The Dissertation Committee for Nicholas Alan Pedrazas Certifies that this is the approved version of the following dissertation:

Dynamic Abnormal Grain Growth in Selected Refractory Metals

Committee:

Eric M. Taleff, Supervisor

David L. Bourell

Todd Ditmire

Desiderio Kovar

Llewellyn K. Rabenberg

Dynamic Abnormal Grain Growth of Selected Refractory Metals

by

Nicholas Alan Pedrazas, B.S.M.E, M.S.E.

Dissertation

Presented to the Faculty of the Graduate School of

The University of Texas at Austin

in Partial Fulfillment

of the Requirements

for the Degree of

Doctor of Philosophy

The University of Texas at Austin

August 2013

Dedication

To my mom, dad, and brother.

Acknowledgements

I would first like to thank my supervisor Eric Taleff for his help and guidance over the years. I have had the pleasure of working in his research group since I was an undergraduate. One could not ask for a more supportive advisor.

I thank my dissertation committee members, professors Bourell, Ditmire, Kovar, and Rabenberg for their advice and time in consideration of my dissertation, as well as all the help in both undergrad and grad school. A special thank you also goes to Jim Ciulik, whom I had the pleasure of working with as an undergraduate research assistant.

I thank my former and current fellow researchers, especially Daniel Worthington, Aravindha Antoniswamy, Philip Noell, Alexander Carpenter, and Jakub Jodlowski for all of our discussions and help in the lab. I was lucky to have such great labmates.

I also need to thank the researchers at Sandia National Laboratories that I worked with and who supported this project, Tom Buchheit and Liz Holm. Their interest in my research and support has helped me immensely.

Dynamic Abnormal Grain Growth of Selected Refractory Metals

Nicholas Alan Pedrazas, Ph.D.

The University of Texas at Austin, 2013

Supervisor: Eric M. Taleff

Abstract: Dynamic abnormal grain growth (DAGG) is a phenomenon by which single crystals up to centimeters in length are produced at elevated temperature during the application of strain. DAGG was previously demonstrated in commercial-purity molybdenum (Mo) materials. This is the first investigation to confirm DAGG in another material, tantalum (Ta). Previous experiments initiated and propagated DAGG using constant true-strain rate tensile tests, but this study demonstrates that DAGG can also occur under constant true-stress tensile conditions. A Mo material was tested under constant true stress, and two Ta materials were tested under constant true-strain rate. The effects of temperature, stress, strain rate, initial microstructure and texture on tensile test data and the resulting microstructures are examined. The microstructures of the Ta materials are analyzed using electron backscatter diffraction (EBSD) data to quantify the orientation, deformation, grain boundary character, and slip properties of the DAGG grains and unconsumed microstructure. The DAGG grains were found to be relatively undeformed compared to the unconsumed microstructure following DAGG and to not be oriented favorably, or unfavorably, for slip. The grain boundaries between DAGG grains in one Ta material were found to commonly have $\Sigma 3$ character. This was likely due to a strong initial <111>-fiber texture. Previous investigations of DAGG in Mo indicated that DAGG grains commonly grow along the surface of the specimen, but this was not

observed with significant frequency in Ta. Results suggest that the distance the DAGG grain boundary travels is proportional to the accumulated strain during DAGG, and the velocity of the DAGG grain boundary is proportional to the applied strain rate but is not related to the orientation of the DAGG grain or its slip properties.

Table of Contents

1 Introduction

Dynamic abnormal grain growth (DAGG) is a phenomenon shown to produce large single-crystals, up to centimeters in length, in the solid-state. DAGG occurs at elevated temperature, approximately 0.55 to 0.65 T_M for molybdenum (Mo), and only while the material is undergoing plastic deformation. The primary difference between DAGG and static abnormal grain growth (SAGG) [Ciulik 2009], otherwise simply known as abnormal grain growth (AGG), is the requirement for continuous plastic deformation. Additionally, much higher temperatures are required for SAGG than for DAGG. Plastic deformation is required for both initiation of DAGG and growth of the resulting abnormal grain (or grains) by rapid boundary migration. During constant strain rate tensile testing at elevated temperature, DAGG produces a rapid drop in load, which corresponds to the growth of one or more large crystals across the gauge region of the specimen. The lower flow stress of the large crystal(s) compared to the prior polycrystalline microstructure produces this load drop.

The purpose of this study is to better understand the DAGG process by producing and characterizing microstructures exhibiting different stages of DAGG and determining the influences of various experimental conditions on DAGG. The DAGG process was previously used to produce large single-crystals in commercial-purity Mo materials [Ciulik 2007, 2009, Worthington 2011, 2013]. This work led to many questions about the causes of DAGG, including whether DAGG is possible in other materials. Tantalum (Ta) is also a BCC refractory metal, like Mo, but with a slightly higher melting temperature, 3290 K versus 2896 K. Therefore, it is logical to investigate Ta for DAGG potential. This study will extend understanding for DAGG by furthering research on Mo, as well as investigating Ta. Parameters investigated include the effects of temperature, strain rate, and stress on DAGG initiation and the propagation of DAGG, the orientations

of DAGG grains, the role of grain boundary character on DAGG, and the mechanism(s) behind the high boundary migration rates observed during DAGG. A model based on creep theory and the movement of dislocations is tested as a possible explanation for observed boundary migration rates. A determination is sought as to whether boundary movement during DAGG is strain enhanced or stress driven.

1.1 MOTIVATION

The investigation of DAGG is important for both technical and commercial reasons. DAGG is not yet well understood but has the potential to dramatically affect the microstructure and properties of a material. Single-crystals can be beneficial or detrimental, depending on the application.

High brittle-to-ductile transition temperatures that are well above room temperature often limit the use of refractory metals in structural applications [Schwartzberg 1959]. Brittle fracture has been shown in Mo [Tsurekawa 1994,1999], tungsten (W) [Gumbsch 2003], and other refractory metals to commonly initiate and propagate at grain boundaries, particularly in recrystallized material. Eliminating these boundaries can substantially increase room-temperature ductility. This is demonstrated in Figure 1.1, which shows a single crystal of Mo that was twisted 180° at room temperature. By contrast, recrystallized polycrystalline Mo has effectively zero ductility at room temperature.

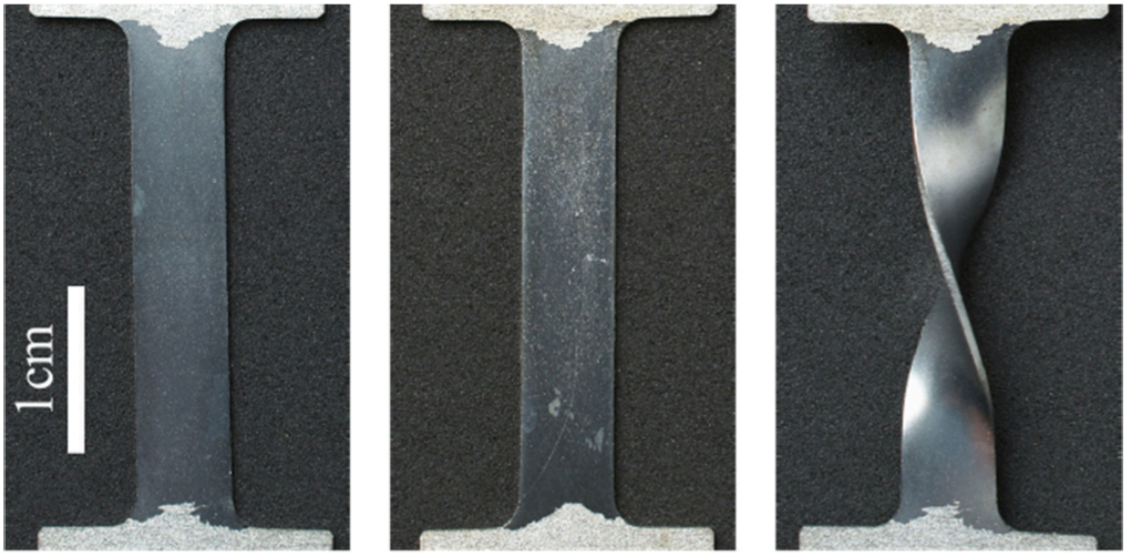

Figure 1.1: Shown is (a) the front and (b) back sides of a single crystal of Mo, and (c) the single crystal twisted 180° at room temperature. Image from [Worthington 2011].

Refractory metals are commonly used in high temperature applications due to their high melting temperatures. In high temperature applications, the effects of grain boundaries can limit service life. A common example of this is observed in W filaments, where a reduction in creep life is caused by a weakening at grain boundaries due to a buildup of impurities and grain boundary sliding [Horacsek 1980]. Single crystals are immune to both of these potential failure mechanisms.

The use of DAGG to create single-crystals also has advantages over traditional methods for crystal growth, such as those of Bridgman [Bridgman 1931] and Czochralski [Czochralski 1918]. These rely on melt-solidification techniques and require higher temperatures and longer times than are used for DAGG, both of which increase the cost and difficulty of production.

The increase in ductility and creep life by using single-crystals, however, is gained at the expense of decreased yield strength. DAGG may inadvertently occur

during hot deformation processing and result in a material ill suited for its intended application due to a reduction in its strength. A better understanding is required to both promote and prevent DAGG.

1.2 MATERIAL SELECTION

Ta was chosen to further investigate DAGG because it does not present some of the challenges that other BCC materials of interest, such as α-Fe and W, do. Iron is polymorphic, and its high-temperature phase change from α to γ at approximately 0.65 T_H (912 °C, where $T_H = T/T_M$ is the homologous temperature and T_M is the melting temperature in K) is within the homologous temperature range of interest for DAGG, based on the previous work with Mo. This phase change prevents the formation of Fe single crystals from melt-solidification methods since the single crystal cannot be retained down to room temperature. It is unknown if the phase change will inhibit the use of DAGG to form single crystals in Fe. W has the highest melting temperature of all refractory metals, at 3422 ˚C. Testing W up to 0.65 T_H (2129˚C) is difficult because reaching such temperatures requires highly specialized equipment. Ta has a crystal structure identical to Mo and has similar properties, making it a likely candidate for DAGG. It can be tested at 0.65 T_H (1866 ˚C), using instruments similar to those used to test Mo. It is for these reasons that Ta was chosen for study. The findings for Ta, in combination with those for Mo, will help give direction to the investigation of DAGG in other materials.

1.3 PROBLEM STATEMENT

Four primary goals are the focus of this investigation.

1. Determine if DAGG can be produced in a material other than Mo, i.e. Ta.
2. Determine the effects of temperature, strain rate, and strain on DAGG in Ta, and compare to results from Mo.
3. Investigate the crystal orientations produced through DAGG and the roles of texture and microstructural features, such as grain boundary character, in their production.
4. Investigate the mechanism of boundary migration during DAGG using the results of microstructural observations and by testing theories of strain-enhanced mobility *versus* stress-driven boundary migration.

2 Materials Background

In this section, the basic principles of deformation and annealing phenomena will be introduced to provide context for understanding DAGG and the microstructural analyses to be subsequently presented. Topics addressed include the microstructural effects of deformation, recovery, recrystallization, grain growth, and abnormal grain growth.

2.1 DEFORMATION

Deformation results from straining a material using a mechanical process and may be considered either elastic or plastic. Elastic deformation occurs only at small strains for metals and is distinguished from plastic deformation in that it does not result in permanent deformation, i.e. the material returns to its original dimensions when the force causing deformation ceases. During plastic deformation of metals and alloys, volume changes so little that this can typically be assumed constant, but a permanent change in the shape does occur. Plastic deformation in crystalline solids generally occurs by dislocation activity. Defects can be in the form of a point (i.e., vacancies), line (i.e. screw and edge dislocations), or plane/surface (grain boundaries), but it is line defects that are most intimately related to plastic deformation. The total dislocation length in the crystal lattice structure per unit volume, a measure of the dislocation density, typically increases with increasing plastic strain. The rate of formation and morphology of dislocations depend on many parameters, such as the deformation rate, temperature, crystal structure and orientation, and initial microstructure, including grain size and particle content. Discussions of dislocation formation and interactions are found in the literature [Hull 2001]. Dislocations are thermodynamically unstable but often remain at low

temperatures due to the activation energy required for their movement toward annihilation. Annealing or deformation at high temperatures allows for dislocations to migrate by climb and other pathways, by which they may encounter another dislocation or surface at which annihilation is possible. Deformation at low temperatures (T_H<0.3) and warm temperatures ($0.3 < T_H < 0.5$) may result in strain hardening due to an increased resistance to further deformation caused by dislocation interactions. At higher temperatures ($T_H > 0.5$) dislocations move more easily and recovery (a small reduction in dislocation density) may occur, reducing the required force for continued deformation. Deformation can result in an increase in dislocation density, deformation cell formation and changes in the shape of grains. Recovery, recrystallization and grain growth are restorative processes that reduce the stored energy caused by defects in the microstructure system, and these will be discussed in a subsequent section.

2.1.1 Creep

Creep is time-dependent deformation at elevated temperature. It is most commonly studied by applying constant stress (or constant load) to a material as tension at an elevated temperature and observing strain *versus* time or strain rate *versus* time, as demonstrated in the schematics of Figure 2.1. Typical creep behavior exhibits three stages: primary (stage I), steady-state or secondary (stage II), and tertiary (stage III). In primary creep, plastic deformation builds dislocation structures, primarily subgrains, which slow the creep rate until it becomes constant. This type of *normal* primary, as demonstrated in Figure 2.1, is typical of pure metals and many of their alloys. Some alloys, referred to as Class I or Class A alloys, exhibit an *inverted* primary during which strain softening occurs [Kassner 2009 p.157]. However, this *inverted* primary behavior is not pertinent to the present study. Primary creep often leads to steady-state creep,

stage II, in which the strain rate remains constant due to a balance between hardening and recovery. For some materials, stage II is so short that it is not considered to provide steady-state creep, but is considered to produce only a minimum in creep rate. In tertiary creep, stage III, the strain rate increases as damage, such as cavitation and necking, occurs and reduces the resistance of the specimen to plastic deformation. Damage weakens the material and produces in an increase in strain rate. At the end of stage III, the material ruptures if the test is not halted. This basic view of creep behavior provides a general context for understanding, but it should be kept in mind that this is perhaps the simplest behavior possible. Many more complex behaviors can occur, but these will only be mentioned when directly pertinent to specific experimental results.

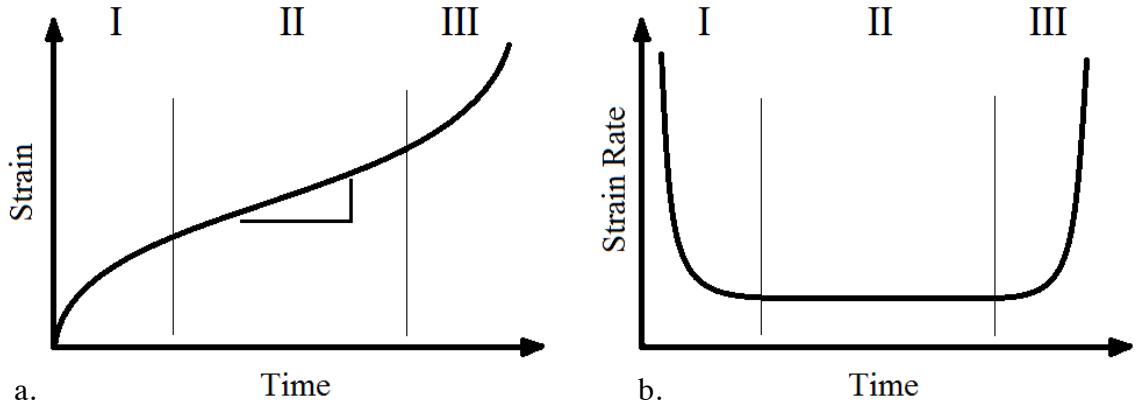

Figure 2.1: Schematic of (a) strain *versus* time and (b) strain rate *versus* time for a constant-stress creep test.

Creep can also be studied using a tensile test at constant true-strain rate. In such a test, a material is strained at elevated temperature at a specified true-strain rate, which requires the use of a test frame with active displacement control. A plot of true stress *versus* true strain, or time, can be used to determine the stages of creep, as indicated in Figure 2.2. In stage I, the stress increases with increasing time (or strain) until becoming constant, assuming a *normal* primary creep behavior. After stage I, stage II begins, and

the true stress remains constant until the beginning of stage III, when damage decreases the resistance to plastic deformation. The material begins to fail, and the stress drops accordingly until fracture occurs.

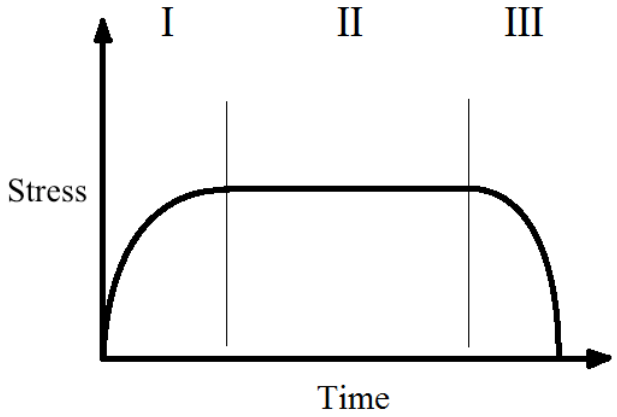

Figure 2.2: Stress *versus* time of a constant strain-rate creep test.

Steady-state creep is generally observed to follow the phenomenological equation for creep, which can be written in terms of the Zener-Holloman parameter, Z, as [Sherby 1967]:

$$Z = \dot{\varepsilon}\exp\left(\frac{Q}{RT}\right) = A\left(\frac{\sigma}{E}\right)^{n}, \qquad \text{Eq. 2.1}$$

where $\dot{\varepsilon}$ is the strain rate, Q is the activation energy for creep, R is the universal gas constant, T is temperature in K, A is a material constant, σ is the flow stress, E is the dynamic unrelaxed Young's modulus and n is the stress exponent. Different creep regimes are often identified by the stress exponent, n, which equals approximately 5 for dislocation climb creep of many polycrystalline pure metals, and by the activation energy, Q, which varies by material and the creep mechanism active at a particular temperature and strain rate.

2.1.2 Slip

Plastic deformation can be produced by either slip or twinning in crystalline metals. However, twinning is generally uncommon in materials with a high stacking fault energy γ_{SFE}, such as BCC metals. Slip in BCC metals occurs in <111> directions and is commonly cited as occurring on either {110}, {112} or {123} planes. There are 12 {110}<111>, 12 {112}<111> and 24 {123}<111> slip system combinations, i.e. permutations of the slip directions within possible slip planes. The number of slip combinations for each system doubles if slip in the negative direction is also considered.

Controversy exists as to the planes on which slip occurs at different temperatures. This is complicated by the fact that slip appearing to occur on a {110} plane may actually be the result of successive slip on 2 {112} planes, and vice-versa. In general, the slip system active below 0.25 T_H is {112}<111>, between 0.25 and 0.5 T_H is {110}<111> and above 0.5 T_H is {123}<111> [Humphreys 2004 p.25]. At high temperatures slip is thought to occur by the "pencil slip" process along a <111> direction, which means that slip occurs equally well on any plane that allows for slip in a <111> direction. In theory, pencil slip may be thought of as occurring on any of an infinite number of planes that can be created as one rotates about a <111> direction. A simpler theory is that of "mixed slip," in which all three slip systems are considered to be simultaneously active. This assumption produces 12 possible slip planes when rotating about any single <111> direction.

2.1.3 Single slip

The Schmid law states that slip will occur when a critical resolved shear stress is reached on a particular slip plane in a particular slip direction [Schmid 1935]. The active

slip system for a particular crystallographic orientation relative to the direction of the applied force will be that with the highest resolved shear stress,

$$\tau_{ns} = \sigma \cos\lambda \cos\phi \qquad \text{Eq. 2.2}$$

where τ_{ns} is the shear stress resolved on the slip plane, σ is the applied stress normal, λ is the angle between the slip direction and the and force vector causing the applied normal stress and ϕ is the angle between the slip plane normal and force vector. If τ_{ns} is greater than a critical value, called the critical resolved shear stress, then slip will occur. The Schmid factor is defined as,

$$m = \cos\lambda \cos\phi, \qquad \text{Eq. 2.3}$$

such that Eq. 2.2 can be defined as

$$\tau_{ns} = m\,\sigma\,. \qquad \text{Eq. 2.4}$$

The Schmid factor can be calculated for each possible slip system to determine which system is active for a particular normal stress caused by the applied force. The active slip system predicted is the one that produces the highest Schmid factor.

The Schmid law is generally applicable to close-packed crystal structures, such as FCC and HCP. Behaviors not predicted by the Schmid law in BCC, and other non-close-packed structures, have been known since the studies of Taylor on the deformation of α-iron and β-brass [Taylor 1926, 1928]. These included observations that slip does not always occur on a definite crystallographic plane and that the resistance to slip in one direction is not the same as in the opposite direction. Non-Schmid effects can lead to slip on a system that does not have the highest Schmid factor. In BCC metals, the asymmetry of shearing in the positive or negative <111> direction causes slip to be directionally dependent and results in the formation of twinning-antitwinning behavior [Christian 1983, Duesbery 1989, Vitek 1975]. It has also been observed that components of the stress state that do not exert any Peach-Koehler force (force on a dislocation) can affect

the shape of the dislocation core and thus alter the Peierls stress (force required to move a dislocation) [Escaig 1974, Duesbery 1973, 1984, Groger 2005, Ito 2001]. This is commonly attributed to the complex atomic geometry in the core of the screw dislocation in BCC metals [Vitek 1970, Basinski 1971, 1972, Duesbery 1973, 1989, 1998, Christian 1983].

2.1.4 Multiple Slip

The Schmid factor assumes slip on one slip system, which may be applicable to single crystals that do not have boundary constraints. But multiple slip, in which more than one slip system is active simultaneously, is preferred in polycrystalline microstructures. The activation of multiple slip systems provides greater internal accommodation of applied external strains. The underlying mechanisms of plasticity in a single crystal are the same for polycrystalline deformation, but polycrystalline deformation is much more complex than single-crystal deformation because of the constraints imposed by neighboring grains. Efforts to accurately predict the mechanical behaviors of BCC (and FCC) materials continue, particularly by using computational methods [Liang 1999, Buchheit 2005]. Difficulties arise from the complexity of the interactions involved, understanding of the underlying phenomena, computational power required to simulate realistic microstructures and the difficulty of experimentally characterizing microstructures for comparison to simulation predictions.

One model of multiple-slip in polycrystals is that of Sachs [Sachs 1928]. The Sachs model for multiple-slip deformation assumes isostress conditions, allowing for grain rotations to accommodate slip [Sachs 1928]. However, this leads to problems with geometric compatibility, especially near grain boundaries [Taylor 1938].

The most widely accepted model of slip in polycrystals is that of Taylor [Taylor 1938]. The Taylor model requires compatibility between all grains during deformation and is an isostrain model such that each grain is assumed to undergo the same strain as the bulk of the sample. Because the strain tensor is symmetric, there are 6 independent strains, which reduce to 5 under the assumption that volume is conserved [von Mises 1928]. It follows that a material is capable of deforming into any general shape if 5 or more independent slip systems are available. The {110}<111> family of slip systems in BCC crystals (analogous to {111}<110> in FCC crystals) has 12 slip systems that may be combined to form groupings containing at least 5 independent slip system components to meet this requirement. There are 792 possible combinations of 5 slip systems from these 12. According to Taylor, the particular combination of 5 slip systems that causes slip is the one that produces the minimum internal work in the material to accommodate the applied strain. The internal work per volume, dw, expended by the active slip systems is

$$dw = \tau \, \Sigma_i \, |d\gamma_i|, \qquad \text{Eq. 2.5}$$

where τ is the magnitude of the resolved shear stress for slip and is assumed equal among all slip systems, and $\Sigma_i \, |d\gamma_i|$ is the sum of the magnitudes of the shear strains from slip over the individual active slip *systems i* and is often denoted $d\gamma$. The Taylor model also assumes uniaxial tension, such that the strain state is,

$$d\varepsilon_y = d\varepsilon_z = -\tfrac{1}{2} \, d\varepsilon_x \text{ , and } d\gamma_{yz} = d\gamma_{zx} = d\gamma_{xy} = 0 \text{ ,} \qquad \text{Eq. 2.6}$$

for uniaxial tension along the x direction. The internal work is then defined as

$$dw = \tau \, d\gamma = \sigma_x \, d\varepsilon_x \qquad \text{Eq. 2.7}$$

where σ_x is the applied normal stress resulting from tension along x. The Taylor factor, M, is then defined as the sum of the shear strains from the slip components for an increment in tensile normal strain, given by

$$M = d\gamma / d\varepsilon_x \text{ .} \qquad \text{Eq. 2.8}$$

An average Taylor factor $\overline{M}$ can be calculated by averaging M for all orientations in a polycrystalline sample to determine an approximate relationship between stress and critical resolved shear stress for a material with a particular texture, such that,

$$\sigma_x = \overline{M}\ \tau\ . \qquad \text{Eq. 2.9}$$

The Taylor factor gives a measure of the resistance to slip for a given crystallographic orientation and strain state. M and m have an inverse relationship, as is demonstrated by comparing Eq. 2.4 and Eq. 2.9, such that a higher M represents a "harder" texture.

The method of calculating Taylor factor presented here assumes isotropic hardening and that the deformation path is independent of strain rate, and it ignores stress discontinuities at grain boundaries. Despite these deficiencies, this method presents a reasonable description of multiple slip for the purposes of this study.

The Taylor method considers only the geometric feasibility of the individual shears matching the imposed strain. Bishop and Hill developed a measure of the Taylor factor using a stress-based approach [Bishop 1951]. This method requires there to exist a stress state that is capable of activating the required slip systems to accommodate the external strain. The stress tensor must exert a shear stress on each active slip system greater than a critical shear stress for yielding, while the shear stress on non-active systems must not cause slip. This method involves first calculating each stress state that can simultaneously activate at least 5 slip systems. The active stress state is the one that produces the maximum work on the material for an increment of strain [Bishop 1951]. The possible stress states have been tabulated in the literature for the {110}<111> system [Bishop 1951], {112}<111> system [Hosford 1969] and {123}<111> system [Chin 1970]. For the {110}<111> system, the Taylor model includes 384 possible slip system

combinations, but the Bishop and Hill method reduces this to 56. The result of the Bishop and Hill method is equivalent to that of the Taylor method.

2.2 GRAIN BOUNDARY PROPERTIES

Grain boundaries are planar dislocation structures separating differently oriented crystals. The properties and movement of grain boundaries are defined by both atomistic and energetic mechanisms. Full geometric characterization of the grain boundary requires knowledge of all 5 degrees of freedom defining the boundary; three are determined by the orientation between the crystals, and two are defined by the orientation of the boundary plane. However, the complete grain boundary definition is not required to develop some orientation-property relationships. Of particular interest are *special* boundary types, such as Σ boundaries, that may give rise to geometric compatibility along the boundary. Properties that affect the energetic mechanisms are due to gradients in thermodynamic properties within the material, such as stored deformation energy and impurity content.

2.2.1 Grain Boundary Characterization

Grain boundary characters of interest include low $\sum$ and low-angle (aka, $\sum 1$) boundaries. These boundary types can have energy and mobility characteristics very different from boundaries with similar misorientations that do not have a $\sum$ orientation relationship.

$\sum$ boundaries, are defined by the presence of a coincident cite lattice (CSL). If two misoriented crystal lattices are overlaid, there exists a regular array of positions where points from both lattices are congruent. This defines the CSL. The CSL has a

minimum repeating unit, and the ratio of the size of this unit to the size of the original lattices determines the ∑ character of a boundary between the two crystal orientations. As a result, a ∑3 boundary, for example, is often described as having approximately every 1 out of 3 lattice points along the boundary in common with both crystals. Low-angle boundaries are those that separate lattices with nearly the same crystallographic orientation. These may be viewed as having a CSL congruent everywhere on the original lattices, to within the small "low-angle" misalignment. Thus, these are sometimes described as ∑1 boundaries. Virtually any misorientation will have a CSL, but only low ∑ boundaries are of interest because they are more likely to exhibit particular grain boundary properties, particularly a low grain-boundary (surface) energy. The conditions for ∑3, ∑5, ∑7, ∑9, and ∑11 are listed in Table 2.1. A ∑3 boundary, for example, is the special case for which the lattice of one grain can be rotated 60° about a <111> axis to be coincident with the lattice of the other grain.

Table 2.1: Definition of ∑3 through ∑11 boundary misorientations for cubic materials.

∑	Angle, degrees	Axis
3	60	<111>
5	36.87	<100>
7	38.21	<111>
9	38.94	<110>
11	50.48	<110>

The deviation allowed from the ideal misorientation for a ∑ boundary, for the purposes of measuring the fraction of such boundaries, is commonly defined by the Brandon criterion [Brandon 1966],

$$\theta_B = 15° \Sigma^{-1/2} \quad \text{Eq. 2.10}$$

where θ_B is the allowed deviation from a perfect Σ misorientation, in degrees, and Σ refers to the Σ value of the grain boundary being analyzed. This definition distinguishes between high- and low-angle boundaries by a misorientation (disorientation) of 15°. A note on terminology: it is common to define *misorientation* as the deviation in orientation between two points, however, since a material with cubic symmetry has 24 equivalent orientations, a second term may be used, *disorientation,* which implies that the deviation in orientation is specifically taken as the lowest among the 24 possible variations for the crystal's orientation. This will be discussed further in subsequent sections. Misorientation is the more widely used term and will be used here in all cases where the disorientation is not required.

2.2.2 Grain Boundary Migration

The migration of a grain boundary is fundamentally a process of atoms detaching from one crystal and joining an adjacent crystal, such that one crystal is sacrificed for the growth of the other. The boundary moves to reduce its Gibbs free energy. The change in Gibbs free energy, dG, as a function of driving force, P, and volume swept out by the moving boundary, dV, is:

$$dG = -P\, dV. \quad \text{Eq. 2.11}$$

Therefore, P is the free energy difference per unit volume and can be thought of as a force per unit area, or pressure. The velocity of a boundary, v, is typically calculated from,

$$v = m\, P \quad \text{Eq. 2.12}$$

where P is the driving force and m is the mobility of the boundary. (Note that the symbol m is customarily used for both mobility and Schmid factor, but the context generally allows the meaning to be easily distinguished.)

2.2.2.1 Driving Force

Grain growth is commonly the result of a driving force from stored deformation energy and the energy associated with grain boundary curvature. However, other factors are also known to increase the driving force for boundary migration. These factors are summarized in Table 2.2.

Table 2.2: Grain boundary driving forces. From [Gottstein 2009, p.141].

Source	Equation	Approximate value of parameters	Estimated driving force, MPa
Stored deformation energy	$P = \frac{1}{2}\rho\mu b^2$	ϱ = dislocation density ~ 10^{15} m^{-2} $\mu b^2/2$ = dislocation energy ~ 10^{-8} J/m	10
Grain boundary curvature	$P = \frac{2\Delta\sigma_b}{R}$	σ_b = grain boundary energy ~ 0.5 J/m^2 R = grain boundary radius of curvature ~ 10^{-4} m	10^{-2}
Surface energy	$P = \frac{2\Delta\sigma_s}{d}$	d = sample thickness ~ 10^{-3} m $\Delta\sigma_s$ = surface energy difference of two neighboring grains ~ 0.1 J/m^2	$2x10^{-4}$
Chemical driving force	$P = R(T_1 - T_0)c_0 \ln c_0$	c_0 = concentration = max. solubility at T_0 T_1 (< T_0) annealing temperature (5% Ag in Cu at 300°C)	$6x10^{2}$
Magnetic field	$P = \frac{\mu_0 H^2 \Delta\chi}{2}(\cos^2\Theta_1 - \cos^2\Theta_2)$	Material: bismuth H = magnetic field strength (10^7 A/m) $\Delta\chi$ = difference of magnetic susceptibilities ~ 1.8x10-7 (250°C) Θ = angle between c-axis and field direction $\Theta_1 = 0°$; $\Theta_2 = 90°$	$3.5x10^{-4}$
Elastic energy	$P = \frac{\tau^2}{2}\left(\frac{1}{E_1} - \frac{1}{E_2}\right)$	τ = elacic stress ~ 10 MPa E_1, E_2 = elactic moduli of neighboring grains ~ 10^5 MPa	$2.5x10^{-4}$
Temperature gradient	$P = \frac{\Delta S \cdot 2\lambda grad T}{\Omega_a}$	ΔS = entropy difference between grain boundary and crystal (approx. equivalent to melting entropy) ~ $8x10^3$ J/Kmol *grad T* = temperature gradient ~ 10^4 K/m 2λ = grain boundary thickness ~ $5x10^{-10}$ m Ω_a = Molar volume ~ 10 cm^3/mol	$4x10^{-5}$

The estimated driving forces in Table 2.2 represent general approximations and are not specific to a particular material, except where stated. The driving forces that may influence the present investigation are from stored deformation energy, grain boundary curvature and possibly surface energy. The chemical driving force applies to solid solutions and thus is not of interest herein, despite its potentially large effect.

2.2.2.2 Mobility

Grain-boundary mobility is affected by material, impurity content, temperature and orientations of the crystals and boundary [Gottstein 2009]. The mobility is generally expected to, approximately, follow the Arrhenius relation, such that [Gottstein 2009, p.138]

$$m = m_0 \exp(-H/kT) \,, \qquad \text{Eq. 2.13}$$

where m_0 is the mobility constant, H is the activation enthalpy of the mobility, k is the Boltzmann constant and T is the absolute temperature. The activation energy for grain-boundary migration in pure metals is similar to that for grain-boundary diffusion, which is approximately half the activation energy for bulk diffusion [Gottstein 2009, p.138].

Atomistic simulations over a wide range of boundary types using synthetic driving forces determined that mobility cannot be consistently correlated to Σ character, disorientation angle, excessive volume at the boundary or boundary energy [Olmsted 2009a, 2009b]. Shearing of the boundary, which may allow for much larger mobility, was restricted in many of the simulations because it may not be possible to accommodate large shears during grain growth in polycrystalline materials. The largest mobility was found for Σ3 boundaries, but the mobility for Σ3 boundaries varies considerably. Σ3 boundaries were determined to often be high mobility and low energy, although they were also often found to not be thermally activated, and thus did not always abide by Eq. 2.13 [Olmsted 2009b].

2.2.2.3 Stress Assisted Boundary Migration

Stress-assisted boundary migration (SABM) is a process in which a grain boundary migrates by coupling with shear deformation. Observations of shear coupled boundary migration have been observed in experiments and simulations of bicrystals

[Winning 2001a, 2001b; Cahn 2006a, 2006b; Gorkaya 2010], and nanocrystalline thin films [Gianola 2006]. A model for shear coupled boundary migration was presented by Cahn [Cahn 2004]. A dissipation of energy resulting from the applied stress and produced strain provides the driving force for boundary migration. A net shape change of the crystal is observed due to the accumulated shear strain. These mechanisms have a clear affect on bicrystals but their influence on the motion of boundaries in polycrystals is not clear because bicrystals are not subjected to the same boundary conditions as grains in a polycrystalline microstructure. It has been suggested by Cahn [Cahn 2006] that these mechanisms may be possible without a net shear deformation, and thus observable in polycrytals, if the shear deformation is allowed to switch back and fourth. It is unclear that this is possible in a bulk polycrystalline specimen. It is unlikely that all grains will be oriented to facilitate a reduction in energy due to the motion of a boundary in one direction, as is required for DAGG.

2.3 RECOVERY, RECRYSTALLIZATION, AND GRAIN GROWTH

Recovery, recrystallization and grain growth are all restorative processes that reduce the overall energy stored in a material. They vary in the degree and morphology of their restoration. Both the static and dynamic variants of these phenomena are introduced here. Static processes occur upon annealing following deformation, while dynamic implies that strain is actively being applied as restoration occurs. In addition, recrystallization and grain growth may also be classified as either continuous or discontinuous, depending on the homogeneity of the process.

2.3.1 Recovery

Recovery is the reduction in energy through the annihilation or rearrangement of defects. Recovery occurs at elevated temperature, where the movement of dislocations becomes easier, particularly through climb, and can result in dislocation annihilation, dislocation rearrangement and subgrain formation and growth. This is often accomplished in BCC metals by dislocation glide at lower temperatures and dislocation climb at higher temperatures. In high γ_{SFE} materials, such as Mo and Ta, subgrains and cellular dislocation structures may form from agglomerations of dislocations.

Active straining may also cause some recovery processes to occur, such as dislocation annihilation and rearrangement of dislocations to lower energy configurations, even at low temperatures. Recovery produced by active straining is classified as *dynamic recovery* (DRV).

2.3.2 Recrystallization

Recrystallization (RX) is the formation of new, unstrained grains that grow to consume the original deformed microstructure. It is governed by both nucleation and growth mechanisms. Recrystallization is a thermally activated process that uses stored deformation energy as its primary driving force. It is in competition with recovery, which is simultaneously decreasing the stored energy. A new grain is often observed as nucleating from a relatively strain-free segment of a previous grain, separated from its surrounding microstructure by high-energy boundaries. Growth of the nucleus results in consumption of the surrounding microstructure. When both nucleation and growth occur simultaneously throughout the microstructure, the recrystallization is continuous. Discontinuous recrystallization may occur following primary recrystallization, and is thus

termed secondary recrystallization. Secondary recrystallization is also known as abnormal grain growth, which will be discussed in a subsequent section.

Several rules have been developed to describe the recrystallization process [Mehl 1948, Burke and Turnbull 1952, Humphreys 2004 p.220]: a minimum plastic strain is required for initiation, larger deformations generally produce smaller recrystallized grain sizes and the temperature required decreases with increasing annealing time and increasing strain.

Dynamic recrystallization (DRX) is the formation of new grains as a material is actively strained, typically at elevated temperature. This may occur after a critical plastic strain is reached, as with RX. The critical plastic strain is related to the peak stress, which is related to the Zener-Holloman parameter, Z, such that the peak stress increases with decreasing temperature or increasing strain rate. As preexisting grains are deformed, new unstrained, recrystallized grains nucleate and begin to grow, but a build up of dislocations in these and the formation of new recrystallized grains impedes their growth. The initiation of new grains gradually reduces the flow stress during a tensile test, but eventually a constant flow stress is reached, as shown in Figure 2.3, when equilibrium between nucleation of recrystallized grains and deformation of existing grains is reached. The resulting grain size distribution remains constant with increasing strain during DRX. DRX often does not occur in high γ_{SFE} materials because rapid recovery and DRV may prevent the dislocation density from reaching the critical value required for DRX.

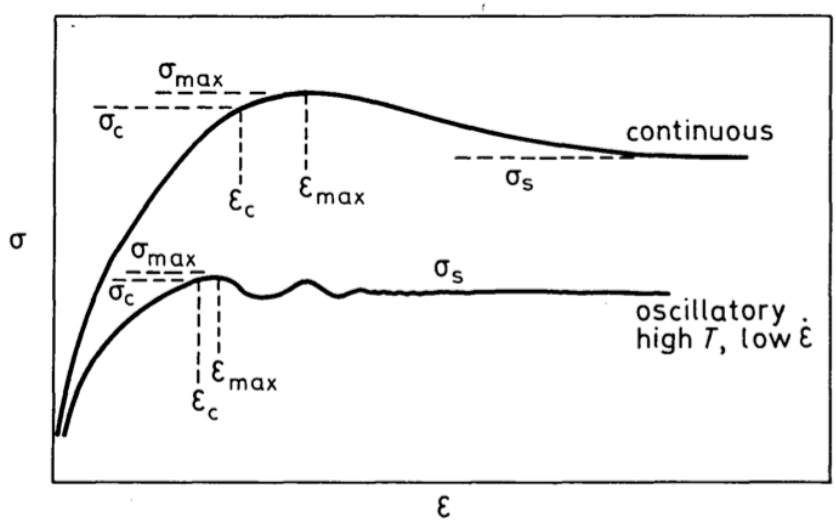

Figure 2.3: Schematic of stress *versus* strain behavior demonstrating the effect of temperature and strain rate on a material that exhibits DRX. From [Roberts 1979].

DRX was observed during plastic deformation of Au, Ag, Cu and Ni single crystals [Mecking 1978, Gottstein 1979, 1983a, 1983b]. As a single crystal is deformed, it builds up dislocation and subgrain structures. When DRX initiates, a sudden drop in flow stress is observed, as demonstrated in Figure 2.4. This drop is much more rapid in a single crystal than is observed in DRX of polycrystals, and it corresponds to the nucleation of a new, recrystallized grain or grains. Investigations by Gottstein *et al*. on copper single crystals indicate that DRX in single crystals occurs at a critical stress, which was not related to the critical strain or *Z* as with DRX of polycrystals [Gottstein 1979]. Rather it can be related to the material, orientation, temperature and strain rate [Gottstein 1979,1983, Stuitje 1980]. Often only one grain nucleated, and it originated from either a subgrain [Gottstein 1979] or at a transition band formed during deformation [Ardakani 1992].

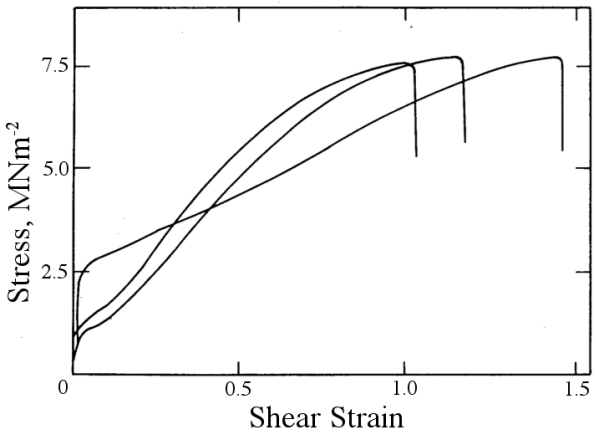

Figure 2.4: Stress *versus* shear strain for three single crystals of copper, of nearly identical orientation, deformed at a strain rate of 6×10^{-4} s^{-1} and temperature of 857 °C (0.83 T_H). Image adapted from [Gottstein 1979].

2.3.3 Grain Growth

Grain growth may continue after recrystallization to further reduce the Gibbs free energy of the microstructure system. This growth is slower than that observed during primary recrystallization because of reduced driving force. Common factors influencing grain growth rate and final grain size are: temperature, particle content [Zener 1948, Hillert 1965, Gladman 1966, Wörner 1987, Andersen 1995a], texture [Humphreys 1997] and the specimen's dimensions [Mullins 1958, Frost 1990]. Higher temperatures increase grain growth by increasing the mobility of grain boundaries. Particles and solutes may pin boundaries by residing at energetically favorable positions within the boundaries. This increases the energy requirement to move a boundary, making grain growth difficult. The amount of pinning depends on many factors, such as the particle size, volume fraction and their dissolution or agglomeration at temperature [Rios 1987, Andersen 1995a]. Strong textures will have grains often separated by low angle boundaries. Low-angle boundaries are often low energy and low mobility and thus may be less likely to migrate, inhibiting grain growth. A specimen's size may affect growth

as the grain size surpasses the thickness of a specimen [Beck 1949, Palmer 1987] because this may affect the curvature of the grains, a driving force for grain-boundary migration [Burke 1952, Mullins 1956]. Additionally, grain boundary grooving at the surface may impede further grain growth [Mullins 1958].

Dynamic grain growth has not been studied in much depth, but pertinent observations of grain-boundary migration during creep tests of lead were made by Gifkins [Gifkins 1952,1953a, 1953b,1957,1959].

2.3.3.1 Abnormal Grain Growth

Grain growth that occurs homogeneously is termed continuous or *normal* grain growth. A subset of grains grow and consume the remaining grains, and the mean grain size increases. This differs from discontinuous or abnormal grain growth (AGG) in which a smaller subset of grains grow rapidly to several times the size of the of the remaining matrix grains, creating a bimodal grain size distribution. Because this also resembles a second recrystallization process, after recrystallization has already occurred, it sometimes termed *secondary recrystallization*. AGG that occurs without concurrent plastic deformation is termed static abnormal grain growth (SAGG) [Ciulik 2005]. This is used to distinguish traditional AGG from dynamic abnormal grain growth, which will be discussed subsequently.

There are several factors found to influence AGG. The suppression of normal grain growth is a commonly recognized precursor for AGG. AGG is promoted by:

- particle pinning [Hillert 1965, Rios 1987,1994, Andersen 1995b]
- strong texture [Dunn 1966, Humphreys 1997]

- diffuse grain size distribution and the presence of a grain much larger than the average [Hillert 1965, Srolovitz 1985]
- solute drag [Kim 2008]
- orientation based surface energy differences [Dunn 1966, Frost 1992]
- grain boundary mobility advantage [Frost 1988, Rollett 1989,1997a]

It has been demonstrated theoretically and computationally that AGG is more likely to occur when a particular "seed" grain has boundaries with higher mobilities than those of other grain boundaries [Frost 1988, Rollett 1989, 1997a]. An abnormal grain is often assumed to have a size advantage over other matrix grains [Hillert 1965], although a large size advantage alone is not sufficient to cause AGG, and this perturbation in grain size distribution disappears for long simulation times in an *ideal* microstructure, i.e. a microstructure absent of impurities and with a uniform grain boundary energy [Thompson 1987].

The influence of grain boundary pinning by particles on initiation of AGG is well recognized. Particle pinning is a major contributor to grain growth inhibition and is predicted to have a role in AGG when the average grain size is below a threshold, as determined by the size and spacing of particles [Hillert 1965]. Small pinning forces may not significantly inhibit normal grain growth, thus making AGG unlikely. Additionally, very high pinning forces may delay the occurrence of AGG [Hillert 1965]. Particle content may not be static across time and temperature because of the dissolution or agglomeration of particles, which should be expected to affect AGG [Hillert 1965, Rios 1987,1992, Andersen 1995b].

Solute drag and particle pinning can occur both on grain boundaries and on single dislocations. These have similar effects in that they restrict migration of either until a critical point is reached, at which the dislocation or grain boundary breaks from the

impediment (solute atmosphere or particle) and moves freely through the material. Simulations indicate that AGG is possible from solute drag effects, even in the absence of texture, mobility or energy anisotropy, pinning particles or grain size advantages [Kim 2008].

Grains in materials with strong textures, which have narrow distributions of boundary misorientations and energies, are less stable than in random textures and are more prone to AGG [Humphreys 1997]. A strong texture may still contain some grains outside the majority texture, which will inherently have higher boundary angles and higher boundary energies than the majority of grains. These grains may act as seed grains for AGG. High-angle boundaries are generally expected to be more mobile than low-angle boundaries. The theoretical relationship between mobility and energy with misorientation angle is given in Figure 2.5.

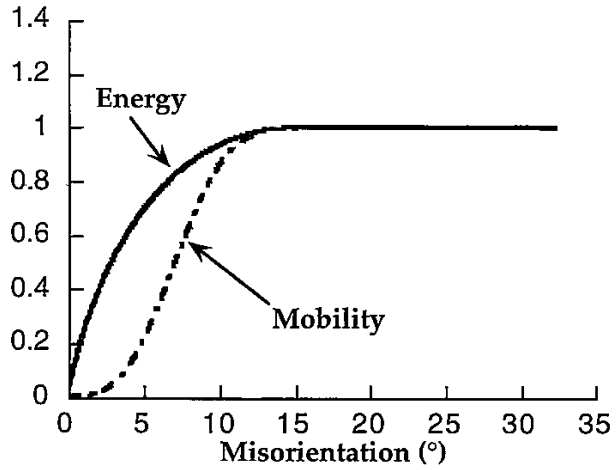

Figure 2.5: Schematic demonstrating general relationship between boundary energy and mobility with misorientation angle. Values normalized to that for the largest misorientation. Figure adapted from [Rollett 1997b].

The presence of high-angle boundaries is not a sufficient condition for AGG; the grain boundaries must also be highly mobile [Rollett 1989,1997a]. Simulations indicate that abnormal grain growth is most likely to occur when a grain has a high-mobility, low-

energy boundary with its neighbors, relative to the boundaries between the remaining grains in the matrix [Rollett 1997a, 1997b, Holm 2003]. Boundaries with both high mobility and low energy may be possible in some Σ boundary configurations, as were discussed in §2.2.1, although special boundary character is not a consistent predictor of low energy boundary character [Olmsted 2009a, 2009b, Janssens 2006, Rohrer 2011].

Surfaces may have a significant effect on AGG because of both orientation-based surface energy differences between grains and migration inhibition from grain-boundary grooving. The effect of surfaces increases with decreasing thickness of the specimen, relative to grain size. Observations of AGG in thin films have demonstrated growth in the opposite direction expected from their boundary curvature, indicating that surface energy effects can be a dominant mechanism for AGG [Walter 1960]. Simulations of thin film microstructures indicate that only small differences in surface energy are required between a grain and its neighbors for the grain to overcome stagnation forces and grow abnormally [Frost 1992].

Most observations and simulations of AGG demonstrate a limitation on the maximum size to which an abnormal grain will grow. This limit depends on many of the same factors that promote or inhibit AGG, such that larger abnormal grains (relative to the size of the matrix grains) are predicted with: thicker sheet materials [Frost 1992, Nakashima 1994], a greater boundary mobility advantage of the abnormal grain boundary [Rollett 1989, 1997b, Humphreys 1997] and stronger initial texture [Humphreys 1997].

2.3.3.2 Dynamic Abnormal Grain Growth

Abnormal grain growth that occurs concurrently with active straining is termed dynamic abnormal grain growth (DAGG) [Ciulik 2005]. Materials that exhibit DAGG

are also expected to exhibit SAGG, but higher temperatures and longer annealing times are required for SAGG.

DAGG is best observed using a constant true-strain rate tensile test at elevated temperature. An illustrative example of DAGG during a constant true-strain rate test is provided in Figure 2.6. As the material is strained, it plastically deforms, as expected. At a particular strain, approximately 0.18 true strain in this case, the flow stress drops rapidly. This corresponds to the initiation of a large DAGG grain. The decrease in flow stress is because of the ease of plastic deformation in the new single crystal compared to that of the prior polycrystalline microstructure. As the material is strained further, the large DAGG grain continues to grow until it reaches the ends of the gauge region of the specimen. At this point, the rate of decrease in flow stress slows until the stress levels out and briefly becomes constant. Straining beyond this point results in plastic deformation of the single crystal(s) produced by DAGG and eventual rupture of the specimen. The specimens shown in Figure 2.6 were produced from different experiments using identical test conditions. Each test was halted at a specific true strain to view the microstructure corresponding to various features on the true stress *versus* true strain curve. The abnormal grains grew at rates up to ~0.5 mm/sec. DAGG grains of 10 cm in length were produced in Mo wire [Worthington 2011]. The resulting DAGG grain size appears to be only a function of specimen geometry and physical limitations of the testing apparatus.

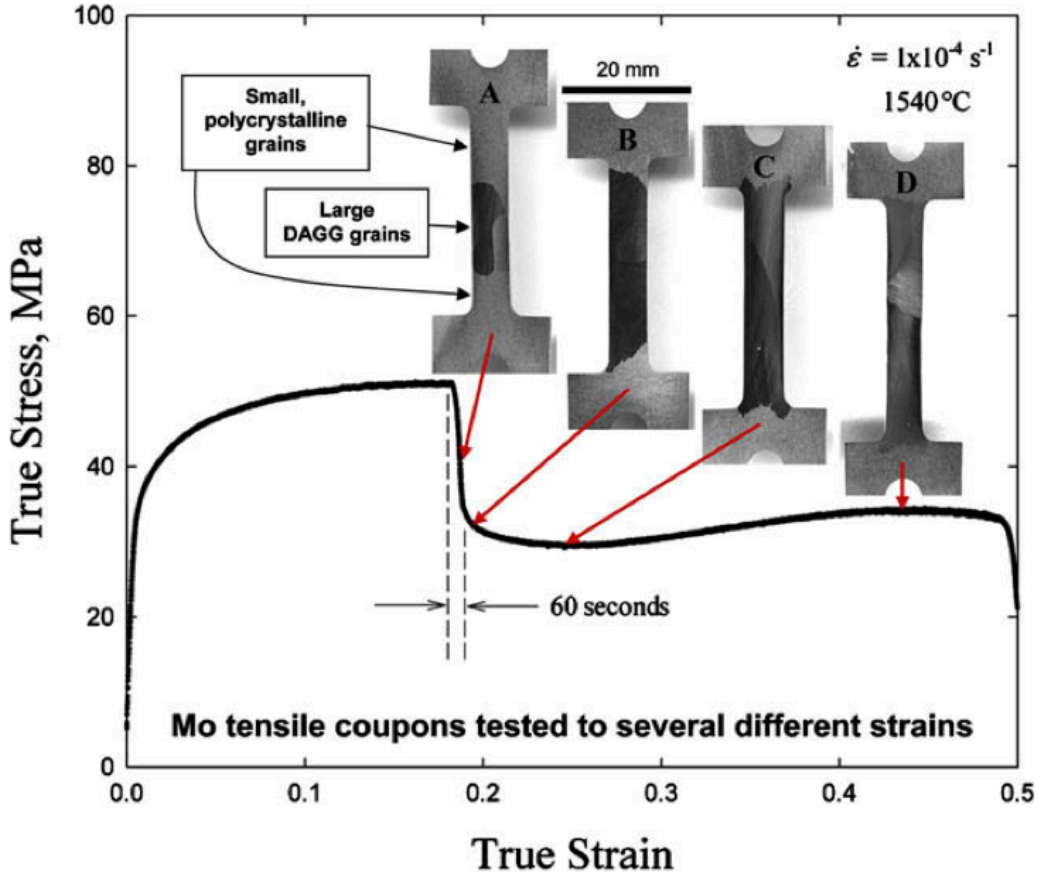

Figure 2.6: DAGG in Mo is demonstrated for a constant true strain rate of 10^{-4} s^{-1} at 1540 °C. Microstructures shown are from separate tests halted along various points along the test curve. Figure from [Ciulik 2009].

2.4 Review of Previous DAGG Investigations: Mo, U, Fe

DAGG was previously tested for in three BCC refractory materials: Mo [Ciulik 2005, 2009, Worthington 2011, 2013], U [Worthington 2007], and α-Fe [Tran 2008, Thanh 2009]. Experiments on U and α-Fe demonstrated AGG, but the observation of DAGG was inconclusive.

2.4.1 DAGG in Mo

Mo is the material in which DAGG has been most extensively investigated. DAGG was demonstrated in three commercially-pure Mo materials: one produced using the arc-melting process (Mo-AM), and two materials produced by powder metallurgy techniques (Mo-PMA, Mo-PMB). The tests performed for prior investigations were all constant true-strain rate tensile tests at elevated temperature. DAGG was observed in Mo at temperatures from 1540 to 1850 °C under applied strain rates from 10^{-6} to 10^{-4} s^{-1}. Some conclusions from the previous studies of DAGG in Mo are summarized below.

1. A minimum temperature and strain rate are required to initiate DAGG.
2. The strain at which DAGG initiates is observed to be a strong function of temperature, with decreasing required strain with increasing temperature.
3. The strain at which DAGG initiates varied between the three Mo materials.
4. The strain at which DAGG initiates was largely unaffected by the strain rate within the range of rates studied.
5. The three Mo materials displayed different initial textures, which depended on their processing histories, but all exhibited DAGG.
6. DAGG grains in all three materials preferred to align their <110> direction parallel to the tensile direction.
7. Large recrystallized grains occasionally remain unconsumed by the growing DAGG grain, becoming island grains. This was more commonly observed in the Mo-AM material, which had a larger recrystallized grain size than either the Mo-PMA or Mo-PMB materials.
8. Initiation of multiple DAGG grains was more common in Mo-AM than in either Mo-PMA or Mo-PMB.

9. DAGG grains often prefer to grow at the surface of the specimen.
10. The length of a DAGG grain along the tensile axis is proportional to the plastic strain accumulated during the drop in flow stress associated with DAGG.
11. DAGG boundary migration rates at 1650 °C are approximately 0.6 to 1.3 cm/min, which is one to two orders of magnitude faster than boundary migration rates expected for SAGG.
12. Driving forces from stored deformation energy and boundary curvature alone are not sufficient to explain the rapid boundary migration rates during DAGG. Plastic strain accumulation likely increases the mobility of DAGG grain boundaries.

2.4.2 Investigations for DAGG in U

Constant crosshead experiments were conducted at elevated temperature on U-238 at Los Alamos National Laboratories by Worthington [Worthington 2007] in an effort to observe DAGG. These tests used a constant crosshead speed of 10^{-4} s^{-1} and temperatures of 475, 550 and 650 °C (0.53, 0.59 and 0.66 T_H, respectively). Tests at 475 and 550 °C showed no signs of AGG, however, the 650 °C test did. The 650 °C test was conducted to failure, unlike the 475 °C and 550 °C tests, and exhibited a bimodal grain size distribution in the gauge region of the specimen. The resulting abnormal grains were limited in size to approximately 1 mm. No AGG was observed in the grip regions. The test data did not exhibit the characteristic drop in stress that is seen in Mo. Thus, it is not certain whether the AGG occurred during testing or after fracture and before the specimen cooled.

2.4.3 Investigations for DAGG in α-Fe

Constant-stress tests were performed on α-Fe at a temperature of 850 °C (~0.6 T_H) by Tran *et al*. in an effort to initiate DAGG [Tran 2008]. Strain rates were in the range of 10^{-4} to 10^{-7} s^{-1}. AGG grains on the order of 2 mm in diameter were observed at the tip of the fractured specimens [Tran 2008]. It was concluded that the AGG observed was likely due to the deformation gradient created during necking [Thanh 2009].

3 Experimental Procedure

DAGG was produced using both constant true-stress and constant true-strain rate tensile tests. Constant true-strain rate testing procedures were adapted from the work of Ciulik [Ciulik 2009] and Worthington [Worthington 2011], and all tensile tests were performed on the same electromechanical test frame. Microstructural analysis was performed using optical and electron imaging, including electron backscatter diffraction (EBSD), and X-ray diffraction (XRD). Customized algorithms were developed to analyze the EBSD data.

3.1 MATERIALS

Three different materials were studied in this investigation: a commercial purity Ta (Ta-A), a Ta with small alloying additions to inhibit grain growth (Ta-B), and a Mo produced through powder metallurgy techniques. The Mo of the present study is the same as previously investigated by Worthington [Worthington 2011, 2013] and is referred to here as Mo-PMB for continuity with those previous studies.

The Mo-PMB and Ta-B materials were obtained from H.C. Starck, Inc. (Euclid, OH). Mo-PMB was received as sheet of 0.76 mm (0.030 inch) thickness and was produced using powder-metallurgy techniques. The Ta-B was received as sheet of 1.016 mm (0.040 inch) thickness and was produced by arc-melting Ta with small alloying additions to reduce normal grain growth, followed by rolling into sheet. The compositions of Mo-PMB and Ta-B are provided in Tables 3.1 and 3.2. Ta-A was received from Eagle Alloys Corporation of Talbott, TN, as sheet of 0.76 mm (0.030 inch) thickness and meets the ASTM B 708 R05200 annealed grade specification for

commercially pure Ta produced using arc-melting processing [ASTM 2005]. The composition of Ta-A, as provided by its manufacturer, is provided in Table 3.2.

Table 3.1: Maximum limits of composition for Mo-PMB, in ppm by weight.

Mo	Mg	Mn	Ni	Al	Cu	Pb	Ti	Ca	Si	Sn	Cr	C	Fe
Bal.	10	10	20	20	20	20	20	30	30	30	50	50	50

Table 3.2: Maximum limits of composition for Ta-A and Ta-B, in ppm by weight.

	Ta	C	Cr	Cu	Fe	H	Mo	N	Nb	Ni	O	Si	Ti	W	Y
Ta-A	Bal.	30	8	8	25	15	8	14	250	5	130	30	10	30	n/a
Ta-B	Bal.	9	1	1	6	1	4	5	133	4	39	2	1	311	20

Tensile coupons were machined from the sheet materials with the tensile axis aligned perpendicular to the sheet rolling direction, i.e., the rolling direction is along the long-transverse direction of the coupons, as shown in Figure 3.1. The coupons used a dog-bone geometry with a gage length of 25.4 mm (1.00 inch), a gage width of 6.4 mm (0.250 inch) and a gage-to-grip transition radius of 1.6 mm (0.063 inch). The thicknesses of the as-received sheet materials were retained in the tensile coupons. The grip regions measured 19.05 by 19.05 mm (0.75 by 0.75 inch). Holes were machined into the grip ends to accommodate loading pins used for testing of the coupons. The hole diameter for the Mo-PMB and Ta-A coupons was 6.35 mm (0.25 inch), and the pin hole diameter for Ta-B was 7.24 mm (0.285 inch). The loading pins used are fully dense, sintered silicon carbide rods with diameters of 6.22 mm (0.245 inch) or 7.11 mm (0.280 inch), corresponding to the appropriate specimen pinhole size. The grips and loading pins for testing Ta-B were different form those used for testing Mo-PMB and Ta-A because of Ta-B's greater thickness. A schematic of the specimen dimensions is shown in Figure 3.1. The specimen directions are referenced according to the designations given in Figure 3.2, where TD is the tensile direction, LTD is the long-transverse direction, which

is also the rolling direction, and STD is the short-transverse direction, which is also the sheet normal direction.

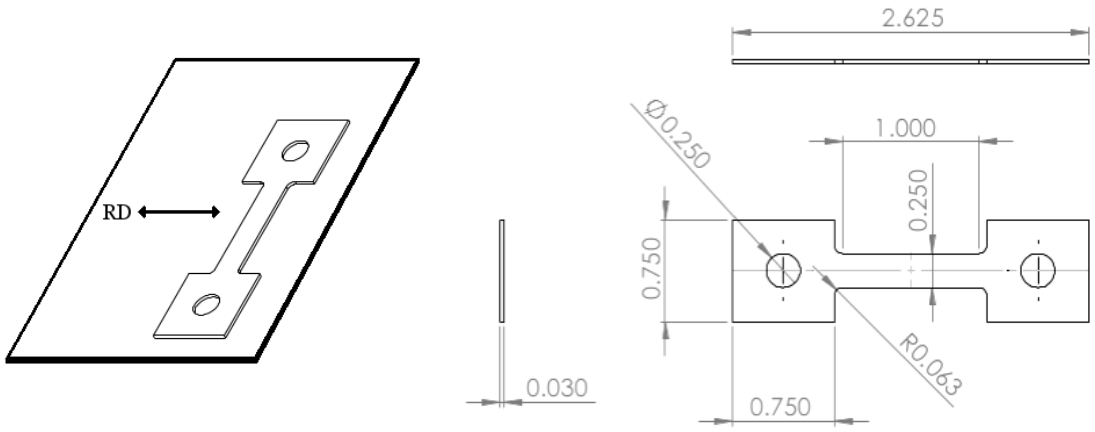

a. b.

Figure 3.1: Schematic of specimen orientation and geometry used for Ta-A and Mo-PMB. Ta-B has identical dimensions except for the pinhole diameter and sheet thickness, which are 7.24 mm (0.285 inch) and 1.016 mm (0.040 inch) respectively. Dimensions are in inches. Tolerances are ±0.005 inch, except for the gauge length and width, which are ±0.002 inch.

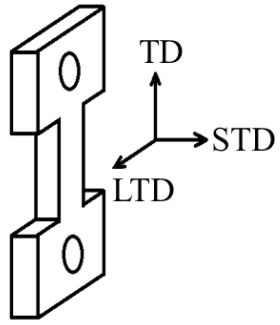

Figure 3.2: Specimen reference orientations for the tensile direction (TD), short-transverse direction (STD), and long-transverse direction (LTD).

3.2 TESTING

Tensile tests were conducted at constant temperature and either constant true-strain rate or constant true stress in a high-temperature vacuum furnace attached to a computer-controlled, electromechanical test frame.

3.2.1 Furnace and Test Frame Setup

Specimens were tested using an MTS Systems (Eden Prairie, MN) Alliance RF/100 test frame in combination with a Thermal Technology LLC (Santa Rosa, CA) Testmaster 3-8-3-W furnace. TestWorks® 4 software was used to control the MTS test frame. Tungsten resistance heating elements in the furnace are capable of providing test temperatures up to 2000 °C. The temperature of the furnace was held constant during each test by a digital electronic controller. The furnace temperature typically fluctuated less than ±2 °C from its set-point. A vacuum system reduces oxidation of the furnace components and specimen. The vacuum is held in the range of 10^{-5} to 10^{-6} Torr when the furnace is at temperature. This is accomplished by using a roughing pump backing a turbo vacuum pump. The electromechanical test frame displacement measurement is accurate to within 0.0005 mm (0.00002 inch).

Specimens were tested in tension using pin-loaded grips on tungsten pull rods within the hot zone of the furnace. Images of the test setup are shown in Figure 3.3 and 3.4. The pull rods are connected to the electromechanical testing frame through bellows on the top and bottom of the furnace. This allows for the top pull rod to travel with the electromechanical machine crosshead through approximately 3 inches while vacuum is maintained in the furnace.

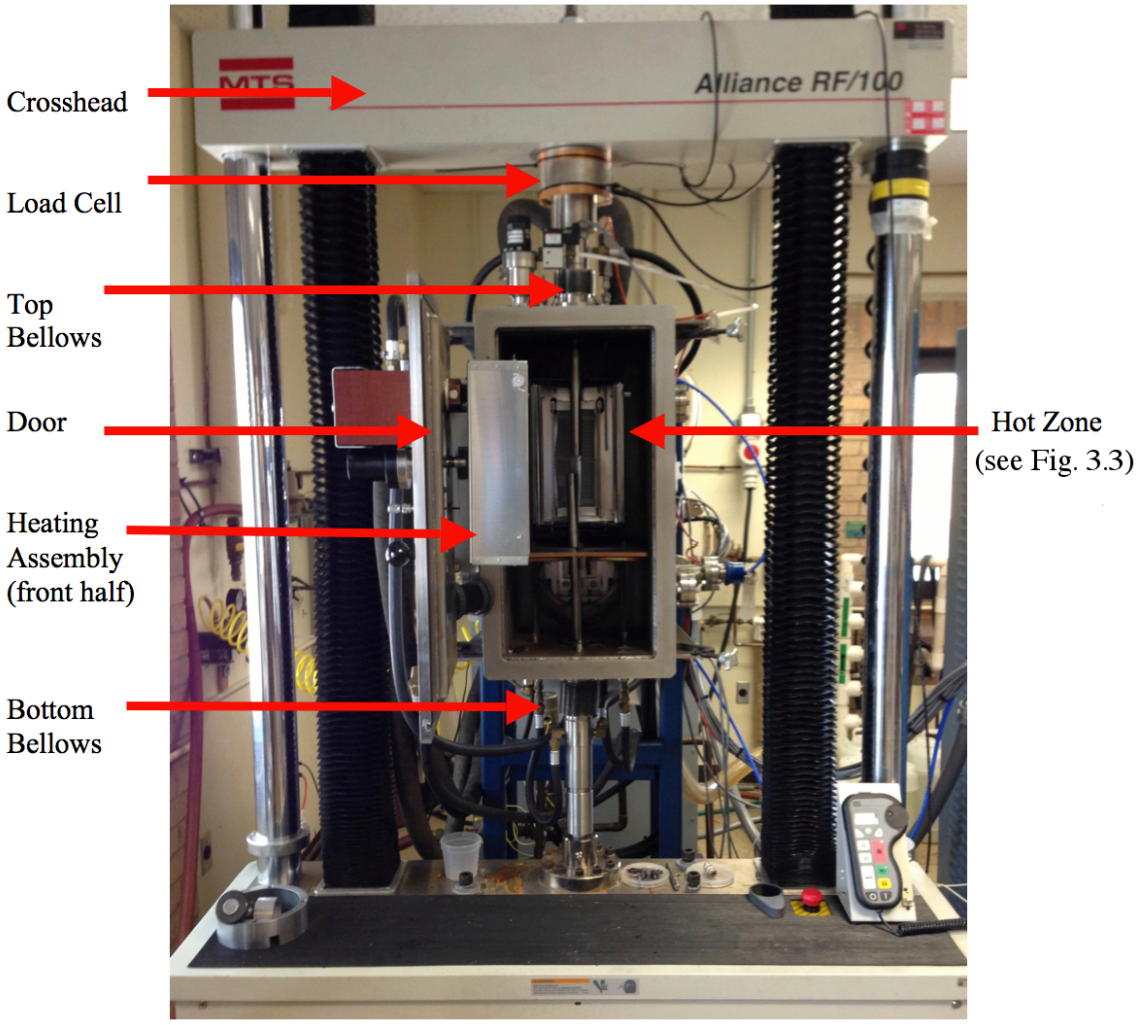

Figure 3.3: Furnace assembly.

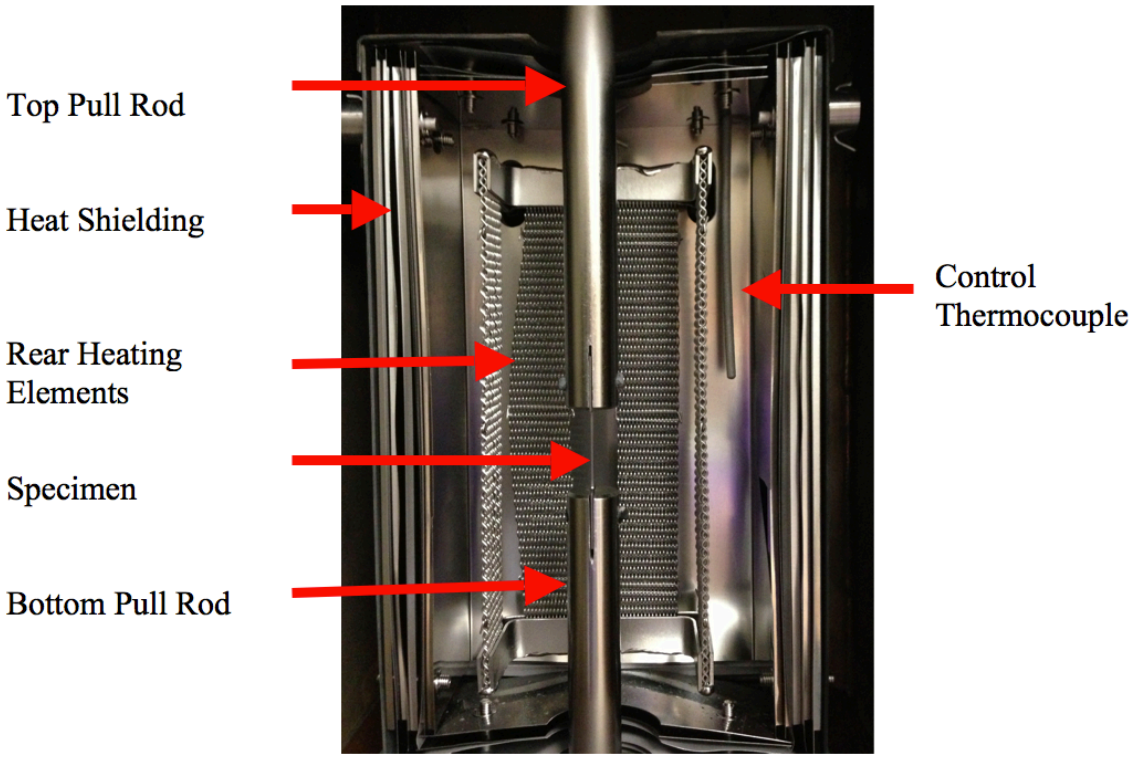

Figure 3.4: Furnace hot zone showing specimen loaded in grips.

The bottom pull rod is connected through a bellows to the frame of the electromechanical testing machine but remains stationary during testing. The load applied by the extension of the top bellows as the crosshead moves upwards, measured through independent calibration tests, must be subtracted from the test data. This load is measured by independently measuring the load *versus* extension without a specimen connected to the pull rods inside the furnace. An example of a bellows test used for correcting the load in test data is shown in Figure 3.5. Although the relationship between load and extension is nearly linear within the range of extension shown in Figure 3.5, a second order polynomial fit is used to correct the load in the test data to improve accuracy.

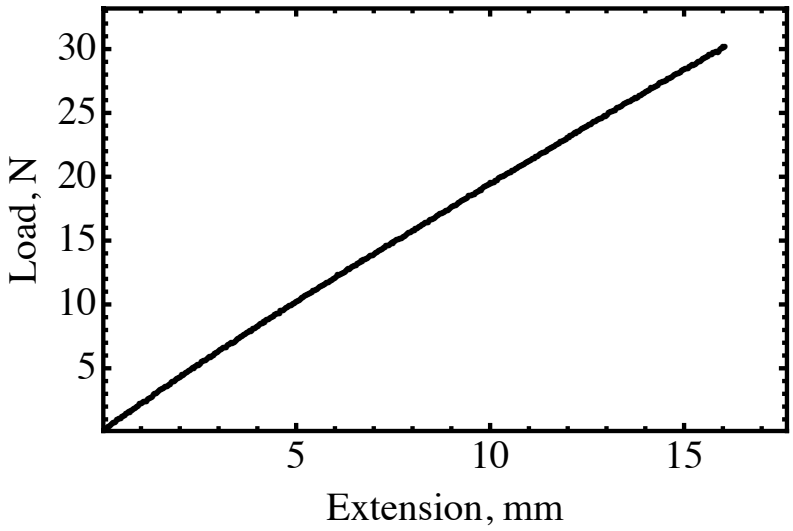

Figure 3.5: An experimentally determined calibration curve illustrates the bellows contribution to load as a function of crosshead extension.

The hot zone of the furnace is shielded with tungsten sheet, and the walls, power lines, and bellows couplings are water-cooled. Measurements of temperature at different locations within the furnace hot zone are made by replacing the top pull rod with a second thermocouple inserted along the centerline of the hot zone to a specified height within it solely to measure the temperature at that location, without any tensile coupon present. This method is used to create reference data for furnace temperature profiles. The temperature variations within the hot zone as a function of vertical distance are shown in Figure 3.6. The reference point is approximately 0.75 in. (19 mm) above the bottom pull rod, making it a height of 0.18 in. (4.6 mm) above the center of the specimen, if the specimen was loaded for testing. This reference point is also approximately 0.25 in. (6.4 mm) above the center point along the vertical centerline of the furnace heating elements. The distance from the reference point is measured vertically from this point and corresponds with the direction in which tensile coupons are pulled during testing. Very little difference in temperature is expected between this reference point and the true

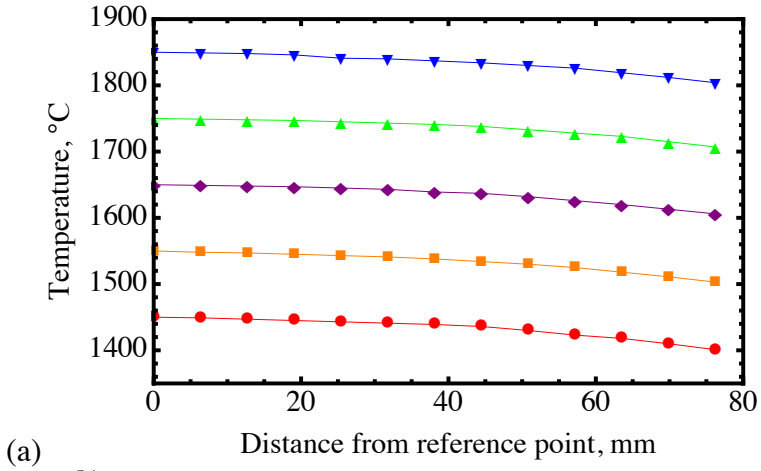

(a)

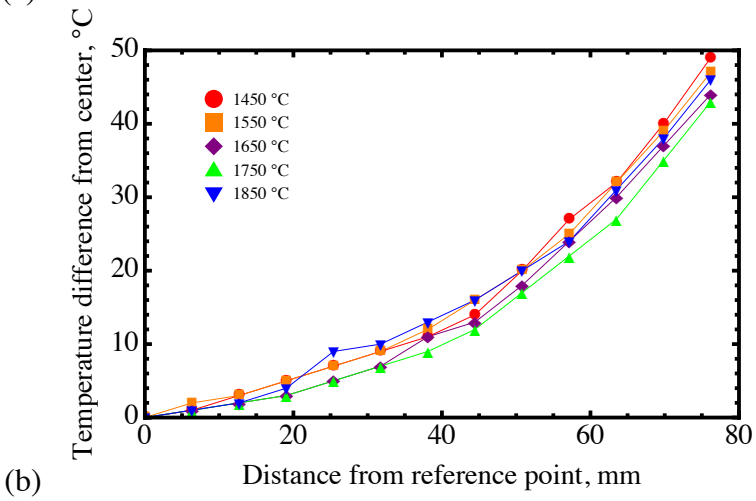

(b)

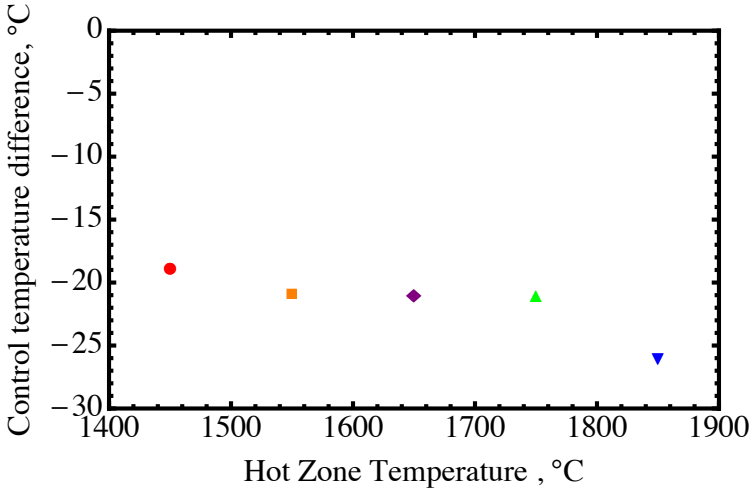

(c)

Figure 3.6: Temperature as a function of height in the furnace (a), the variation in temperature from the reference point (b), and the difference in temperature between the reference point and the control thermocouple, for various test temperatures.

center of the furnace due to the small variations in temperature at small deviations from the reference point, as shown in Figures 3.6(a) and 3.6(b).

The control thermocouple used for monitoring and controlling the furnace temperature during testing is located just outside the hot zone, as shown in Figure 3.4. The measured differences between the temperatures along the centerline of the hot zone and outside it at the control thermocouple, as shown in Figure 3.6(c), are used to offset and correct the set-point temperature during testing to better achieve the desired temperature at the specimen location in the furnace. The slow shifting or deflection of heating elements or the control thermocouple during normal operation over many test cycles can change the furnace temperature profile and the offset of the control thermocouple's temperature measurement compared to the hot zone centerline. Thus, temperature-profiling experiments must be conducted periodically. Periodic profiling data are used to keep the actual test temperature controlled to ±10 °C or better.

3.2.2 Heat-up and Cool-down Procedures

A heat-up procedure is designed for every test to prevent compressive loads on the specimen due to thermal expansion of the specimen and tungsten pull rods during heating. In this procedure, a small load is applied to the load train, typically 5 lbs., as the furnace temperature increases to the set point. Temperature is ramped up gradually over approximately 15 minutes to the desired set point. Vacuum is maintained during the gradual heating. Contaminates within the furnace outgas upon heating and lower the vacuum, thus requiring rather slow heating to maintain a good vacuum quality. The load is held constant by controlling displacement to account for thermal expansion of the rods

and specimen. An example of the crosshead extension as a function of time as temperature increases is shown in Figure 3.7.

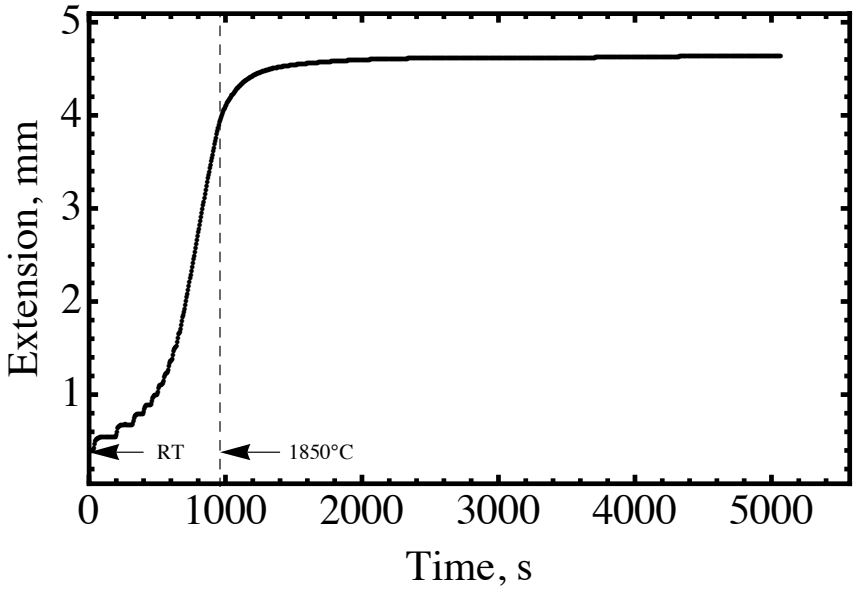

Figure 3.7: Crosshead extension applied to compensate for thermal expansion over time during heat-up is shown. Temperatures indicated are those corresponding to the temperature in the hot zone at select times, as determined by correcting the temperature observed at the reference thermocouple. "RT" indicates room temperature.

Once the furnace reaches its set point, the heat-up process continues for approximately 1 to 2 hours as the temperature in the furnace and thermal expansion of the components stabilize. This stabilization period is required prior to performing a test since the continued expansion of the load train will cause the extension observed at the crosshead to differ from the strain experienced at the specimen. This is particularly important for a constant true-strain rate test because the test conditions are directly dependent on the amount of strain in the sample. After temperature and thermal expansion stabilize, the rate of expansion of the rods is less than 5% of the strain rate to be applied in the test. If a test is halted prior to rupture, an approximately inverse procedure must be employed to minimize stress on the specimen during cool-down from

thermal contraction of the pull rods. This thermal-contraction stress is avoided by reducing the load until there is no load on the specimen, meaning that the only load is that of the bellows contribution, holding this load constant and requiring the computer to adjust displacement as the furnace cools to maintain this small load. Example test results from this procedure are provided in Figure 3.8. If a specimen ruptures during tensile testing, the furnace can be cooled down safely without this additional procedure. Some recovery or recrystallization is possible because of the rather long period of time required for the specimen to cool down following testing.

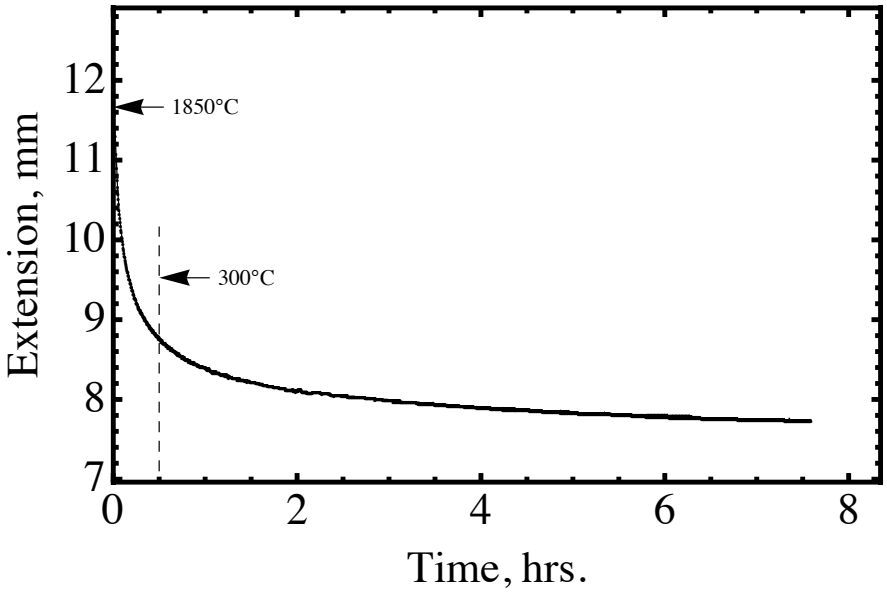

Figure 3.8: Crosshead extension reduction applied to compensate thermal contraction during cool-down is shown as a function of time. Temperatures at select times are indicated.

3.2.3 Constant True-Stress Tensile Testing

Previous studies of DAGG only used constant true-strain rate tensile tests. In this study, constant true stress tensile tests were performed on Mo-PMB. This was accomplished by continuously calculating the true stress through measuring elongation

and force and factoring in the original length, cross-sectional area and force contribution from the bellows, which is based on the position of the crosshead. The equation for true stress is:

$$\sigma = s\,(1+e) \qquad \text{Eq. 3.1}$$

where s and e are the engineering stress and strain, respectively, which are given by:

$$s = F/A_o \qquad \text{Eq. 3.2}$$

$$e = \Delta l/l_o \qquad \text{Eq. 3.3}$$

where F is the applied force, A_o is the initial cross-sectional area, Δl is the change in length, and l_o is the original length. The true stress was held constant using the TestWorks® 4 *hold* function, in which a proportional feedback controller is used to hold load constant by varying displacement of the crosshead. Standard deviation of true stress from the set-point, arising from fluctuations in the load and response of the control system, was 0.34 MPa, which corresponds to a standard deviation of 1.2% or less for the range of true stresses investigated. The variation in the bellows contribution between tests was ± 0.15 lbs, which corresponds to an additional potential error of approximately ± 0.14 MPa for the specimen geometry investigated. The range of true-stresses investigated spans 28 to 40 MPa, and the test temperature was 1650 °C, which is a homologous temperature (T_H) of 0.66. A full list of test conditions and a summary of results are provided in Table 3.3. The test temperature and range of stresses were chosen based on the flow stress previously observed for DAGG initiation and on other observations of DAGG in Mo.

Table 3.3: Constant true-stress testing conditions. All tests conducted on Mo-PMB at 1650°C.

True Stress, MPa	Number of Tests
28	1
30	3
32	2
35	4
37	2
38.5	1
40	2

3.2.4 Constant True-strain Rate Tensile Testing

Constant true-strain rate tests of Ta-A and Ta-B were conducted similarly to previous studies of DAGG in Mo [Ciulik 2005, 2009, Worthington 2011, 2013]. The range of true-strain rates investigated is approximately 3×10^{-5} to 5×10^{-4} s^{-1}, and test temperatures range from 1450 to 1850 °C (0.52 to 0.65 T_H). Both Ta-A and Ta-B were tested in tension under constant true strain rates, and the test conditions are listed in Figure 3.9. These strain rates and homologous temperatures were chosen for study based upon previous observations of DAGG in Mo. Constant true-strain rates were applied in displacement control by continuously updating extension rate every second. Applied extension rate was calculated as:

$$v = \dot{\varepsilon}\ (\underline{l_o} + x), \qquad \text{Eq. 3.4}$$

where v is the velocity, $\dot{\varepsilon}$ is the desired true-strain rate, l_0 the initial length, and x the crosshead displacement. Calculations to determine appropriate extension rate histories assumed conservation of specimen volume and no necking. Observations of tested specimens support these assumptions as reasonable. Tensile tests were stopped at either a

predetermined elongation following the load drop associated with DAGG or after specimen rupture.

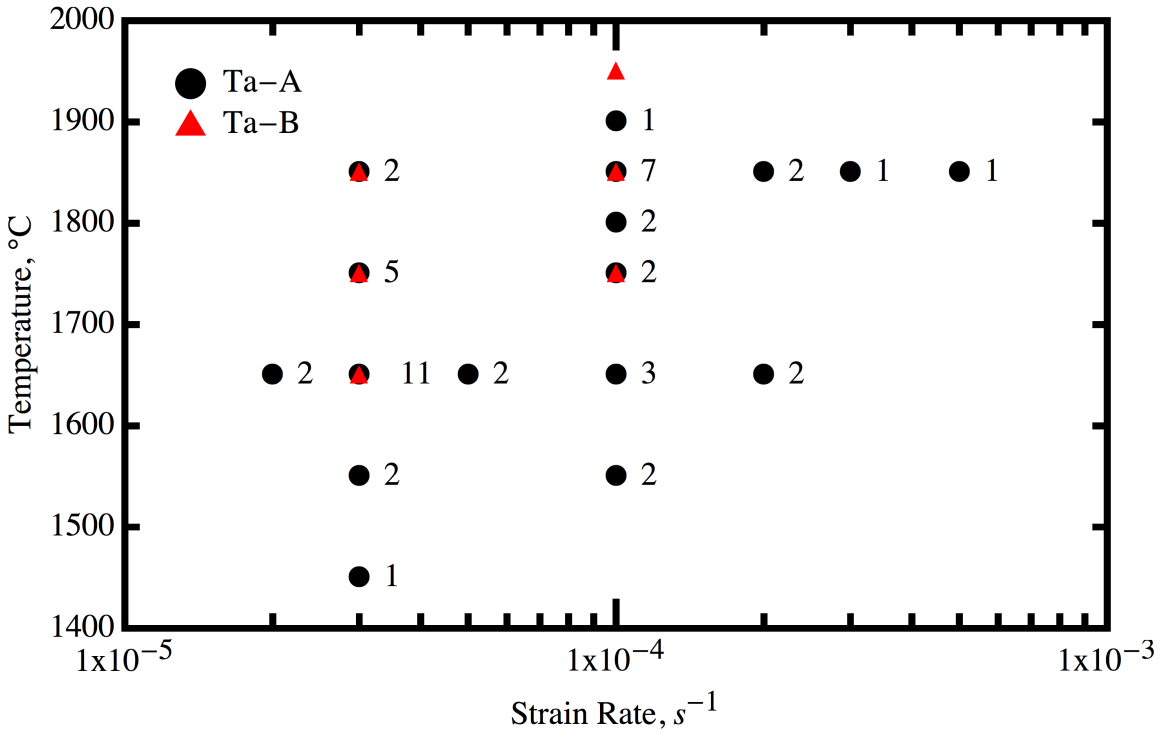

Figure 3.9: Constant true-strain rate tensile testing conditions for Ta-A (black) and Ta-B (red). Numbers indicate the number of tests conducted at each test condition for Ta-A. Only one test at each test condition was conducted for Ta-B.

3.3 CHARACTERIZATION

Characterization of the materials' microstructures used mechanical grinding and polishing to prepare specimens for optical microscopy, electron microscopy, EBSD, and Laue XRD. Analysis of EBSD was performed using customized algorithms developed to characterize and quantify unique features observed in the DAGG microstructures.

3.3.1 Metallography

After testing, specimens were prepared for observation and analysis using standard metallographic procedures. The process for preparing the Mo samples was based on the method of Ciulik [Ciulik 2009] and Worthington [Worthington 2011]. Grinding and polishing procedures for Mo are listed in Table 3.5. After polishing, Mo specimens were etched using a solution of one part nitric acid (69%), one part sulfuric acid (97%) and one part distilled water.

Metallographic preparation steps for Ta are provided in Table 3.6. The procedure is similar to that for Mo, but in general a lighter force and longer times must be used for Ta. The process was amended when preparing Ta for EBSD analysis by allowing for more time during each of the polishing steps. A clean, undeformed surface is very important to obtain a clear and accurate diffraction pattern for EBSD. Longer polishing times are necessary to remove the surface deformation from the previous polishing step. After polishing, the Ta was etched for optical and scanning electron microscope observations with a solution of 2 parts nitric acid (69%), 2 parts hydrofluoric acid (49%) and 5 parts sulfuric acid (97%). Specimens prepared for EBSD analysis remained unetched.

Table 3.5: Grinding and polishing schedule for Mo. Surface and abrasives consumables are listed by Struers product designations. Polishing was performed on a Struers Rotopol-15™ automated polisher.

Polishing Surface	Lubricant/ Abrasive	RPM	Force, N	Time, min.
MD-Piano 220	Water	300	35	Until planar
MD-Piano 600	Water	300	35	3
MD-Piano 1200	Water	300	35	3
MD-Allegro	9μm DiaoDuo	150	35	3
MD-Largo	9μm DiaoDuo	150	30	3
MD-Dur	3μm DiaoDuo	150	25	3
MD-Chem	1 part (by volume) 30% H_2O_2 99 parts 0.05μm colloidal silica	150	25	3

Table 3.6: Grinding and polishing schedule for Ta. Standard procedures are adequate for optical microscopy, but additional time is needed at specific steps, as indicated, for preparation for EBSD.

Polishing Surface	Lubricant/ Abrasive	RPM	Force, N	Time, min. (Additional time for EBSD preparation)
MD-Piano 220	Water	300	30	Until planar
MD-Piano 600	Water	300	30	3
MD-Piano 1200	Water	300	30	3
MD-Plan	9 μm DiaoDuo	150	25	8 (+2)
MD-Dur	3 μm DiaoDuo	150	20	8 (+12)
MD-Chem	0.05 μm colloidal silica	150	20	8 (+12)

Following polishing and etching, microstructures could be observed using an optical microscope or a scanning electron microscope (SEM) with back-scatter imaging (BSI). Regions where DAGG occurred were typically evident to the naked eye following etching. Grain size measurements were made using the lineal intercept method [ASTM 1996].

3.3.2 Laue Backscatter Diffraction

Laue backscatter X-ray diffraction was performed on DAGG grains to determine their orientations relative to the specimen's geometry. This was accomplished using a custom jig to hold the specimen and adjust its vertical and horizontal placement to align the point of interest on the specimen with the X-ray beam. A photosensitive image plate was use to collect the X-ray diffraction pattern. The specimen was placed 2.6 cm from the image plate. The image plate was exposed for 1 minute using an X-ray source with an accelerating voltage of 35 kV and current of 20 mA. The resulting image was scanned, and indexed with OrientExpress software [Laugier]. Pole figures and inverse pole figures were produced using a custom algorithm built in the *Mathematica*^{TM} software package [Mathematica 2010].

3.3.3 EBSD

EBSD is a powerful tool for studying microstructural features and can provide information on orientation, texture, misorientation, grain boundary character, and deformation patterns, to name a few important applications. EBSD is performed in an SEM and works by rastering the electron beam across the surface of a tilted specimen while a phosphorescent screen collects the Kikuchi pattern diffracted from the surface. The Kikuchi pattern is automatically indexed at every raster point to determine crystal orientation, and these orientation data are stored electronically. EBSD data were collected at Sandia National Laboratories on a Zeiss Supra 55VP SEM using Oxford HKL Channel5 [HKL] software and at The University of Texas at Austin in the Department of Geological Sciences on an FEI XL30 ESEM using either Oxford HKL Channel5 [HKL] software or HKL AZtec software [HKL]. Large orientation maps

comprised of multiple adjacent scans on a single specimen were stitched together using HKL MapStitcher.

EBSD data were analyzed using custom algorithms built in *Mathematica*™ [Mathematica 2010]. Functions included orientation mapping, point-to-point misorientation mapping, grain finding, grain boundary characterization, reference orientation deviation mapping, grain orientation spread mapping, and Taylor and Schmid factor mapping. The methods used to make these calculations will be presented here, and the full code developed for this analysis is provided in Appendix A.

Orientation imaging microscopy (OIM) is used to show the crystallographic orientation as a function of spatial position on a specimen surface, for the 2-D technique used in the present investigation. A colorized map can be used to visualize crystallographic directions, typically with the <100> direction red, <110> direction green, and <111> direction blue. This color system is represented on an inverse pole figure using the standard stereographic triangle for cubic materials such as Mo and Ta. The OIM map is thus produced with respect to a particular specimen direction, i.e. the map will be colored to show the crystallographic direction normal to the STD, LTD or TD.

3.3.3.1 Defining Grains

The definition of a grain is important to determine misorientation between grains, deformation within individual grains and grain boundary character. To define a grain a series of steps is employed which gradually builds individual grains by comparing each point in the data set (x-y location defined in the imaged area) to its neighboring points. This method may be described as a percolation process and is detailed as follows:

1. The definition of a grain begins with the selection of a seed point. The seed point is chosen as the first entry in a master list of all points in the

data set that have not been assigned to a grain. A point has a set of up to 4 adjacent neighbors that could potentially belong to the same grain as itself.

2. When the point-to-point misorientation between the seed datum point and a neighbor is less than a predefined threshold amount, then the points are determined to belong to the same grain, and the neighboring point is added to a list of data points that comprise that grain. For this study, a threshold of 2.5° was used. This threshold value was determined based on a sensitivity study in which various threshold values were applied and the grains calculated were compared to those manually determined by inspection of microstructural data. Each symmetrically equivalent orientation for a cubic crystal system is tested when comparing the orientations of the neighboring data points. Un-indexed points and points already assigned to another grain are ignored and must be worked around.
3. The neighbor of the seed point that is determined to belong to the same grain is deleted from the master list of all points in the image that have not been assigned to a grain. The neighbor point is also added to a list of seed points for that grain, thus when a point is added to a grain, its neighboring points are then potential candidates for belonging to the grain as well.
4. As the process continues, neighbors of points are tested and added to the grain, if necessary, and the neighbors of those points are tested and possibly added to the grain, and so on, until every neighbor of every point belonging to the grain has been either added to the grain or is disoriented beyond the threshold.
5. Once all neighbors of all points in a grain are exhausted, the process restarts with the formation of a new grain. The first seed datum point for

the next grain is the next point in the master list of data points that are not yet assigned to a grain. Grains are built one-by-one until all indexed points in the map are assigned to a grain. A minimum grain size of 3 adjacent data points was required to reduce the noise that occasionally occurs from computer misindexing and surface contamination.

This process results in grain boundaries defined as continuous lines drawn between data point pairs disoriented greater than the threshold. The threshold should be chosen so that all grains are identified, subgrains are not separated from the remainder of the grain to which they belong, and surface imperfections, such as scratches, do not divide grains. The 2.5° threshold provides a reasonable balance between these requirements.

Occasionally, computational errors in analyzing the Kikiuchi pattern may produce a misindexed point or leave it unindexed due to a poor quality Kikuchi pattern. These points can be corrected to improve the accuracy and clarity the resulting maps. A common method of correction is to copy the orientation of a neighboring point to an adjacent unindexed point in a predetermined direction (*method 1*) [Randle 2009]. This can lead to unrealistic microstructural features, especially near grain boundaries or where multiple adjacent points are unindexed. An alternative method, used in this study, applies the grain definitions previously established around the questionable point. "Votes" for the orientation of a questionable point are based on the number of similar neighbors it has (*method 2*). The detailed method is as follows:

1. A list of all points not assigned to a grain is created, and the first point in the list is selected.

2. This point has up to 8 surrounding points, 4 adjacent horizontally or vertically and 4 diagonally. The grain to which the greatest number of neighboring points belongs becomes the grain to which the questionable point belongs. If this point does not have any neighbors that belong to a grain already, it is skipped and reexamined once the other unindexed points are assigned.
3. Once the point has been assigned to a grain, its orientation is defined as the average orientation of the neighboring points that belong to the same grain.
4. This process is repeated until all unassigned points belong to a grain.

This method produces more realistic grain boundary character than *method 1*. An example of the difference between the two methods is demonstrated in Figure 3.10.

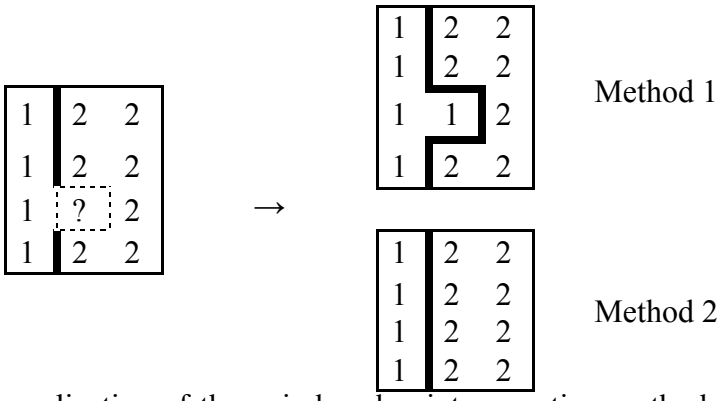

Figure 3.10: Example application of the unindexed point correction methods. Numbers represent grain identifications, and bold lines represent grain boundaries.

If an unindexed point lies on the boarder of two or more grains, *method 1* may arbitrarily assign the unindexed point's orientation to the orientation of the point to its left. However, a more realistic, stable grain boundary structure is obtained by assigning the unindexed point to its majority neighbor grain. In Figure 3.10, *method 1* produces a

perturbation in the grain boundary, while *method 2* does not. Unindexed points that lie completely within one grain are largely unaffected by the method chosen, and the only difference is that *method 2* averages the neighboring orientation, while *method 1* does not.

3.3.3.2 Misorientation Mapping

There are several ways to quantify and view the misorientations between various elements in an EBSD map. These can provide an indication of lattice curvature, subgrain development and deformation patterns. In this study, three mapping methods are presented: point-to-point misorientation (PTP), reference orientation deviation (ROD), and grain orientation spread (GOS). (Note: "GOS" is not to be confused with the commonly cited "Goss" texture description.)

Point-to-point misorientation mapping is the simplest method of viewing misorientation. In this method, a point is colored based on its misorientation with its neighbors. This can be calculated using orientation matrices, Euler angles, quaternions, or Rodrigues vectors to name a few. The orientation matrix is used in this case. The orientation matrix is a 3x3 matrix composed of the direction cosines that relate the 3 coordinate axes of one system to the 3 coordinate axes of another system. The orientation matrix $\boldsymbol{G}$ here relates the orientation of the specimen $\mathbf{g}_S$ to the crystallographic orientation $\mathbf{g}_C$, such that

$$\mathbf{g}_C = \boldsymbol{G} \bullet \mathbf{g}_S \,, \qquad \text{Eq. 3.5}$$

where $\mathbf{g}_C$ represents the [100], [010], and [001] crystal axes, and $\mathbf{g}_S$ represents the X, Y, and Z axes relative to the EBSD image, such that X aligns along right-left, Y along up-down, and Z is normal to the image. The orientation matrix is then defined as

$$G = \begin{bmatrix} g_{11} & g_{12} & g_{13} \\ g_{21} & g_{22} & g_{23} \\ g_{31} & g_{32} & g_{33} \end{bmatrix} = \begin{bmatrix} \cos\alpha_1 & \cos\beta_1 & \cos\gamma_1 \\ \cos\alpha_2 & \cos\beta_2 & \cos\gamma_2 \\ \cos\alpha_3 & \cos\beta_3 & \cos\gamma_3 \end{bmatrix} \quad \text{Eq. 3.6}$$

$$\text{where} \quad \begin{matrix} \alpha_1,\beta_1,\gamma_1 \text{ are angles between [100] and } X,Y,Z \\ \alpha_2,\beta_2,\gamma_2 \text{ are angles between [010] and } X,Y,Z \\ \alpha_3,\beta_3,\gamma_3 \text{ are angles between [001] and } X,Y,Z \end{matrix} \quad \text{Eq. 3.7}$$

The misorientation angle between two orientation matrices, φ (in degrees), is defined as:

$$\varphi = \cos^{-1}[\tfrac{1}{2}* (\mathrm{tr}(\boldsymbol{G}_M) - 1)] *180/\pi \,, \quad \text{Eq. 3.8}$$

$$\text{where} \quad \boldsymbol{G}_M = \boldsymbol{G}_1 * \boldsymbol{G}_2^{\,T}, \quad \text{Eq. 3.9}$$

and where $\boldsymbol{G}_1$ and $\boldsymbol{G}_2$ are the 3x3 orientation matrices of the two points being examined. All symmetrically equivalent orientations are considered by multiplying $\boldsymbol{G}_1$ (or $\boldsymbol{G}_2$) by the 24 equivalent symmetry operations for cubic symmetry ($\mathbf{G}_{CS}$), and the lowest misorientation among the 24 possibilities is the misorientation, or *disorientation*, defining the boundary, such that

$$\boldsymbol{G}_{M,j} = \boldsymbol{G}_1 * \boldsymbol{G}_{CS,j} * \boldsymbol{G}_2^{\,T} \,, \quad \text{Eq. 3.10}$$

where each permutation of j from 1 to 24 represents a particular cubic symmetry operation. Thus, each $\boldsymbol{G}_{M,j}$ represents the misorientation between two points after one has been rotated about at particular symmetry operation. The disorientation between the points is defined by the $\boldsymbol{G}_{M,j}$ that produces the lowest misorientation angle using Eq. 3.8.

A ROD map colors each point in the map according to its misorientation relative to a reference orientation [Wright 1993, 2011]. This can be the same reference orientation for the whole map or specific to a region or grain. In this study, the reference orientation used is the average orientation of the grain to which the point belongs. An alternative reference orientation, not used in this study, is the orientation of the point in each grain that has the lowest misorientation with its neighbors, which represents the

orientation of the part of the grain that is deformed the least [Brewer 2002]. A ROD map is beneficial for observing substructure within grains, lattice curvature and deformation patterns.

A GOS map is a simplified method of viewing the data from a ROD map. For the GOS map, the misorientations of all points in a grain relative to the average grain orientation are averaged. This produces a single value representing the average misorientation within a grain. Thus, a GOS map can be used to easily identify the grains with the least and greatest internal misorientations. In this study, the GOS map is compared to both the type of grain (from within the polycrystalline microstructure, DAGG grain, etc.) and the grain's orientation.

3.3.3.3 Averaging Orientations

The average orientation of any set of points is determined using the accepted method of averaging the quaternion description of the orientation [Morawiec 1989, Kunze 1993, Humbert 1996, Humphreys 2001, Cho 2005]. This method is applied whenever orientations are averaged, such as when correcting points or determining the average orientation of a grain. The EBSD data were acquired in rotation matrix form and were converted to quaternions for averaging. An algorithm for converting between rotation matrices and quaternions is provided in Appendix A Part 1.

A quaternion is a four dimensional vector, $\mathbf{q} = \{q_0, q_1, q_2, q_3\}$, where $\sum \mathbf{q}_i^2 = 1$, and is an alternative representation of an axis and angle. The first term, q_0, is a scalar term and the remaining terms represent the vector component, such that:

$$q_0 = \cos(\theta/2), \qquad \text{Eq. 3.11}$$

$$\{q_1, q_2, q_3\} = \sin(\theta/2)\hat{\mathbf{u}}, \qquad \text{Eq. 3.12}$$

where θ is the angle of rotation and $\hat{\mathbf{u}}$ is a unit vector representing the axis of rotation. The average orientation using quaternions is simply the normalized arithmetic mean of the quaternions, i.e.

$$\bar{\mathbf{q}} = \mathbf{q_m}/||\mathbf{q_m}|| \text{ , where } \mathbf{q}_m = \frac{1}{N}\sum_{k=1}^{N}\mathbf{q}_k \text{ .} \qquad \text{Eq. 3.13}$$

Using quaternions can be beneficial over other methods, such as rotation matrices that require a much more complicated procedure for averaging, or Euler angles that have a singularity at the origin of Euler angle space, potentially making its components linearly dependent.

3.3.3.4 Grain Boundary Characterization

The definition of grains allows for analysis of grain boundaries. The grain boundary character is determined by comparing the orientation of the two points on either side of each grain boundary segment. Grain boundary characters of interest include the presence of low-$\sum$ and low-angle ($\sum 1$) boundaries.

Low-angle boundaries are determined simply by comparing the rotation matrices of two points defining a boundary. This method is identical to the misorientation determination described previously, but in this case only the grain boundary points are examined. A low-angle grain boundary is generally considered one with a misorientation less than 10°, although more restrictive cases may be considered. In this study, grain boundaries with disorientations below 10° and below 5° were both considered because low-angle grain boundaries can have particularly low mobility [Huang 2000, Yang 2001, Winning 2010].

$\sum$ boundary character is determined by first determining all variants of the rotations that define each $\sum$ boundary type in rotation matrix form ($\boldsymbol{G}_{\sum}$). The number of

variants depends on the number of permutations of the axis of rotation. The rotation matrices representing each ∑ boundary type are provided in Appendix B. Each pair of adjacent points that are separated by a grain boundary is multiplied by each variant of each ∑ boundary type and each cubic symmetry operation. The lowest misorientation among the computed values defines the boundary. This is a similar process to that for finding boundary disorientation, except $\boldsymbol{G}_{\mathrm{M}}$ takes the form

$$\boldsymbol{G}_{\mathrm{M}\,i,j} = \boldsymbol{G}_1 * \boldsymbol{G}_{\sum,i} * \boldsymbol{G}_{\mathrm{CS},j} * \boldsymbol{G}_2^{\mathrm{T}} \quad , \qquad \text{Eq. 3.14}$$

where $\boldsymbol{G}_{\sum,i}$ represents all permutations i of the type of ∑ boundary under investigation. Each component of $\boldsymbol{G}_{\mathrm{M}\,i,j}$ represents a rotation matrix that describes the misorientation of the two points from a particular ∑ boundary type. This is produced by multiplying the orientation matrices of the two points, the orientation matrix of one of the cubic symmetry operations, and the orientation matrix of a rotation describing a particular ∑ boundary. The $\boldsymbol{G}_{\mathrm{M}\,i,j}$ that results in the lowest misorientation defines the boundary disorientation and possible ∑ character. For example, if the disorientation between two points can be described by a 60° rotation about the <111> axis, then multiplying by the ∑3 variant, 60° about $<\bar{1}\,\bar{1}\,\bar{1}>$, will bring the two point orientations in line with each other. If the disorientation calculated from this combination is below the Brandon criterion [Brandon 1966] for a ∑3 boundary, then the two points are determined to have ∑3 boundary character. This process is repeated for each grain boundary point pair, ∑ type and its variants, and symmetry operation. In this investigation, low angle boundaries and special boundaries ∑3, ∑5, ∑7, ∑9, and ∑11 were identified.

3.3.3.5 Schmid Factor

The Schmid factor (*SF*, sometimes denoted *m* in literature) [Schmid 1935] is calculated by first defining the tensile direction. The component of each point's

orientation matrix that corresponds to the tensile direction is used to calculate the *SF* at that point. All permutations of the slip system(s) of interest must be considered. For a BCC crystal structure, the common slip systems are {110}<111>, {112}<111>, and {123}<111>, where { } represents the family of slip planes and < > the family of slip directions. The slip directions must lie in the slip plane, i.e. their dot product equals zero. This results in 12 (twelve) {110}<111>, 12 (twelve) {112}<111>, and 24 (twenty-four) {123}<111> possible slip combinations. The SF is calculated for each point as follows:

$$SF = \mathrm{Max}\left[\frac{\mathbf{g}_\mathrm{T} \bullet \mathbf{b}_i}{\left\|\mathbf{g}_\mathrm{T} \bullet \mathbf{b}_i\right\|} \times \frac{\mathbf{g}_\mathrm{T} \bullet \mathbf{n}_i}{\left\|\mathbf{g}_\mathrm{T} \bullet \mathbf{n}_i\right\|}\right]_{i=1\ldots N}, \qquad \text{Eq. 3.15}$$

where $\mathbf{g}_\mathrm{T}$ is the component of the orientation matrix aligned in the tensile direction, i.e. the vector of direction cosines describing the orientation between the crystal axes and particular direction, **b** is the vector normal to a slip plane, **n** is the slip direction, and *N* depends on the number of possible slip combinations for the particular slip system. The *SF* is determined by the combination of slip plane and slip direction in the slip system that produces the largest value. The *SF* will always be ≤ 0.5. *SF*s calculated as a function of orientation are presented in Figure 3.11 for each slip system, a combined mixed-slip case, and two examples from literature [Hosford 1993 p.36, 42].

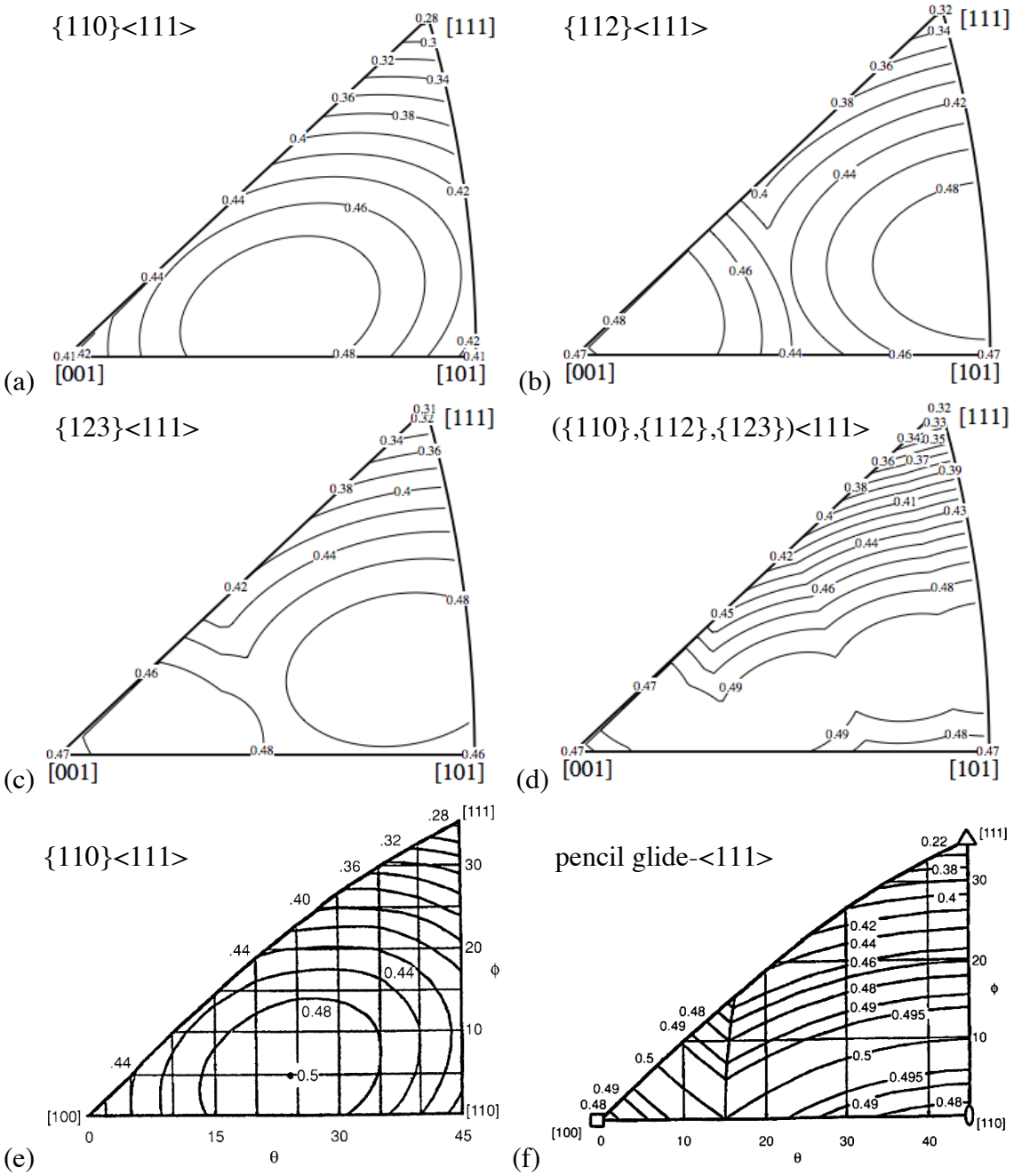

Figure 3.11: SF as a function of orientation, shown on inverse pole figures for slip systems (a) {110}<111>, (b) {112}<111>, (c) {123}<111>, and (d) the combined, highest, *SF* among each system at each orientation. Published maps of {110}<111> (e), and pencil glide (f) are reproduced for comparison [Hosford 1993 p.36, 42]. Note: in (e) and (f) the plot is distorted slightly from the standard triangle dimensions so that ϕ is displayed vertically.

The calculated *SF* for the {110}<111> system is nearly identical to that published previously by Hosford [Hosford 1993]. The calculated combined slip is similar, but not identical, to the published map for pencil glide along <111>. This is expected since <111>-pencil glide considers a continuum of possible slip planes allowing for slip in the <111> directions, but the combined slip presented here only considers a limited number of slip planes (12). Nevertheless, the trend is similar in both cases, and the calculated combined slip provides a reasonable approximation for the case where pencil glide is assumed.

3.3.3.6 Taylor Factor

There are two primary methods for calculating Taylor factor (*M*). The first was proposed by Taylor [Taylor 1938] and involves finding the combination of 5 slip components that accommodate a prescribed macroscopic external strain that result in the least amount of internal strain. The theory behind this method was introduced in §2.1.4, as was the second method, that of Bishop and Hill [Bishop 1951]. More detailed descriptions of each method will be presented here. A *Mathematica*^{TM} [Mathematica 2010] script for calculating multiple-slip Taylor factor over a standard triangle is provided in Appendix C.

Taylor Method

Because all tests were in uniaxial tension, axisymmetric strain conditions about the tensile axis are assumed. The strain state for axisymmetric deformation is

$$\delta\varepsilon''_{ij} = \begin{bmatrix} \delta\varepsilon & 0 & 0 \\ 0 & -\delta\varepsilon/2 & 0 \\ 0 & 0 & -\delta\varepsilon/2 \end{bmatrix}. \qquad \text{Eq. 3.16}$$

The Cartesian axis must be related to the crystal axes. This is done by first calculating the longitude, θ, and latitude, ϕ, of **x**", which represents the axisymmetric direction, i.e. the orientation of the tensile axis, from the coordinate axis on a stereographic projection. These angles are shown in Figure 3.12 on the stereographic projection, simplified to its inverse pole figure form.

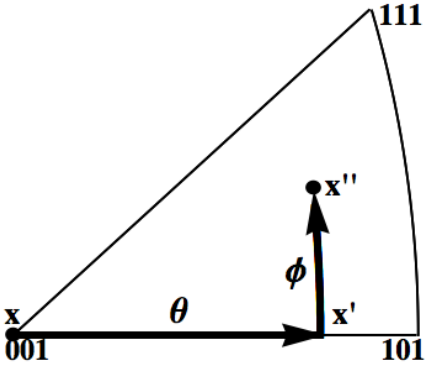

Figure 3.12: A standard triangle of a stereographic projection showing the orientation of a direction x'' in terms of θ and ϕ, relative to the [001] crystal axes.

This transformation is defined by two separate transformations, one from **x** to **x**' about an angle θ around the [100] axis, and one from **x**' to **x**'' about an angle ϕ around the [010] axis. Transformations have the form:

$$\mathbf{x}'_j = \boldsymbol{G}_{jk}\mathbf{x}_k \,, \qquad \text{Eq. 3.17}$$

where $\boldsymbol{G}_{jk}$ is the direction cosines matrix from the original coordinate system to the primed coordinate system. Combining the two rotations with the applied strain results in the imposed strain state now represented in terms of the crystallographic directions, as opposed to the specimen coordinates. The applied strain is then

$$\delta\varepsilon_{kl} = \boldsymbol{G}_{ik}" \, \boldsymbol{G}_{jl}" \, \delta\varepsilon_{ij}" \qquad \text{Eq. 3.18}$$

where, $$G'' = \begin{bmatrix} \cos\theta\cos\phi & \cos\phi\sin\theta & \sin\phi \\ -\sin\theta & \cos\theta & 0 \\ -\sin\phi\cos\theta & -\sin\phi\sin\theta & \cos\phi \end{bmatrix}. \quad \text{Eq. 3.19}$$

Thus, $$\delta\varepsilon = \frac{1}{2}\begin{bmatrix} 3\cos^2\phi\cos^2\theta - 1 & 3\cos^2\phi\sin\theta\cos\theta & 3\sin\phi\cos\phi\cos\theta \\ 3\cos^2\phi\sin\theta\cos\theta & 3\cos^2\phi\sin^2\theta - 1 & 3\sin\phi\cos\phi\sin\theta \\ 3\sin\phi\cos\phi\cos\theta & 3\sin\phi\cos\phi\sin\theta & 3\sin^2\phi - 1 \end{bmatrix}. \quad \text{Eq. 3.20}$$

Next, the contribution of each component of each slip system is calculated as

$$m_c = \tfrac{1}{2}\,(\mathbf{b}\,\mathbf{n} + \mathbf{n}\,\mathbf{b})\,, \quad \text{Eq. 3.21}$$

where **b** is the normalized vector perpendicular to the slip plane and **n** is the normalized slip direction vector. This results in a symmetric 3×3 matrix, which can be reduced to 5 components, since volume is conserved, to form a new vector:

$$\boldsymbol{m} = \{m_{22}, m_{33}, m_{23}, m_{13}, m_{12}\} \quad \text{Eq. 3.22}$$

This is calculated for every slip direction and slip plane combination in each slip system of interest. These contributions are then combined in every possible group of 5 out of all of the slip components of all the slip systems for mixed slip, or for just one system if only one slip system is active. For mixed slip, this results in examining every combination of 5 slip components out of 48 possible, for a total of approximately 1.7×10^6 combinations. However, this number reduces considerably after eliminating those combinations of 5 that are not linearly independent. Each linearly independent group of 5 ***m***'s are combined to form a 5×5 matrix, ***E***, to represent that particular combination.

$$\boldsymbol{E} = \begin{bmatrix} \boldsymbol{m}^{(1)} \\ \boldsymbol{m}^{(2)} \\ \boldsymbol{m}^{(3)} \\ \boldsymbol{m}^{(4)} \\ \boldsymbol{m}^{(5)} \end{bmatrix} = \begin{bmatrix} m_{22}^{(1)} & m_{33}^{(1)} & m_{23}^{(1)} & m_{13}^{(1)} & m_{12}^{(1)} \\ m_{22}^{(2)} & m_{33}^{(2)} & m_{23}^{(2)} & m_{13}^{(2)} & m_{12}^{(2)} \\ m_{22}^{(3)} & m_{33}^{(3)} & m_{23}^{(3)} & m_{13}^{(3)} & m_{12}^{(3)} \\ m_{22}^{(4)} & m_{33}^{(4)} & m_{23}^{(4)} & m_{13}^{(4)} & m_{12}^{(4)} \\ m_{22}^{(5)} & m_{33}^{(5)} & m_{23}^{(5)} & m_{13}^{(5)} & m_{12}^{(5)} \end{bmatrix} \quad \text{Eq. 3.23}$$

The strain relative to the crystal direction, $\delta\varepsilon$ from Eq. 3.20, can be condensed, similarly as $\boldsymbol{m}$, since it is also symmetric. This results in a vector, $\mathbf{D}$, defined as

$$\mathbf{D} = \{\delta\varepsilon_{22}, \delta\varepsilon_{33}, \delta\varepsilon_{23}, \delta\varepsilon_{13}, \delta\varepsilon_{12}\}. \qquad \text{Eq. 3.24}$$

Next, a vector defined by the shear strains, $\delta\gamma$, from each of the 5 slip components can be defined as

$$\mathbf{d\gamma} = \{\delta\gamma^{(1)}, \delta\gamma^{(2)}, \delta\gamma^{(3)}, \delta\gamma^{(4)}, \delta\gamma^{(5)}\}. \qquad \text{Eq. 3.25}$$

The relationship between $\mathbf{D}$, $\boldsymbol{E}$ and $\mathbf{d\gamma}$ is

$$\mathbf{d\gamma} = (\boldsymbol{E}^{\mathrm{T}})^{-1}\,\mathbf{D}\ . \qquad \text{Eq. 3.26}$$

Since M is the sum of the components of strain for the set of 5 components for which the sum is the least,

$$M = Min\left[\left|\sum_{j}^{5}\left|\delta\gamma_{j}\right|_{x}\Big/\delta\varepsilon_{11}^{''}\right|_{x=1\ldots N}\right], \qquad \text{Eq. 3.27}$$

where N is the number of combinations of 5 linearly independent slip components. Given Eq. 3.26 and that $\delta\varepsilon_{11}$" = 1 (the component of the macroscopic strain in the tensile direction, from Eq. 3.16), Eq. 3.27 becomes

$$M = Min\left[\left|\sum_{j}^{5}\left|(\boldsymbol{E}_{j}^{T})_{x}^{-1}\mathbf{D}\right|\right|_{x=1\ldots N}\right]. \qquad \text{Eq. 3.28}$$

This method was used to compute M as a function of θ and ϕ at 0.5-degree incriments over the range of orientations spanning the standard triangle, as shown in Figure 3.13 (a) for the mixed-slip case (see Appendix C). This matched well with published results, as shown in Figure 3.13 (b) [Chin 1967]. The variation in M over the standard triangle for mixed slip can also be compared to published data for <111>-pencil slip, as shown in Figure 3.13 (c). The differences between these two cases are subtle, and not expected to be significant for the purposes of this investigation. Thus mixed slip will be assumed to reduce the complexity of the computations. M was also calculated for the

three slip systems individually and compared to published results, as shown in Figure 3.14, and demonstrated considerable agreement.

An interpolation algorithm was used to determine *M* at each point using the data set computed for Figure 3.13 (a) for large EBSD scans. This was done to because calculating *M* directly for each point's orienation would take a prohibitively long time for the number of points in the larger EBSD scans presented. *M* is a smooth, continuous function, and the difference in *M* between interpolation points is typically less than 1%; thus, little error is introduced by interpolation.

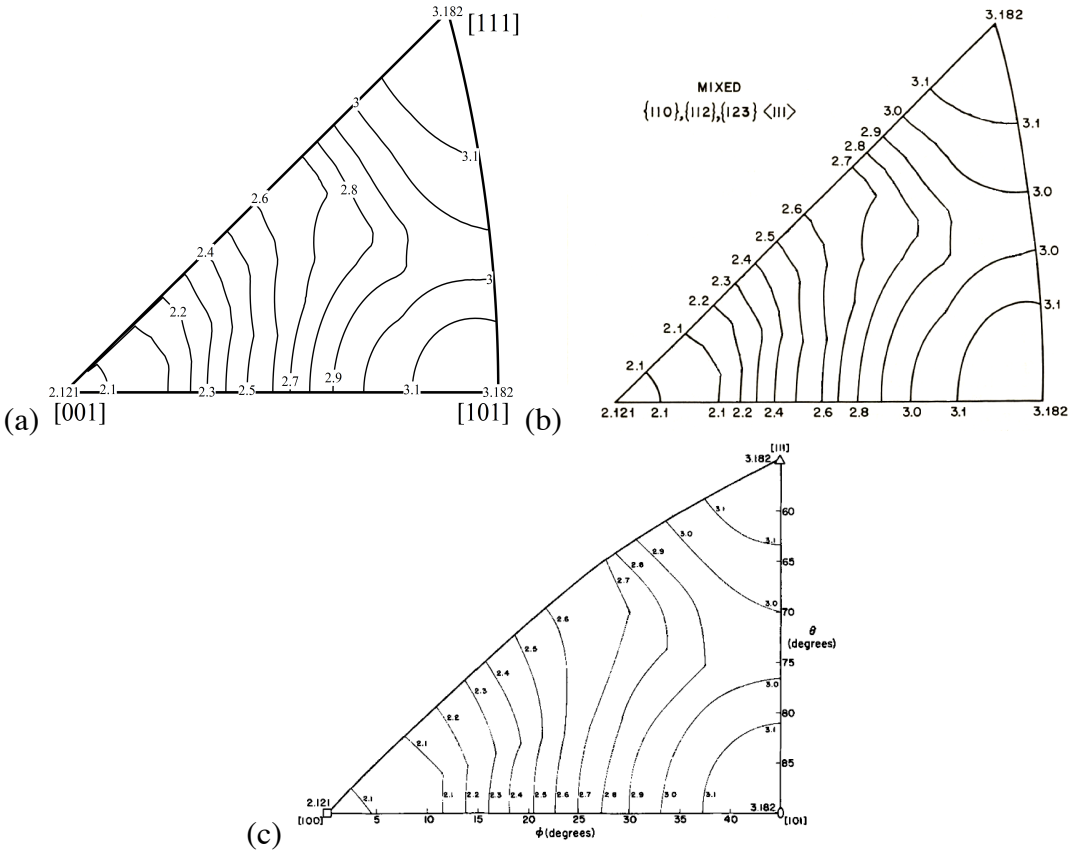

Figure 3.13: The mixed-slip Taylor factor calculated as a function of orientation spanning the range of a standard triangle (a), and as reported in Chin et al. (b) [Chin 1967]. Pencil glide (c) is shown as reported by Rosenberg and Piehler [Rosenberg 1971]. Note: in (c) the plot is distorted slightly from the standard triangle dimensions so that ϕ is displayed vertically.

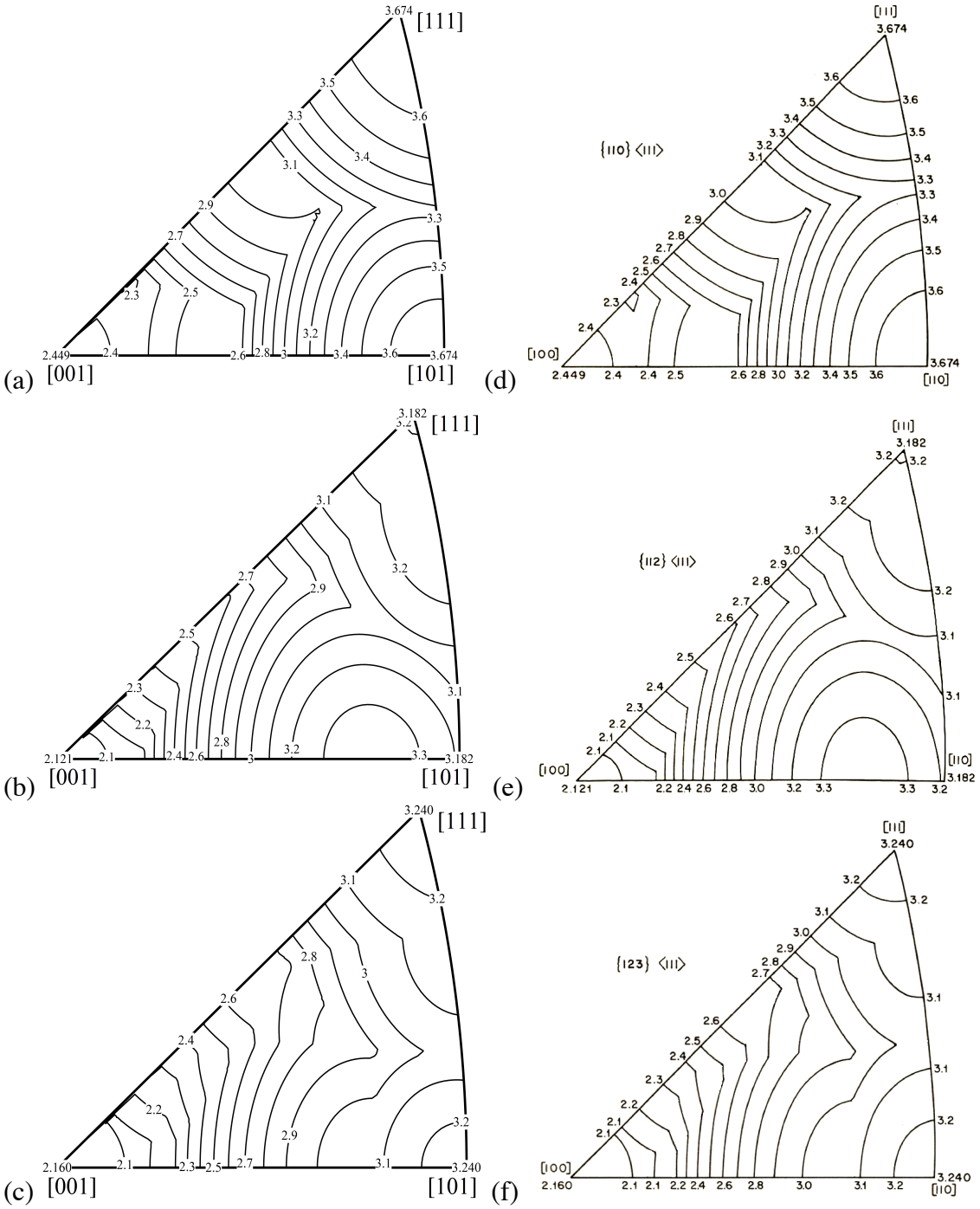

Figure 3.14: Inverse pole figures indicating *M* computed here (a-c) and from published data of Chin *et al* (reproduced)[Chin 1967] (d-f), for slip systems: {101}<111> (a, d), {112}<111> (b, e), and {123}<111> (c, f).

Bishop and Hill method

The method of Bishop and Hill [Bishop 1951] for calculating M was also examined. The process used is similar to that described by Reid [Reid 1973 p.145-169]. M is calculated in this method by determining which stress state produces the maximum work due to the imposed strain. The stress state is

$$\sigma = \begin{bmatrix} \sigma_{11} & \sigma_{12} & \sigma_{13} \\ \sigma_{21} & \sigma_{22} & \sigma_{23} \\ \sigma_{31} & \sigma_{32} & \sigma_{33} \end{bmatrix} , \qquad \text{Eq. 3.29}$$

and the shear stress acting on a particular slip system is

$$\tau = \mathrm{b}_i \sigma_{ij} \mathrm{n}_j . \qquad \text{Eq. 3.30}$$

Bishop and Hill defined a set of coefficients of the shear stress, τ, to characterize each possible stress state for the {110}<111> system. These were termed A, B, F, G, and H, and are defined as

$$\begin{aligned} A &= \sigma_{22} - \sigma_{33} \\ B &= \sigma_{33} - \sigma_{11} \\ F &= \sigma_{23} \\ G &= \sigma_{13} \\ H &= \sigma_{12} \end{aligned} \qquad \text{Eq. 3.31}$$

For each slip system, there are a limited number of combinations of stress states to activate a sufficient number of combinations of slip within that system. Therefore, there exists a stress state to activate a particular set of 5 components of the slip system for an imposed strain. For {110}<111> there are 56 stress states (i.e. possible sets of values for A-H) [Bishop 1951], for {112}<111> there are 90 [Hosford 1969] and for {123}<111> there are 212 [Chin 1970]. The increment work done due to the increment strain is

$$\delta w = \sum_{ij} \sigma_{ij} \delta\varepsilon_{ij} = -B\delta\varepsilon_{11} + A\delta\varepsilon_{22} + 2F\delta\varepsilon_{23} + 2G\delta\varepsilon_{13} + 2H\delta\varepsilon_{12} \cdot \qquad \text{Eq. 3.32}$$

Each of the sets of values of A-H are entered into Eq. 3.32, along with the strain state, to determine the work that is performed by that stress state when the material is strained as prescribed. The stress state that produces the greatest work is the one that is active and is used to calculate M, which is defined as

$$M = \text{Max}[\ \Sigma\, \delta\gamma\ /\ \delta\varepsilon_{11}''\ ] = \text{Max}[\ \delta w\ /(\tau_c\ \delta\varepsilon_{11}'')]. \qquad \text{Eq. 3.33}$$

Thus, by calculating Eq. 3.32 using the A-H coefficients reported, which include τ_c, for each stress state, M can be identified. See Reid [Reid 1973, p.161-69] for a worked example of this process.

Calculations of M using the Bishop and Hill method produced results equivalent to those produced using the Taylor method. The Bishop and Hill method allows for faster calculation of M than the Taylor method, but the Taylor method is simpler and allows for a more straightforward calculation of mixed-slip M.

4 Materials Characterization

The materials studied in this investigation were characterized in their as-received and annealed states using EBSD and optical microscopy to determine their texture and susceptibility to normal grain growth and SAGG. The microstructures of as-received and annealed Ta-A and Ta-B are presented. A similar characterization of the Mo-PMB material was previously performed by Worthington [Worthington 2011] and will be re-presented as needed.

4.1 TEXTURE

Texture is characterized by a preferred crystallographic orientation in a polycrystalline material. All of the materials in this study were produced by rolling to the final sheet thickness. The deformation from rolling bcc materials often results in the formation of α-fiber or γ-fiber textures. An orientation distribution function (ODF) can be used to visualize texture components, and an ODF as a function of Euler angles ϕ and ψ_1 at $\psi_2 = 45°$ is shown in Figure 4.1. The α-fiber is a preferential alignment of the <110> axis along the rolling direction, and spreads from {001}<110> to {111}<110>, where the directions in { } and < > indicate the orientations in the sheet normal direction and tensile directions, respectively. The α-fiber includes {001}<110>, {112}<110>, {111}<110>, and {110}<110> components. The γ-fiber is a preferred allignment of the <111> parallel to the sheet normal direction. This includes crystallographic orientations from {111}<110> to {111}<112>. Primary texture components of the α-fiber and γ-fiber are shown on 100, 110, and 111 pole figures in Figure 4.2.

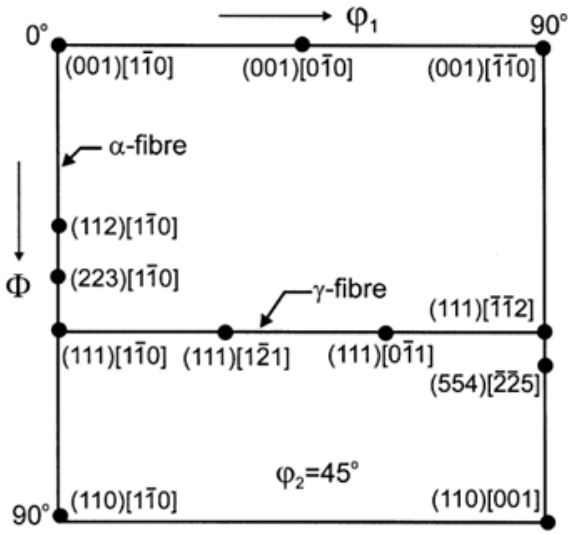

Figure 4.1: Section of ODF where $\psi_2 = 45°$ showing the orientations defined by the α-fiber and γ-fiber as a function of ϕ and ψ_1. Major orientations are also indicated for reference. From [Humphreys 2004 p.76].

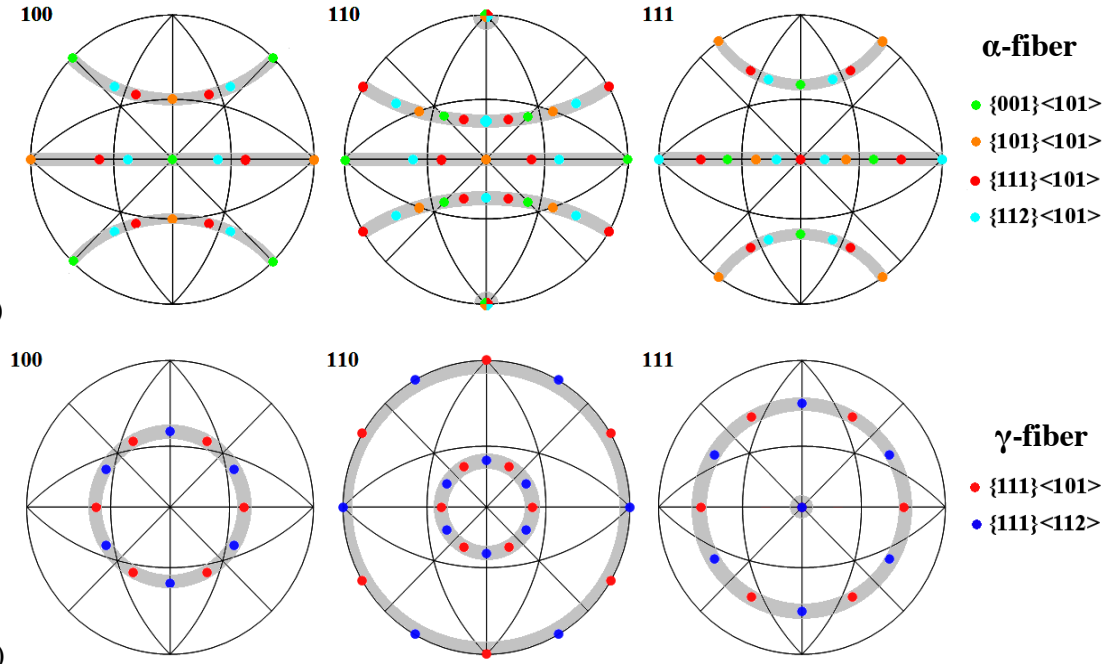

Figure 4.2: Pole figures showing texture of the α-fiber (a) and γ-fiber (b) shaded gray, with components of each fiber highlighted.

4.2 AS-RECEIVED MICROSTRUCTURE

The as-received microstructures of the Ta-A and Ta-B materials are shown in Figure 4.3. Both materials were nearly fully recrystallized and have equiaxed grains. The initial lineal-intercept grain sizes of Ta-A and Ta-B were 44 μm and 26 μm, respectively. The Mo-PMB material was heavily deformed in its as-received state, as shown in Figure 4.4, with grain elongation along the rolling direction.

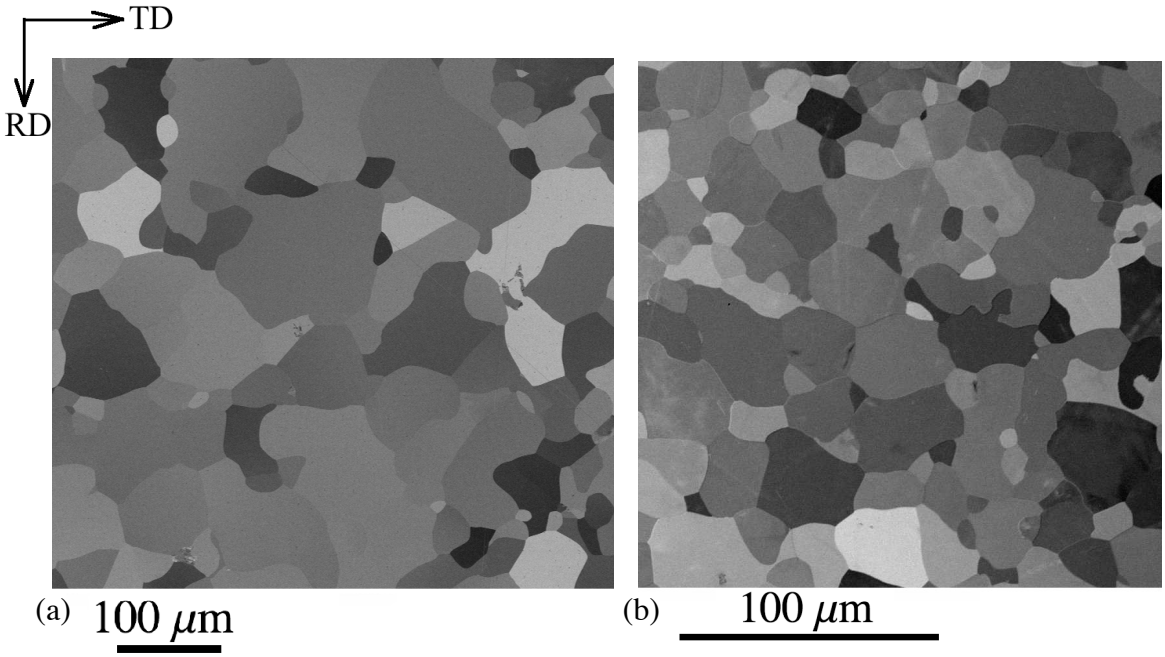

Figure 4.3: Backscatter SEM images of as-received Ta-A (a) and Ta-B (b). Color variations are due to channeling contrast. The rolling direction is vertical and the transverse direction is horizontal.

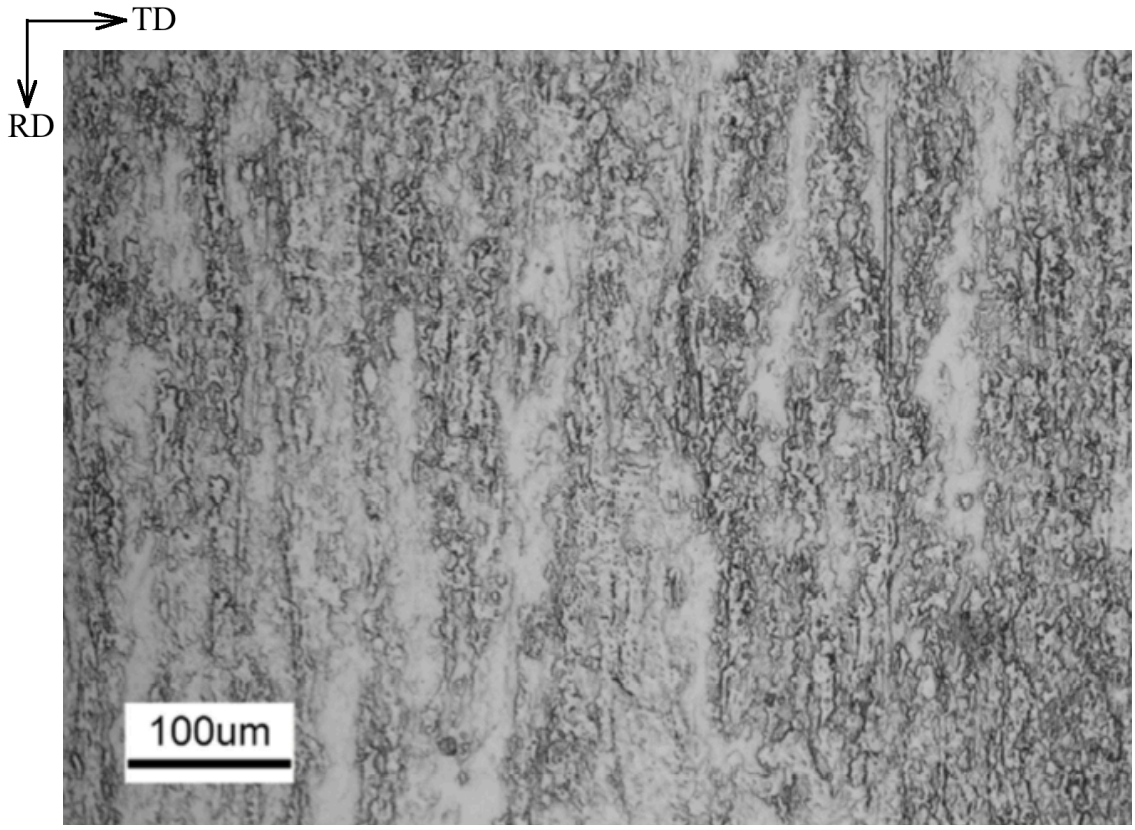

Figure 4.4: Optical image of as-received, etched Mo-PMB. The rolling direction is vertical and transverse direction is horizontal. From [Worthington 2011].

EBSD data were collected to determine texture characteristics of the Ta sheet materials in both the sheet normal direction and normal to its cross section. The cross sections of the Ta sheet materials were examined because Ta sheet may have a variation in texture through its thickness [Wright 1994a, 1994b]. EBSD maps of as-received Ta-A and Ta-B in the sheet normal direction (ND) and in the rolling direction (RD) are shown in Figures 4.5 and 4.8, respectively. Three maps for each scanned area are shown and are colored according to the inverse pole figure coloring scheme to indicate the crystallographic direction parallel to the rolling, transverse, or sheet normal directions.

The textures of as-received Ta-A and Ta-B are similar. Both demonstrate a preference for crystallographic directions between approximately <101> and <112> to

align along the rolling and transverse directions, as shown in Figure 4.5. This preference is also demonstrated in the inverse pole figures of Figure 4.6. Considerable deviation from this trend is also apparent, with slightly more variation seen in the rolling direction. Both materials also show a strong preference for the <111> direction to align along ND, although a small fraction of grains align the <100> direction along ND. Both of these orientations are expected from rolling bcc materials and have been observed in rolled and annealed Ta [Clark 1991]. In Ta, there is often an increased presence of a <111> fiber along ND (γ-fiber) following annealing as annealing temperature and deformation prior to annealing increase [Raabe 1994, Park 1998, Briant 2000].

Pole figures produced from the data of Figure 4.5 are shown in Figure 4.7. A strong γ-fiber is demonstrated in the <111> pole figure for both materials by the intensity of <111> along ND and the ring on intensity about the center. The weak intensity along ND in the <100> pole figure is indicative of the {001}<101> component of the α-fiber.

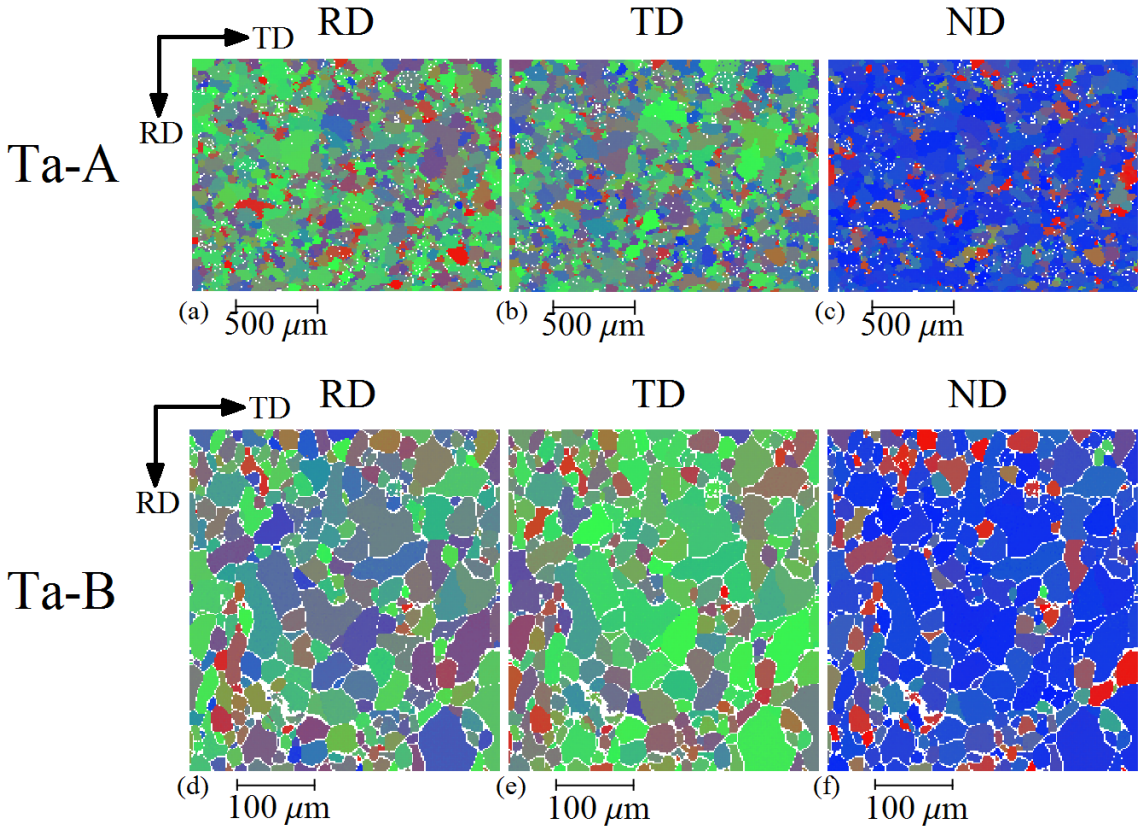

Figure 4.5: EBSD maps of as-received Ta-A (a-c) and Ta-B (d-f), colored according to the inverse pole figure coloring scheme relative to the crystallographic direction along: RD (a,d), TD (b,e), or ND (c,f). The data was collected along (ND). The rolling direction (RD) is vertical and the transverse direction (TD) is horizontal. Unindexed pixels are left white.

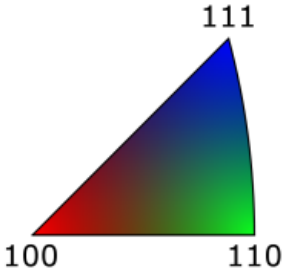

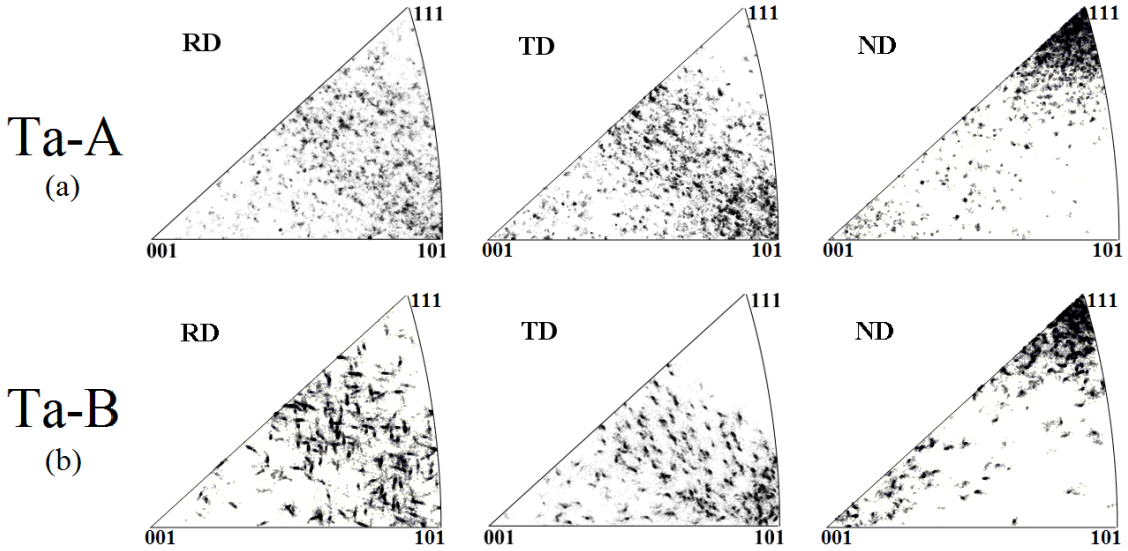

Figure 4.6: Inverse pole figures of as-received Ta-A (a) and Ta-B (b) relative to sheet directions: RD, TD, and ND.

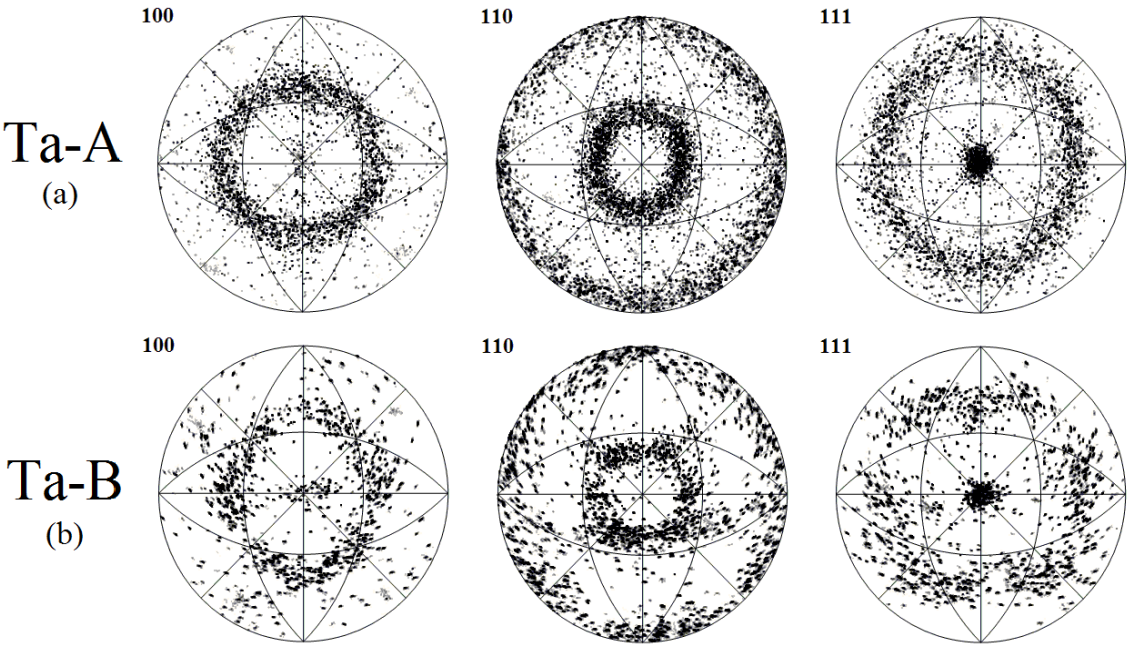

Figure 4.7: Pole figures produced from the EBSD data of Figure 4.5 of the <100>, <110>, and <111> directions of as-received Ta-A (a) and Ta-B (b).

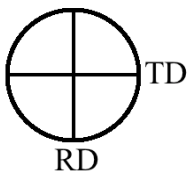

Tantalum is known to display texture variations through its thickness when rolled, and these variations depend on processing conditions, annealing times, and annealing temperatures [Clark 1991, Raabe 1994]. Through-thickness texture gradients often do not persist following recrystallization. Annealing at higher temperatures or increasing deformation strain prior to annealing produces more homogeneous textures. Raabe *et al*. found a strengthening of the α-fiber following annealing at lower temperature and lesser deformation, weakening of the α-fiber and strengthening of the γ-fiber at higher temperature and greater deformation, and a through-thickness texture gradient at intermediate conditions [Raabe 1994]. Through-thickness EBSD maps of as-received Ta-A and Ta-B are shown in Figure 4.8. The microstructures observed in the as-received Ta materials are consistent with materials that have been annealed at moderate to high temperatures because of the lack of a significant texture gradient and a dominance of the γ-fiber.

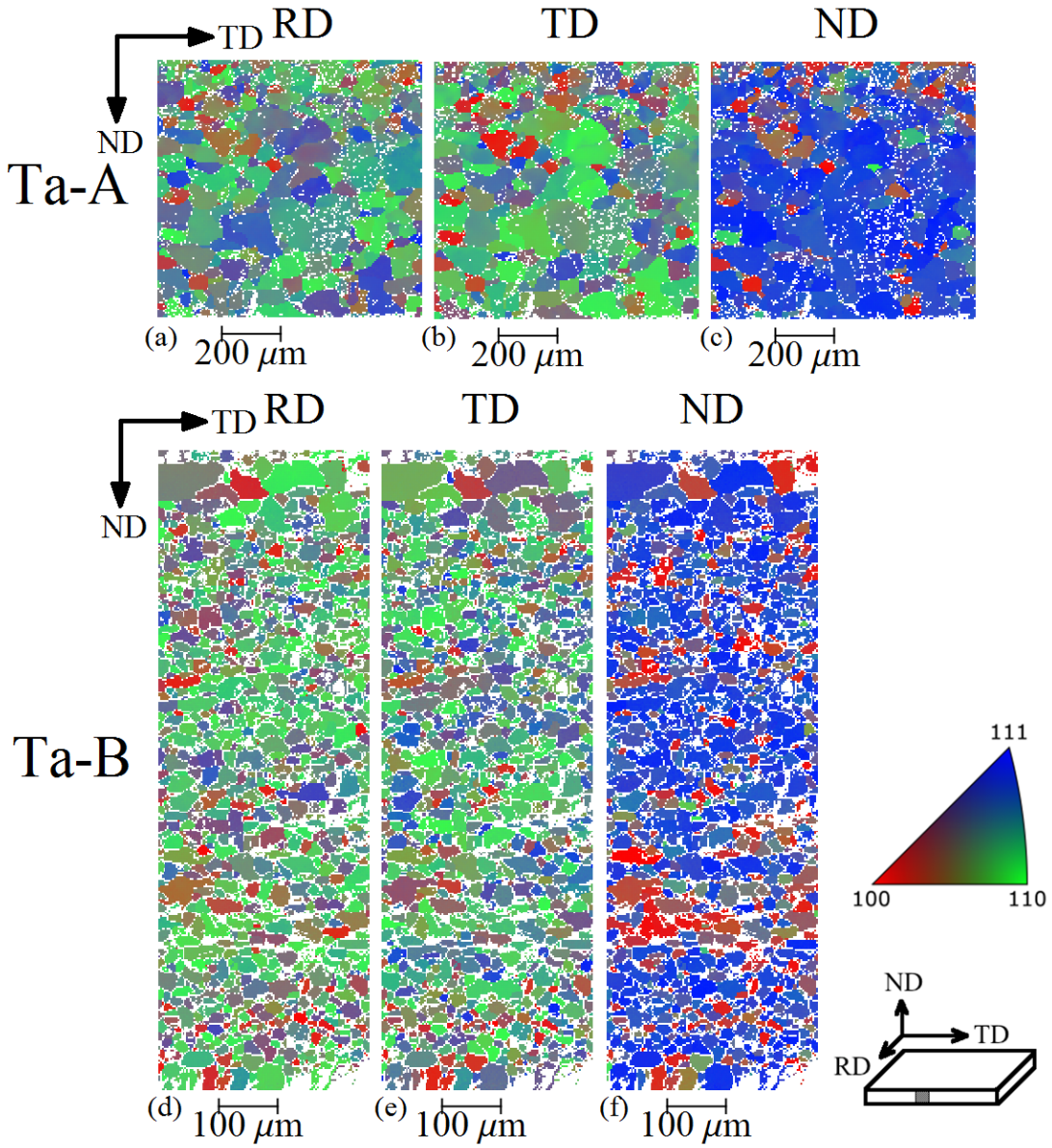

Figure 4.8: EBSD maps of as-received Ta-A (a-c) and Ta-B (d-f), colored according to the inverse pole figure coloring scheme relative to the crystallographic direction along: RD (a,d), TD (b,e), or ND (c,f). The data was collected in along RD. The normal direction (ND) is vertical and the transverse direction (TD) is horizontal. Unindexed pixels are left white. A schematic of the sheet is provided with the reference directions indicated and the area of the EBSD scan shaded. Note: the scales are different for Ta-A and Ta-B.

4.3 GRAIN GROWTH

Microstructures of Ta-A and Ta-B annealed at 1650 °C and 1850°C for 8 hours are shown in Figure 4.9. The Ta-A undergoes considerable normal grain growth when annealed, while Ta-B does not. This is expected since Ta-B is specially alloyed to inhibit grain growth. The as-received and annealed grain sizes (lineal intercept) for Ta-A and Ta-B are listed in Table 4.1. Grain sizes remained equiaxed upon annealing. Large grains, with diameters approximately 3 to 4 times that of the remaining microstructure, were observed along one edge of the Ta-B material after annealing at 1850 °C for 8 hours, as shown in Figure 4.10. The reason for this is unknown, but may be due to a processing artifact or small variation in composition in this region. No other instances of SAGG were observed in either Ta material at any of the conditions examined.

The grain growth behavior of Mo-PMB is described in Table 4.2, and microstructures of Mo-PMB annealed at 1650 °C and 1800 °C for 9.5 hours are provided in Figure 4.11 and 4.12. Mo-PMB exhibited grain sizes 5 to 33% larger in the rolling direction than in the transverse direction. Only moderate growth was observed at 1650 °C between 0.2 and 2.2 hours, and no significant further growth was observed upon annealing up to 9.5 hours. At 1800 °C after 2.2 hours, the grain size was similar to that after 2.2 hours at 1650 °C; however, after annealing at 1800 °C for 9.5 hours SAGG was observed, as demonstrated in Figure 4.12. The abnormal grains grew to hundreds of μm in diameter while the unconsumed polycrystalline microstructure did not experience significant grain growth.

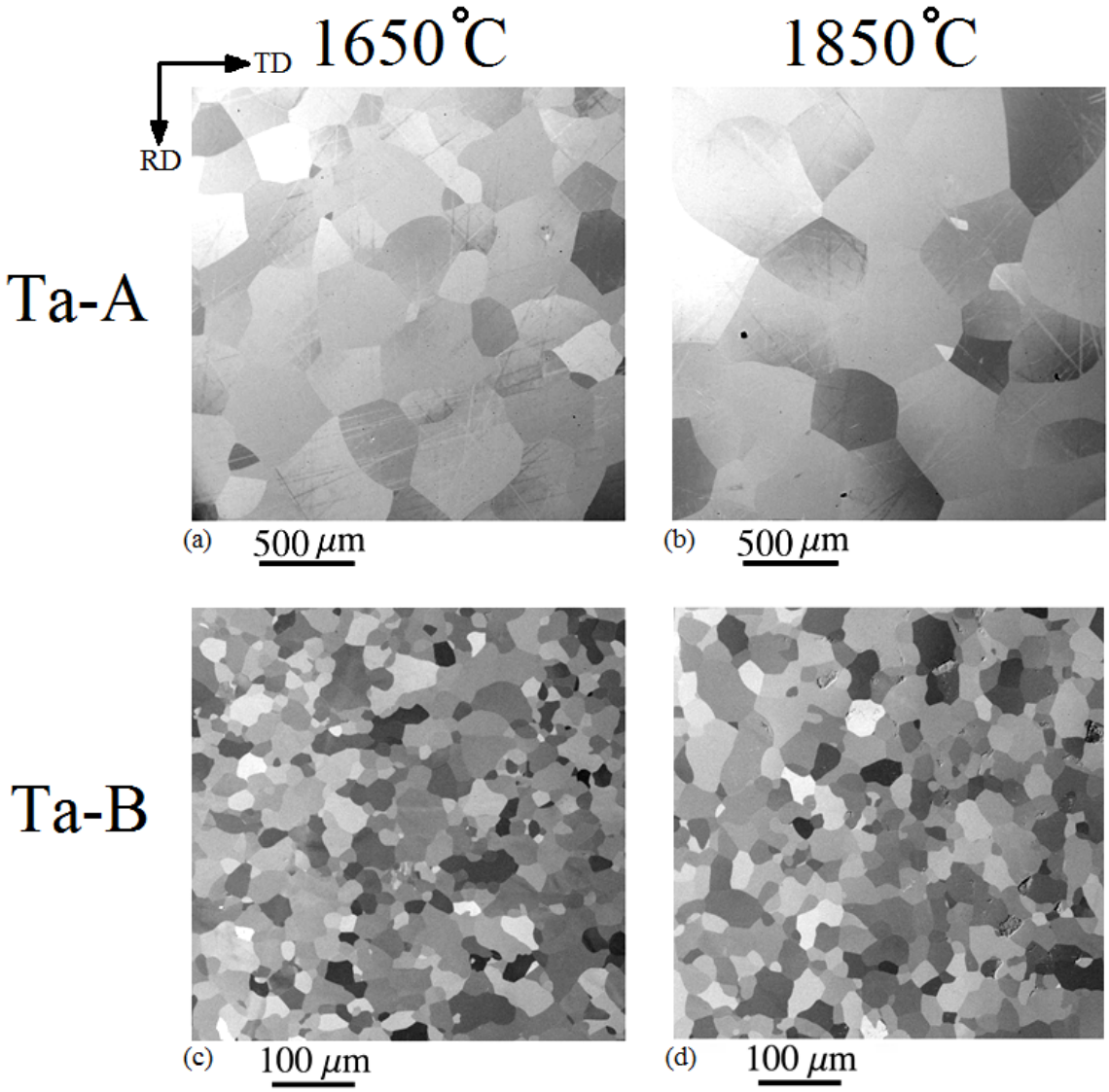

Figure 4.9: Backscatter SEM images of Ta-A (a,b) and Ta-B (c,d) annealed at 1650 °C (a,c) and 1850 °C (b,d) for 8 hours. Color variations are due to channeling contrast. The rolling direction (RD) is vertical and the transverse direction (TD) is horizontal.

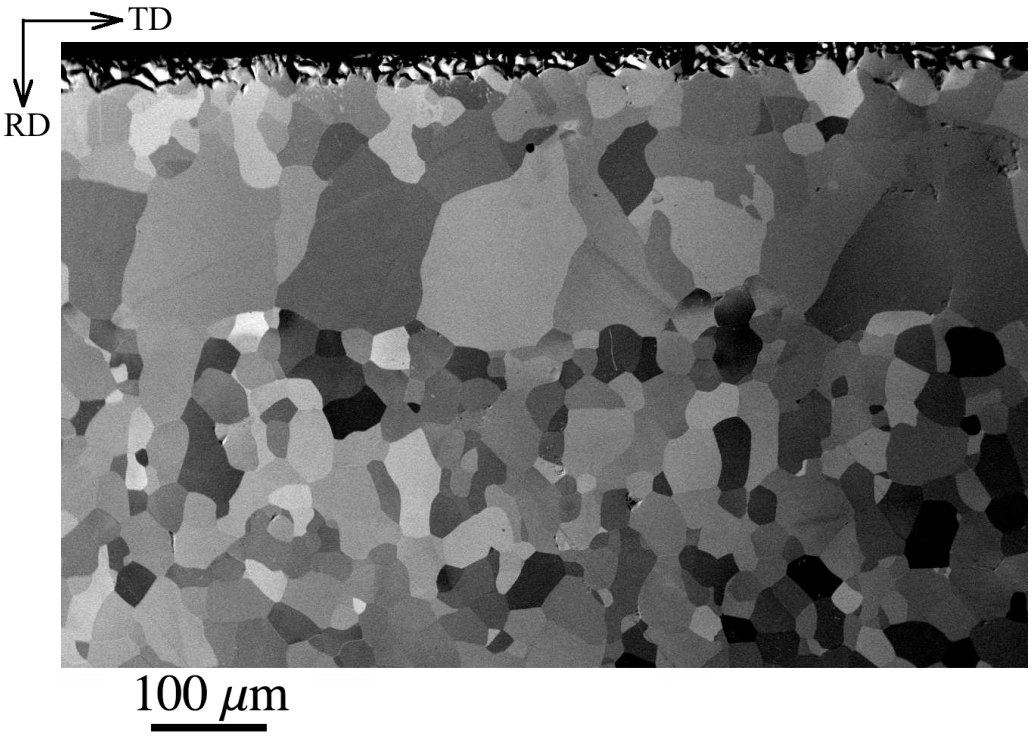

Figure 4.10: Backscatter SEM image of Ta-B annealed at 1850°C for 8 hours showing normal polycrystalline microstructure (bottom) and large grains that grew near one edge of the sheet material (top). The rolling direction (RD) is vertical and the transverse direction (TD) is horizontal.

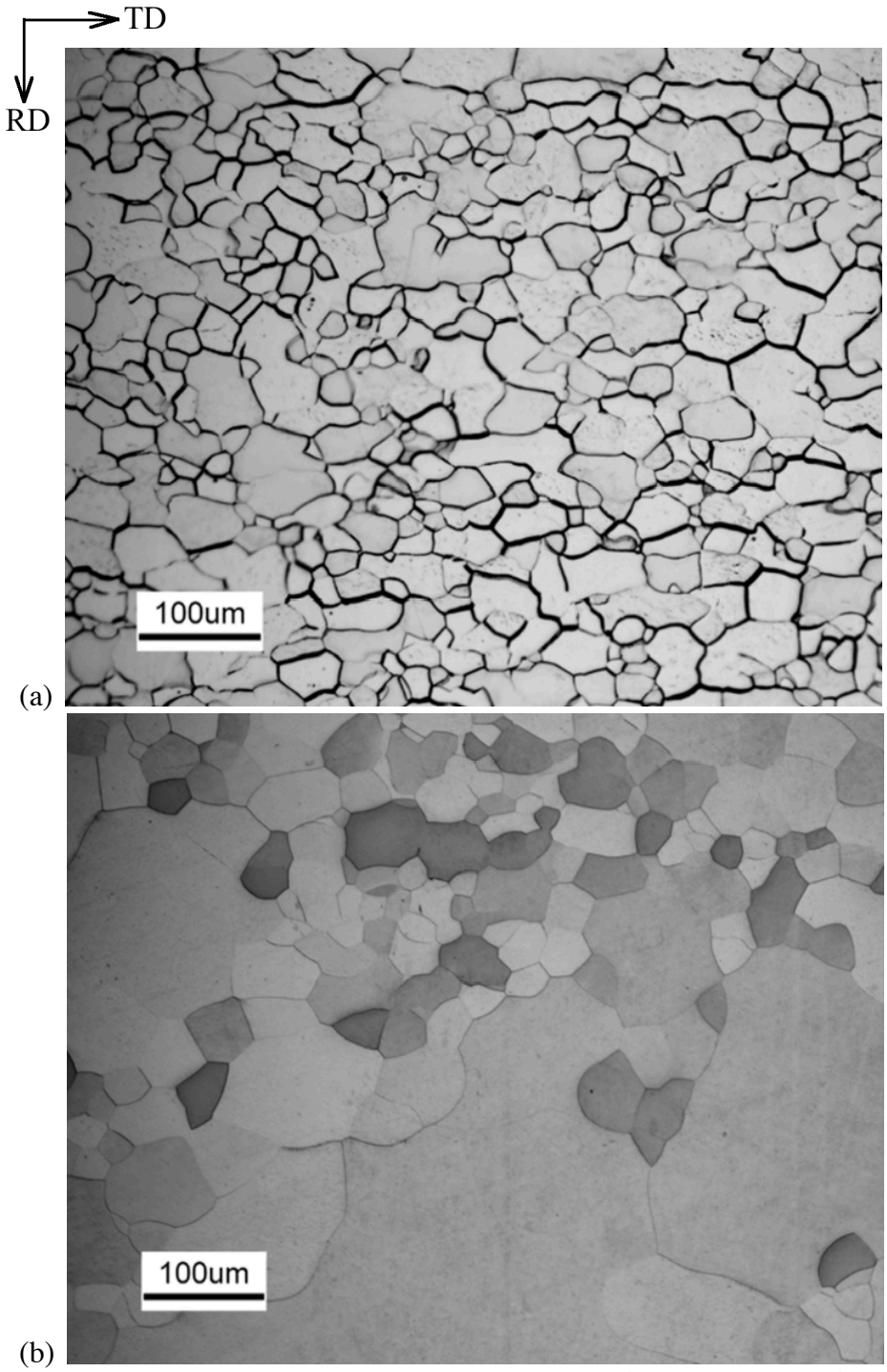

Figure 4.11: Microstructures of Mo-PMB annealed for 9.5 hours at (a) 1650 °C and (b) 1800 °C. The rolling direction (RD) is vertical and the transverse direction (TD) is horizontal. From [Worthington 2011].

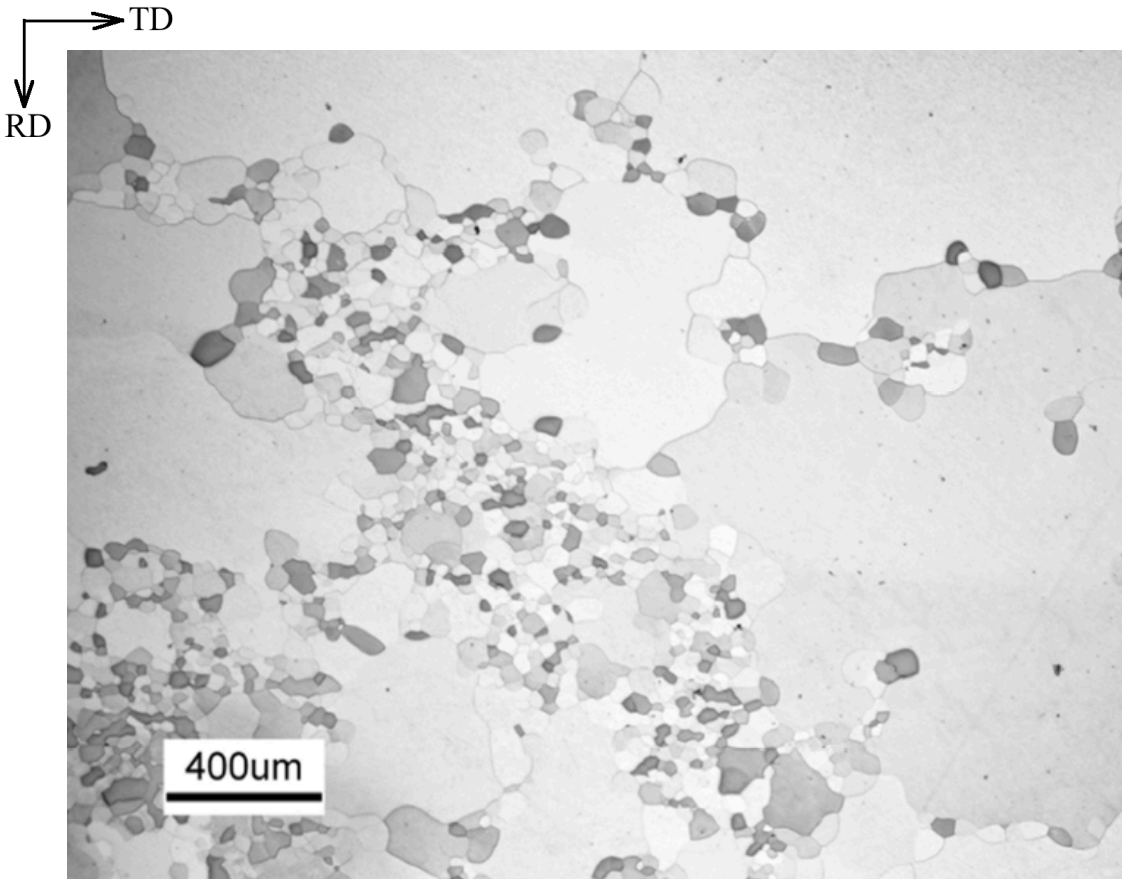

Figure 4.12: Microstructure of Mo-PMB annealed at 1800 °C for 9.5 hours showing polycrystalline grain segments and SAGG. The rolling direction (RD) is vertical and the transverse direction (TD) is horizontal. From [Worthington 2011].

Table 4.1: Grain sizes of as-received and annealed Ta-A and Ta-B determined by lineal intercept method using EBSD data.

	Ta-A	Ta-B
As-received	44 ± 3 μm	26 ± 6 μm
Annealed: 1850°C, 480 min.	441 ± 134 μm	32 ± 6 μm

Table 4.2: Grain sizes of Mo-PMB in its rolling direction d_{RD} and transverse direction d_{TD} determined by lineal intercept method using optical microscopy. From [Worthington 2011].

M-PMB	d_{RD}, μm	d_{TD}, μm
Annealed: 1650°C, 0.2 hrs.	21 ± 3	17 ± 3
Annealed: 1650°C, 2.2 hrs.	28 ± 9	21 ± 5
Annealed: 1650°C, 9.5 hrs.	27 ± 5	22 ± 3
Annealed: 1850°C, 2.2 hrs.	21 ± 3	20 ± 3
Annealed: 1850°C, 9.5 hrs.	Bimodal: fine equiaxed of ~20 μm and large abnormal grains of 100s of μm in size.	

Ta-A is the only material of the three that exhibits significant normal grain growth. The grain growth character of Ta-A was analyzed further by measuring the grain sizes in the grip regions of several tensile specimens, which do not accumulate significant strain during testing since the stresses in the grip region are small. The effects of temperature and time at temperature are shown in Figures 4.13 and 4.14, respectively. These indicate that normal grain growth in Ta-A is a strong function of temperature, but a very weak function of time at temperature in the range of temperatures and annealing times of interest for DAGG. The grain size initially increases with increasing annealing temperature from 1550 to 1750 °C, but grain size does not increase significantly for temperatures higher than these. This may be due to the grain size approaching the thickness of the sheet or a reduction in the driving force due to a decrease in grain boundary curvature, both of which may slow or inhibit further grain growth. The grain size at 1850 °C was constant for annealing times of 0.5 to 4.2 hours. This indicates that

most grain growth occurs rapidly during heating to temperature prior to tensile testing. Thus, no normal grain growth is likely during the tensile tests at elevated temperature for DAGG investigations. Note: grain sizes reported in Figures 4.13 and 4.14 were calculated using optical microscopy, while the grain sizes reported in Table 4.1 are calculated from EBSD data. Grain sizes measured from EBSD data will often be smaller than those measured from optical microscopy due to the increased accuracy in identifying grain boundaries from EBSD data [Gao 2005, Mingard 2009]. Chemical etchants used to reveal grain boundaries for optical microscopy often do not act uniformly across all boundary types, leaving some boundaries unidentifiable. In this instance, grain sizes determined using optical microscopy are approximately 18% higher than those determined using EBSD data at similar temperatures.

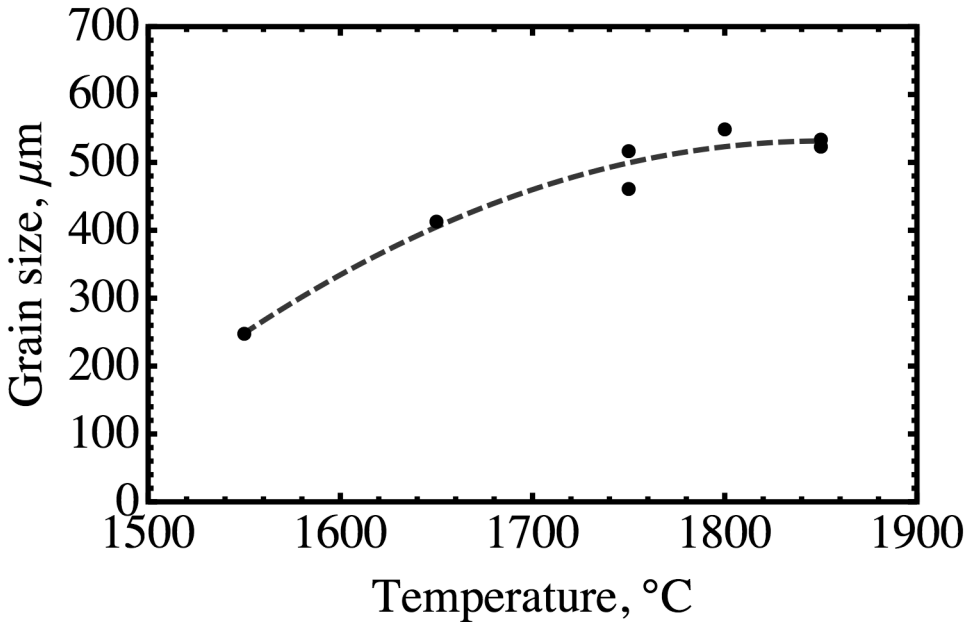

Figure 4.13: Grain size *versus* temperature for Ta-A at annealing times of 2-3 hours. The range in annealing time is not expected to significantly affect the grain size, as demonstrated subsequently in Figure 4.14.

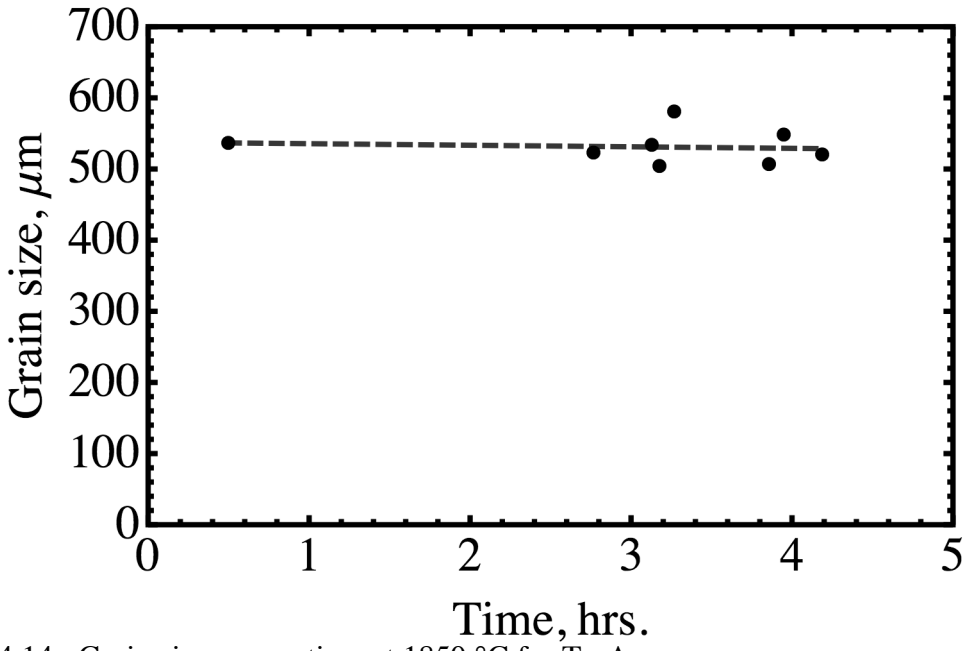

Figure 4.14: Grain size *versus* time at 1850 °C for Ta-A.

EBSD was conducted on annealed Ta-A and Ta-B to determine any texture changes upon heating which may occur prior to straining when conducting a tensile test. EBSD maps constructed of data collected from annealed Ta-A and Ta-B normal to the sheet surface and normal to the rolling direction are shown in Figures 4.15 and 4.19. EBSD results from annealed Mo-PMB are shown in Figure 4.16.

The textures of annealed Ta-A and Ta-B, as shown by the EBSD data of Figure 4.15, are similar to each other and to their as-received textures, although annealed Ta-A shows an increased presence of the <111> orientation along ND and a decrease in <100> and <111> orientations along RD and TD. This is consistent with a sharpening of the original γ-fiber texture. The inverse pole figures of Figure 4.17(a) indicate a strengthening of the primary texture seen in Figure 4.6(a). Grains with orientations outside the primary texture components were likely consumed by the grains in the primary texture due to generally higher boundary energy between adjacent grains that are

not from the same texture component. The pole figures of Figure 4.18a demonstrate the dominance of the γ-fiber in the annealed Ta-A.

The texture of the Ta-B did not significantly change upon annealing, as seen in comparing Figures 4.5 (d-f) and 4.15 (d-f). The inverse pole figures of Figure 4.17(b) show a distribution of orientations similar to the as-received Ta-B in Figure 4.6(b). Thus, Ta-B consistently shows a strong γ-fiber, with possibly some weak {001}<101> and {111}<101> components of the α-fiber, for the range of conditions examined. The observation of these texture components is also supported by the pole figures provided in Figure 4.18(b).

The annealed texture of Mo-PMB is markedly different from those of Ta-A and Ta-B. The EBSD data provided in Figure 4.16 show a spread of orientations from <100> to <111> along ND, with the <100> orientation dominating. The inverse pole figures of Figure 4.17(c) demonstrate a spread of orientations from <110> to <112> in RD and TD, as is generally seen in Ta-A and Ta-B, but <110> is favored along RD and <112> along TD. The distribution from <100> to <111> in ND is also seen in Figure 4.17(c). This indicates that this spread in orientations is not continuous. The primary texture preferentially aligns <100> along ND and a minor component aligns <111> along ND. The 100 pole figure of Figure 4.18(f) indicates that the preferential alignment of <100> along ND is not a fiber; although, this is a component of the α-fiber. Thus, the Mo-PMB texture shows a strong α-fiber and weak γ-fiber character.

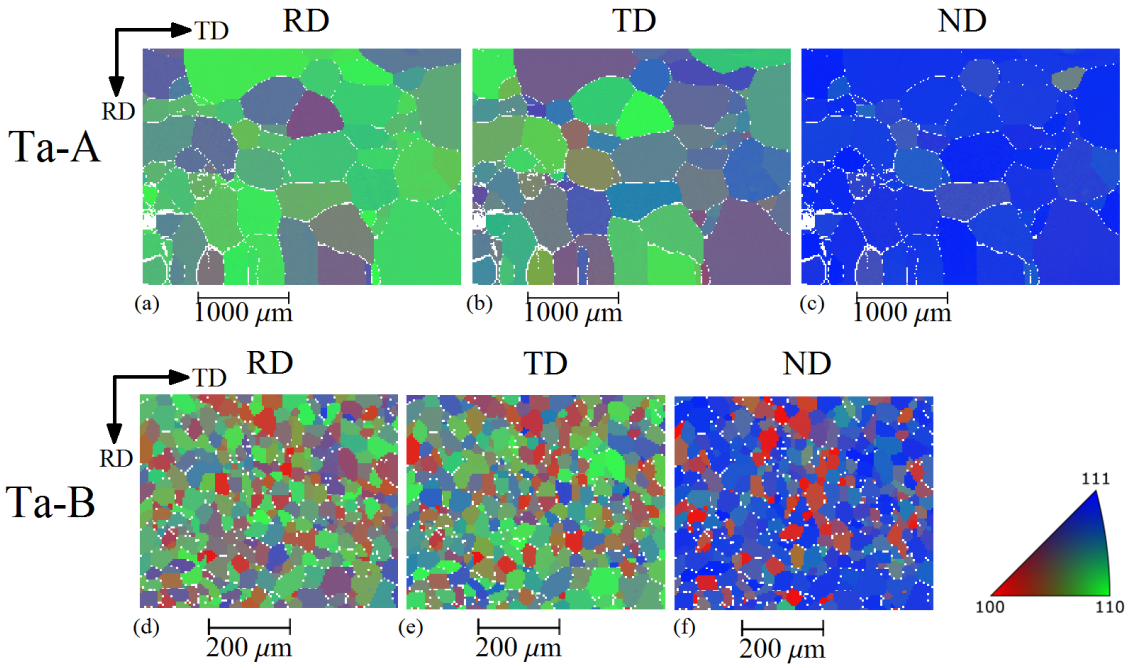

Figure 4.15: EBSD maps of Ta-A (a-c) and Ta-B (d-f) annealed at 1850 °C for 8 hours, colored according to the inverse pole figure coloring scheme relative to the crystallographic direction along: RD (a,d), TD (b,e), or ND (c,f). The data was collected along ND. The rolling direction (RD) is vertical and the transverse direction (TD) is horizontal. Unindexed pixels are left white.

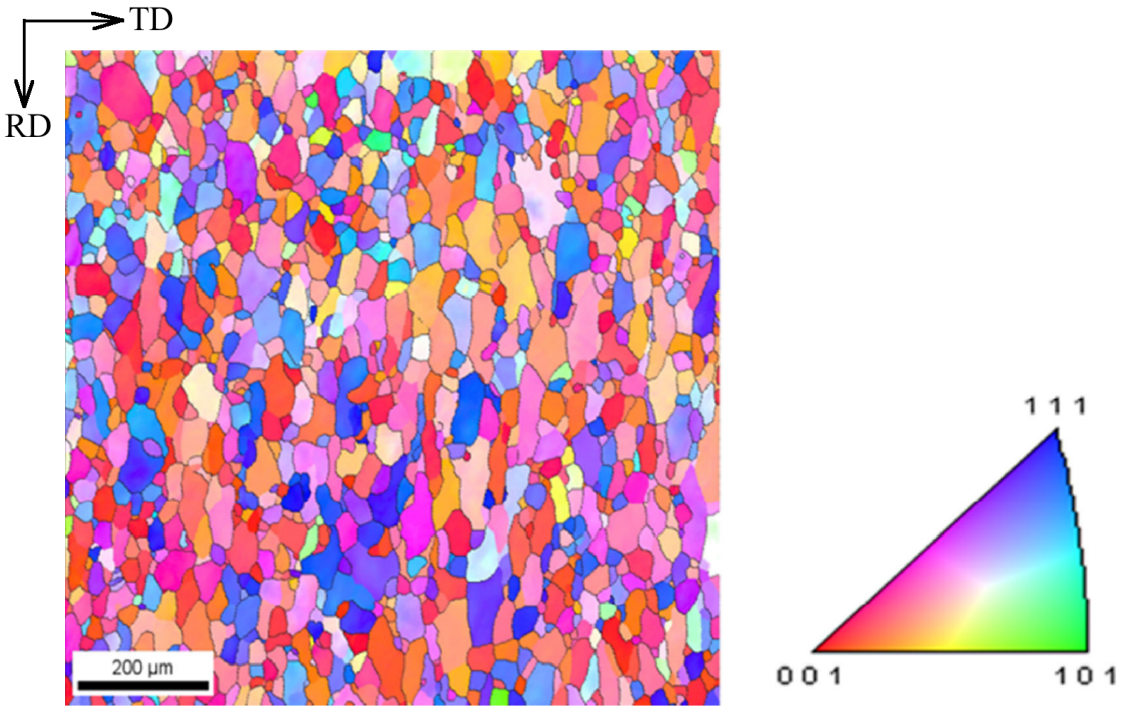

Figure 4.16: EBSD maps of Mo-PMB annealed at 1650 °C for 2.2 hours, colored according to the inverse pole figure coloring scheme relative to the crystallographic direction along ND. The data was collected along ND. The rolling direction (RD) is vertical and the transverse direction (TD) is horizontal. From [Worthington 2011].

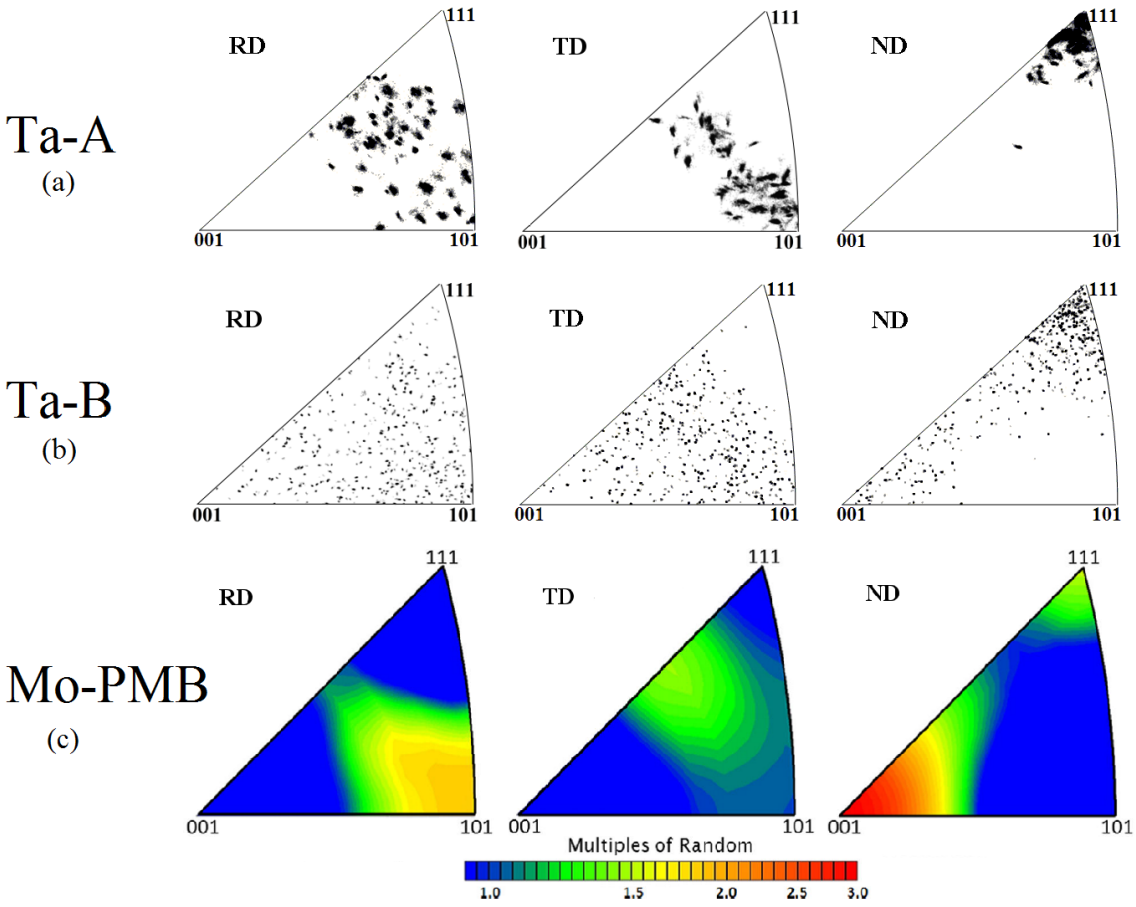

Figure 4.17: Inverse pole figures of (a) Ta-A and (b) Ta-B annealed at 1850 °C for 8 hours, and (c) Mo-PMB annealed at 1650 °C for 2.2 hours (from [Worthington 2011]), relative to RD, TD, and ND.

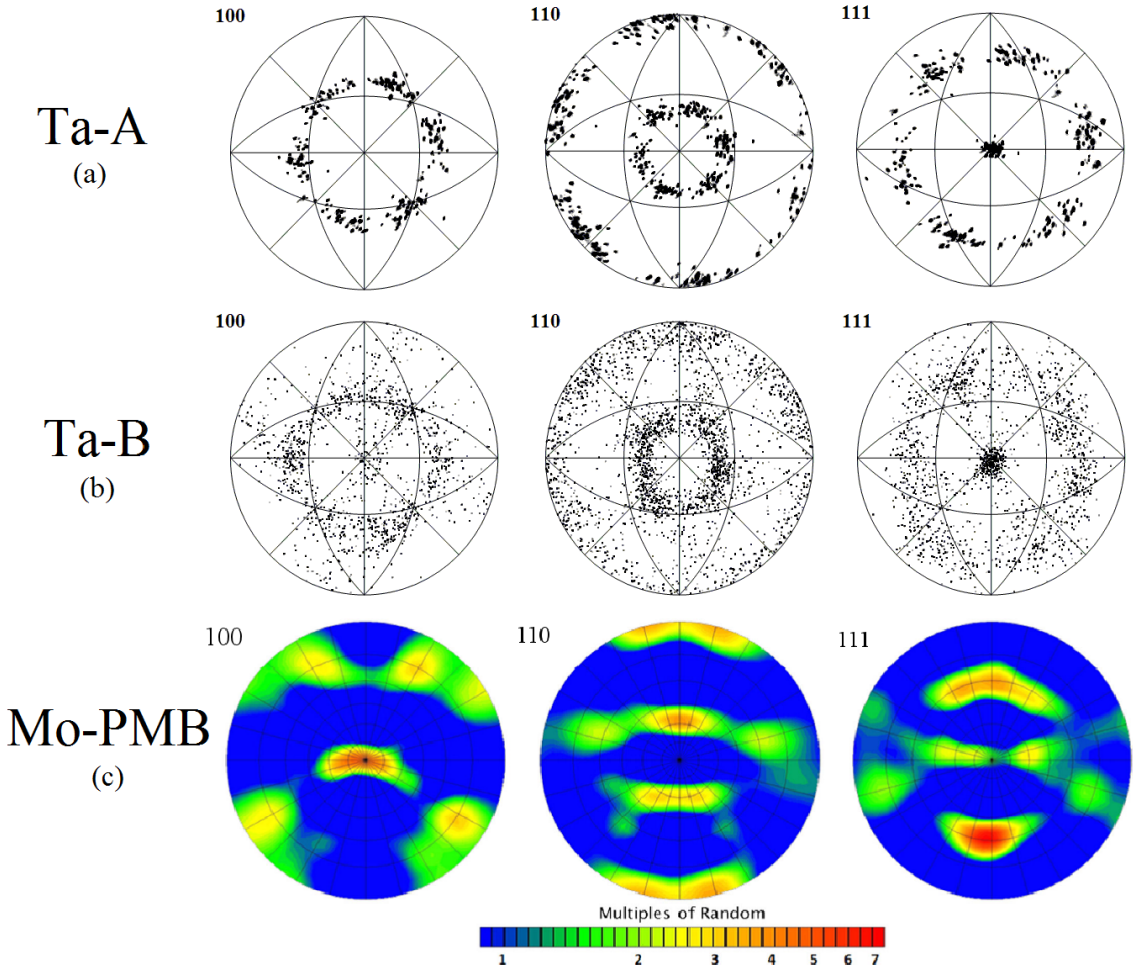

Figure 4.18: Pole figures produced from the EBSD data of Figures 4.15 and 4.16 of the <100>, <110>, and <111> directions of Ta-A (a) and Ta-B (b) annealed at 1850 °C for 8 hours, and Mo-PMB (c) annealed at 1650 °C for 2.2 hours (from [Worthington 2011]).

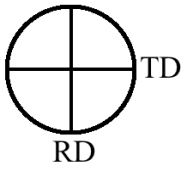

The cross sections of annealed Ta-A and Ta-B were also examined using EBSD, and results are shown in Figure 4.19. In Ta-A, the dramatic grain growth produced grains that spanned the thickness of the specimen, and thus no through-thickness texture gradient is observed. In Ta-B, there was no significant change in texture through the thickness of the sheet, as shown in Figure 4.19 (d-f). Thus, any preferential grain growth

on the surface of a specimen, or at a specific depth from the surface, cannot be attributed to texture variations in these Ta materials.

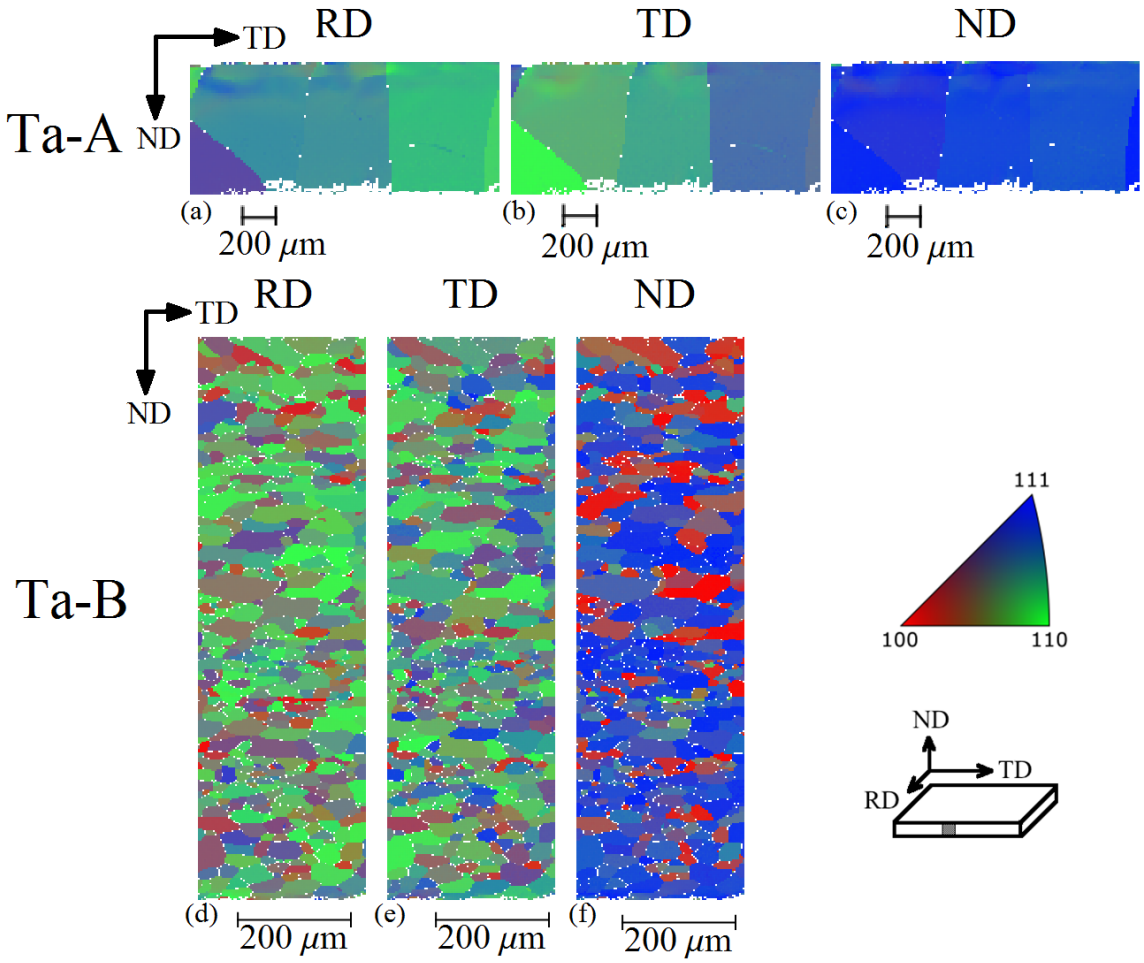

Figure 4.19: EBSD maps of Ta-A (a-c) and Ta-B (d-f) annealed at 1850 °C for 8 hours, colored according to the inverse pole figure coloring scheme relative to the crystallographic direction along: RD (a,d), TD (b,e), or ND (c,f). The data was collected along RD. The normal direction (ND) is vertical and the transverse direction (TD) is horizontal. Unindexed pixels are left white. A schematic of the sheet is provided with the reference directions indicated and the orientation of the EBSD scan shaded. Note: the map aspect ratio is different for a-c and d-f, but all cross sections have the same orientation.

4.4 GRAIN BOUNDARY CHARACTER

The grain boundary character of Ta-A and Ta-B, as shown in Figure 4.20, was characterized using the EBSD data of Figure 4.15. This was done to later compare the distribution of various boundary types before and after creep testing. The grain boundaries in this Ta-A sample are often Σ3 (~19%) or angles below 10° (~21%), although some Σ7 boundaries are also observed. In Ta-B, Σ3 (~7%) and angles below 10° (~8%) also dominate, but to a lesser extent. Minor contributions of Σ 5, 9, and 11 are also observed in Ta-B. The large proportions of Σ3 and low angle boundaries, especially for Ta-A, are due to the strong <111> texture. A strong texture will inherently have a higher percentage of low angle boundaries than a randomly oriented microstructure. In addition, since a Σ3 boundary is characterized by a 60° rotation about a <111> axis, and the texture has very strong <111>-fiber, Σ3 boundaries may form from adjacent grains rotated about the <111> fiber axis. Two grains with their <111> axes parallel must only be rotated 60° ± θ_B (where $\theta_B(\Sigma 3) = 8.66°$) from each other to have a Σ3 boundary between them.

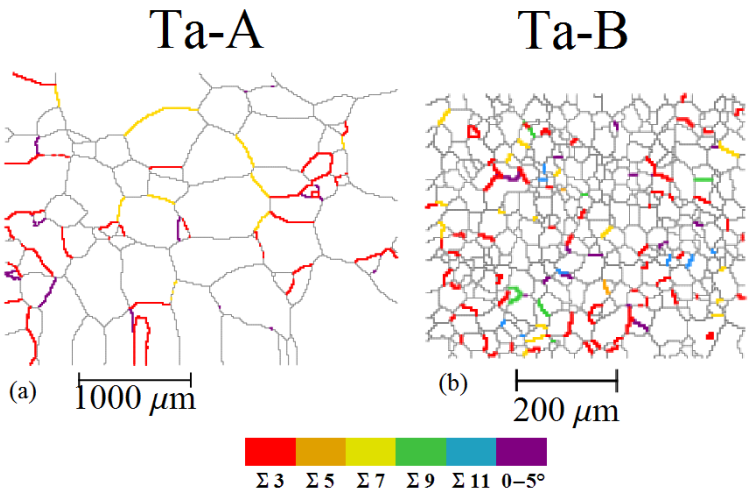

	Ta-A, %	Ta-B, %
Σ 3	18.6	7.0
Σ 5	0.0	0.2
Σ 7	5.9	1.9
Σ 9	0.0	0.8
Σ 11	0.0	0.6
0-5°	3.9	1.4
5-10°	17.2	6.9

Figure 4.20: Grain boundary character for Ta-A (a) and Ta-B (b) annealed at 1850 °C for 8 hours. Boundaries classified as Σ 3, 5, 7, 9, and 11, and grain boundarys with disorientations less than 5° are indicated by color on the EBSD map. The percentage of the total length of each indicated boundary type relative to the total length of all boundaries is provided in the table.

5 DAGG Under Constant True Stress

The experimental observation of DAGG currently relies upon both changes in mechanical response during deformation and the subsequent characterization of microstructure. As a DAGG grain, or grains, propagate during plastic deformation, the mechanical response of the specimen transitions from that of a polycrystalline material to that of a single-crystal, or nearly single-crystal, material. This involves the elimination of grains and substructure (subgrains) that resist plastic deformation, as per creep theory [Kassner 2009, p.41]. A rapid drop in flow stress is observed during a constant strain-rate test, and this corresponds to the initiation of a DAGG grain. Standard creep-like and DAGG behaviors are demonstrated in Figures 5.1 (a) and (b), respectively.

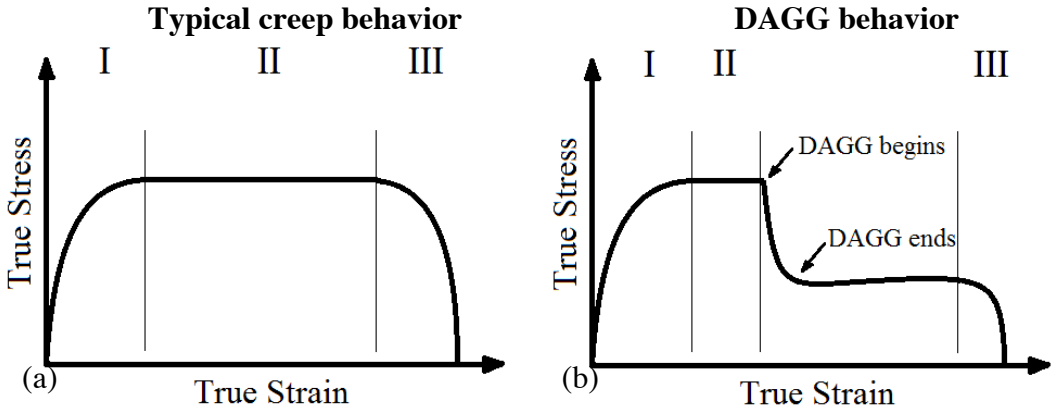

Figure 5.1: Schematics show true stress *versus* true strain of (a) a typical constant true-strain-rate test to failure and (b) one in which DAGG occurred. The rapid drop in true stress in (b) corresponds to the initiation and growth of one or more DAGG grains across the width and along the gauge length of the specimen.

The initial drop in stress in Fig. 5.1(b) results from the lower flow stress of the DAGG single crystal(s) compared to that of the prior polycrystalline microstructure. However, the situation is more complicated if stress is held constant, i.e., a constant true-

stress test. Under constant true stress, DAGG is expected to produce a rapid increase in plastic strain rate. The increase in strain rate could easily be misinterpreted as the beginning of tertiary creep and specimen rupture, which is a plausible explanation for DAGG not having been previously observed in creep tests. Thus, using constant-stress tests to initiate DAGG is expected to be experimentally challenging.

Schematics of data from tensile tests conducted under constant stress at elevated temperature are shown in Figure 5.2 (a) and (b) for creep in a typical pure metal and in (c) and (d) for a specimen in which DAGG occurs. The typical stages of creep behavior are indicated as: primary (stage I), steady-state (stage II, secondary), and tertiary (stage III). The occurrence of DAGG changes this behavior in a subtle but important way. It introduces a new region of rapid plastic strain rate. This change is easy to miss when viewing the data as strain *versus* time, but viewing the data as strain rate *versus* time more clearly reveals the effect of DAGG. Figures 5.2(c) and (d) are schematics of strain *versus* time and strain rate *versus* time, respectively, demonstrating the material response expected from DAGG between stages II and III. DAGG can occur prior to the initiation of stage III creep and increases the strain rate from $\dot{\varepsilon}_1$, observed during steady-state creep, to $\dot{\varepsilon}_2$, observed at DAGG completion. This change is revealed by comparing $\dot{\varepsilon}_1$ and $\dot{\varepsilon}_2$ in Figure 5.2(c). When DAGG ceases, the strain rate may briefly remain constant at $\dot{\varepsilon}_2$ before it increases further and tertiary creep, stage III, begins. The requirement to continuously monitor strain rate makes DAGG particularly difficult to identify during a constant-load or a constant-stress tensile test. The revelation of one or more abnormal grains after testing and an identifiable sharp increase in strain rate, separate from tertiary creep, are required to verify that DAGG has occurred.

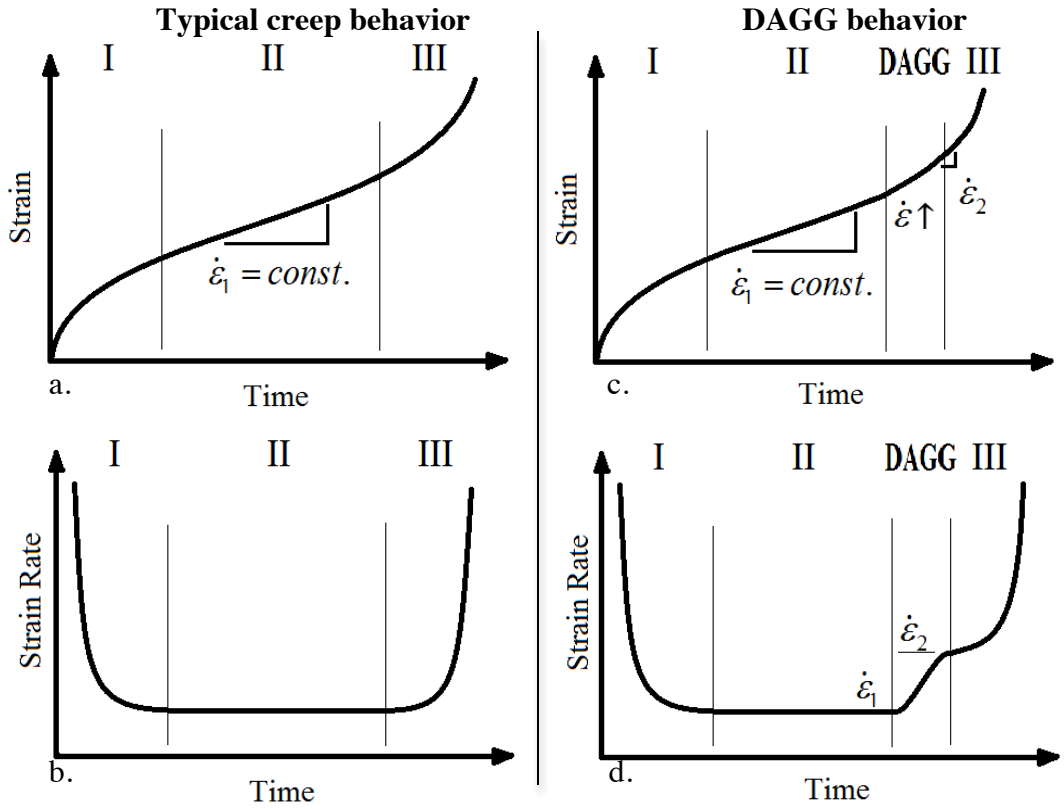

Figure 5.2: Schematics of constant true stress test results are plotted as (a, c) strain *versus* time, and (b, d) strain rate *versus* time, with the three stages of creep indicated. These show (a, b) characteristic creep behavior, and (c, d) a case where DAGG occurred during testing.

Constant-stress tests on α-Fe [Tran 2008, Thanh 2009] showed AGG, but were unsuccessful at definitively inducing DAGG since all specimens were tested to failure and it is not known if the AGG observed was the result of a stress concentration during necking or if DAGG weakened the material locally allowing for necking and failure. The increase in strain rate due to DAGG may be easily misattributed to tertiary creep, and any abnormal grains observed in the microstructure may be mistakenly attributed to SAGG following specimen rupture. The present study, however, demonstrates that it is possible to both induce and simultaneously identify the onset of DAGG in Mo tested in tension under a constant true stress.

A summary of test conditions and results of 15 constant true-stress tests are provided in Table 5.1. All tests were conducted on the Mo-PMB material at a temperature of 1650 °C. Both the length of the largest DAGG grain in the tensile direction and the cumulative length, when two DAGG grains occurred, were measured and are reported in Table 5.1. The test temperature was chosen because it is a temperature at which DAGG occurs consistently in Mo-PMB, which was demonstrated in the investigations of Worthington [Worthington 2011]. The range of true stresses investigated was selected based on the average true stress at DAGG initiation under constant true-strain-rate conditions at the same temperature. The average true stress at DAGG initiation was 35.9 ± 1.38 MPa, and the average strain at initiation was 0.152 ± 0.055 for 22 tests on Mo-PMB at 1650 °C [Worthington 2011]. The specimen dimensions and furnace setup for the present study are identical to those used in the investigations by Worthington.

Table 5.1: Summary of test conditions and results for Mo-PMB at 1650 °C.

Test	True Stress	DAGG observed	True Strain at DAGG		Strain rate at DAGG		Elapsed time during DAGG	Number of DAGG grains	Length of largest DAGG grain	Cumulative length of DAGG grains
			Start	End	Start	End				
Mo cs #	MPa				10^{-5} s^{-1}		s		mm	mm
3	30	No	*	*	*	*	*	*	*	*
4	35	Yes	0.246	0.282	7.38	11.23	371	1	39	39
5	35	Yes	0.314	0.331	8.13	11.41	176	1	21	21
6	35	No	*	*	*	*	*	*	*	*
7	35	No	*	*	*	*	*	*	*	*
8	30	Yes	0.246	0.252	2.77	3.906	170	1	25	25
9	37	Yes	0.19	0.213	9.066	13.68	185	1	21	21
10	40	No	*	*	*	*	*	*	*	*
11	40	No	*	*	*	*	*	*	*	*
12	38.5	No	*	*	*	*	*	*	*	*
13	37	No	*	*	*	*	*	*	*	*
14	32	Yes	0.267	0.287	3.973	9.2	285	2	19	33
15	28	Yes	0.349	0.361	2.362	4.188	320	1	29	29
16	32	Yes	0.331	0.34	4.787	6.382	154	2	15	20
17	30	Yes	0.129	0.138	3.392	5.674	185	1	26	26

5.1 MODEL FOR DAGG GRAIN BOUNDARY MIGRATION

A model proposed by Worthington suggests that the migration rate of DAGG grain boundaries is increased by a plasticity-induced increase in boundary mobility [Worthington 2011]. This model predicts that the distance a grain boundary migrates

during DAGG is proportional to the plastic strain accumulated. A summary of this theory is as follows:

Active straining, which is the primary difference between DAGG and SAGG, may affect either the driving force for boundary migration or the boundary mobility, or both. The boundary migration rate, v, is a function of both the driving force, P, and mobility, m, given previously by Eq. 2.12, where $v = mP$. Driving force depends on a number of factors, such as grain boundary energy, stored deformation energy, and surface energy, among others discussed in §2.2.2.1. It is hypothesized that the increase in boundary migration rate cannot be explained by an increase in driving pressure alone, but rather that active straining increases the mobility constant, m_o in Eq. 2.13 ($m = m_0 e^{-H/kT}$), by moving dislocations to or from the boundary.

The creation and annihilation of dislocations at a grain boundary may affect boundary pinning, such as at fine particles that can act as pinning sites. Pinning sites that inhibit normal grain growth may act as dislocation nucleation sites because of localized stress concentrations, and the dislocations emitted may assist unpinning of the boundary. The grain boundary migration rate may then be defined as in Eq. 5.1, where α is a constant related to the number of dislocations formed at a pinning site for the site to unpin it, R is the rate at which dislocations are produced per site, and l is the average spacing between pinning sites, assumed to make up an array on a pinned grain boundary.

$$v = \alpha R l \qquad \text{Eq. 5.1}$$

Unpinning will result in dislocations traveling through the DAGG grain to a point of annihilation, such as at a free surface. This distance traveled, w, can then be used to define an area swept by the dislocation, A, as simply $A=wl$. The density of dislocation sources, which are pinning sites on the boundary within the DAGG grain, is then

$M=\beta/wl^2$, where β is a constant related to the geometry of slip. From creep theory [Weertman 1968], the strain rate is then

$$\dot{\varepsilon} = RAMb \quad , \qquad \text{Eq. 5.2}$$

where b is the Burgers vector magnitude. R can then be defined as

$$R = \dot{\varepsilon} l / \beta b . \qquad \text{Eq. 5.3}$$

This leads to the following relations for v and $\bar{x}$, the average DAGG boundary migration rate and distance,

$$v = \frac{\alpha l^2}{\beta b}\dot{\varepsilon} \qquad \text{Eq. 5.4}$$

$$\bar{x} = \frac{\alpha l^2}{\beta b}\varepsilon . \qquad \text{Eq. 5.5}$$

This model suggests that the distance that the DAGG boundary travels is directly proportional to the amount of strain produced after the onset of DAGG initiation, which is consistent with observations of DAGG in Mo by Ciulik and Worthington [Ciulik 2005, 2009; Worthington 2011, 2013]. The spacing of pinning sites, however, has not been studied.

In pure metals and Class II (Class M) alloys under power-law creep conditions, strain rate and applied stress are related by the power-law equation [Ciulik 2007, Sherby 1967],

$$\dot{\varepsilon} = AD\left(\frac{\sigma}{E}\right)^n \qquad \text{Eq. 5.6}$$

where A is a material-dependent constant, D is lattice diffusivity, E is the unrelaxed dynamic temperature-dependent elastic modulus, and n is the stress exponent. Combining and simplifying Eq. 5.4 and 5.6 gives the following relationship for strain enhanced boundary migration,

$$v \propto \sigma^n . \qquad \text{Eq. 5.7}$$

This result can be contrasted with that predicted for stress-driven boundary migration [Gottstein 2009 p.139]. For stress-driven migration, the applied stress couples with the strain produced during boundary movement to dissipate work. For a simple tilt boundary, the driving force, P, can be simply considered as a shear stress τ acting to create a strain swept out over an angle θ, as $P = \tau\,\theta$. When combining this result with Eq. 2.12, v is then directly proportional to the applied stress, leading to the relationship shown in Eq. 5.7, with n=1. For strain assisted boundary migration, n is significantly greater than 1, and n~5 for polycrystalline Mo [Ciulik 2007].

In theory, this relationship between applied stress and boundary velocity can be used to determine whether DAGG is a stress-driven or a strain-assisted process. Constant true-strain-rate tests cannot be used to validate this theory because the stress is constantly changing during DAGG. Constant true-stress tests may be used to directly probe the relationship between applied stress and boundary velocity, and it is the purpose of this investigation to attempt to do so. The resulting data will be used to explore whether DAGG is more likely caused by stress-driven or strain-assisted boundary migration.

5.3 RESULTS AND DISCUSSION

Of the 15 specimens tested, 8 produced DAGG under constant true stresses ranging from 28 to 37 MPa. Applied true stresses less than 35.9 MPa, the average true stress at DAGG initiation under constant true strain rate, were more likely to exhibit DAGG; 70% of tests below 35.9 MPa produced DAGG, but only 20% of tests above 35.9 MPa produced DAGG. At 35 and 37 MPa the likelihood of DAGG was 50%.

Examples of test data and microstructures resulting from constant true-stress tests are shown in Figures 5.3 and 5.4. Additional information on each specimen is provided in Appendix D. Figure 5.3 presents strain *versus* time, strain rate *versus* time, and the

microstructure of a specimen tested at 35 MPa (Test # Mo cs 5). The results shown in Figure 5.3(a) and (b) are similar to the schematics of Figure 5.2(c) and (d). This specimen was tested (nearly) to rupture, as indicated by the dramatic increase in strain rate at the end of the test in 5.3(b) and partial specimen fracture shown in 5.3(c). During secondary creep, prior to DAGG initiation, the strain rate is relatively constant and only increases modestly. At DAGG initiation the strain rate begins to increase rapidly for approximately 200 seconds. The cessation of DAGG is observed as a distinct decrease in the rate of strain rate increase. If the test is allowed to continue, as is the case for this test, the strain rate increases from this point until rupture occurs. The increase in strain rate continues gradually before becoming more dramatic near rupture; however, this transition is smooth and does not produce discontinuities. The benefits of using strain rate instead of stress to identify DAGG are clear from comparing Figure 5.3(a) and (b).

Figure 5.4 presents data from a test conducted at 32 MPa (Test # Mo cs 14). Figure 5.4 differs from the schematics of Figure 5.2(c) and (d) and from Figure 5.3 in that the specimen was not tested to failure, but rather halted just following DAGG completion. Figure 5.4(a) shows an increasing rate of true strain *versus* time near the end of the test, which could easily be confused with the start of tertiary creep preceding specimen rupture. However, it is obvious from Figure 5.4(c) that the specimen was not close to rupture. This increase in strain rate corresponds to the occurrence of DAGG. The completion of DAGG is followed by a constant strain rate, as opposed to a continually increasing one as would occur during tertiary creep. The microstructure shown in Figure 5.4(c) confirms DAGG because it shows two DAGG grains spanning nearly the entire gauge length. This also confirms that the change in material behavior is from DAGG and is not the result of SAGG following tensile testing or a stress concentration produced during failure.

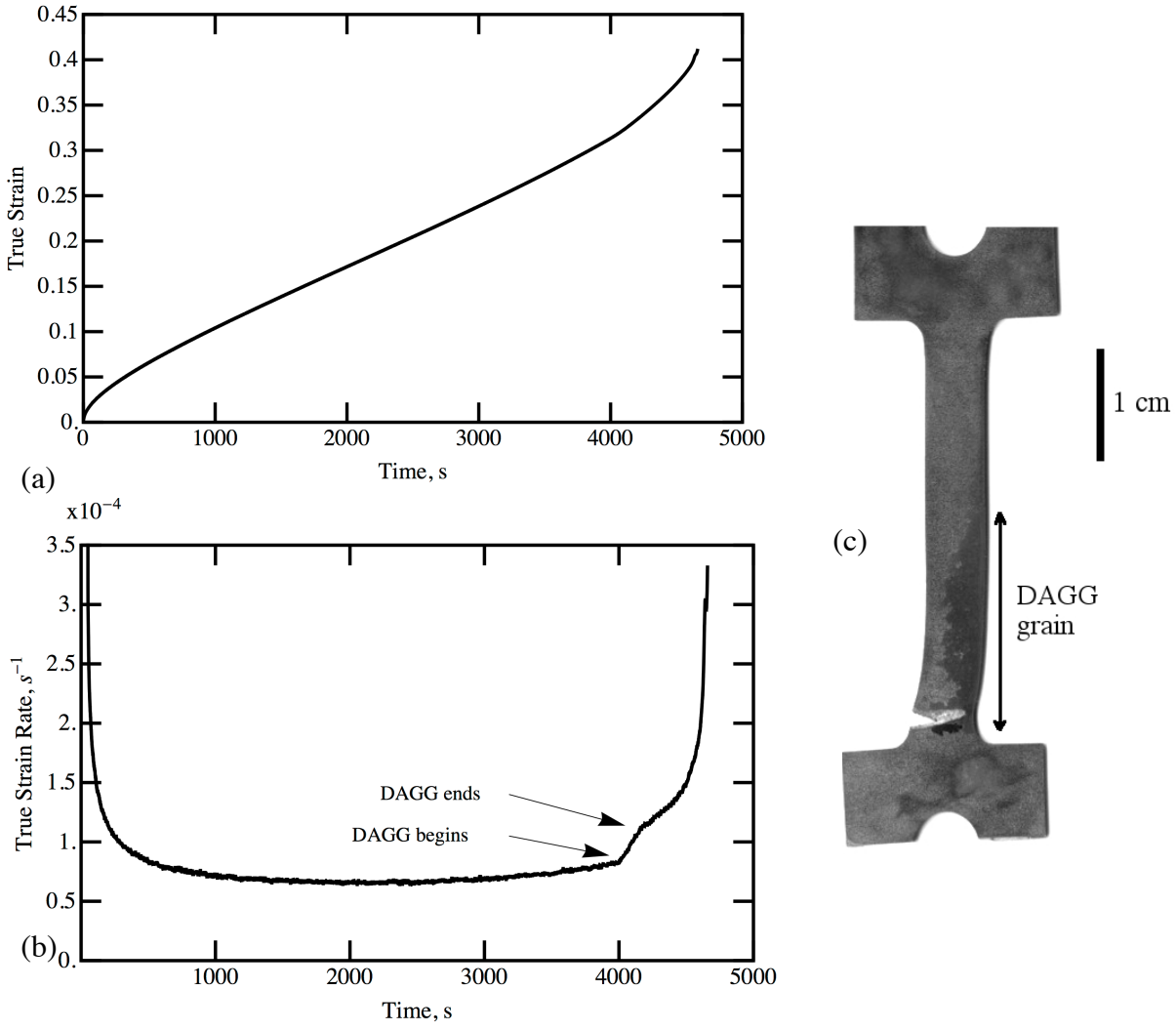

Figure 5.3: Plots of (a) true strain *versus* time, and (b) true-strain rate *versus* time, and (c) an optical image showing the resulting microstructure of a specimen tested just prior to complete rupture (Test # Mo cs 5) are shown. DAGG occurred between approximately 4000 and 4200 seconds. The DAGG grain grew primarily along one edge of one side of the specimen and reached a final length of 21 mm.

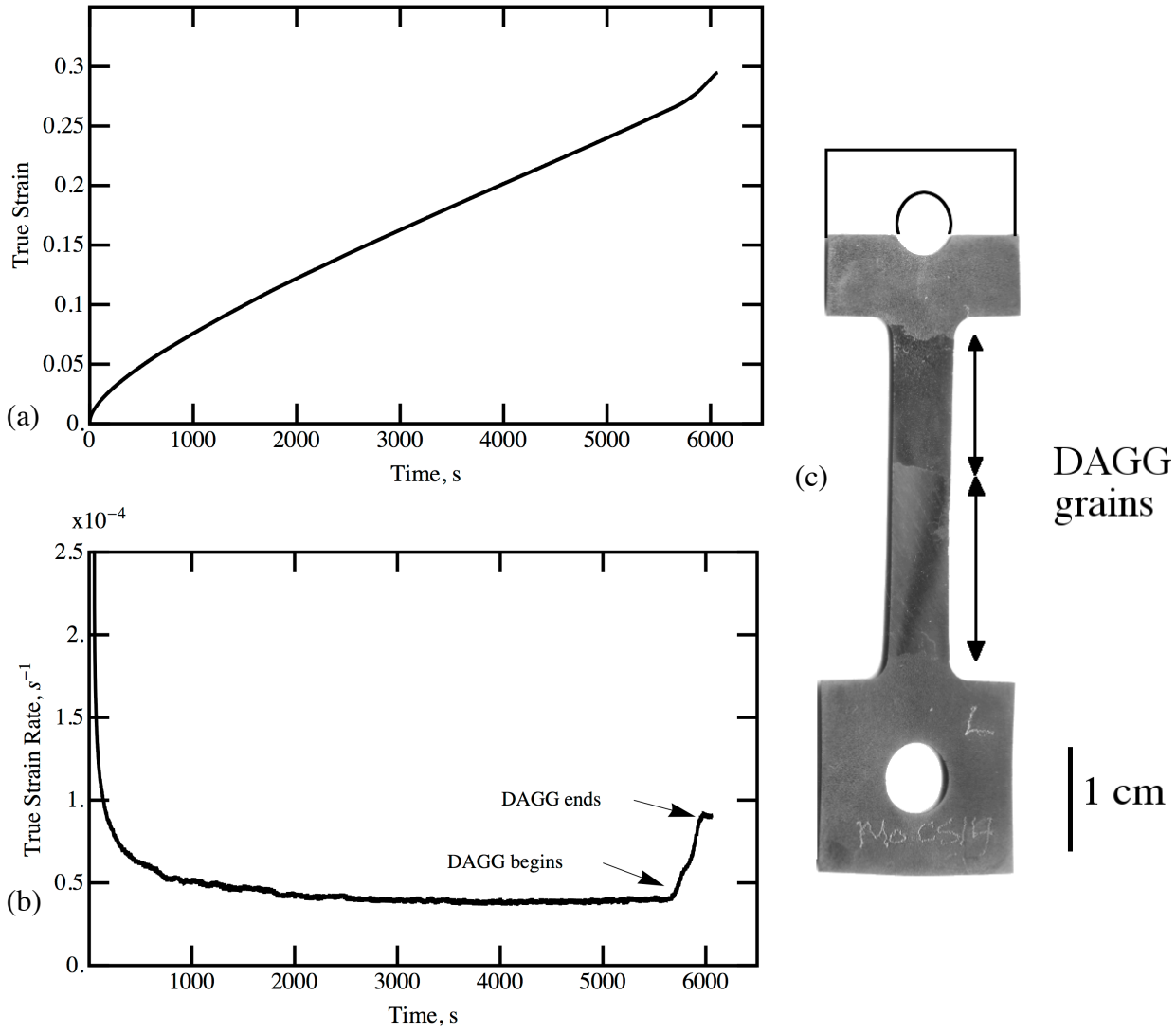

Figure 5.4: Plots of (a) true strain *versus* time, and (b) true-strain rate *versus* time, and (c) an optical image showing the resulting microstructure of a specimen tested just prior to complete rupture (Test # Mo cs 14) are shown. DAGG occurred between approximately 5700 and 6000 s. In this particular case, two DAGG grains grew, as shown in (c). The test was halted prior to rupture.

5.3.1 Orientation of DAGG Grains

The orientations of the DAGG grains produced are shown on the inverse pole figure standard triangles of Figure 5.5(a). These indicate that the DAGG grains produced under constant true stress are of approximately the same orientations as those produced

under constant true-strain rate conditions for the same material, as shown in Figure 5.5(b). Figure 5.5(b) demonstrates the differences in orientation observed between the three Mo materials investigated by Worthington [Worthington 2011].

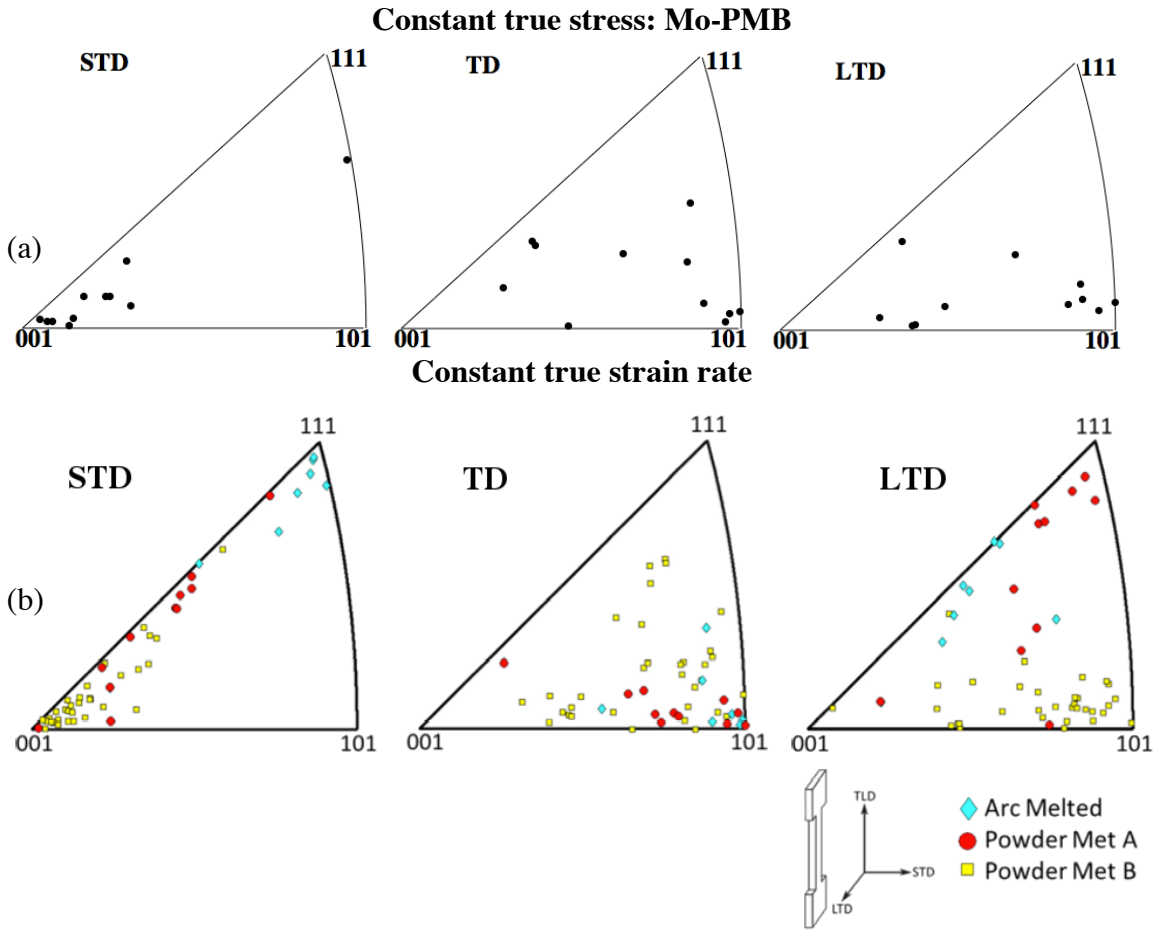

Figure 5.5: Inverse pole figures show orientations, relative to the short transverse (STD), tensile (TD), and long transverse (LTD) specimen directions, of (a) DAGG grains produced under constant true stress conditions and (b) under constant true-strain rate conditions. Figures in (b) are from [Worthington 2011].

5.3.2 Effect of Applied Stress

The strain rate at DAGG initiation increased with the applied true stress, as shown in Figure 5.6. The strain rate at DAGG initiation is very closely related to the strain rate

during steady-state creep, which sometimes occurs just prior to DAGG initiation. Increasing applied stress is expected to increase the strain rate observed during steady-state creep. This relationship between strain rate and flow stress is thought the result of normal creep behaviors, not a result specific to DAGG. The data of Figure 5.6 can be used to calculate the stress exponent, n from Eq. 5.6, for this material as the slope of the logarithm of strain rate *versus* the logarithm of stress. This calculation provides $n = 5.3 \pm 0.4$, which is consistent with the stress exponent of 5 that expected for polycrystalline Mo [Ciulik 2007]. The strain rates ranged from approximately 2×10^{-5} to 8×10^{-5} s^{-1}, which are similar to the strain rates that produced DAGG in Mo during constant true-strain rate tests [Ciulik 2005, 2009; Worthington 2011, 2013]. Ciulik and Worthington observed a decrease in both initiation strain and stress at initiation as temperature increased [Ciulik 2005, 2009; Worthington 2011, 2013]. They did not observe any effect of strain rate on the DAGG initiation strain in Mo. These previous conclusions are consistent with the present results for Mo.

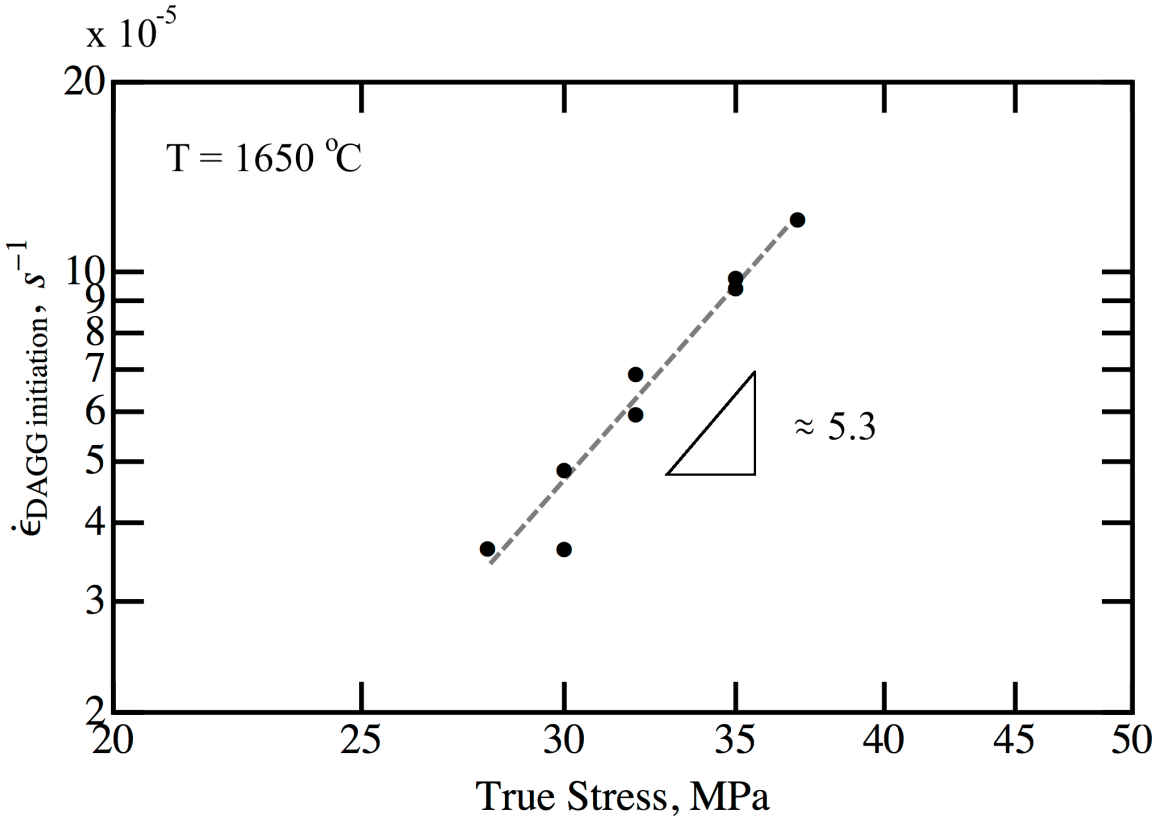

Figure 5.6: DAGG initiation true-strain rate is plotted *versus* applied true stress for eight (8) Mo specimens.

A linear correlation coefficient between strain at DAGG initiation as applied stress is -0.18, indicating that no correlation exists. A correlation coefficient above 0.8, or below -0.8, generally indicates a strong correlation between two parameters, while a coefficient between -0.5 and 0.5 indicates a weak or no correlation [Pearson 1896]. Thus, the average strain at DAGG initiation under constant true stress is roughly constant, and is 0.259 ± 0.074 at 1650°C. This is slightly larger (0.107) than the average for the same material and temperature using constant true-strain rate tensile test [Worthington 2011]. This difference may be because the constant true-strain rate tests were performed at 10^{-4} s^{-1}, whereas the constant true stress tests produced slightly slower strain rates prior to DAGG initiation, as indicated in Figure 5.6. The slower strain rates allow more time for

recovery to occur, which increases the strain required to initiate DAGG. The amount of time prior to DAGG initiation decreases with increasing stress, with a linear correlation coefficient between time and stress of -0.75. This is expected since higher stresses produce faster strain rates, and the critical strain is roughly constant.

Because the strain rate is constantly changing during DAGG under constant true stress, the average strain rate, calculated from the initiation and completion times and strains for DAGG, can only be compared between tests that were conducted to DAGG completion, or nearly to completion. Attempts were made to halt tests near the end of DAGG without straining past the point of DAGG completion, but it is not always clear when DAGG is complete while conducting a test. Microstructural observations post-test indicated that five of the specimens had a DAGG grain, or grains, consume at least 80% of their gauge length. One of these specimens, however, did not grow across the width of the specimen, and at least one other did not grow through the thickness of the specimen along its entire length. It is unclear whether growth through the width and thickness of the gauge affects growth in the tensile direction.

The relationship between the time elapsed from DAGG start to DAGG finish and the strain accumulated during that time is shown in Figure 5.7 for the five specimens for which DAGG was at least 80% complete. The applied constant stress, in MPa, is indicated by color. In general, a higher applied stress produces a greater strain accumulation during DAGG. This becomes clearer when a linear fit is applied at each constant stress for accumulated strain *versus* time, assuming that the accumulated strain must be zero when the elapsed time is zero. The rate of strain accumulation during DAGG increases as applied stress increases. Higher applied stresses are also associated with a higher strain rates during secondary creep and at DAGG initiation, as observed in Figure 5.6. The strain rates observed during DAGG follow a similar trend. The

relationship between the logarithm of applied stress and the logarithm of the rate of strain accumulation during DAGG is shown in Figure 5.8 to be nearly linear. A stress exponent of 4.7 ±1.0 is calculated from this fit, which is slightly lower than 5, as observed in the polycrystalline material; however, this the standard deviation implies that this difference may not be significant. The stress exponent of the polycrystalline material is calculated using data just prior to DAGG initiation and the stress exponent of the single crystal would be calculated from data just after DAGG completion. Thus, this stress exponent represents the intermediate condition when the microstructure is transforming from polycrystalline to a single crystal.

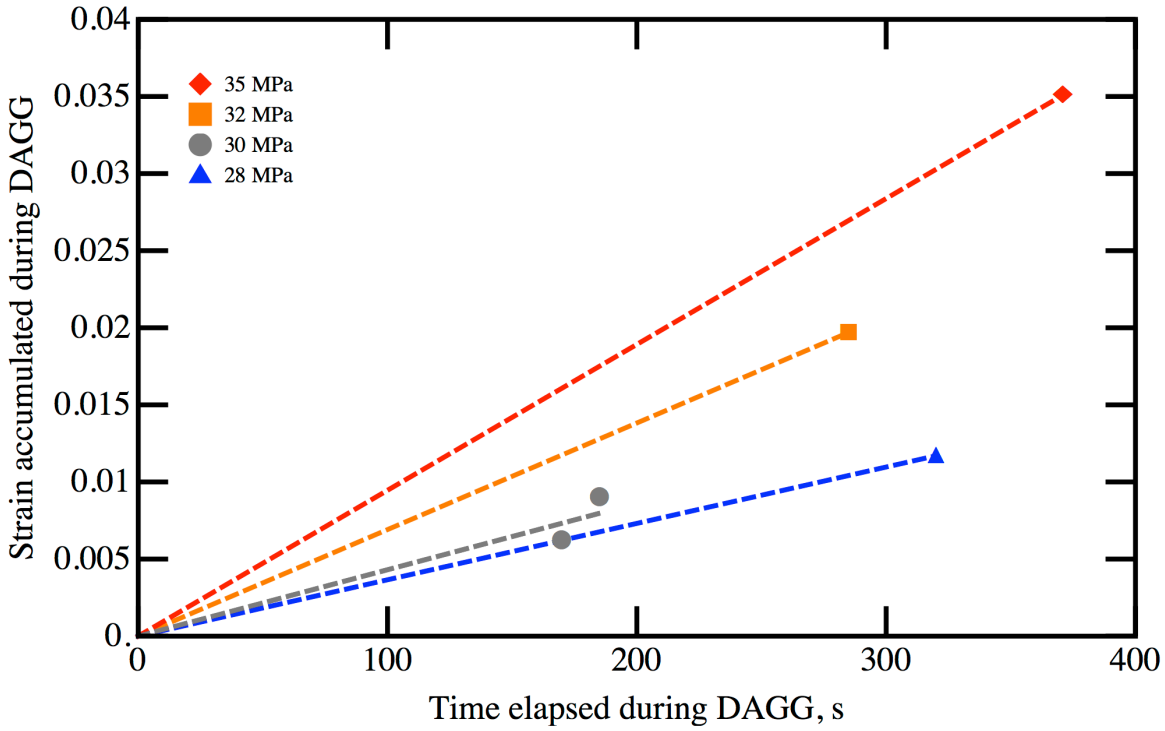

Figure 5.7: The strain accumulated during DAGG is plotted *versus* the time elapsed during DAGG for five (5) Mo specimens that DAGG was at least approximately 80% complete. The color code indicates constant true stress, in MPa, for each data point.

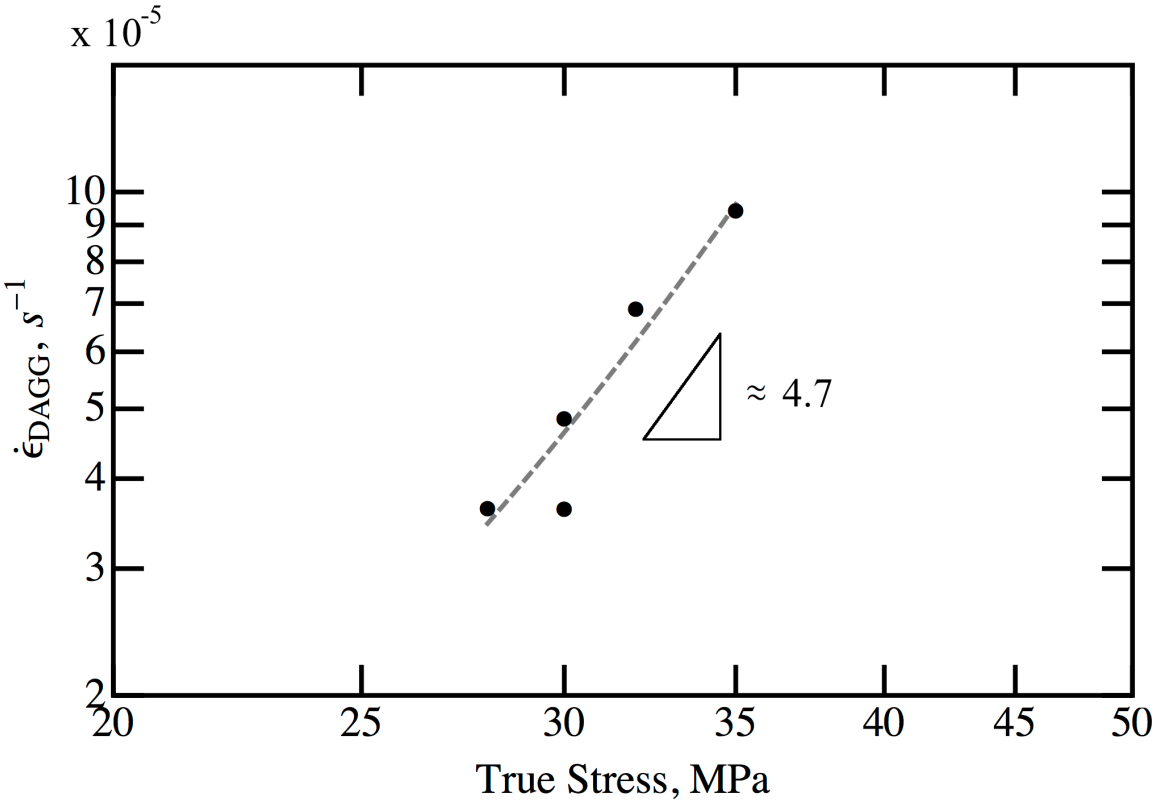

Figure 5.8: Rate of strain accumulation during DAGG is plotted *versus* applied true stress for five (5) Mo specimens that DAGG was at least approximately 80% complete.

5.3.3 DAGG Grain Size and Boundary Velocity

Following testing, microscopy was performed on all specimens that exhibited any indications of DAGG in the strain rate *versus* time data. Of the fifteen specimens tested, eight exhibited DAGG and five had DAGG grow at least nearly to completion. Of these five, one grew more than one DAGG grain and at least one other exhibited DAGG growth primarily on one side of the specimen. The preferential growth of DAGG on one side of the specimen was commonly observed in Mo-PMB by Worthington [Worthington 2011]. The preferential growth on the surface may be due to surface energy differences or variations of texture or grain size through the thickness of the material.

The length of the DAGG grain was measured along the tensile direction. In cases where more than one DAGG grain formed, the cumulative length of the DAGG grains is considered. The DAGG boundary migration distance of each boundary is unknown; however, a range of possible migration distances can be calculated for which the boundaries in each specimen must fall. The boundary migration distance is at a maximum if only one boundary migrates at a time, and is simply the length of the DAGG grain, or grains, in the tensile direction. The lower limit for migration distance is calculated by assuming that all boundaries of each DAGG grain are migrating at the same time, and is $l/(2*n_d)$ where l is the length of the DAGG grain, or grains, and n_d is the number of DAGG grains. These minimum and maximum values define the ranges presented in the subsequent analysis.

The DAGG grain boundary migration distance is plotted *versus* the strain accumulated during DAGG in Figure 5.9. DAGG migration distance appears to increase with accumulated strain, and a linear correlation is suggested by its correlation coefficient of 0.94. In §5.2 it was proposed that the DAGG migration distance is proportional to the strain accumulated during DAGG (Eq. 5.5). Following this reasoning, it is reasonable to assume that the DAGG grain will not have traveled a significant distance when no strain has been accumulated. A linear fit suggests that the size of the DAGG grain at zero strain is approximately 16 mm, before growing linearly with accumulated strain. Thus, a linear fit may not be applicable for all values of accumulated strain under the condition of constant true stress. The model from §5.2 was formed from observations under constant true strain rate, but the continually varying strain rate in the present tests may prohibit a direct comparison between the former and present tests since the strain rate may affect the velocity of the DAGG boundary.

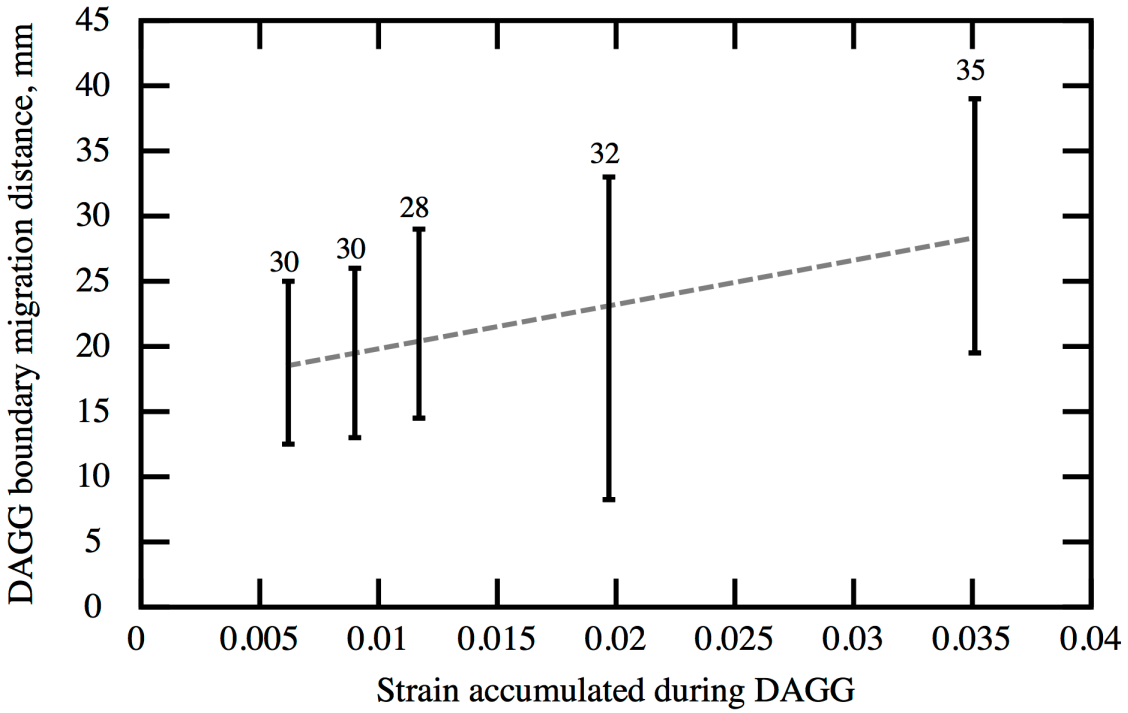

Figure 5.9: DAGG boundary migration distance is plotted *versus* the strain accumulated during DAGG for five (5) Mo specimens for which DAGG was at least 80% complete, as determined by microstructural analysis. Labels indicate applied true stress, in MPa. The range of possible DAGG boundary migration distances observed in each of the specimens is shown.

The average velocity of each DAGG grain boundary is $v = d/t$, where d is the DAGG boundary migration distance range as defined previously, and t is the time elapsed during DAGG. The velocity of the DAGG grain boundary was not significantly affected by applied stress, as shown in Figure 5.10 and indicated by the correlation coefficient of -0.15. From Eq. 5.7 it was postulated that increasing the applied strain may increase the velocity of the DAGG boundary, but this does not appear to be true for the range of stresses investigated here. The models proposed in §5.2 suggest that DAGG boundary velocity and stress are related by a stress exponent, which defines whether the DAGG process is stress driven or strain enhanced; however, the data indicate that DAGG boundary velocity is relatively constant, and independent of applied stress. Additionally,

these models assume that the velocity of the boundary and the mobility are independent, which may not be true for all cases, such as when solute drag effects are prominent [Humphreys 2004 p.337].

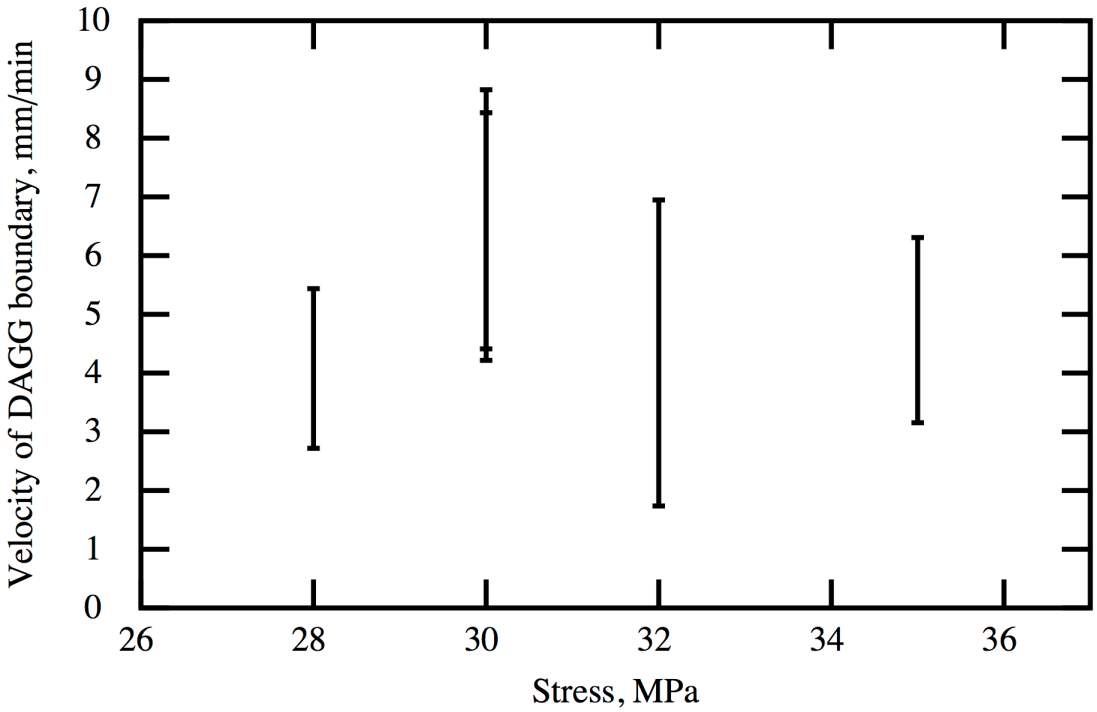

Figure 5.10: The velocity of the DAGG boundary is plotted *versus* applied stress during DAGG for five (5) Mo specimens for which DAGG was at least 80% complete, as determined by microstructural analysis. Labels indicate applied true stress, in MPa. The range of DAGG boundary velocities are calculated from the range of possible DAGG boundary migration distances and time elapsed during DAGG for each specimen.

Since the strain rate is continually changing, it may not be accurate to compare the calculated velocity with a singular value for strain rate (i.e. the starting, final, or average strain rate). The DAGG boundary velocity is believed to be proportional to strain rate, thus the velocity would continuously increase as the strain rate increases. Specimens whose strain rates increased at a faster or slower rate may have different average calculated velocities but the same average strain rate. Comparing only those

specimens that grew nearly to completion should reduce these differences, but will not eliminate them.

The failure of DAGG to continue to completion, preferential growth along a surface, and initiation of multiple grains may all potentially affect the analysis of the constant true stress tests. A larger sample size with consistent microstructural features and tensile behavior would be advantageous to confirm the trends observed.

5.4 CONCLUSIONS

DAGG was observed in Mo sheet tested at 1650 °C under constant true stress. Of 15 specimens tested with a constant true stress between 28 and 40 MPa, 8 produced DAGG. Few clear trends were observed between DAGG initiation strain, accumulated strain during DAGG, DAGG grain size, stress, and DAGG boundary velocity. Overall, the data exhibit much more variation than was observed for constant true-strain rate tests. Although the data show significant scatter, the results of these tests are as follows:

1. The observed strain rate prior to DAGG initiation and during DAGG is directly related to the applied stress, with higher stress resulting in faster strain rates.
2. Higher applied stresses cause a larger increase in the strain rate from DAGG start to finish, i.e. a larger DAGG induced increase in strain rate.
3. A minimum applied stress and strain rate may exist for the initiation of DAGG.
4. The velocity of DAGG grain boundaries is not definitively correlated to the applied stress.
5. The resulting length of the DAGG grain is possibly related to the amount of strain accumulated during DAGG.

6 DAGG in Ta-A

DAGG was initiated and propagated in Ta under constant true-strain rates at elevated temperatures. Specimens were tested until either rupture or shortly after the point when the stress begins to drop rapidly. This point at which stress first drops defines the stress at DAGG initiation and the strain at DAGG initiation, or critical strain. In this chapter, observations of DAGG in Ta will be presented and discussed, including the effects of temperature, strain rate, and crystallographic orientation relative to the specimen geometry on DAGG initiation and propagation. A list of experimental conditions and a summary of test results from tensile tests are provided in Table 6.1. Additional information on each test is provided in Appendix E.

Table 6.1: Summary of tests conducted for Ta sheet.

Specimen number	Temperature	True-strain rate	Stress at DAGG initiation	Critical true strain	Largest DAGG grain size	Number of DAGG grains
	°C	10^{-4} s^{-1}	MPa		mm	
1	1850	1.0	7.24	0.159	39	1
2	1850	1.0	*	0.186	12	4
3	1850	1.0	*	*	5	>7
4	1850	1.0	*	*	18	2
5	1850	1.0	*	0.222	15	1
6	1850	1.0	7.83	0.147	15	4
7	1750	1.0	9.81	0.231	21	3
8	1800	1.0	8.93	0.235	16	2
9	1850	1.0	*	*	5	6
10	1750	0.8	8.07	0.205	6	2
11	1650	1.0	*	0.196	4	2
12	1550	1.0	18.44	0.178	3	7
14	1850	5.0	10.90	0.266	11	6
15	1850	3.0	8.51	0.270	8	4
16	1850	2.0	8.32	0.219	9	3
17	1850	2.0	8.04	0.257	10	3
18	1650**	0.5	10.61	0.238	12	3
19	1650**	0.3	9.18	0.206	24	1
20	1450	0.3	24.17	0.215	8	>7
21	1650	0.3	*	0.179	20	1
22	1550	0.3	17.85	0.170	7	4
23	1750	0.3	9.71	0.200	8	1
24	1850	0.3	6.37	0.311	5	2
25	1650	0.3	*	*	17	2
26	1650	0.3***	10.5***	0.224	4	2
27	1750	0.3	8.60	0.126	4	1
28	1550	0.3	16.54	0.162	4	4
29	1750	0.3	8.76	0.174	*	*
30	1650	0.3	14.22	0.155	5	2
31	1650	0.3	13.03	0.163	3	1
32	1650	0.3	12.25	0.167	2	3
33	1650	0.3	12.73	0.164	3	1
34	1650	0.3	13.27	0.183	10	2
35	1650	0.3	12.75	0.198	7	3
36	1650	0.3	13.12	0.162	7	2
37	1650	0.3	12.42	0.184	6	2
38	1750	0.3	9.15	0.247	18	2
39	1750	0.3	10.64	0.282	8	1
41	1650	1.0	16.43	0.265	5	7
42	1650	1.0	17.70	0.177	6	4
43	1650	2.0	19.89	0.234	5	7
44	1650	0.2	12.90	0.213	12	3
45	1650	2.0	17.73	0.239	4	4
46	1650	0.5	13.38	0.278	12	5
47	1650	0.2	12.07	0.202	7	2
48	1550	1.0	20.69	0.231	6	5
49	1800	1.0	10.68	0.194	12	2
50	1850	0.3	6.79	0.202	9	4

* Data not available or DAGG drop not identifiable

**Data unreliable due to thermocouple failure following test and inconsistent tensile behavior.

*** Tensile data indicate that loading pin may have shifted during testing

An example of a large grain produced by DAGG in Ta at 1850 °C under a constant true-strain rate of 1×10^{-4} s^{-1} is presented in Figure 6.1(a). This DAGG grain consumed the entire gage length of the specimen. Laue back-scatter diffraction was performed at each end of the DAGG grain to confirm the presence and continuity of the single crystal along the length of the specimen. Figure 6.1(b) shows the corresponding true stress *versus* true strain data and indicates where DAGG initiates and terminates. The test continued following completion of DAGG but was halted prior to specimen rupture.

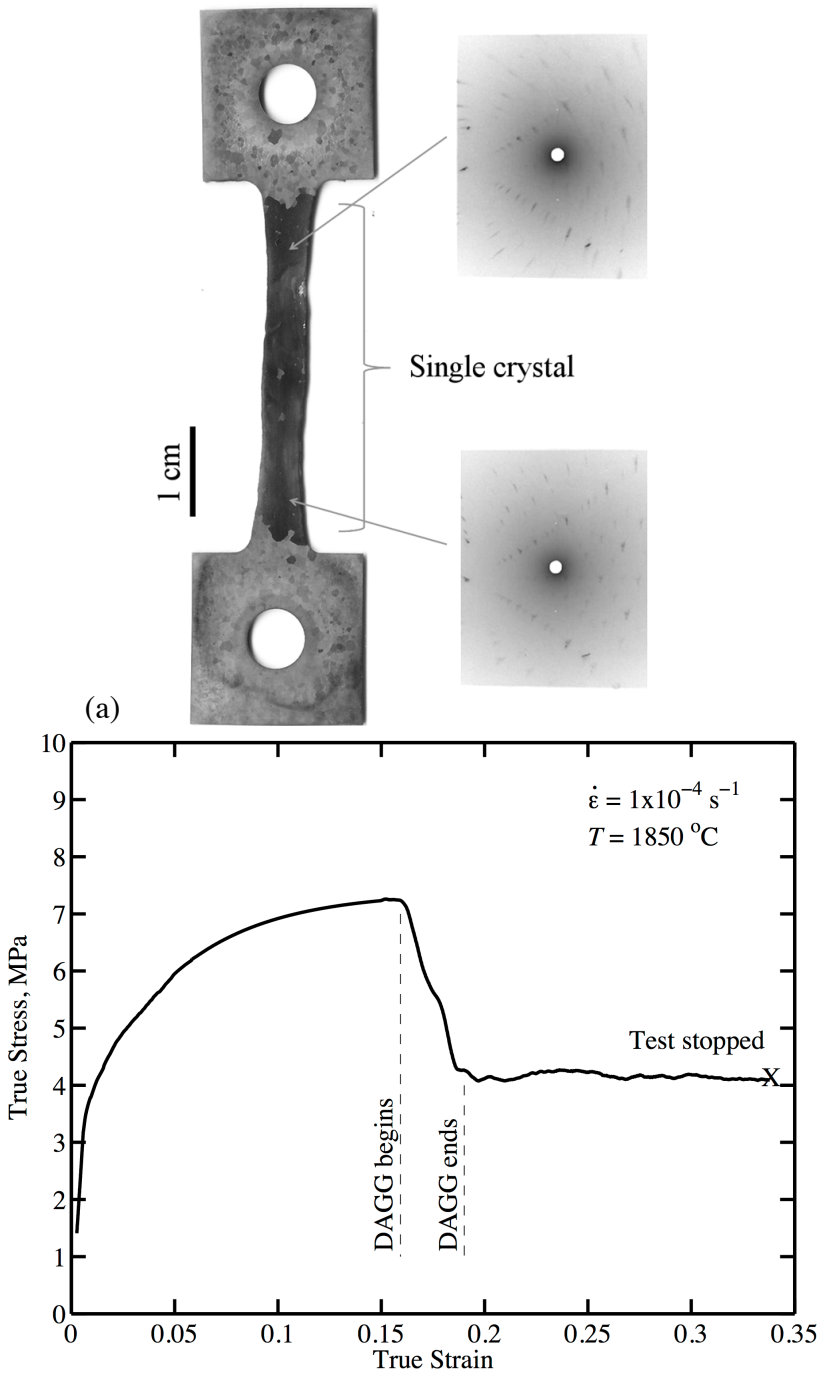

Figure 6.1: The Ta specimen in (a) evidences a DAGG grain produced at 1850°C. Laue X-ray back-scatter diffraction images are shown from the extremes of the single-crystal region to demonstrate that the DAGG grain has a single orientation. The corresponding true stress *versus* true strain tensile test data in (b) show a rapid drop in stress at approximately 0.15 true strain, indicating initiation and growth of the DAGG grain.

6.1 EFFECT OF TEMPERATURE AND STRAIN RATE ON DAGG INITIATION

Data for tests conducted at 1550, 1650, 1750 and 1850 °C and strain rates of 1×10^{-4} and 3×10^{-5} s^{-1} are shown in Figure 6.2. All tests shown were halted prior to rupture except for one at 1850 °C and 1×10^{-4} s^{-1}, which ruptured at approximately 0.45 true strain. Figure 6.2 demonstrates a general decrease in the flow stress at DAGG initiation with increasing temperature. Steady-state creep is generally not observed at temperatures of 1650 °C and lower. The flow stress plateaus only at higher temperatures. However, the data suggest that a steady-state flow stress may be achieved at 1750 °C.

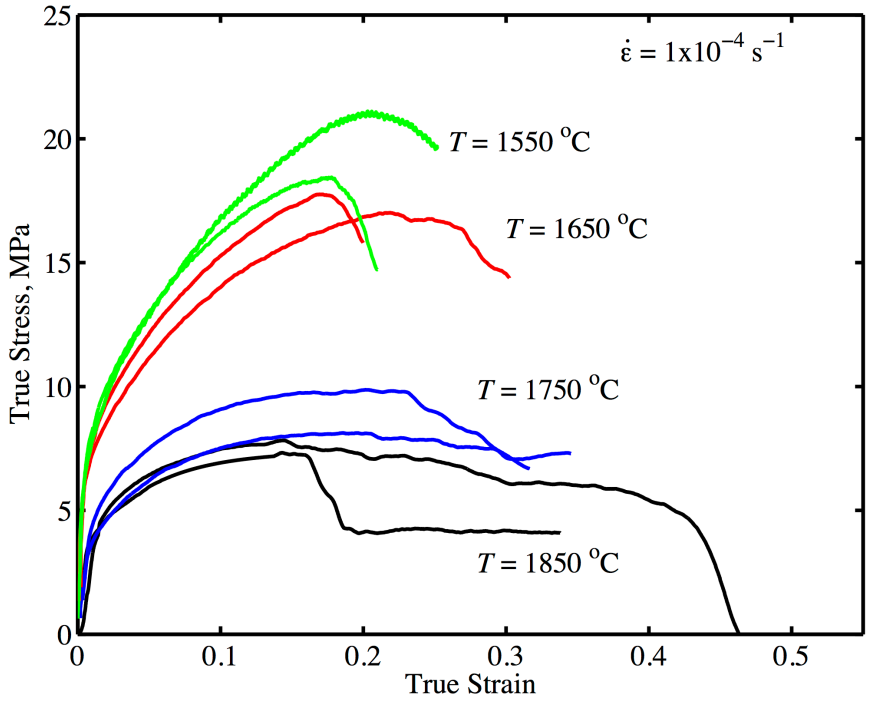

(a)

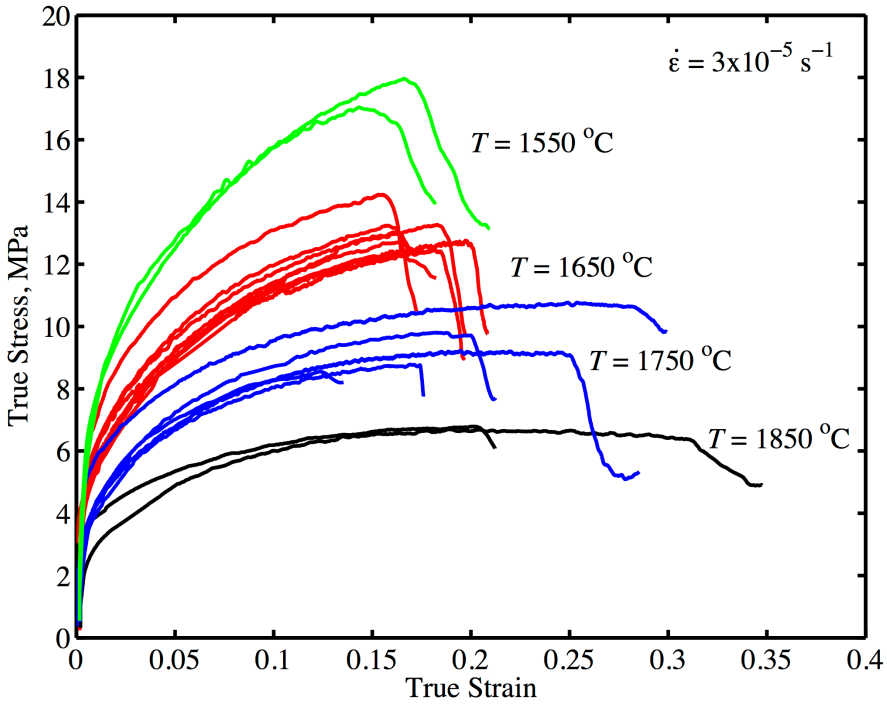

(b)

Figure 6.2: True stress *versus* true strain data are shown for Ta tests conducted at temperatures of 1550, 1650, 1750 and 1850 °C at strain rates of (a) 1×10^{-4} s^{-1} and (b) 3×10^{-5} s^{-1}.

These data demonstrate that the drop in stress from DAGG is often not a single rapid drop but may be a gradual decrease or consist of multiple drops. The variations in hardening rate and steady-state flow stress in Ta are greater than those observed for Mo-PMA and Mo-PMB [Ciulik 2009, Worthington 2011]. These variations between stress-strain data curves obtained under the same testing conditions may be due to inhomogeneities in the material or small variations in the temperature of the furnace. Maag and Mattson reported that small changes in composition or thermomechanical history could have a notable effect on the creep behavior of several refractory metal alloys [Maag 1969]. Green reported annealing creep specimens for 8 hours prior to creep testing to reduce variations in the creep rate of commercial-purity Ta due to changing chemical composition with respect to carbon, oxygen, nitrogen, and hydrogen [Green 1965].

The temperature difference required to produce the observed differences in the steady state flow stress for two tests at the same strain rate can be calculated using a relationship derived from the Zener-Holloman parameter,

$$\sigma \propto \exp\left(\frac{Q}{RT}\right). \qquad \text{Eq. 6.1}$$

The flow stresses obtained in two separate tests can be compared using the relation

$$\frac{\sigma_1}{\sigma_2} = \frac{\exp\left(Q/RT_1\right)}{\exp\left(Q/RT_2\right)}. \qquad \text{Eq. 6.2}$$

If T_1 and Q are known, solving for T_2 provides the furnace temperature required to account for the known ratio of σ_1 to σ_2. The steady-state flow stress at each temperature and strain rate can be compared to the average flow stress for all tests under the same conditions. The average temperature difference required (T_1 - T_2) to account for the variation about the mean flow stress observed for a given test condition is ±3.85 °C for the data presented in Figure 6.2. The largest variation in flow stress was observed at

1750 °C and 3×10^{-5} s^{-1}, and this would require a temperature variation of 9.0 °C from the set-point. The required temperature variations are within or near the uncertainty of the temperature measurements described in Ch. 3. Other factors, such as varying annealing time or inhomogeneities in the composition of the starting material may also be a factor.

6.1.1 Effects of Temperature on DAGG Initiation

Because DAGG proceeds by grain-boundary migration, a thermally activated process [Burke 1952, Gottstein 2009], it is important to study the effects of temperature on DAGG. Both the critical strain and the flow stress immediately prior to DAGG initiation in Mo depend on temperature [Ciulik 2005, 2009; Worthington 2011, 2013]. These effects are considered here for Ta. The rate of boundary migration in Mo following DAGG initiation depends strongly on the rate of plastic strain accumulation [Worthington 2011, 2013]. The effect of strain rate is, thus, potentially important.

Although the strain at which DAGG initiates, the critical strain, is a strong function of temperature in Mo [Worthington 2011, 2013], this relationship is not apparent in the data from Ta. Figure 6.3 presents the critical strain for DAGG as a function of temperature. There is no temperature dependence evident for the average critical strain. However, the scatter in critical strain values generally increases with increasing temperature. This is potentially a result of normal grain growth prior to DAGG decreasing the total number of grains in the specimen, thus decreasing the number of grains susceptible to abnormal grain growth. This effect of normal grain growth increases with increasing temperature. With fewer well-suited grains available for DAGG initiation, the critical strain observed for DAGG at a given temperature and strain rate will vary more widely between tests. This is a direct result of the statistics of small

numbers for nucleation (initiation) sites. To demonstrate this effect, Figure 6.4 shows the relationship between the standard deviation of the critical strain and the grip region grain size. The standard deviation of the critical strain clearly increases with grain size, which increases with temperature because of normal grain growth.

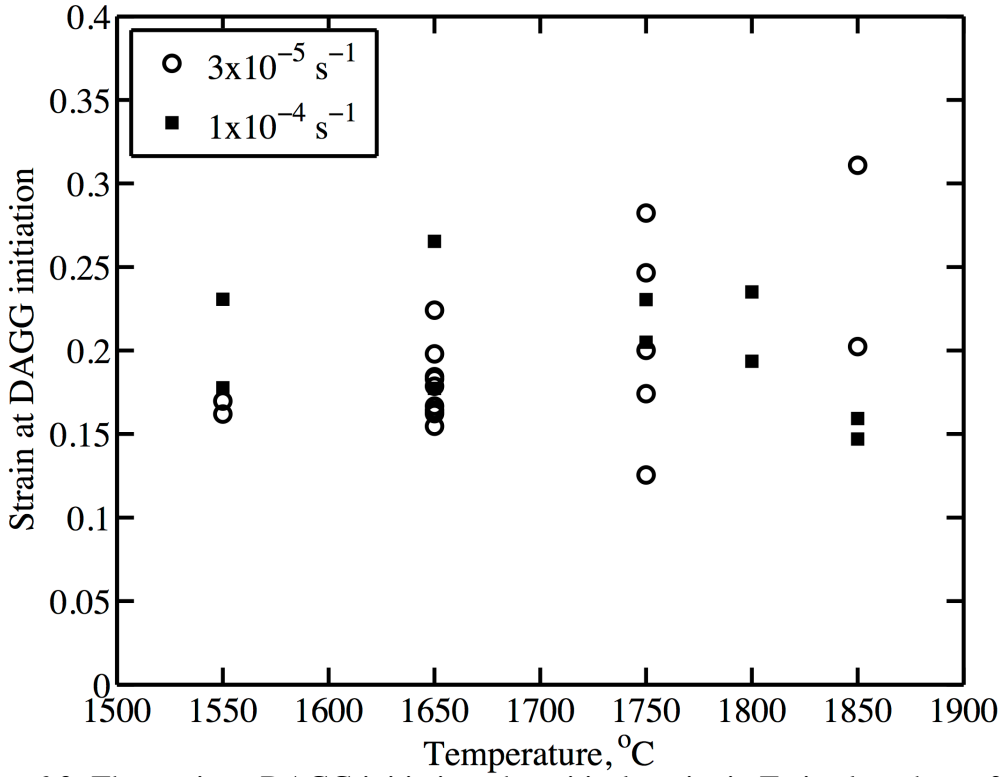

Figure 6.3: The strain at DAGG initiation, the critical strain, in Ta is plotted as a function of temperature for two strain rates.

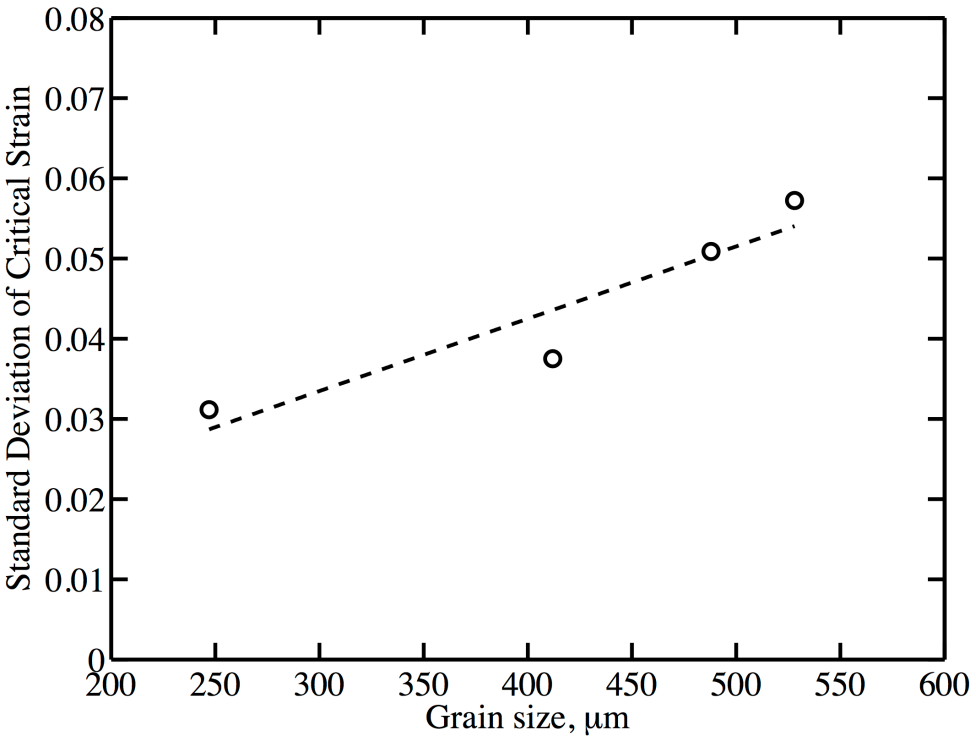

Figure 6.4: The standard deviation of the critical strain in Ta is plotted as a function of grain size in the grip region. Standard deviations are calculated from sample sizes (number of tests producing a critical strain measurement) of 4 to 17. Average grain size is calculated after annealing for approximately 2 to 3 hours at the temperature corresponding to each calculation.

The effect of temperature on the flow stress observed at DAGG initiation is shown in Figure 6.5. This flow stress decreases with increasing temperature for both strain rates shown. This is an expected result of increasing temperature decreasing the creep flow stress and is not thought to be associated with the mechanisms of DAGG initiation. Figure 6.5 illustrates that strain rate has a small, but noteworthy, effect on stress, with slightly higher stresses produced at the faster rate.

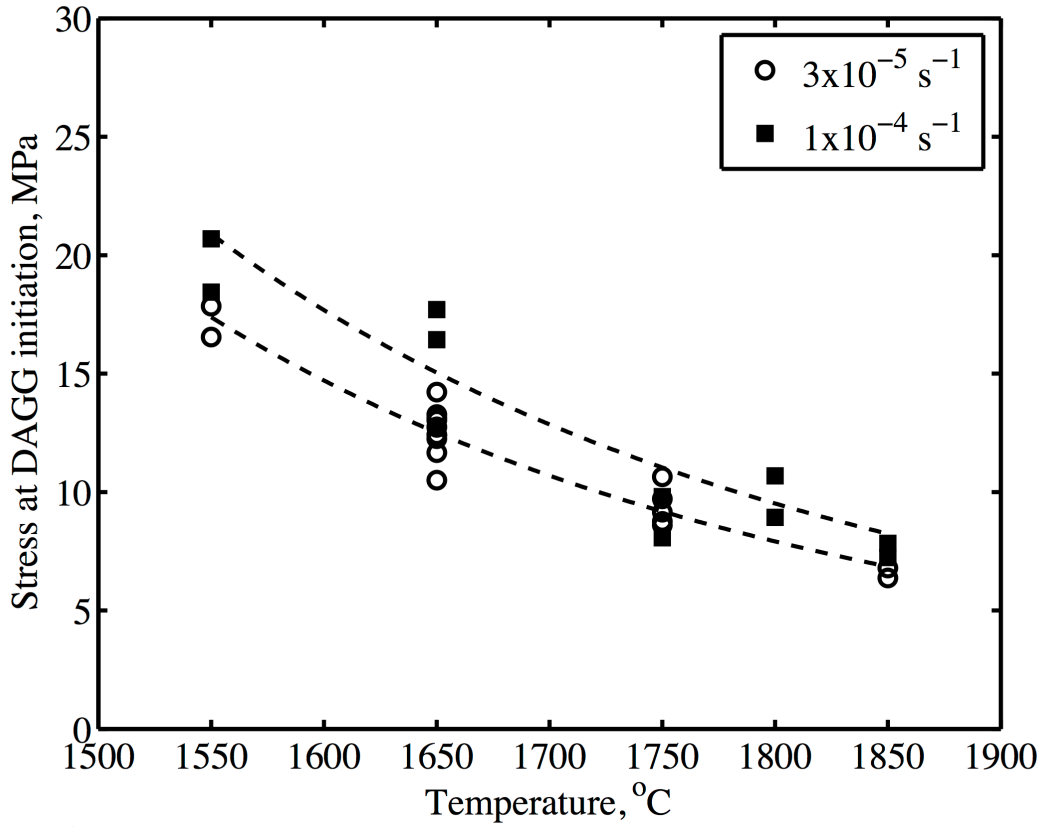

Figure 6.5: The flow stress immediately prior to DAGG initiation in Ta is plotted *versus* temperature for strain rates of 3×10^{-5} and 1×10^{-4} s^{-1}.

6.1.2 Effects of Strain Rate on DAGG Initiation

Figures 6.6 and 6.7 show the effect of strain rate on the flow stress at DAGG initiation and critical strain, respectively. As shown in Figure 6.6, the flow stress increases slightly with increasing strain rate, which is consistent with the theory of creep at constant temperature [Zener 1944]. The stress is a stronger function of strain rate at 1650 °C than at 1850 °C. These observations are not thought to be related to the mechanisms of DAGG initiation, but rather to those of creep deformation. Figure 6.7 shows the critical strain versus strain rate for tests at 1650 and 1850 °C. This plot

indicates that critical strain is not a function of strain rate because critical strain does not demonstrate any consistent variation with either strain rate or temperature.

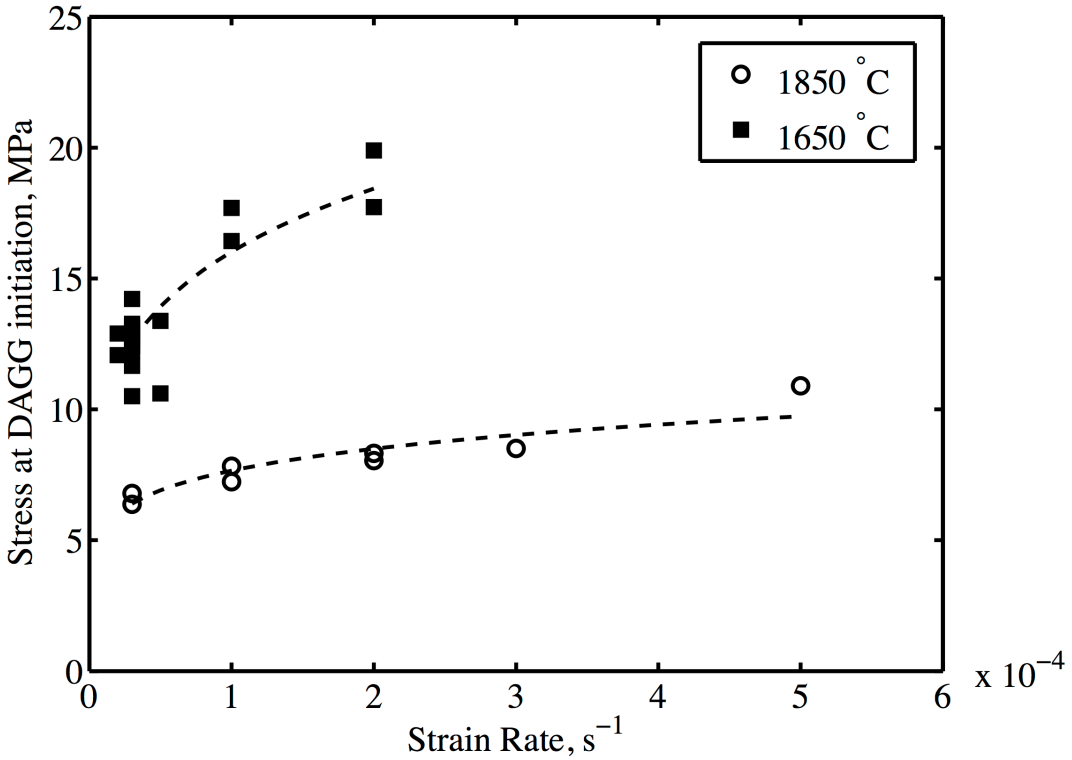

Figure 6.6: The flow stress immediately prior to DAGG initiation in Ta is plotted *versus* strain rate for constant temperatures of 1650 and 1850 °C.

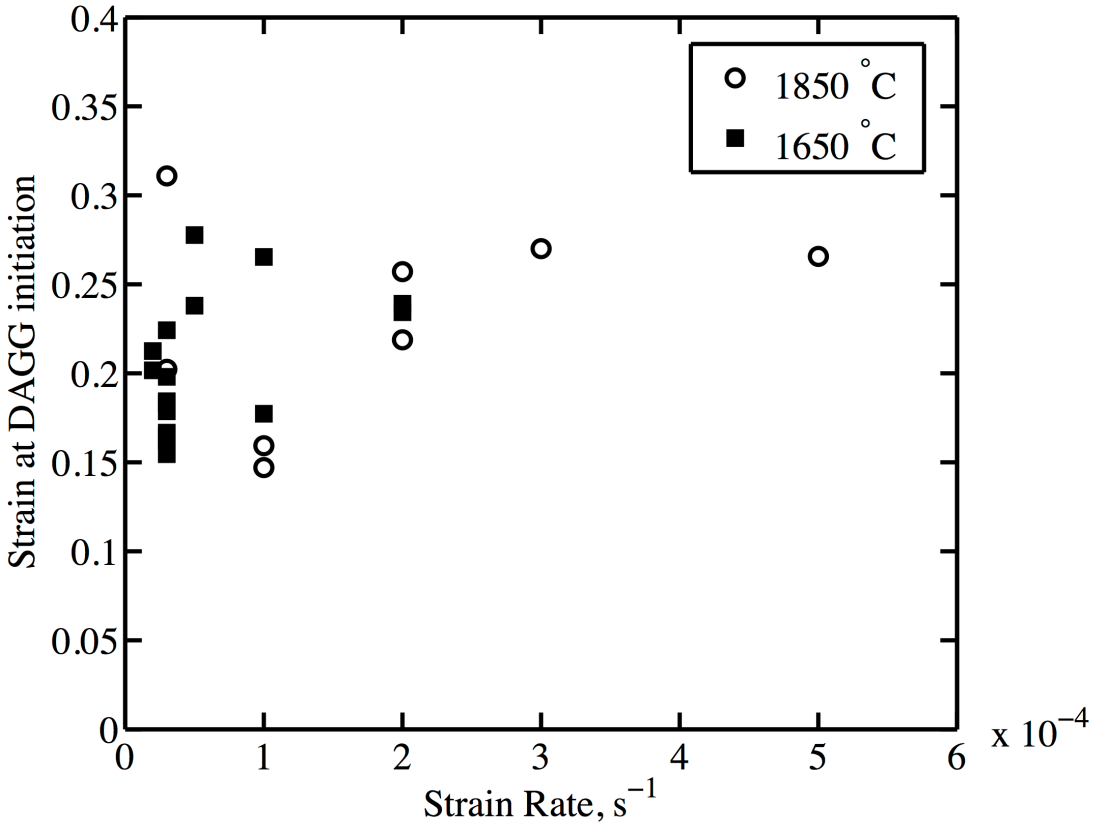

Figure 6.7: The strain at DAGG initiation in Ta is plotted *versus* strain rate at temperatures of 1650 and 1850 °C.

6.2 CREEP DEFORMATION OF TA

Creep theory states that the steady-state flow stress will increase with increasing strain rate and decrease with increasing temperature [Zener 1944, Sherby 1967]. The activation energy and stress exponent for creep in the range of temperatures and strain rates investigated can be calculated from the available Ta data, and these are expected to be approximately constant across the test conditions.

Tensile tests did not always reach steady state prior to DAGG initiation. In order to estimate the steady-state flow stress for such cases, the data are characterized using the

Voce fit hardening law [Kocks 1976; Voce 1948, 1955] by fitting the tensile data to the equation

$$\sigma = \sigma_{sat.} + (\sigma_o - \sigma_{sat.}) \exp[\, -(\varepsilon - \varepsilon_o)/\, \varepsilon_c] \,, \qquad \text{Eq. 6.3}$$

where σ is the observed flow stress; $\sigma_{sat.}$ is the saturation stress, an approximation of the steady-state flow stress; σ_o is the yeild stress; ε is the applied strain; ε_o is the strain at the start of the test, assumed to be zero; and ε_c is a characteristic strain value that is a measure of the hardening rate.

The Zener-Holloman parameter (Eq. 2.1) can be used to calculate the stress exponent from tensile data collected at identical temperatures but varying strain rates. By only considering data at one temperature, Eq. 2.1 is simplified to

$$\dot{\varepsilon} \propto \left(\frac{\sigma}{E}\right)^n \,. \qquad \text{Eq. 6.4}$$

The stress exponent is calculated by plotting $\log(\dot{\varepsilon})$ *versus* $\log(\sigma/E)$ and measuring the slope of the data. This was done for data collected at 1650 °C at strain rates from 2×10^{-5} to 2×10^{-4} s^{-1}, as shown in Figure 6.8, using the σ_{sat} values calculated from Eq. 6.3. A stress exponent of approximately 3.9 ± 0.3 is calculated, which is consistent with the value of 3.9 determined by Green for commercial purity Ta [Green 1965].

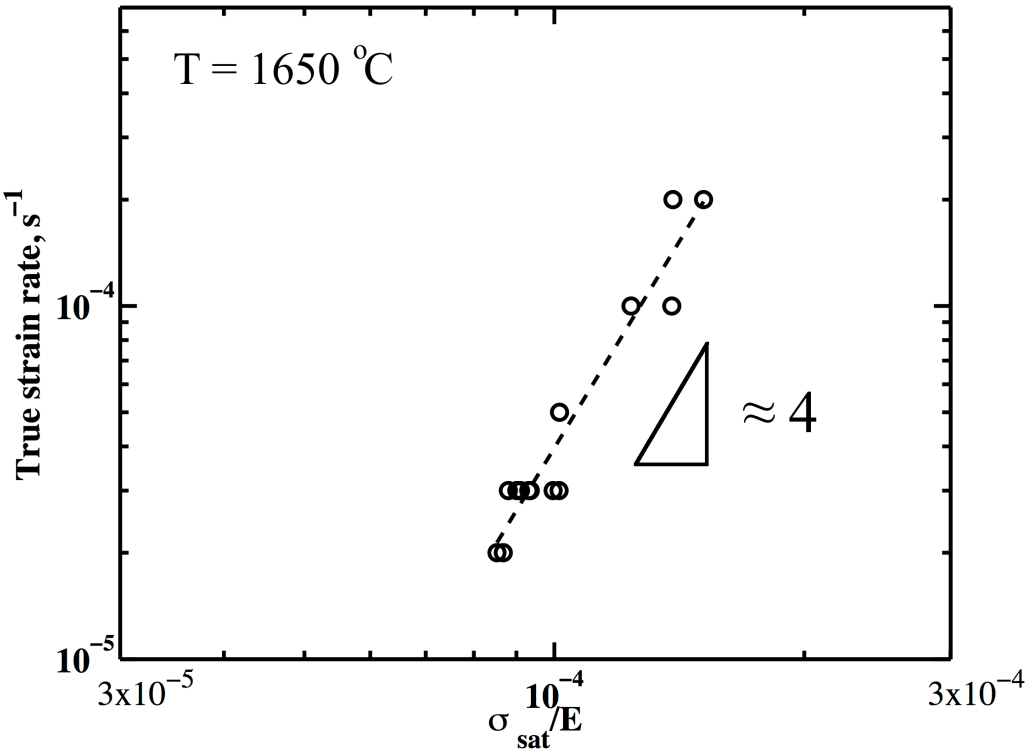

Figure 6.8: Tensile data are shown as the logarithm of strain rate *versus* the logarithm of steady-state flow stress normalized by the temperature dependent Young's modulus. The slope of the data is the stress exponent and equals approximately 4. Elastic modulus was determined from the data of Farraro [Farraro 1979].

The activation energy for creep is calculated by considering tensile data at multiple temperatures using the same strain rate. For this calculation, the Zener-Holloman parameter is reorganized as follows:

$$Z = \dot{\varepsilon}\exp\left(\frac{Q}{\mathrm{R}T}\right) = A\left(\frac{\sigma}{E}\right)^{n}$$

$$\ln\left(\dot{\varepsilon}\right) + \frac{Q}{\mathrm{R}T} = \ln\left(A\right) + n\ln\left(\frac{\sigma}{E}\right)$$

$$\ln\left(\frac{\sigma}{E}\right) = \frac{\ln\left(\dot{\varepsilon}/A\right)}{n} + \frac{Q}{\mathrm{R}n}\frac{1}{T}$$

$$\left.\frac{\mathrm{d}\ln\left(\sigma/E\right)}{\mathrm{d}\,1/T}\right|_{\dot{\varepsilon}} = \frac{Q}{n\mathrm{R}} \qquad \text{Eq. 6.5}$$

Since $\dot{\varepsilon}$, A, and n are constant, Q can be calculated by plotting $\ln(\sigma/E)$ *versus* $1/T$, where $\sigma=\sigma_{sat}$ from Eq. 6.3. The slope of the data in such a plot is Q/Rn, where R and n are known and are the universal gas constant and stress exponent, respectively. This method of activation energy calculation is demonstrated in Figure 6.9. The activation energy calculated is 432 kJ/mol, which is similar to the value 477 kJ/mol reported by Green for Ta [Green 1965].

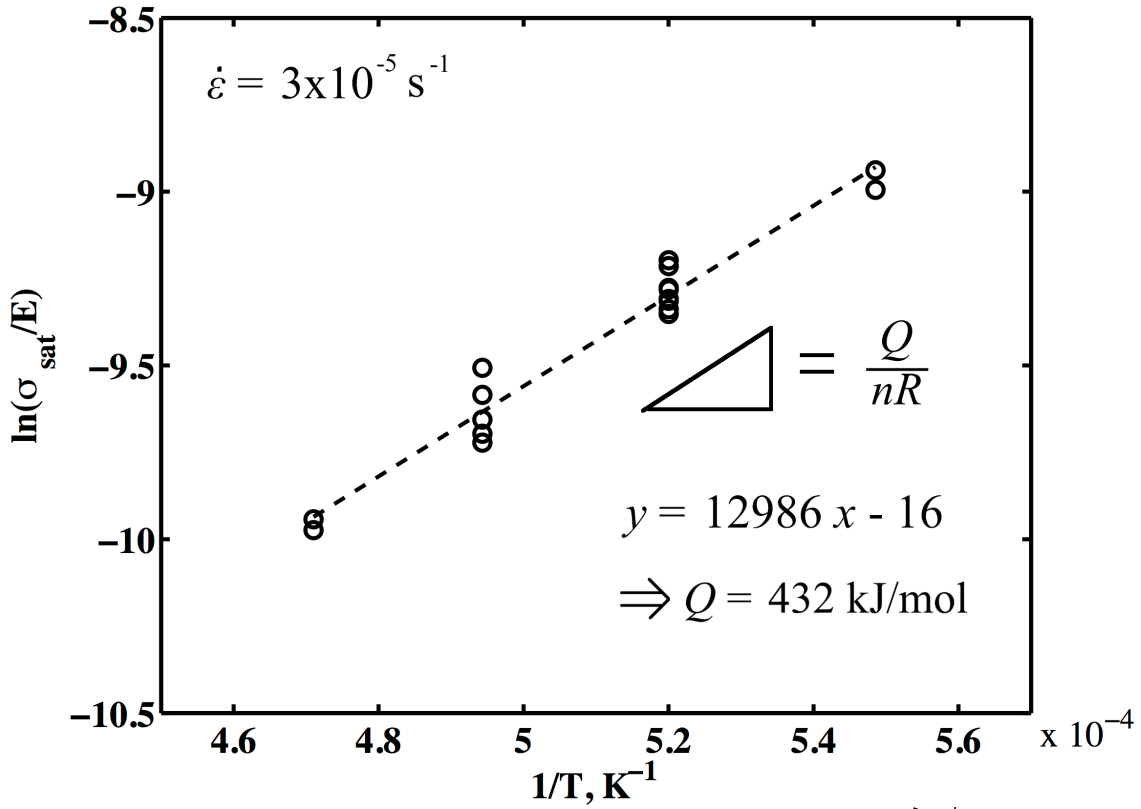

Figure 6.9: Tensile data collected for Ta at a true strain rate of 3×10^{-5} s^{-1} show a linear dependence for the natural logarithm of stress compensated by the temperature dependent dynamic Young's modulus *versus* inverse temperature. The activation energy for creep, Q, is calculated from the slope and equals 433 kJ/mol. The elastic modulus at each temperature was determined from the data of Farraro [Farraro 1979].

6.3 ORIENTATION OF DAGG GRAINS

Studies of DAGG in Mo by Worthington indicated that DAGG grains grow preferentially with the <101> crystallographic axis aligned along the TD and the STD

ranging from the <001> to the <111> directions [Worthington 2011]. The crystallographic orientations relative to the LTD depended on the particular grade of the material, powder metallurgy or arc melted. BCC materials are expected to develop a <101>-fiber texture upon tensile deformation [Rollett 1998 p.194], and the TD orientations of the DAGG grains appear to come from a component of this texture, with orientations close to {001}<101>. The DAGG grains produced in Ta follow this behavior, which is illustrated by the inverse pole figures of Figure 6.10. DAGG grains in Ta prefer the <101> aligned along the TD and favor the STD ranging from <001> to <111>, but generally nearer to the <111>. The LTD ranges from approximately the <112> to the <101>. Overall, the orientation of DAGG grains in Ta-A is more similar to Mo-AM than to either Mo-PMA or Mo-PMB.

When compared to the recrystallization texture before DAGG, the data shown in Figure 6.10(a), DAGG grain orientations appear to arise primarily from the recrystallization texture, but some DAGG grain orientations are clearly not from within that texture. An RP error value [Matthies 1988] of 32% was calculated between the DAGG grain orientations and the ODF of the recrystallized material using MTEX (ver. 3.4.1) quantitative texture analysis software [Bachmann 2010]. An RP value of 0% and corresponds to a perfect overlap between the data sets, and a value of 100% means that there is no overlap of the data. An RP value of 32% implies that some overlap is present, but significant variation is observed between the two textures. A DAGG grain with an orientation outside the recrystallization texture might grow more readily because it will have a higher percentage of more mobile, high-angle boundaries surrounding it than would an orientation from within the recrystallization texture, as discussed in Chapter 2. The scarcity of DAGG orientations from outside the recrystallization texture may be a

result of the strength of that texture and the large recrystallized grain size, which limits the number of grains available for DAGG initiation.

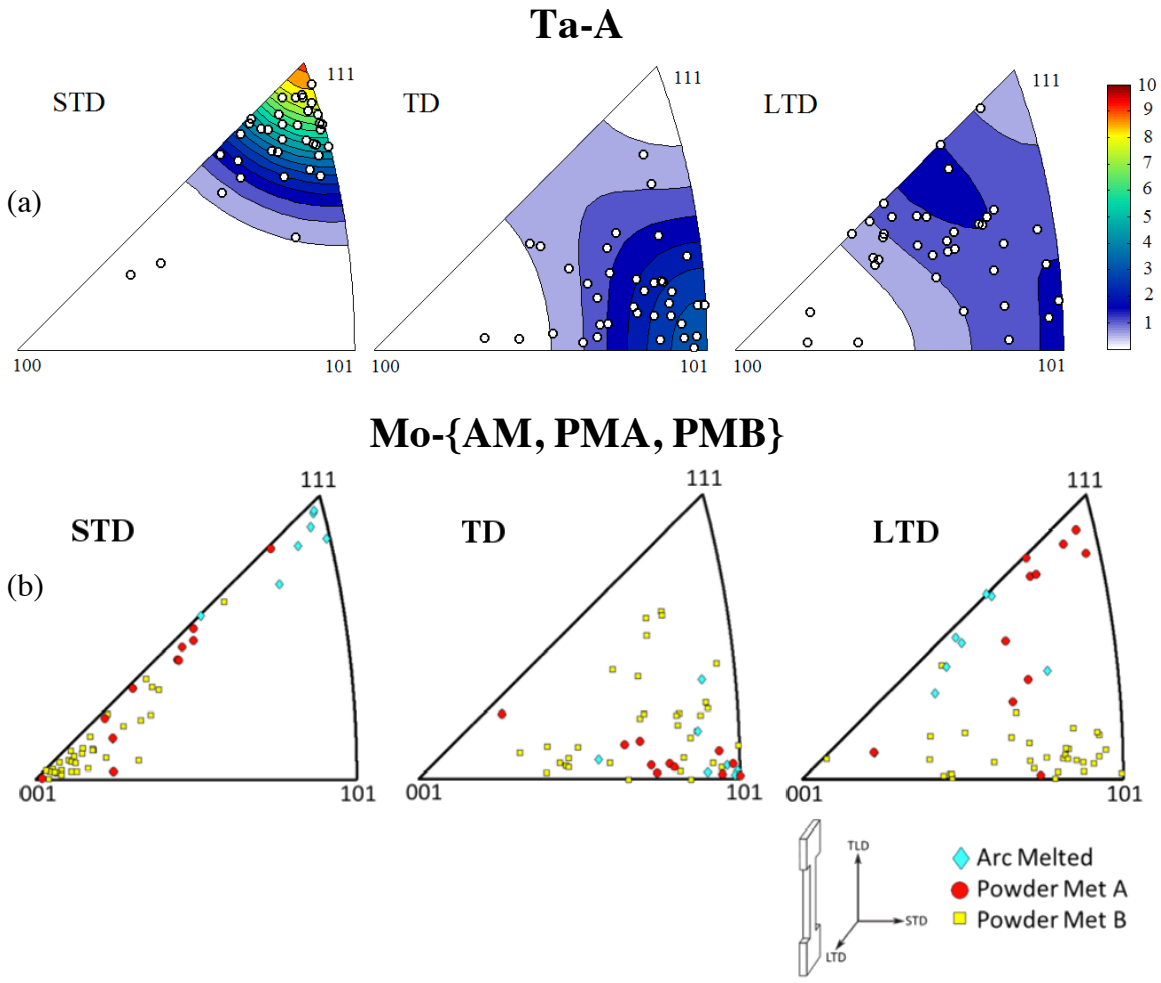

Figure 6.10: Inverse pole figures of orientation are shown relative to the short transverse (STD), tensile (TD), and long transverse (LTD) specimen directions. (a) The orientation distribution function (ODF) of Ta recrystallized at 1850 °C for 8 hours is shown along with the orientations of individual DAGG grains, indicated by the white-filled circles. ODF contour lines are at divisions of 0.5 of multiples of random. (b) DAGG grain orientations produced under constant true strain rate conditions in three Mo materials [Worthington 2011] are shown.

6.4 VARIATIONS IN DAGG BEHAVIOR

DAGG was observed across a range of temperatures and strain rates in Ta, although the "ideal" DAGG behavior with a clear, rapid stress drop, as described in past

investigations [Ciulik 2005, 2009; Worthington 2011, 2013], was not observed at the extremes of temperatures and strain rates investigated. The unpredictability of DAGG in Ta makes it difficult to control the growth of large single crystals. Irregularities observed for DAGG in Ta include multiple DAGG initiations, leading to multiple stress drops; gradual, instead of sudden, DAGG onset in the stress-strain data; and a large number of island grains.

Figure 6.11 shows two examples of stress-strain response associated with the DAGG behaviors observed in Ta. Tensile data are plotted as true stress *versus* true strain for tests conducted at true-strain rates of 3×10^{-5} s^{-1} and 1×10^{-4} s^{-1} for temperatures of 1650 and 1750 °C, respectively. Both the tensile tests of Figure 6.11 were halted after DAGG initiation, but prior to specimen rupture. The 1650 °C test data, the upper curve, demonstrate a characteristic rapid drop in flow stress associated with the initiation and propagation of DAGG. The rate at which the DAGG grain grows through the thickness of the specimen is believed to govern the steepness of the DAGG stress drop. The 1750 °C test data show a more gradual drop, with multiple inflections. The strains at which DAGG begins, slows and restarts (inflections), and finishes are indicated. The inflections likely indicate DAGG intermittently halting and restarting or the initiation and growth of multiple DAGG grains.

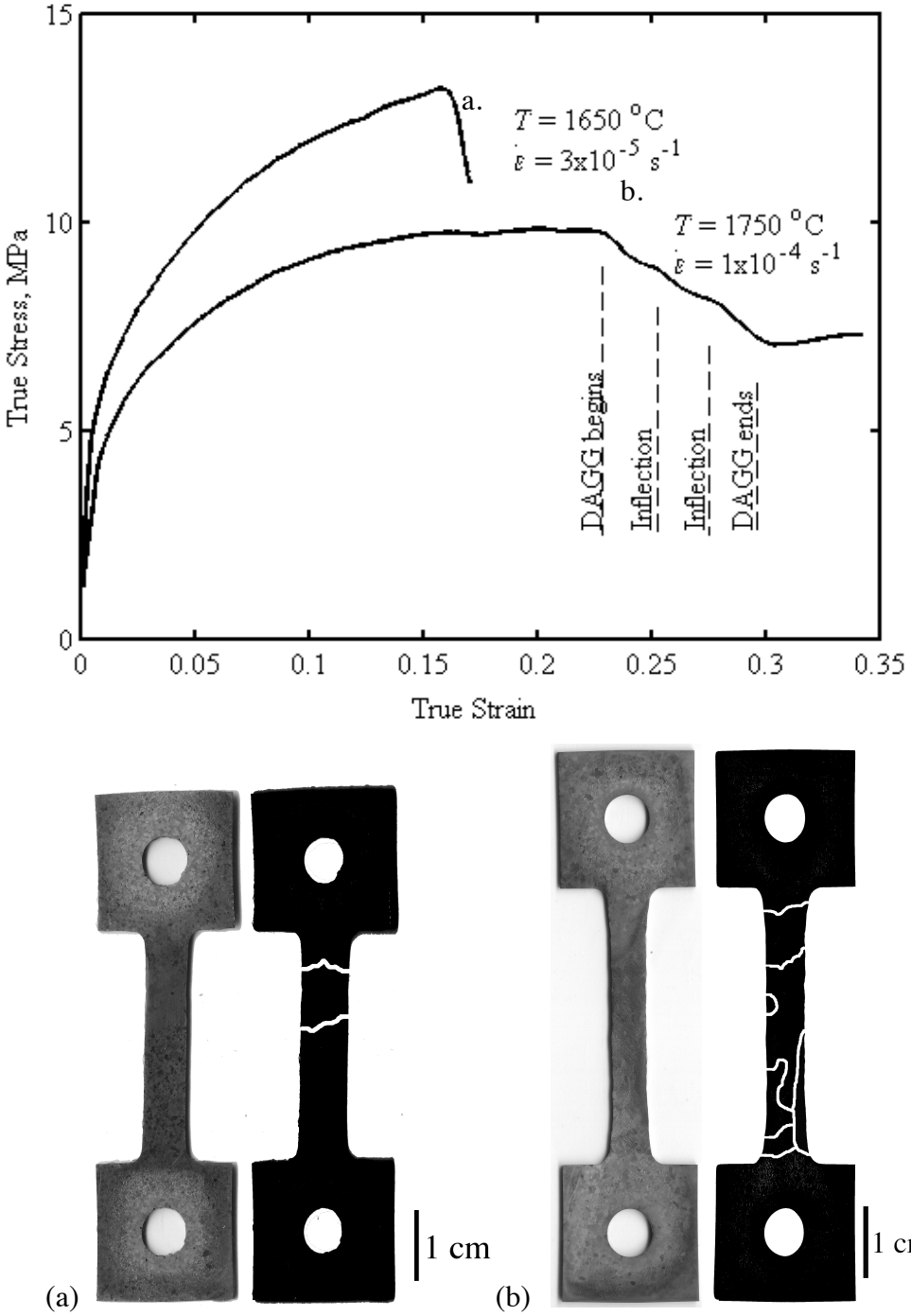

Figure 6.11: Stress-strain data (above) and resulting microstructures (below) are shown for tensile tests conducted on Ta at (a) 3×10^{-5} s^{-1} and 1650 °C and at (b) 1×10^{-4} s^{-1} and 1750 °C. The boundaries of the DAGG grains in the microstructures are highlighted in the traced figures to the right of each specimen image.

The most characteristic and repeatable DAGG behavior, that with the sharpest stress-strain drop, was generally observed at 1650 °C and a strain rate of 3×10^{-5} s^{-1}. Even under these conditions, some tests produced gradual or intermittent stress drops, but such non-ideal behaviors increased with increasing deviation from these optimal conditions. While a test temperature as low as 1450 °C did produce abnormal grains, specimen number 20 in Table 6.1, the associated stress-strain data exhibit a very gradual drop in stress that bears as much similarity to classical dynamic recrystallization behavior as to DAGG.

The characteristics of DAGG in this Ta sheet material are similar to those in a Mo sheet material produced through arc-melting [Ciulik 2009; Worthington 2011, 2013]. Similar characteristics include gradual and intermittent drops in stress following DAGG initiation, numerous large DAGG grains that may not fully consume the specimen gage length, and unconsumed island grains. These characteristics are thought to be a result of large grain sizes produced through normal grain growth prior to the initiation of DAGG. The DAGG grain orientations observed in Ta are most similar to Mo-AM, as demonstrated in Figure 6.10(c). These behaviors contrast sharply with DAGG observed in a Mo material produced through powder metallurgy, which resisted normal grain growth prior to DAGG [Worthington 2011, 2013]. Large grains produced in Ta and Mo materials by normal grain growth inhibit the growth of DAGG grains by increasing the grain-boundary radius of curvature, which reduces the driving pressure for boundary migration, as discussed in Chapter 2. The suppression of normal grain growth promotes DAGG, as it does other abnormal grain growth phenomena [Hillert 1965]. A reduced boundary migration rate, because of a large radius of curvature in the polycrystalline grains, may allow time for additional DAGG grains to form in other parts of the specimen before the original DAGG grain has an opportunity to consume those regions.

6.5 DAGG Boundary Migration Distance and Velocity

Of the fifty (50) Ta tensile specimens tested, nine (9) produced only one DAGG grain, as determined by optical microscopy and Laue back-scatter diffraction. The DAGG boundary migration distance and velocity were calculated from observations of the microstructures and test data of these specimens. These are considered with respect to test conditions and orientation parameters. The DAGG boundary migration distance and velocity are defined similarly to that in §5.3.3. Because the uncertainty of the DAGG boundary migration distance and velocity increase as the number of DAGG grains in a specimen increases, only specimens with one DAGG grain were considered.

Figure 6.12 demonstrates a linear correlation between the DAGG grain boundary migration distance and accumulated strain during DAGG, producing a correlation coefficient of 0.78. The correlation from the data of Figure 6.12 is consistent with the observations of Ciulik and Worthington [Ciulik 2005, 2009; Worthington 2011, 2013], and supports the previous conclusion that DAGG requires active straining for its boundary to continue migrating.

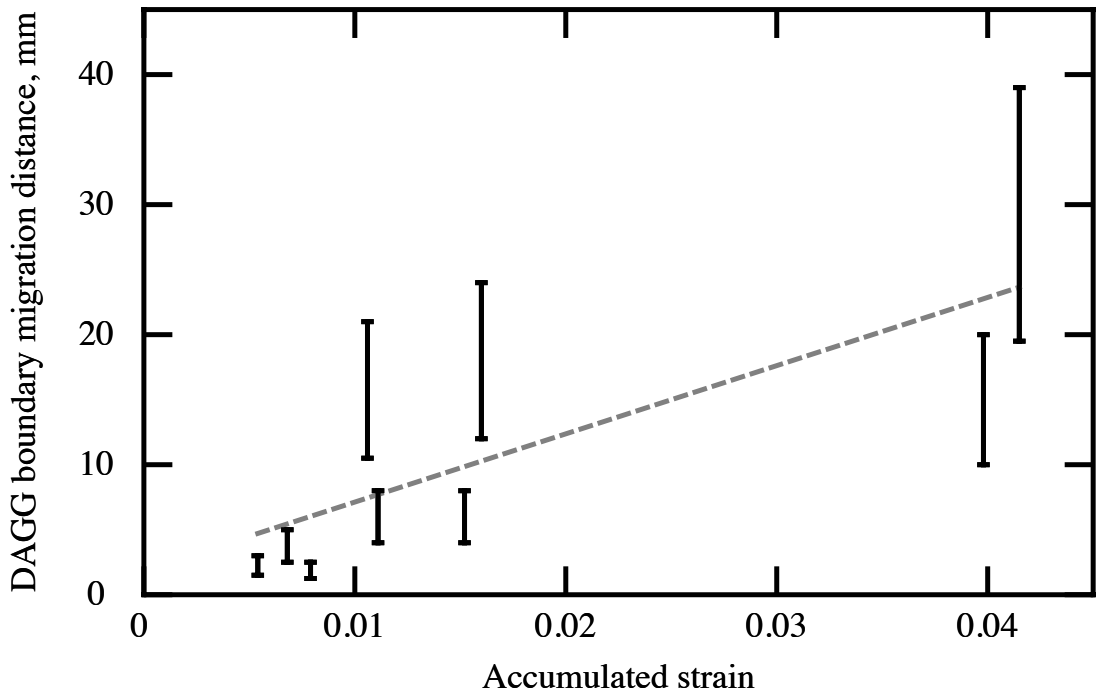

Figure 6.12: DAGG boundary migration distance in Ta is plotted *versus* plastic strain accumulation, revealing a correlation coefficient of 0.78 between these parameters.

Figure 6.13 shows a plot of DAGG boundary migration distance *versus* time elapsed during DAGG. When comparing data of Figure 6.13 for each strain rate or temperature separately, a trend of generally increasing DAGG boundary migration distance with increasing time elapsed during DAGG is observed. This trend between DAGG grain boundary migration distance and time was also observed under constant true stress conditions for specimens tested at the same temperature.

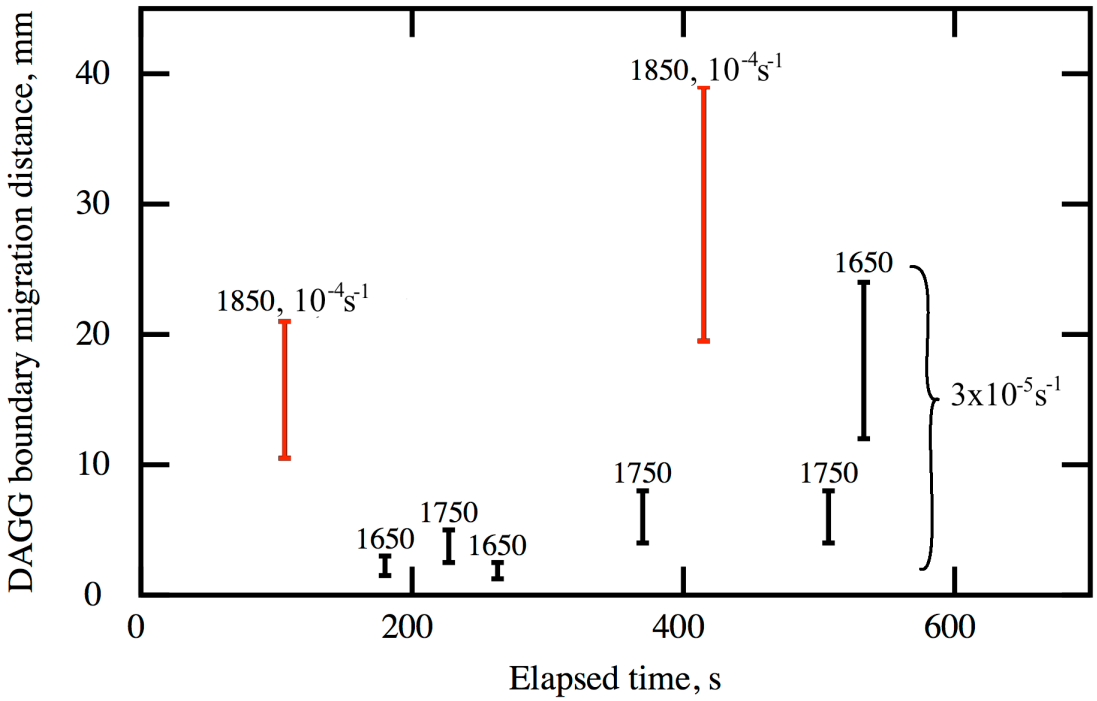

Figure 6.13: DAGG boundary migration distance in Ta is plotted *versus* the elapsed time from DAGG start to end. Labels indicate the test temperature in degrees C. Red and black markers indicate strain rates of 10^{-4} and 3×10^{-5} s^{-1}, respectively.

The average velocity of DAGG grain boundary migration is defined as $v = d/t$, where d is the DAGG boundary migration distance and was defined previously, and t is elapsed time during DAGG, as determined from the test data. The average DAGG boundary velocity is shown in Figures 6.14 and 6.15 as functions of strain rate and temperature. The boundary velocity increases with both of these parameters. Because this sample of specimens does not include tests between every temperature and every strain rate, separating the effects of temperature and strain rate is difficult. The boundary velocity appears relatively constant at temperatures of 1650 and 1750 °C, but increases rapidly at 1850 °C. The 1650 and 1750 °C tests, however, were conducted at a slower strain rate than the 1850 °C tests. The similarity between the 1650 and 1750 °C tests

suggests that the DAGG boundary velocity may be a stronger function of strain rate than temperature.

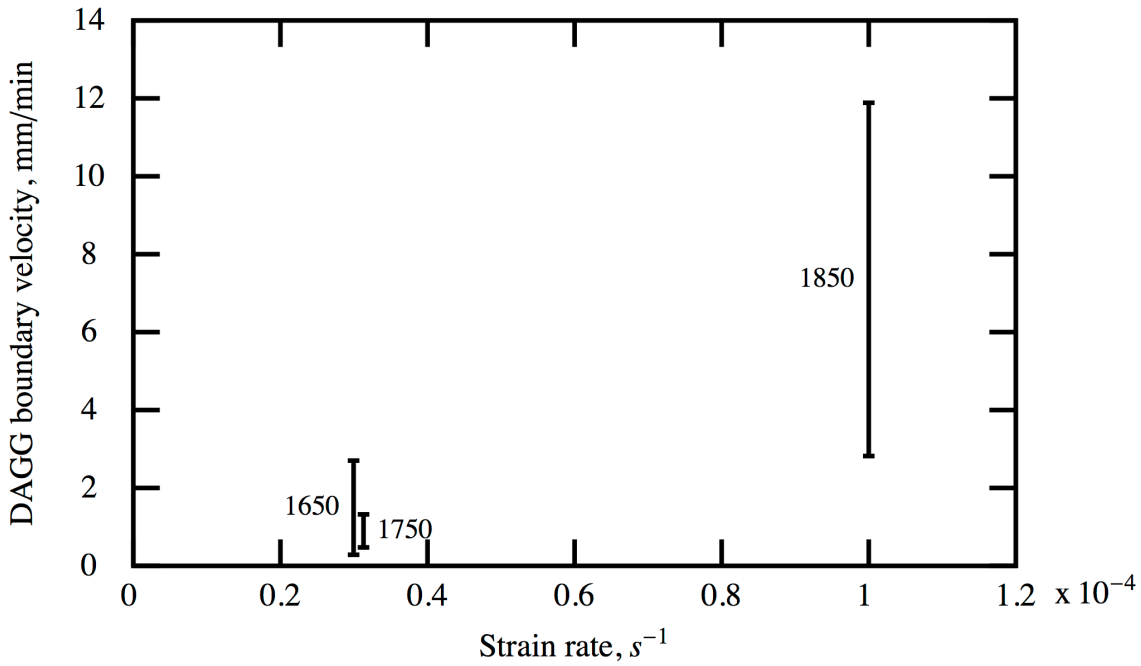

Figure 6.14: The range of DAGG boundary velocities for each combination of temperature and strain rate in Ta is plotted *versus* strain rate. Labels indicate the test temperature in degrees C.

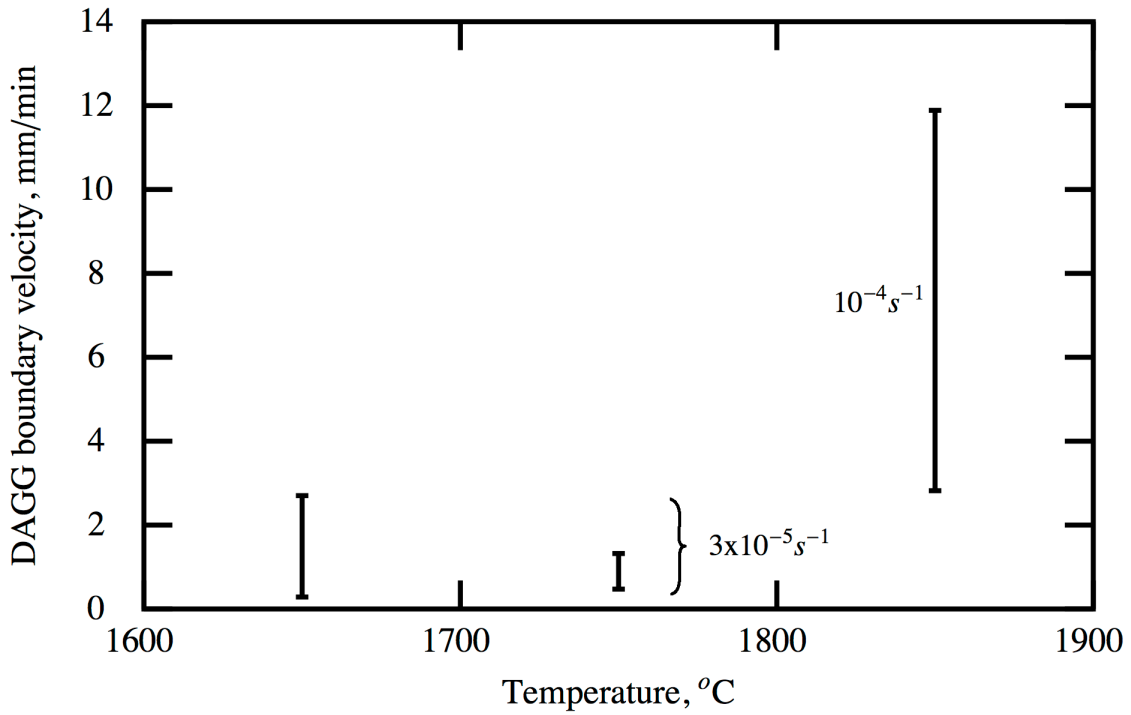

Figure 6.15: The range of DAGG boundary velocities for each combination of temperature and strain rate in Ta is plotted *versus* temperature. Labels indicate the applied true strain rate.

It is plausible that the drop in flow stress associated with DAGG is related to the velocity of the DAGG boundary, such that a steeper drop is seen for a faster DAGG boundary velocity. The drop in stress is characterized as shown in Figure 6.16, where the red curve is approximated as a 3rd order polynomial. The second derivative is used to identify the inflection point near the center of the drop where the slope of true stress *versus* true strain is greatest. The slope at this point, calculated from a polynomial fit to the data, is now compared with the corresponding DAGG boundary velocity. Figure 6.17 shows a linear relationship of increasing negative slope with increasing boundary velocity. The data of Figure 6.17 were obtained at temperatures of 1650 and 1750 °C for a strain rate of 3×10^{-5} s^{-1}. These data indicate that the velocity of the DAGG boundary can be estimated from the slope of the DAGG drop for a specific strain rate. It is unclear

whether or not the slope of the DAGG drop at each point along the curve correlates to the instantaneous velocity of the DAGG grain.

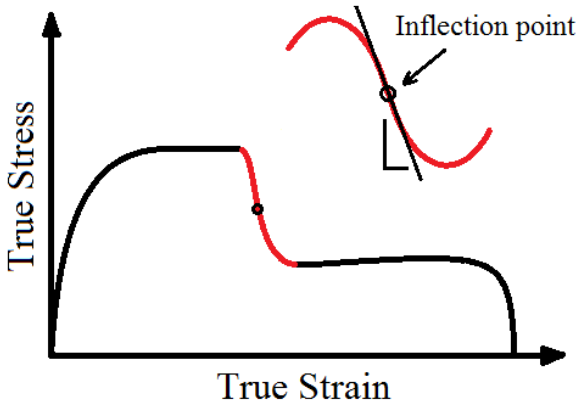

Figure 6.16: This schematic shows the method used to quantify the slope of the drop in stress due to DAGG in the stress-strain test data.

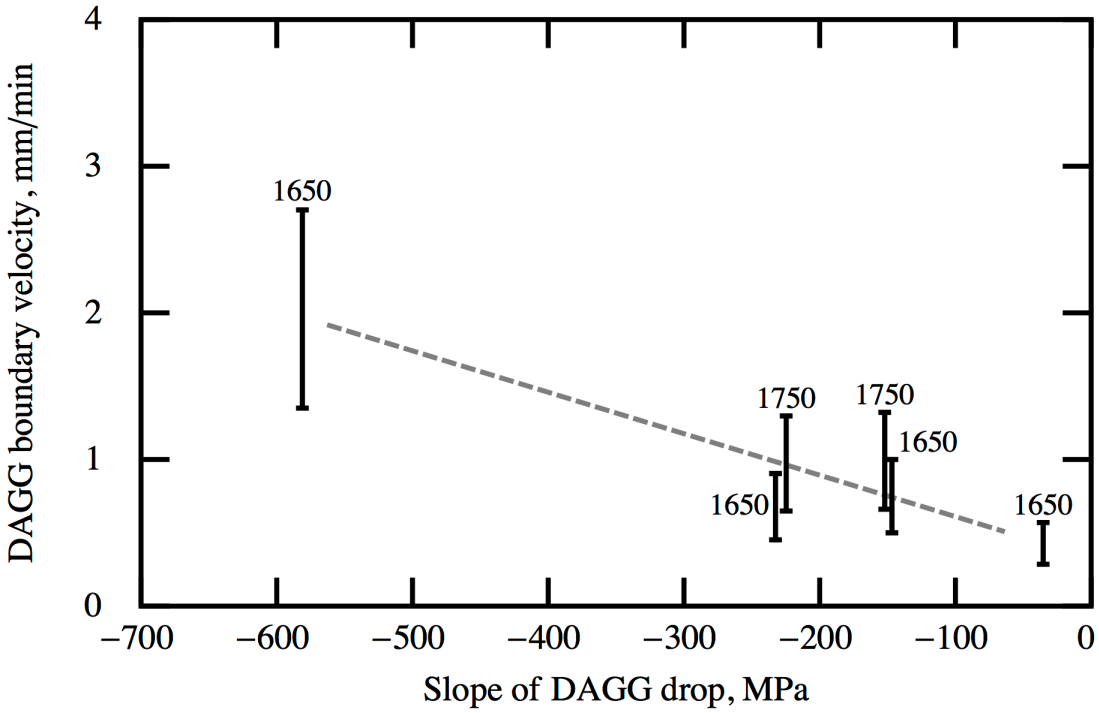

Figure 6.17: DAGG boundary velocity in Ta is plotted *versus* the slope of the DAGG drop, revealing a correlation coefficient of -0.95. All data were collected at a strain rate of 3×10^{-5} s^{-1}. Data labels indicate temperature in degrees C.

Reduction of dislocation density can be a major driving force for grain boundary migration. If DAGG is driven by stored dislocation energy from prior straining up to the point of DAGG initiation, it is expected that the DAGG boundary velocity will be proportional to the strain accumulated at this point, the critical strain. This was tested by calculating the linear correlation coefficient between DAGG boundary velocity and critical strain for 7 specimens tested using the same strain rate and temperatures of 1650 and 1750 °C. The data of DAGG boundary velocity *versus* strain at initiation is shown in Figure 6.18. There appears to be no correlation between critical strain and DAGG boundary velocity, as the correlation coefficient is 0.09. This indicates that the initiation conditions of DAGG may have relatively little effect on the subsequent growth of the DAGG grains.

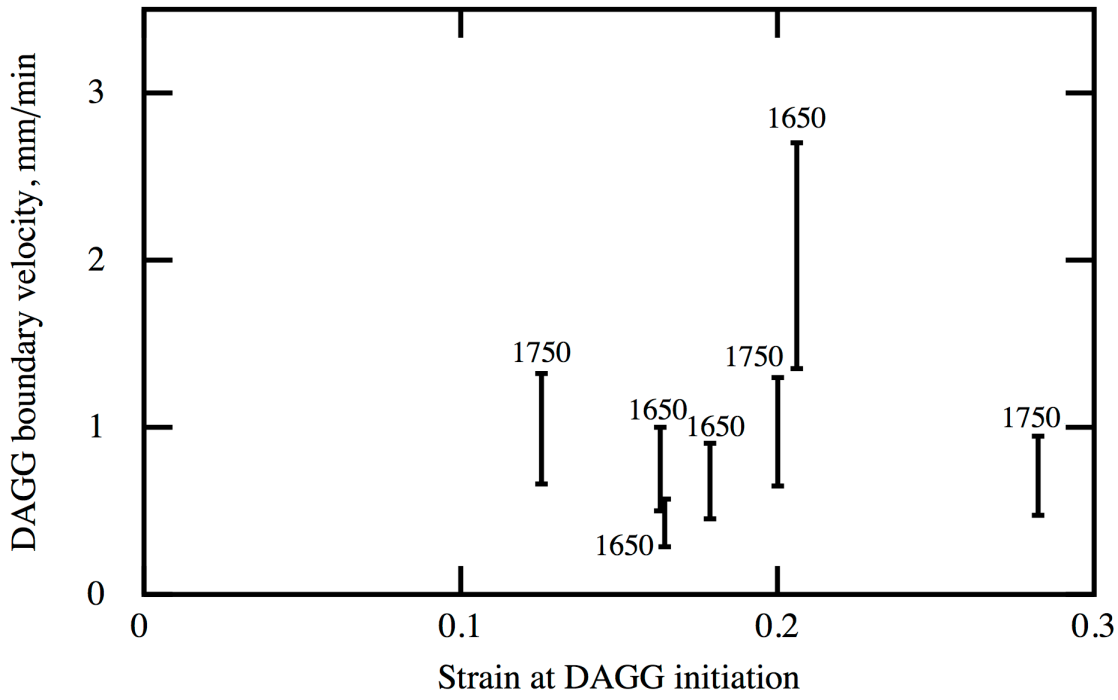

Figure 6.18: DAGG boundary velocity in Ta is plotted *versus* strain at DAGG initiation, revealing a correlation coefficient of 0.09. All data were collected at a strain rate of 3×10^{-5} s^{-1}. Data labels indicate temperature in degrees C.

Because the DAGG grain boundary travels a distance proportional to the amount of strain accumulated, the DAGG grain may prefer orientations for which slip is easier. This may result in higher DAGG boundary velocities for orientations that have a low Taylor factor, or high Schmid factor. Figure 6.19 presents DAGG boundary velocity plotted against the Schmid factor and Taylor factor. There is no significant correlation between Schmid factor and boundary velocity, as the correlation coefficient is 0.32. Only a moderate correlation is observed between Taylor factor and boundary velocity. Increasing boundary velocity with increasing Taylor factor produces a correlation coefficient of 0.56. If the Taylor factor and DAGG boundary velocity are correlated, then DAGG grains prefer to grow from grains initiated with "harder" orientations relative to their slip properties. This is contrary to the hypothesis that DAGG grains may prefer to grow from grains that slip more easily. Because of the small sample size, it is not possible to determine if the increase in velocity with increasing Taylor factor is due to the Taylor factor or is because of the temperature or strain rate of the two specimens with the highest boundary velocities, which also had the largest Taylor factors, as shown in Figure 6.18(b). Additional data would be required to further pursue this possibility.

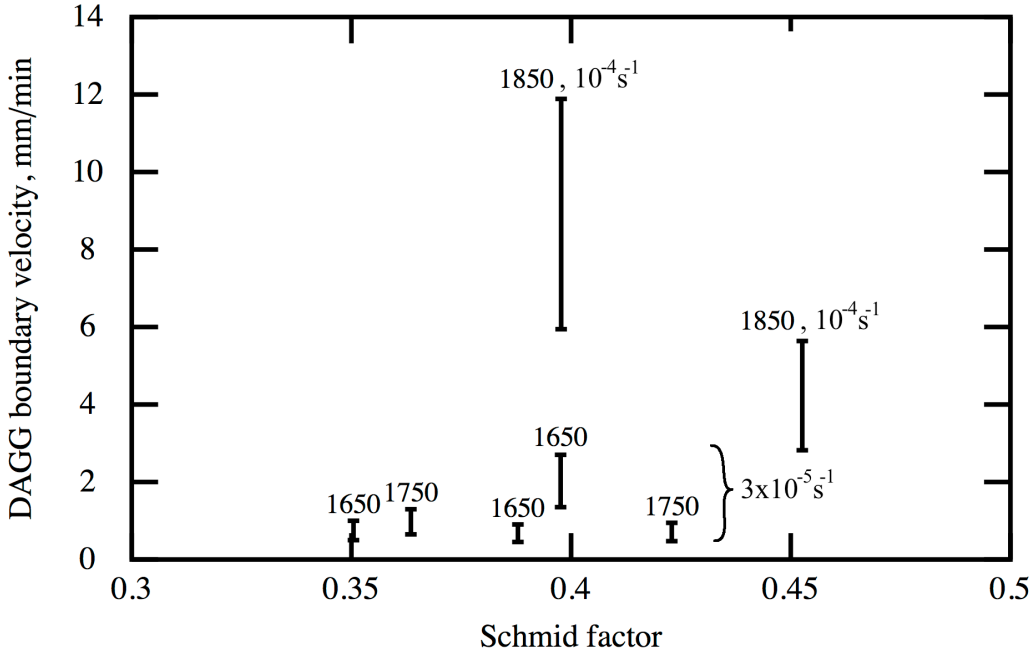

(a)

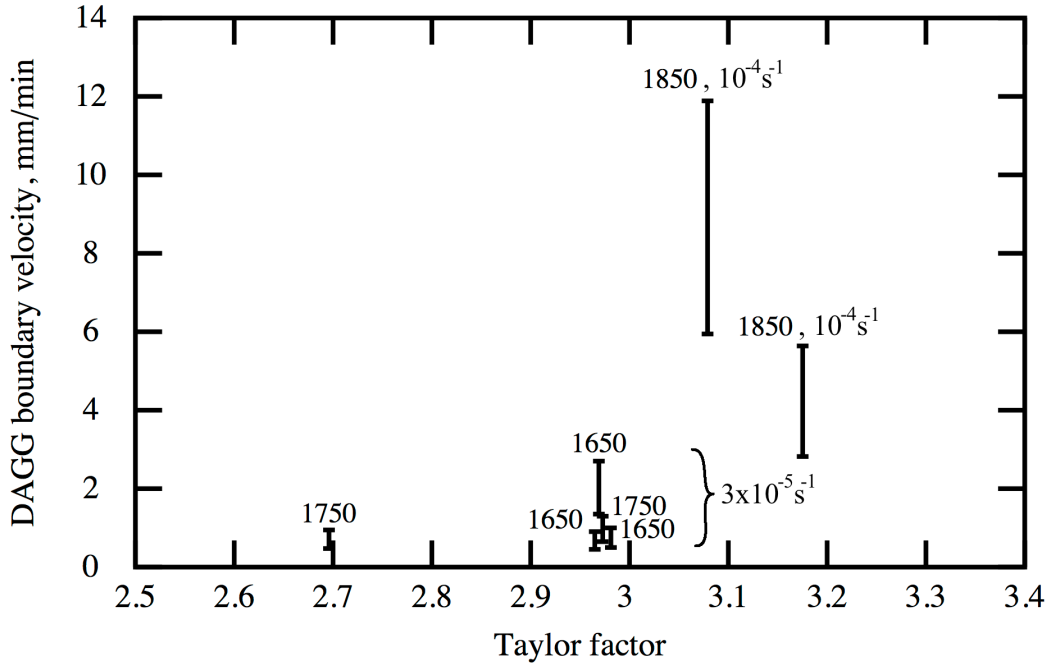

(b)

Figure 6.19: DAGG boundary velocity is plotted *versus* (a) Schmid factor and (b) Taylor factor. The correlation coefficients between DAGG boundary velocity and Schmid factor and Taylor factor are 0.32 and 0.56, respectively.

If DAGG prefers growth along a particular crystallographic direction, the velocity of the DAGG boundary may be higher for grains of a particular orientation. Figure 6.20 shows inverse pole figures relative to the STD, TD, and LTD specimen directions with markers shaded to indicate the DAGG boundary velocity measured for each orientation, darker markers indicating faster DAGG boundary velocities. The fastest boundary velocities are closest to the <101> relative to the TD and lie between <001> and <111>, near <112>, relative to the LTD. In spite of this occurrence, no definitive relationship between orientation and DAGG boundary velocity is observed, as was also observed with Mo-PMB under constant true stress test conditions.

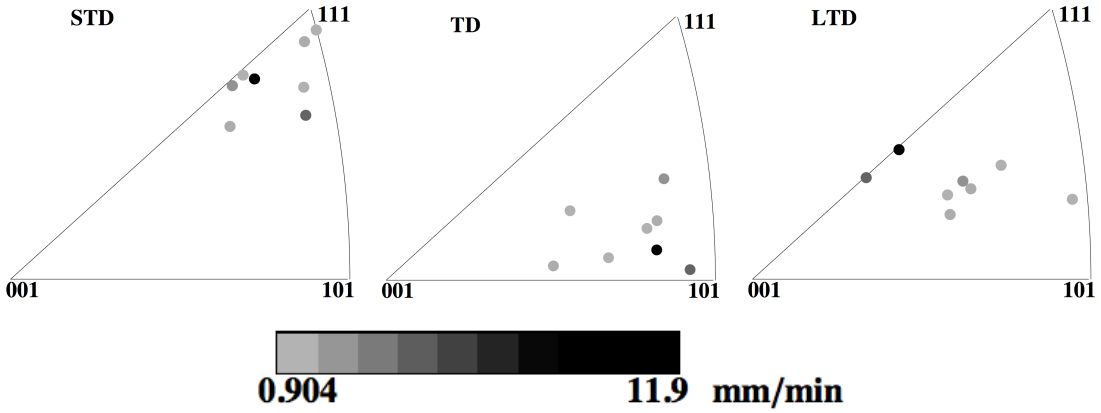

Figure 6.20: Inverse pole figures relative to specimen orientation present the average velocity of DAGG boundaries, indicated by the shade of each marker, where darker points represent faster velocities.

6.6 CONCLUSIONS

1. DAGG was observed in a commercial-purity Ta material between temperatures of 1550 and 1850 °C and strain rates of 2×10^{-5} to 5×10^{-4} s^{-1}.

2. The tensile stress-strain behavior prior to DAGG initiation indicates an activation energy for creep of 433 kJ/mol and a stress exponent of approximately 4.
3. There is no significant correlation between the critical strain for DAGG and either temperature or strain rate. The average critical strain varies little with temperature, but the standard deviation of the critical strain increases with both temperature and grain size.
4. The stress at DAGG initiation decreases with increasing temperature and increases with increasing strain rate. This is consistent with the expected creep behavior and is not thought related to the mechanisms of DAGG initiation.
5. Orientations of the DAGG grains are often similar to that of the primary recrystallized texture. DAGG grains in Ta tend to be oriented with <111> parallel to STD and <101> parallel to TD. The orientations of Ta DAGG grains are most similar to those observed from DAGG grains in Mo-AM.
6. The drop in flow stress corresponding to the initiation and propagation of DAGG is often irregular in Ta-A, displaying multiple inflection points consistent with the slowing, or halting, and resuming of DAGG.
7. The DAGG boundary migration distance is proportional to the strain accumulated during DAGG, as was observed for DAGG in Mo.
8. The average velocity of the DAGG grain boundary increases with increasing strain rate.
9. The slope of the drop in flow stress due to DAGG is proportional to the average DAGG boundary velocity for a specific strain rate.

10. The average velocity of the DAGG boundary is not a function of the critical strain, Schmid factor, or Taylor factor.
11. Testing conditions, such as temperature and strain rate, have a larger effect on the velocity of the DAGG boundary than strain at initiation or orientation of the DAGG grain.

7 Microstructural Observations of DAGG in Ta-A

The microstructures produced by DAGG in Ta-A were observed using optical and scanning electron microscopy to investigate the microstructural factors that may promote or inhibit DAGG. Each specimen was ground, polished and etched, as described in §3.3.1. Two (2) specimens were cross-sectioned along their length to observe the morphology of the DAGG grain as it meets the polycrystalline region through the thickness of the material. Six (6) specimens were chosen for further analysis using EBSD. EBSD analysis includes observations of misorientation and substructure, Schmid and Taylor factors, and grain boundary character.

7.1 CROSS-SECTIONS

Investigations of DAGG in Mo-PMB by Worthington indicated preferential growth of DAGG grains along the surface of the specimen [Worthington 2011]. Preferential surface growth is possibly due to surface energy effects, or through thickness variations in texture, grain size, or composition. The large recrystallized grain size in annealed Ta-A causes grains to frequently span the thickness of the specimen, as shown in §4.3. Thus, no texture or grain size variations were observed through the thickness. DAGG grains were not observed to preferentially grow on one side of the specimen. The shape of the typical DAGG grain as it meets the unconsumed polycrystalline region, however, may indicate if surface energy effects influence DAGG in Ta-A. Two Ta specimens were chosen for analysis of through-thickness DAGG grain morphology, as shown in Figures 7.1 and 7.2. Figures 7.1 and 7.2 present specimens tested at 1650 °C and 3×10^{-5} s^{-1} (Ta30), and at 1850 °C and 3×10^{-5} s^{-1} (Ta50), respectively. The back-scatter electron (BSE) images of Figures 7.1 and 7.2 (b) are produced using channeling

contrast, which is sensitive to crystallographic orientation. The contrast does not vary regularly over large deviations in orientation, so it is difficult to distinguish between grains and subgrains in a deformed material. The optical (c) and BSE (b) images were both used to determine the locations of grain boundaries in (a) in Figures 7.1 and 7.2.

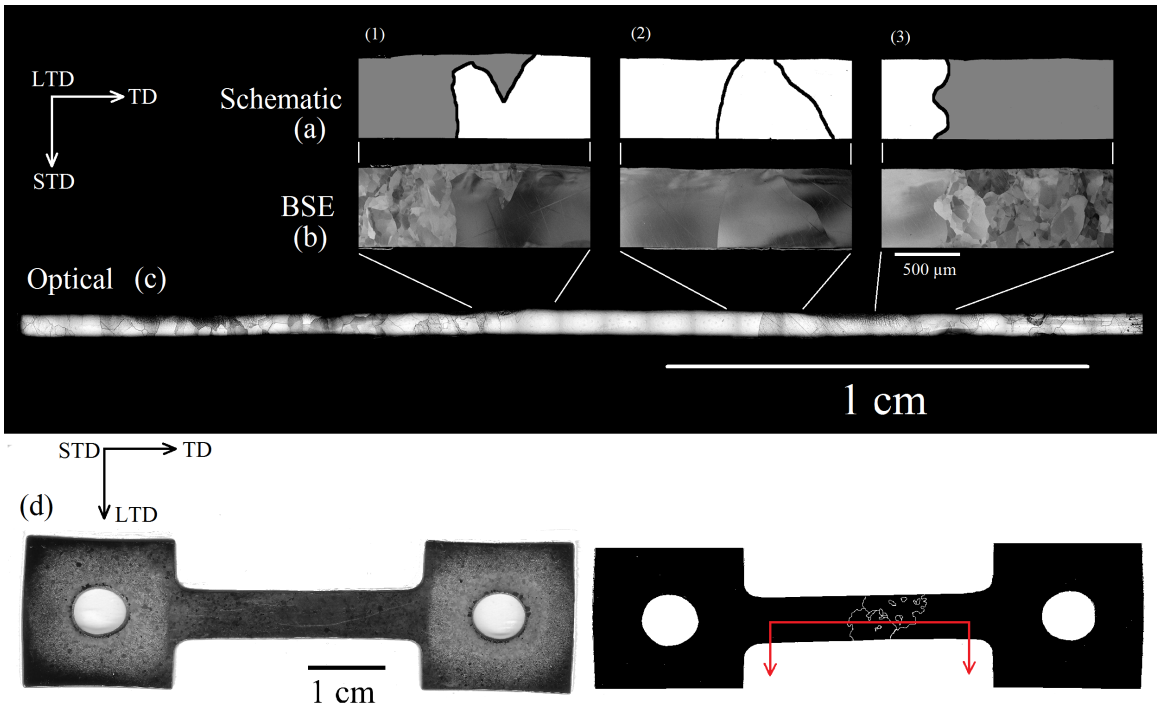

Figure 7.1: Microstructure of a Ta-A specimen tested at 1650 °C and 3×10^{-5} s^{-1} (Test 30), is shown through (a) a schematic of DAGG grain boundaries identified in the specimen cross-section, (b) back-scatter electron images from the cross-section, (c) an optical image of the entire cross-section, and (d) an optical image of the entire specimen. The gray areas in (a) denote polycrystalline regions, and the white areas denote DAGG grains. The red line and arrows in (d) indicate the location of the cross-section cut and the direction of viewing the cross-section. Traces of DAGG grains are shown in the schematic to the right of the specimen in (d).

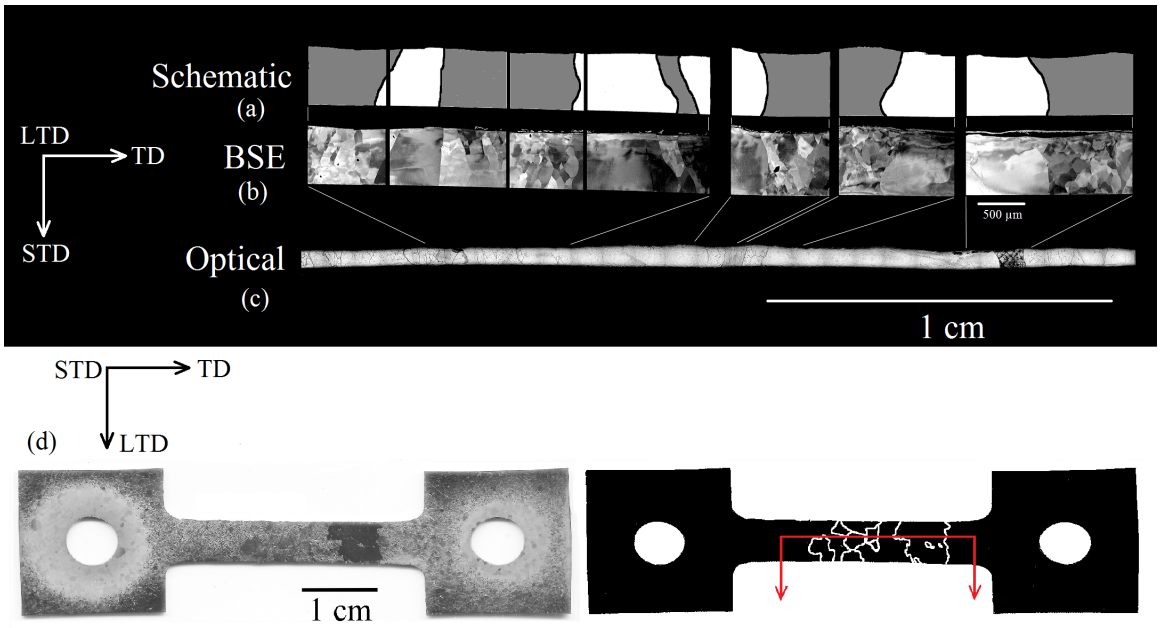

Figure 7.2: Microstructure of a Ta-A specimen tested at 1850 °C and 3×10^{-5} s^{-1} (Test 50), is shown through (a) a schematic of DAGG grain boundaries identified in the specimen cross-section, (b) back-scatter electron images from the cross-section, (c) an optical image of the entire cross-section, and (d) an optical image of the entire specimen. The gray areas in (a) denote polycrystalline regions, and the white areas denote DAGG grains. The red line and arrows in (d) indicate the location of the cross-section cut and the direction of viewing the cross-section. Traces of DAGG grains are shown in the schematic to the right of the specimen in (d).

The bottom edge of each cross-section image, parts (a), (b), and (c) in Figures 7.1 and 7.2, is the side shown in the images of the entire specimen in part (d). The bottom edge is flat and does not show the contours of the specimen surface following testing because material was removed from this surface during grinding and polishing procedures for the initial microstructural characterization prior to cross-sectioning. A thickness of approximately 150 μm was removed from the specimen in Figure 7.1 and 60 μm from the specimen in Figure 7.2.

There is no indication in Figures 7.1 and 7.2 that DAGG in Ta prefers growth at the surface. The interfaces of the DAGG grains as they meet the unconsumed polycrystalline regions are not significantly curved, which would indicate preferred

growth at the surface or center-line. Curvature-driven grain boundary migration causes a grain boundary to travel toward the center of curvature. If DAGG is curvature driven, the shape of the DAGG grain at the interface between it and each polycrystal grain should generally be concave. The lack of a concave DAGG grain shape indicates that surface energy differences are not promoting DAGG along the surface in Ta-A.

Significant thermal grooving was not observed in the cross-sections of Figures 7.1 and 7.2; however, it is possible that small grooves at grain boundaries create stress concentrations that promote the initiation of DAGG grains at the surface. Since DAGG was consistently observed in Mo-PMB, which had an initial grain size much smaller than the thickness of the sheet, thermal grooving may aide in the initiation of DAGG, but is not expected to be a requirement for the suppression of normal grain growth and promotion of DAGG. The influence of grain boundary grooves may, however, have a larger effect on material for which the grain size approaches the thickness of the sheet, such as for Ta-A.

The optical images in Figure 7.3 demonstrate the roughness on the surfaces of Ta-A specimens following testing. This is from the accommodation of plastic deformation at the surface. Slip in the large grains during testing prior to DAGG initiation is accommodated differently for each grain depending on orientation of that grain, orientation of its neighboring grains, and its proximity to the free surface. Differences in plastic deformation of individual grains produces a wavy surface appearance after testing. Figure 7.3 shows optical images of the surfaces of four specimens tested different conditions. Slip bands are observed on the surfaces. Increased surface roughness is observed at higher temperatures. The majority of surface deformation is believed to occur prior to DAGG initiation because the regions in which DAGG occurred do not correlate with the deformation patterns on the surfaces of the specimen. Microstructural

analysis requires the surface to first be ground until flat, which removes up to 200 μm of material from each surface to be observed. It is possible that surface features may affect DAGG by creating stress concentrations on the surface, but since these surface features were not significant in DAGG tests of Mo, this effect is likely not related to DAGG initiation.

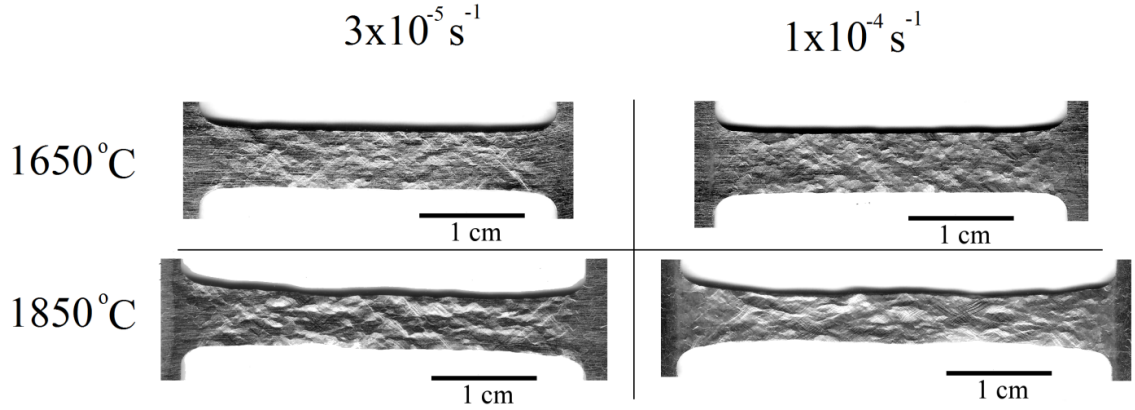

Figure 7.3: Optical images of the gauge region of Ta-A specimens tested at temperatures of 1650 and 1850 °C, and strain rates of 3×10^{-5} and 1×10^{-4} s^{-1} are shown as-tested prior to metallography and microstructural analysis. Surface deformation and slip bands are observed on the surfaces.

7.2 EBSD ANALYSIS

Six (6) Ta-A specimens were characterized using EBSD. Information on the testing conditions, microstructure, and location of EBSD analysis on each specimen is provided in Figure 7.4. Sufficient contrast between grains is often difficult to obtain in optical images of the etched microstructures. Thus, a sketch of the approximate location of observable grain boundaries bordering abnormal grains is also provided for each specimen.

Specimen number	Test conditions	Microstructure
Ta8	1800 °C 1×10^{-4} s^{-1}	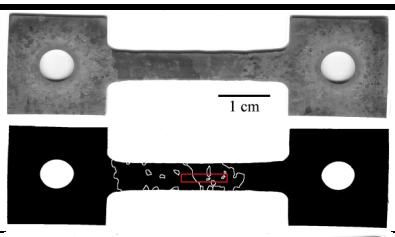
Ta11	1650 °C 1×10^{-4} s^{-1}	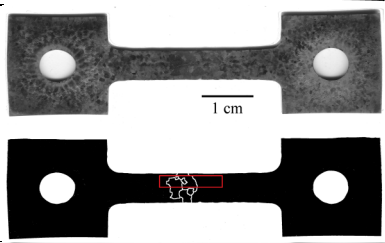
Ta 26	1650 °C 3×10^{-5} s^{-1}	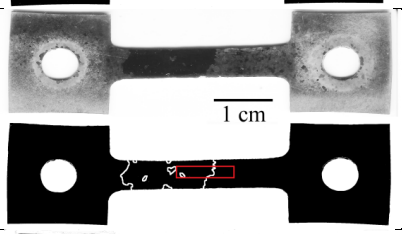
Ta30	1650 °C 3×10^{-5} s^{-1}	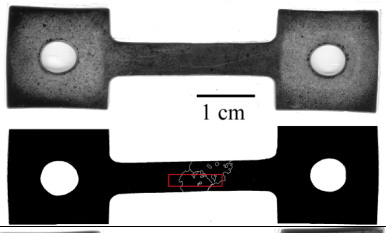
Ta34	1650 °C 3×10^{-5} s^{-1}	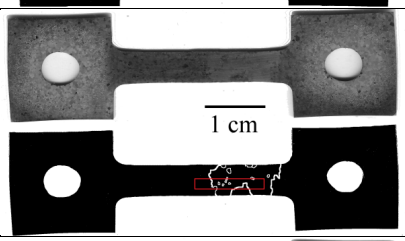
Ta36	1650 °C 3×10^{-5} s^{-1}	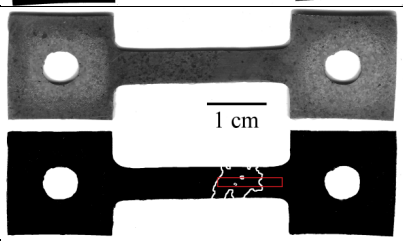

Figure 7.4: Test conditions and resulting microstructures are shown for six Ta-A specimens characterized using EBSD. The top image of each shows the specimen polished and etched, and the bottom image shows a schematic of grain boundaries that could be identified in the DAGG region by eye following etching. The red box indicates the region where EBSD data were collected.

Figure 7.5 shows three maps for each data set, each colored by an inverse pole coloring scheme to indicate crystallographic orientations aligned along either the STD, TD, or LTD. Significantly more microstructural detail is provided in the EBSD data than is observed in the optical images, especially since not all grain boundaries are visible from optical microscopy. In addition, not all grain boundaries are identifiable at every orientation provided in Figure 7.5. Very little contrast is shown between grains in the STD due to the strong <111> texture along this direction. Specimens Ta8, Ta11, Ta34, and Ta36 show large areas that may be interpreted to be one grain when viewing the orientation relative to the TD; however, contrast in the LTD indicates the presence of multiple grains in these regions. The similarity in orientations among these grains is a likely reason that they are also not easily observed using optical microscopy. The etching procedure required for optical microscopy is unlikely to reveal low energy boundaries, and grain boundaries between grains that are similarly oriented or that have special boundary character are often low energy.

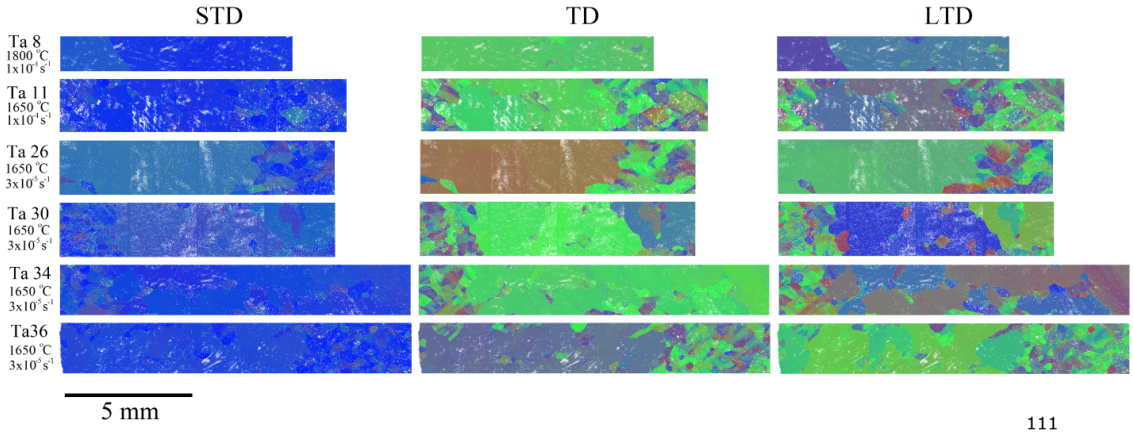

Figure 7.5: EBSD data are shown for six Ta-A specimens. Data are colored by the inverse pole figure coloring scheme to the bottom right and indicate orientations normal to the STD, TD, and LTD specimen directions. Unindexed points are white.

7.2.1 Deformation

Because DAGG grains grow during plastic deformation, it is relevant to investigate the strain accumulated within DAGG grains. One way to inspect the local strain accumulation within a grain is to measure the local lattice misorientations developed within that grain. This might be quantified as a measure of lattice curvature. Grains are first identified using the process described in §3.3.3.1. Reference orientation deviation (ROD) maps (see §3.3.3.2) were created from the EBSD data sets of the specimens in Figure 7.4 and are shown in Figure 7.6. The black curves identify grain boundaries, and a colored scale shows the degree of misorientation for each point in a grain from the average orientation of the grain to which it belongs. The ROD map gives a measure of deformation and lattice curvature within each grain.

The ROD is sensitive to the threshold misorientation for identifying grain boundaries. A *large* misorientation threshold will allow some regions to be included in the DAGG grain that may also be defined as separate grains with low misorientations to the DAGG grain. A *small* misorientation threshold causes subgrains in the polycrystalline region to be classified as individual grains, which will reduce the amount of deformation calculated. The threshold must be chosen to reduce both of these effects, but it is not always possible for these issues to be simultaneously eliminated. The threshold misorientation used for grain boundary identification was 2.5°.

The large, abnormal grains are often less deformed than the unconsumed, polycrystalline grains. This is in spite of the active straining that occurs during growth of the abnormal grains. More deformation is observed in some of the largest grains, but this deformation is still small compared to the deformation in most of the polycrystalline grains. The maximum misorientation in an abnormal grain, relative to its average orientation, is approximately 6.2 ± 4.5° for these six Ta-A specimens. The data of Figure

7.6 do not indicate whether the abnormal grains initiate from a less-deformed polycrystalline grain or from a newly recrystallized grain. The polycrystalline regions experienced deformation at least up to the critical strain required for DAGG initiation. The resulting polycrystalline microstructures reveal the subgrain structures expected from dislocation creep of this commercially-pure, polycrystalline metal.

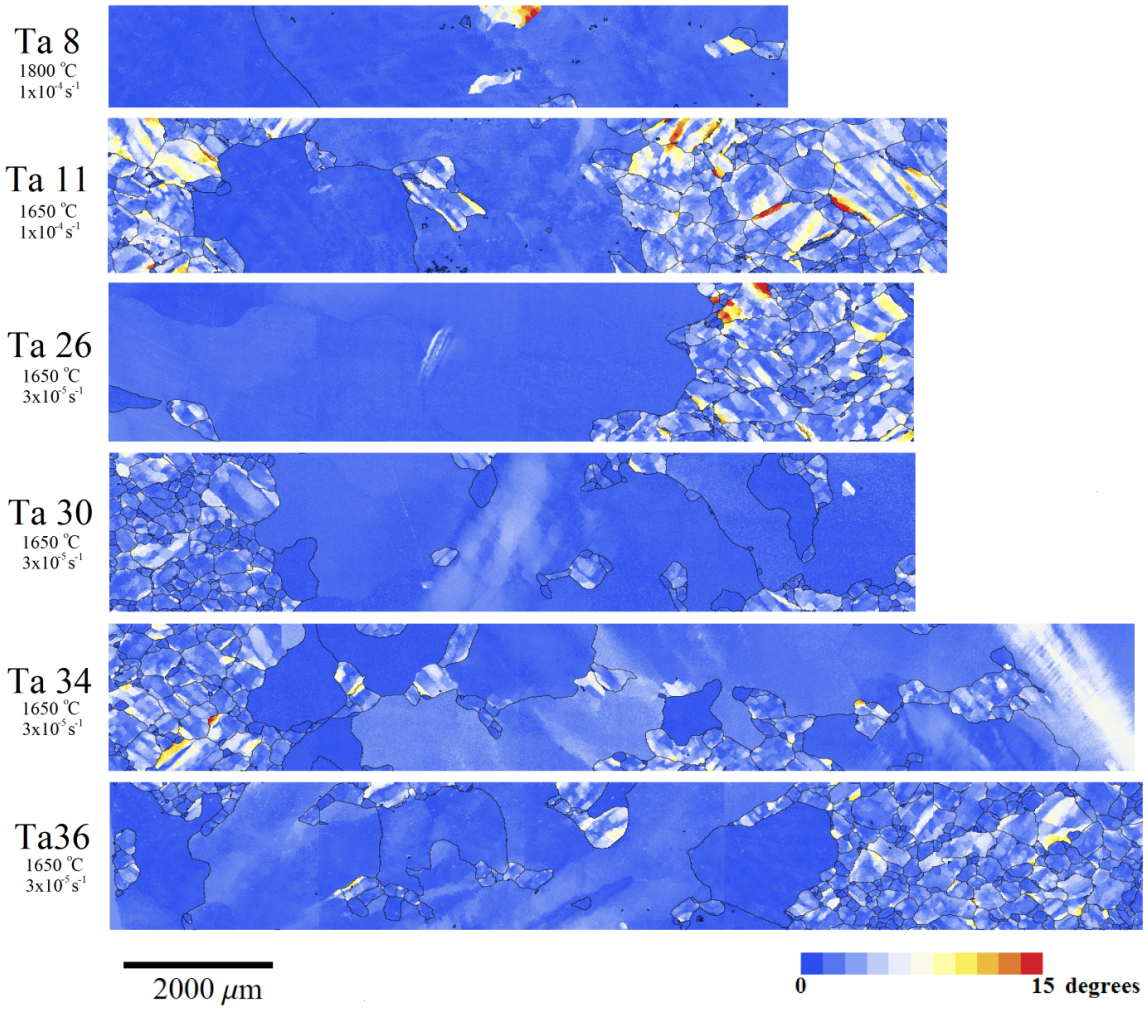

Figure 7.6: Misorientation maps are presented for the six Ta-A specimens of Figure 7.4. Each point is colored by its misorientation relative to the average orientation of the grain to which it belongs.

The grain orientation spread (GOS) provides another method of viewing misorientation and was previously discussed in §3.3.3.2. Figure 7.7 shows the GOS map from each of the specimens of Figure 7.4.

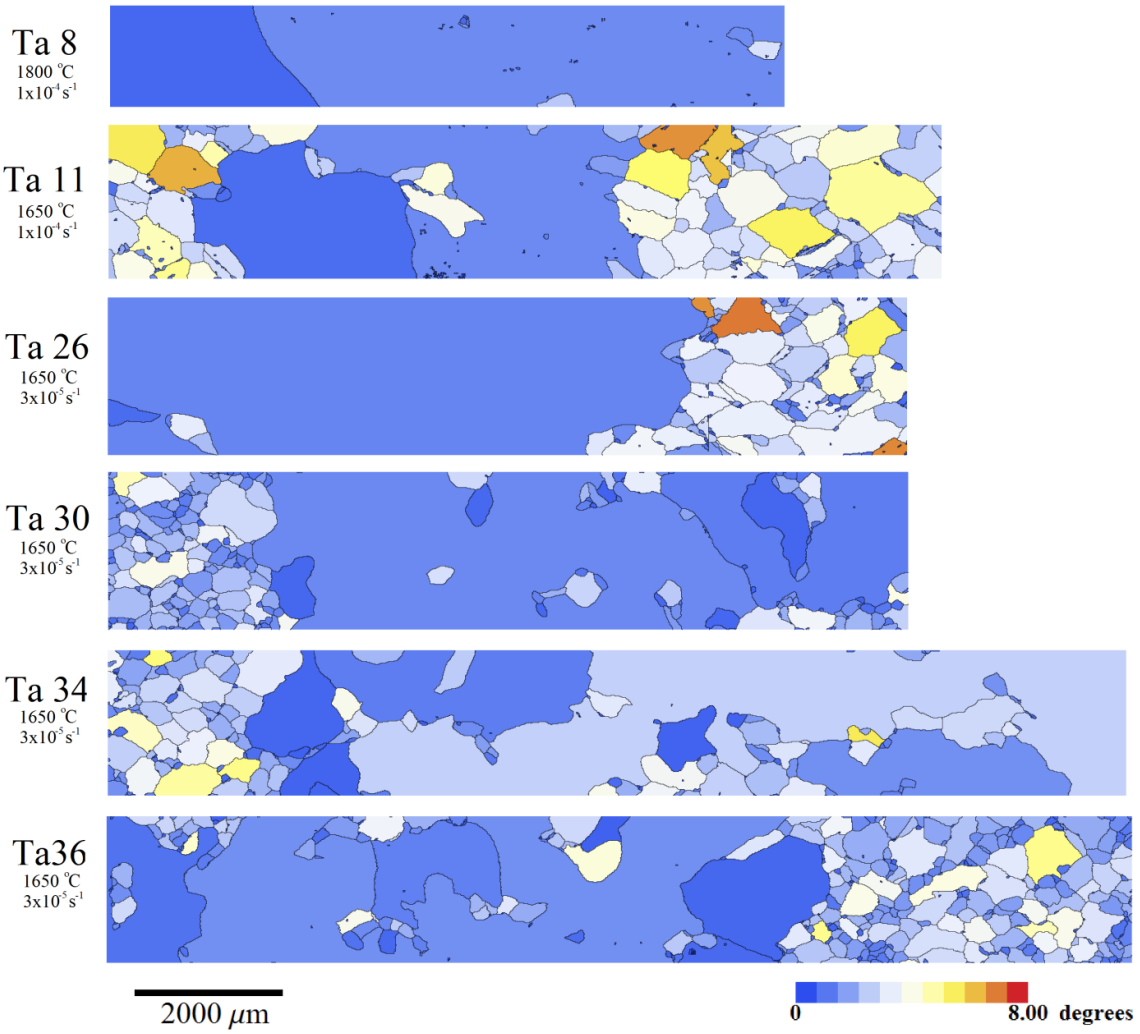

Figure 7.7: Grain orientation spread (GOS) maps are shown for the six Ta-A specimens of Figure 7.4. Each grain is colored to indicate the average misorientation of the points within it from the average orientation of the grain.

The GOS misorientation analysis allows for a comparison of deformation between grains based on their type. This requires specific definitions to distinguish between

DAGG (abnormal), island, and polycrystalline grains. Abnormal grains must be much larger than the average grain size and, in this case, often relatively undeformed. Thus, abnormal grains are defined here as those grains that are at least three times the average grain size and have a GOS of 1.5° or less. An exception was made to the maximum GOS criterion for the largest grain, since the GOS is disproportionally large for a large grain with a specific lattice curvature than a small grain with the same lattice curvature. Island grains are those that border only abnormal grains, such that an island grain may reside entirely within an abnormal grain or at the boarder between two or more abnormal grains. Polycrystalline grains are all grains that are not defined as either abnormal or island grains.

An island grain may occur by growing to a large size prior to growth of the DAGG grain in which it subsequently resides. A large grain size decreases grain-boundary curvature, which decreases the driving force for consumption by a DAGG grain. The grain-boundary character of an island grain, relative to the DAGG grain in which it resides, could also reduce its chance of being consumed by the DAGG grain. Island grains and clusters of grains suspended between abnormal grains were much more common in this Ta material than in the Mo materials of prior investigations [Worthington 2011].

The GOS was calculated for three different categories of grains: (a) abnormal grains, (b) polycrystal grains, and (c) polycrystal grains oriented within 5 degrees of the, or an, abnormal grain in the same map. The degree of deformation produced in the DAGG grains is compared to the deformation observed in the unconsumed regions of the specimen. Polycrystal grains similar in orientation to DAGG grains were singled out to determine if they are more or less likely to accumulate deformation than the average polycrystal grain, which may influence why a particular grain is selected to grow

abnormally. If these grains are relatively undeformed, this may indicate that DAGG grains initiate from relatively strain-free grains that consume their more deformed neighbors. If these grains are more deformed than the DAGG grains, this may indicate that DAGG grains initiate by first recrystallizing and forming a new grain. This metric only considers the orientation of each grain, not the orientation of its neighboring grains that could significantly affect the deformation observed because of interactions at the grain boundary.

The average GOS values for grains in each category (a, b, and c) are shown in Table 7.1. The average GOS of the abnormal grains is approximately half that of the unconsumed polycrystal grains, meaning that, on average, the amount of deformation accumulated in the DAGG grains at the end of testing is approximately half that accumulated in the polycrystalline microstructure. The GOS is ideally suited for comparing grains of roughly the same size, since small lattice curvature over a large area will be interpreted as a large GOS misorientation. The DAGG grains are significantly larger than the polycrystal grains. Thus, the lattice curvature of DAGG grains, in comparison with the polycrystal grains, will be even less than that suggested by the GOS value. The average GOS of polycrystal grains oriented similarly to abnormal grains is slightly higher than that observed in all polycrystal grains, but this difference is not statistically significant. From this analysis, it is concluded that the orientation of a grain is not a predictor of the strain it will accumulate or its likelihood of becoming a DAGG grain.

Table 7.1: Average grain orientation spread (GOS) values are given for three grain classifications in the six Ta-A specimens of Figure 7.4.

	GOS, degrees
Abnormal grains	1.2 ± 0.6
Polycrystal grains	2.3 ± 1.0
Polycrystal grains oriented similarly to abnormal	2.9 ± 1.1

7.2.2 Slip Properties

To further investigate the effects of grain orientation and plasticity on DAGG, the Schmid factor and Taylor factor were determined at each point on each EBSD map. Results are shown in Figures 7.8 and 7.9, respectively, to determine if certain types of grains (abnormal, polycrystal, or island) commonly have orientations that are beneficial or detrimental to slip. Because DAGG requires continued straining, it is hypothesized that DAGG grains may prefer orientations for which plastic strain accumulation is easier.

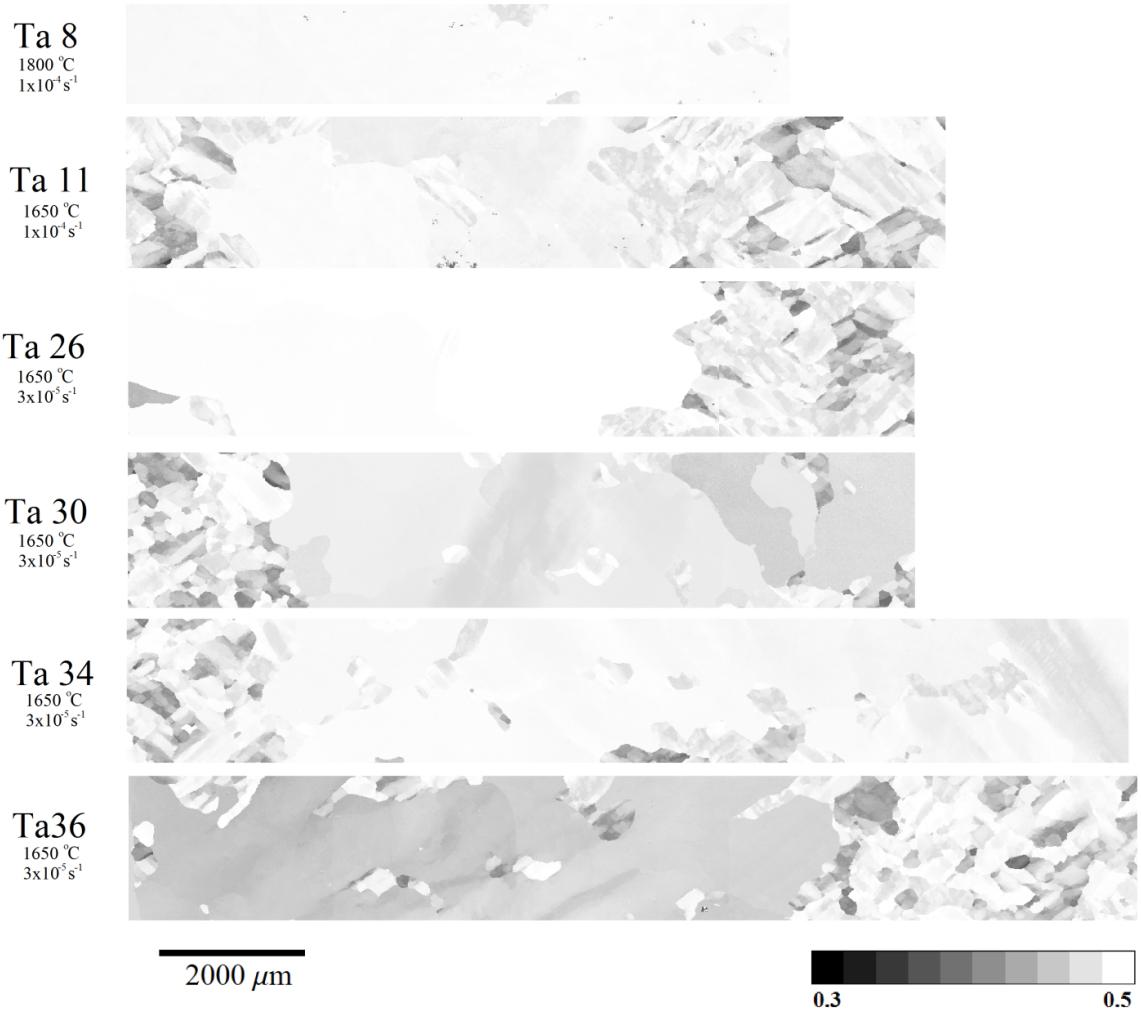

Figure 7.8: Schmid factor maps are shown for the six Ta-A specimens of Figure 7.4. Schmid factor presented at each point is that with the highest value from the three major slip systems: {110}<111>, {112}<111>, and {123}<111>.

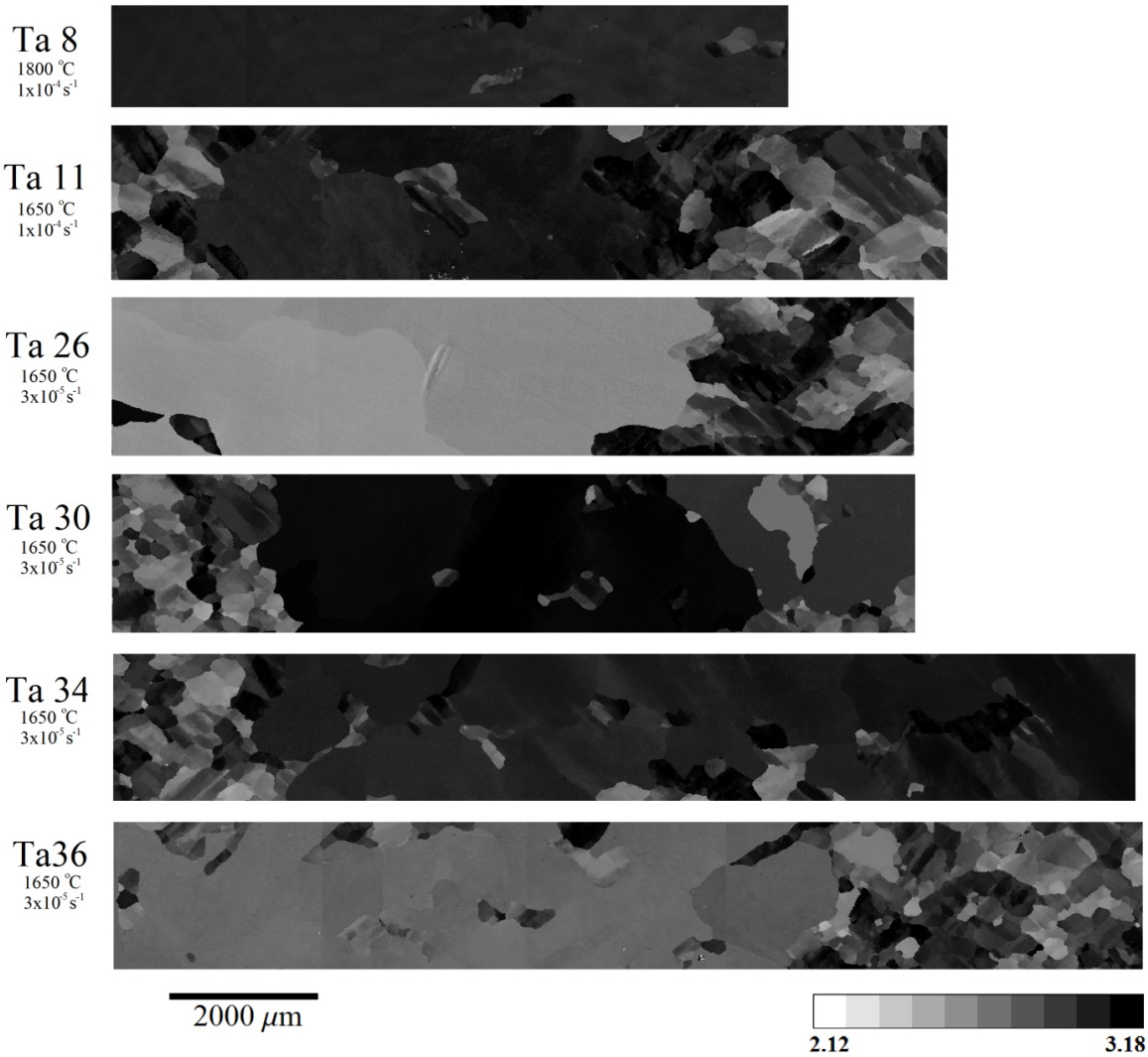

Figure 7.9: Taylor factor (for multiple-slip) maps are shown for the six Ta-A specimens of Figure 7.4.

From Figures 7.8 and 7.9, it is not apparent that DAGG grains or polycrystalline grains consistently have orientations with high or low Schmid or Taylor factors. A summary of the data from Figures 7.8 and 7.9 is shown in Tables 7.2 and 7.3 for Schmid factor and Taylor factor, respectively. The Schmid factor is relatively constant among each grain type for each slip system. The same is true for Taylor factor, which is effectively identical for each grain type. The lack of a definitive preference for Schmid

or Taylor factor with grain type indicates that the orientation preference of DAGG grains is likely not due to favorable slip properties for specific orientations.

Table 7.2: Average Schmid factors for three slip systems, plus combined slip, are shown for various grain types in the six Ta specimens of Figure 7.4.

	Schmid factor			
	{110}<111>	{112}<111>	{123}<111>	{110,112,123}<111>
All grains	0.46 ± 0.02	0.47 ± 0.02	0.48 ± 0.02	0.48 ± 0.02
Abnormal grains	0.46 ± 0.02	0.47 ± 0.02	0.48 ± 0.01	0.49 ± 0.01
Polycrystalline	0.46 ± 0.02	0.47 ± 0.03	0.48 ± 0.02	0.48 ± 0.02
Island grains	0.44 ± 0.03	0.47 ± 0.02	0.48 ± 0.02	0.48 ± 0.02

Table 7.3: Average Taylor factors (for multiple-slip) are shown for various grain types in the six Ta specimens of Figure 7.4.

	Taylor factor
All grains	2.93 ± 0.19
Abnormal grains	2.93 ± 0.2
Polycrystalline	2.93 ± 0.17
Island grains	3.05 ± 0.14

7.2.3 Grain Boundary Characterization

In §6.4, it was suggested that variations in DAGG behavior might be the result of the formation of multiple DAGG grains. The reason for the formation of multiple DAGG

grains, instead of the single or very few DAGG grains commonly observed in Mo-PMB by Worthington [Worthington 2011], is unknown. The grain boundaries are characterized to determine if this character plays a role in the formation of DAGG grains.

The grain boundaries observed from the EBSD data of Ta were characterized as described in §3.3.3.4. Grain boundary character between various grain types was then quantified. Maps of the grain boundaries, colored to indicate grain boundary character, are shown in Figure 7.10. The boundaries indicated include Σ3, Σ5, Σ7, Σ9, Σ11, and low-angle boundaries with a misorientation less than 5°.

It is evident from 7.10 that Σ3 boundaries are dominant between abnormal grains. Only two specimens show any significant boundary character between abnormal grains that is not Σ3: Ta 30 with a Σ7 boundary and Ta 8 with a high-angle, above 10°, boundary with no observed special boundary character.

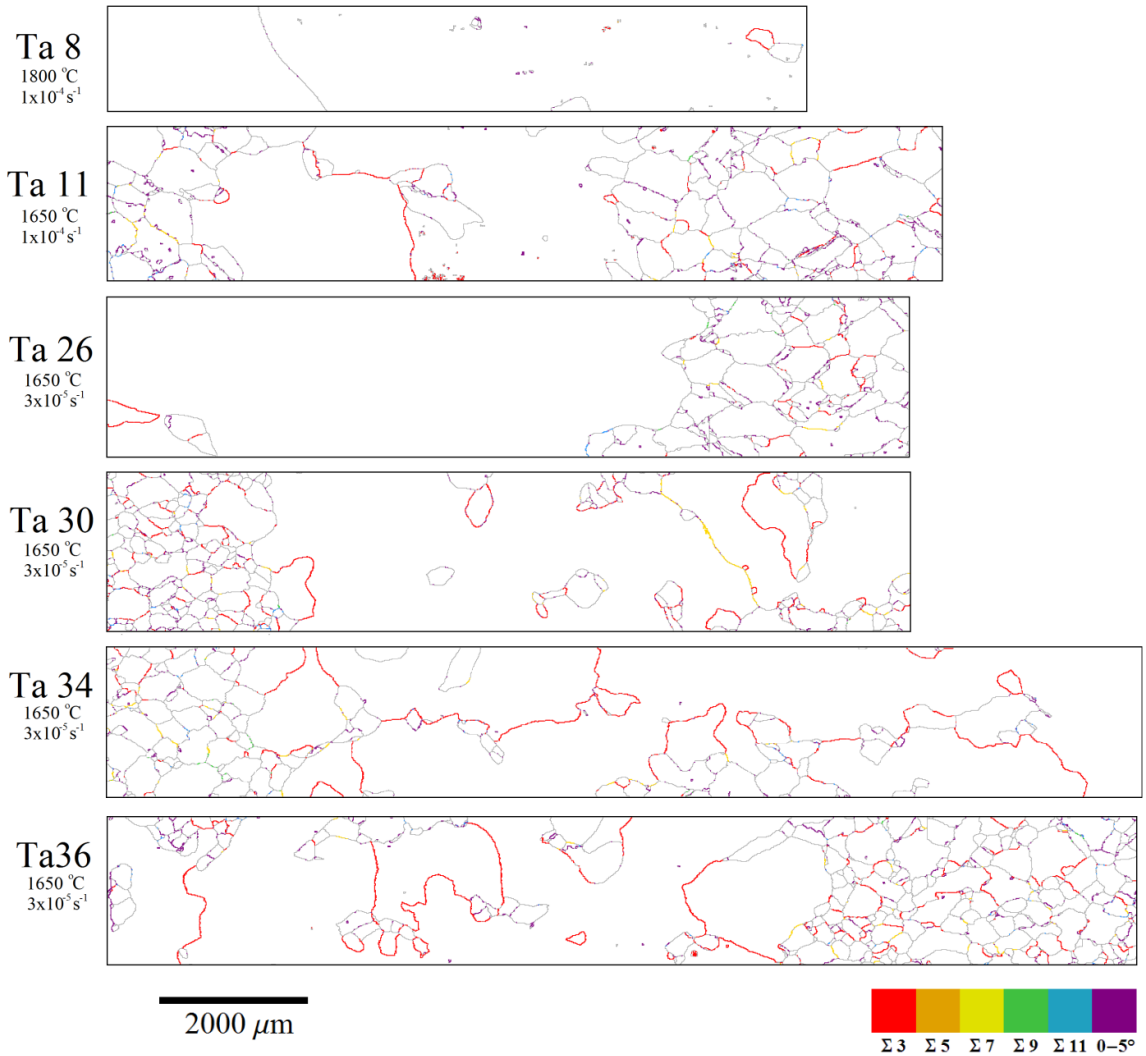

Figure 7.10: Coincident site lattice (CSL) boundaries Σ3, Σ5, Σ7, Σ9, Σ11, and low-angle boundaries, below 5°, are shown for the six Ta-A specimens of Figure 7.4.

Some polycrystal and island grains in Figures 7.6 and 7.7 show noticeably less deformation than the majority of the unconsumed polycrystal grains. These grains appear to be recrystallized. Their GOS is similar to the abnormal grains, but they did not grow abnormally. The recrystallized (RX) and non-recrystallized (non-RX) grains are considered both separately and together in the subsequent analysis. The GOS was used to distinguish RX grains by defining RX grains to have a GOS less than or equal to 1.5°.

Non-RX grains are defined as those grains with a GOS greater than 1.5°. Using this definition, 20 ± 16% of the polycrystalline grains are recrystallized in the six EBSD data sets.

The percentage of character for each grain boundary type (between two abnormal grains, between abnormal grains and island grains, between abnormal grains and recrystallized island grains, etc.) is provided in Table 7.4. The balance of the character of each grain boundary type is high-angle, above 10°. As shown in Figure 7.10, boundaries between abnormal grains are dominated by Σ3 character. Few Σ5 boundaries were observed, and other Σ boundary types, Σ7, Σ9, and Σ11, are uncommon for any of the boundary types.

The boundaries between DAGG and island grains have predominantly either low-angle or Σ3 boundary character. Low-angle boundaries are common because of the strong texture present in the recrystallized material and because these will generally have a lower mobility than high-angle boundaries [Huang 2000, Koo 2000]. The grain boundary character between abnormal grains and the RX and non-RX versions of island and normal grains varies. Boundaries of RX grains are frequently Σ3, while boundaries of non-RX grains are not, and boundaries of non-RX grains tend to be low-angle slightly more often than boundaries of RX grains. Other special boundary types are uncommon between abnormal and island grains. Previous reports on the grain boundary character of island grains within abnormal grains are consistent with these observations. Koo *et al*. observed small-angle boundaries around island grains in Cu [Koo 2000], and Bennett *et al*. observed a large fraction of island grain boundaries in Fe-1%Si to have a Σ3 character [Bennett 2007].

Percentages of grain boundary types between all normal grains, both RX and non-RX, are effectively equivalent. Between abnormal and RX normal grains the boundary is

often Σ3, as mentioned previously; however, between abnormal and non-RX normal grains the boundary character is very similar to that found between normal grains. Thus, the grains that are recrystallizing are often forming with orientations that form a special boundary character with the abnormal grains, while the grain boundary character between the abnormal and non-RX normal grains is not unique from that observed in the material prior to any recrystallization or grain growth.

Table 7.4: Percentages of grain boundary types between various grain classifications are given for the boundaries in the maps presented in Figure 7.10.

	Σ 3	Σ 5	Σ 7	Σ 9	Σ 11	< 5°	5 to 10°	> 10°
Total	17.8	0.0	2.6	0.1	0.1	3.3	14.9	bal.
Abnormal-Abnormal	85.3	0	7.8	0	0	0	0	bal.
Abnormal-Island	20.7	0	0.7	0	0	8.5	15.4	bal.
Abnormal-Island (RX)	29.1	0.1	0.7	0	0	11.6	10	bal.
Abnormal-Island (non-RX)	6.4	0	0.8	0	0	3.2	24.8	bal.
Abnormal-Normal	21.9	0	2.6	0.1	0.4	1.2	14.4	bal.
Abnormal-Normal (RX)	36.5	0	2.3	0.2	0	1.6	12	bal.
Abnormal-Normal (non-RX)	14.1	0	2.8	0.1	0.6	1	15.7	bal.
Normal-Normal	10.6	0	2.3	0.1	0	9.4	23.7	bal.
Normal-Normal (RX)	11.6	0	1.6	0	0	14.3	27.2	bal.
Normal-Normal (non-RX)	10.5	0	2.4	0.1	0	8.7	23.5	bal.

The frequency of Σ3 special boundaries along DAGG grains is an interesting, new observation. Σ3 boundaries are particularly low energy and are not expected to be thermally activated [Olmsted 2009b]. Boundary energy and mobility characteristics are not easily described by simple quantifications of misorientation and Σ character and are not completely understood [Olmsted 2009a, 2009b]. Nevertheless, since these boundaries are often low energy, it is possible that the occurrence of Σ3 boundaries causes the termination of DAGG grain boundary migration, which would then provide sufficient time for the initiation of additional DAGG grains. If a DAGG grain is separated from another grain by a Σ3 boundary, it is less likely to consume that grain, providing an opportunity for the second grain to become an island grain or grow abnormally itself. This may also be the source of the gradual, or intermittent, stress drops associated with DAGG in Ta-A, as demonstrated previously in Figure 6.11.

The frequent presence of Σ3 boundaries may be because of the strong initial texture in the Ta-A sheet. The crystallographic orientation along the STD is primarily <111>, and deviation outside this majority texture is not significant. A Σ3 boundary is defined by a 60° rotation about a <111> axis, so it may be relatively easy for Σ3 boundaries to form because most of the grains already allign the <111> along the STD. The natural spread of rotations about this axis allows for a large number of grain boundaries to fall into the range of misorientations defined as Σ3.

7.3 CONCLUSIONS

1. DAGG grains in Ta-A do not appear to prefer to grow along the surface of specimens, as was observed in Mo by Worthington [Worthington 2011].

2. Specimen surface roughness increases with increasing temperature and is likely because of varying plastic deformation between the large grains prior to DAGG initiation.
3. Multiple DAGG grains frequently form, and optical microscopy is often insufficient for identifying all DAGG grain boundaries.
4. DAGG grains typically do not accumulate a large amount of plastic deformation during DAGG grain formation.
5. There is no indication that the DAGG grains prefer orientations because of their slip properties, as evidenced by analysis of the GOS, Schmid factor, and Taylor factor.
6. Grain boundaries between abnormal grains and between abnormal grains and recrystallized grains often have $\Sigma 3$ character.
7. $\Sigma 3$ and low-angle boundaries are often observed around island grains.
8. The formation of low-energy boundaries, such as $\Sigma 3$ boundaries, may hinder the growth of DAGG grains.

8 DAGG in Ta-B

Constant true-strain rate tests were conducted at temperatures of 1650 to 1950 °C and strain rates of 3×10^{-5} and 1×10^{-4} s^{-1} on a Ta material alloyed to reduce normal grain growth, Ta-B, in an effort to induce DAGG. Six (6) tests were conducted on Ta-B. The true stress *versus* true strain data are presented. The orientation of DAGG grains and microstructural features were analyzed using Laue back-scatter diffraction, EBSD, and optical microscopy. Microstructural analysis of Ta-B specimens was conducted similarly to that of Ta-A in Chapter 7.

A summary of test conditions and microstructural observations is provided in Table 8.1. Additional information on each specimen is provided in Appendix F. Significant AGG was observed in three specimens: Ta-B3, Ta-B4, and Ta-B5. These tests were also those conducted at the highest temperatures, 1850 and 1950 °C. Specimen Ta-B2, tested at 1750 °C and 1×10^{-4} s^{-1}, demonstrated a large abnormal grain at its fracture tip, but it is unclear if this occurred prior to, during, or after rupture. Specimens Ta-B3 and Ta-B4 were tested to rupture, while Ta-B5 and Ta-B6 were not.

Table 8.1: Summary of test conditions and microstructural observations is presented for six constant true-strain rate tests of Ta-B.

Specimen	Temperature, °C	Strain rate, s^{-1}	Test end	Microstructure
Ta-B1	1650	3×10^{-5}	After rupture	No AGG
Ta-B2	1750	1×10^{-4}	After rupture	AGG at fracture tip
Ta-B3	1850	1×10^{-4}	After rupture	AGG along entire gauge length
Ta-B4	1950	1×10^{-4}	After rupture	AGG along entire gauge length
Ta-B5	1850	3×10^{-5}	Prior to necking	DAGG along entire gauge length
Ta-B6	1750	3×10^{-5}	During necking	No AGG

The true stress *versus* true strain data for the six Ta-B specimens are shown in Figure 8.1. Strain softening occurred during tests at 1850 °C, and to a lesser extent at 1750 °C. It is possible that this occurred because of dynamic recrystallization (DRX). Strain softening, however, was not observed at 1950 °C. The cause of this is unknown, but it is possible that a stable grain size from DRX was obtained much earlier than for the lower test temperatures. All test parameters for the 1950 °C test were identical to those of the other specimens except for the temperature and strain rate. Specimens that exhibited AGG, see Table 8.1, did not show the characteristic sharp drop in stress that is associated with the initiation of DAGG. A slight drop in stress was observed during tests at 1850 °C, but that change in stress is gradual. Most of the tests continued until rupture because of the lack of an identifiable stress drop. Ta-B5 is the only specimen that exhibited AGG and was tested short of rupture. It is concluded that the AGG observed in Ta-B5 must have occurred under dynamic conditions and is not due to mechanisms related to the failure of the specimen, such as a stress concentrations created during necking or SAGG following failure. It is possible that the abnormal grains observed in

the other Ta-B specimens also resulted from DAGG, but this cannot be confirmed. All of the specimens except Ta-B5 showed signs of necking. It should be noted that the true stress *versus* true strain test data shown in Figure 8.1 are not accurate once necking begins. The exact point at which necking occurs during each test is unknown. Thus, the data just prior to the end of the test is not representative of the true values.

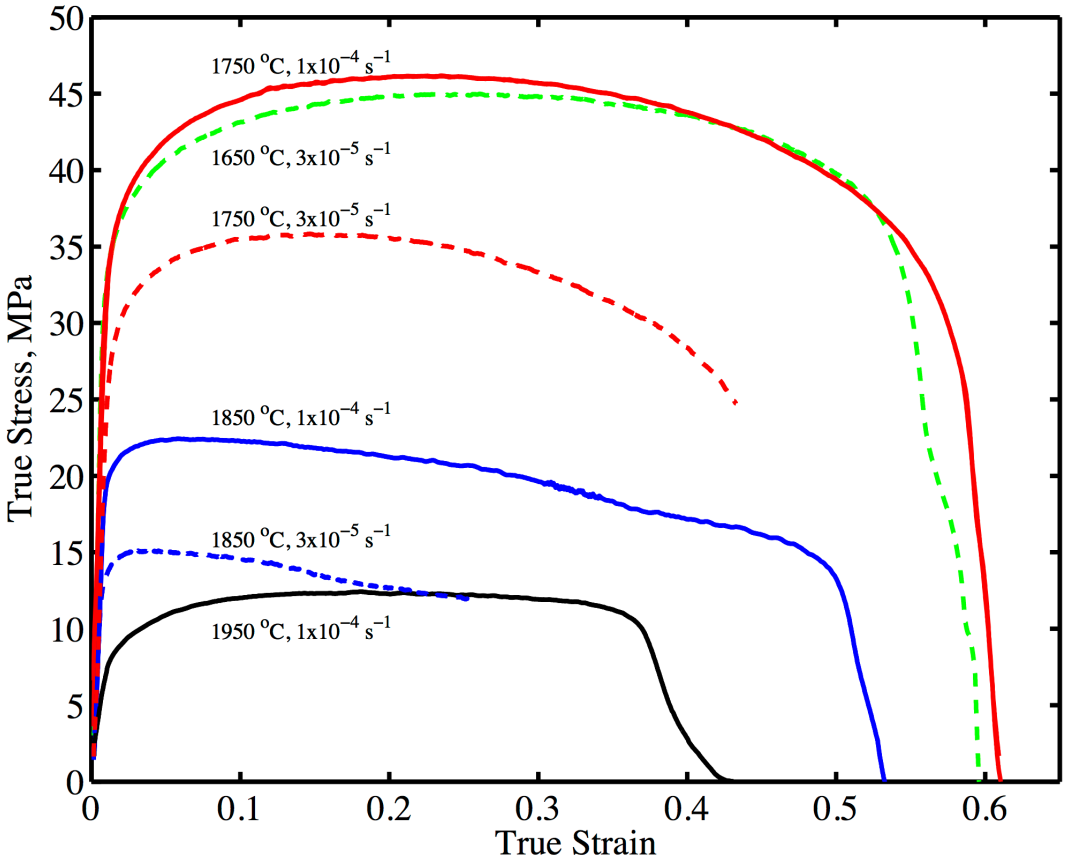

Figure 8.1: True stress *versus* true strain is plotted for six Ta-B specimens.

The data of Figure 8.1 are consistent with creep theory in that the flow stress decreases with increasing temperature and decreasing strain rate. It is difficult to compare the steady-state flow stress under each set of conditions due to the strain softening that occurred in some specimens. The yield stress of Ta-B is considerably

higher than that observed for Ta-A in Chapter 6, especially at the lower test temperatures. This may be, in part, due to grain boundary strengthening mechanisms resulting from the small initial grain size in Ta-B. The alloying additions in Ta-B presumably form pinning sites that restrict grain boundary motion and thus hinder grain growth. The restriction of dislocation motion by the alloying additions would also act to increase the yield stress.

8.1 ORIENTATIONS

The orientations of five abnormal grains produced in Ta-B were obtained using Laue back-scatter diffraction and are shown along with the orientations of DAGG grains produced in Ta-A in the inverse pole figures of Figure 8.2. The abnormal grains in Ta-B orient similarly to those in Ta-A. This is likely due to their similar recrystallized textures, as demonstrated in §4.3. The abnormal grains in Ta-B form with orientations primarily within the texture of the annealed sheet.

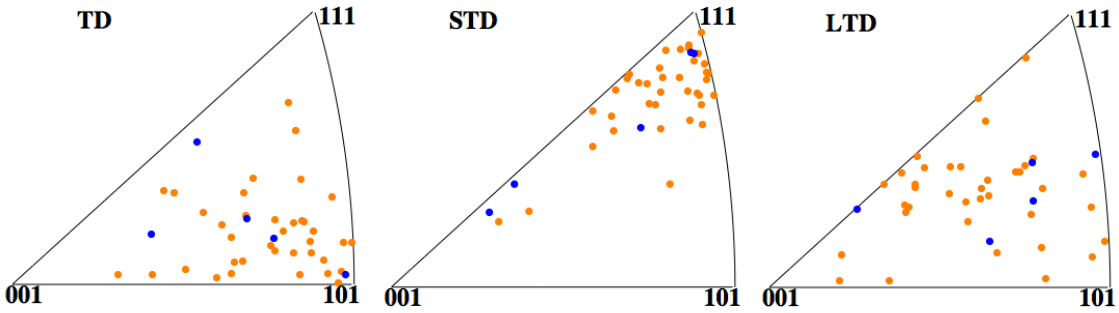

Figure 8.2: Inverse pole figures relative to the TD, STD, and LTD, are shown indicating orientation of DAGG grain produced in Ta-B (blue) and Ta-A (orange).

8.2 CROSS-SECTIONS

The through thickness DAGG grain morphology was observed by cross-sectioning two specimens, Ta-B3 and Ta-B4, to determine if the abnormal grains grow preferentially at the surface of the specimen. This analysis method is identical to that

presented in §7.1, and the cross-sections are shown in Figures 8.3 and 8.4 for Ta-B3 and Ta-B4, respectively.

Figure 8.3 shows significant abnormal grain growth along one side of the specimen tested at 1850 °C. This specimen exhibited some bowing following testing, such that the surface of the specimen shown in Figure 8.3(d) was originally bowed outwards before being ground and polished flat for observation. It is unknown whether the bowing occurred prior to or after AGG. So, it is also not known if the bowing contributed to or is a product of the preferential growth on one side. No significant through-thickness variations in texture or grain size were observed in the annealed cross-section of Ta-B in §4.3 that could provide a cause for a growth preference on one side of the specimen. The grain boundary at the end of the abnormal grain, where it meets the unconsumed polycrystalline region, is relatively straight and does not indicate any preferred growth near the surface.

The specimen in Figure 8.4 (Ta-B4) was tested at 1950 °C, a higher temperature than the specimen in Figure 8.3 (Ta-B3), and has more grain growth in the polycrystalline regions that were not consumed by the large abnormal grains, as shown in 8.4(b) and (c). The grain size was nearly constant in Ta-B when annealed statically up to a time of 8 hours and temperature of 1850 °C. The large grains observed in the unconsumed polycrystalline regions possibly grew due to dynamic recrystallization, a possibility that will be later explored using EBSD data. These grains typically did not span the thickness of the specimen. Two abnormal grains are shown, and the grain boundaries between them and the unconsumed polycrystalline regions are relatively straight. This indicates that the preferential surface growth observed in Figure 8.3 does not consistently occur in Ta-B. The reason for preferential surface growth in Figure 8.3 is unknown, but could be due to a texture variation that was not observed due to the small sample used for

analyzing the through-thickness texture in §4.3, or due to the bowing that occurred under tensile deformation.

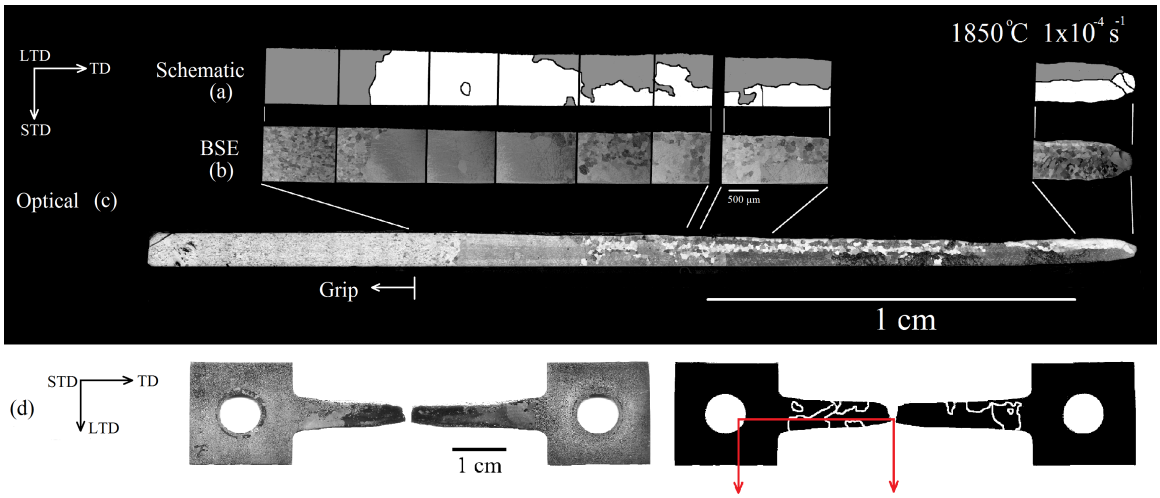

Figure 8.3: Microstructure of a Ta-B specimen tested at 1850 °C and 1×10^{-4} s^{-1} (Test B3), is shown though (a) a schematic of abnormal grain boundaries identified in the specimen cross-section, (b) back-scatter electron images from the cross-section, (c) an optical image of the entire cross-section, and (d) an optical image of the entire specimen. The gray areas in (a) denote polycrystalline regions, and the white areas denote abnormal grains. The red line and arrows in (d) indicate the location of the cross-section cut and the direction of viewing the cross-section. Traces of abnormal grains are shown in the schematic to the right of the specimen in (d).

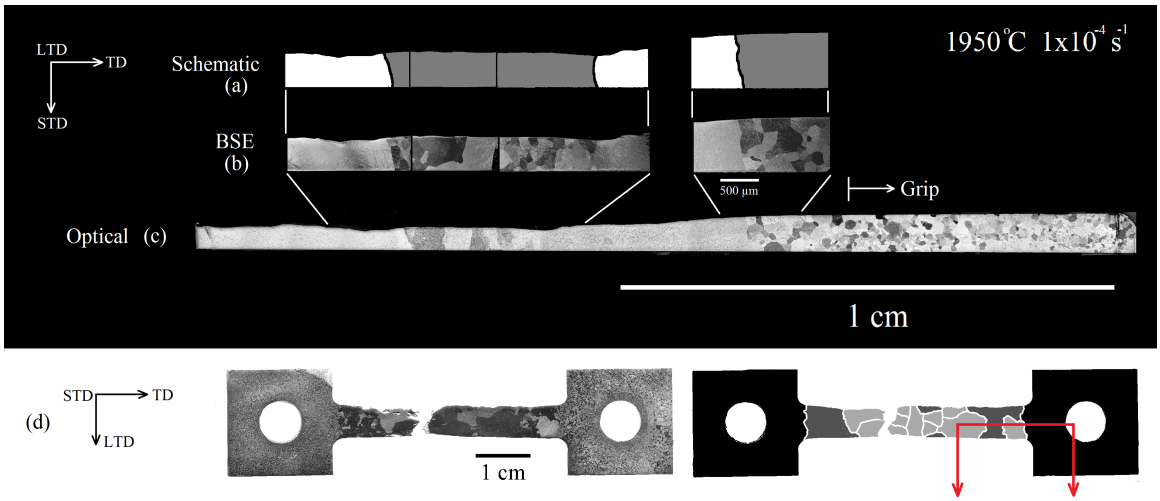

Figure 8.4: Microstructure of a Ta-B specimen tested at 1950 °C and 1×10^{-4} s^{-1} (Test B4), is shown through (a) a schematic of abnormal grain boundaries identified in the specimen cross-section, (b) back-scatter electron images of the cross-section, (c) an optical image of entire cross-section, and (d) and optical image of entire specimen. The gray areas in (a) denote polycrystalline regions, and the white areas denote abnormal grains. In (d) the red line and arrows indicate the location of the cross-section cut and the direction of viewing the cross-section, and the schematic is shaded to indicate large abnormal grains in light-gray, regions of recrystallized grains in dark-gray, and unconsumed regions in black.

8.3 EBSD

Three Ta-B tested specimens were analyzed using EBSD in a manner similar to that given in §7.2. Information on the test conditions, microstructures of the specimens analyzed using EBSD, and locations of EBSD analysis are shown in Figure 8.5. Grain boundaries along abnormal grains observed following etching are indicated in the schematic below each specimen image.

Specimen number	Test conditions	Microstructure
Ta B3	1850 °C 1×10^{-4} s^{-1}	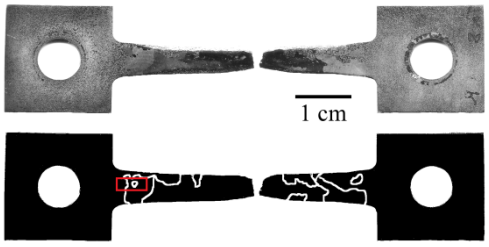
Ta B4	1950 °C 1×10^{-4} s^{-1}	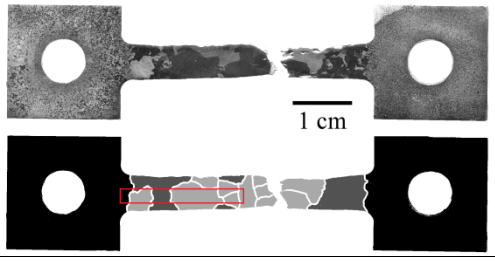
Ta B5	1850 °C 3×10^{-5} s^{-1}	

Figure 8.5: Test conditions and resulting microstructures are shown for thee Ta-B specimens characterized using EBSD. The top image of each shows the specimen polished and etched, and the bottom image shows a schematic of grain boundaries that could be identified in the DAGG or abnormal grain growth region by eye following etching. The schematic for Ta-B4 also distinguished between regions with large abnormal grains (light-gray), recrystallized grains (dark-gray), and unconsumed polycrystalline regions (black). The red box indicates the region where EBSD data were collected.

Figure 8.6 shows three maps from EBSD data sets, each colored by the inverse-pole-figure (IPF) coloring scheme to indicate crystallographic orientations aligned along the STD, TD, or LTD. The size of each scan was adjusted based on grain size and to observe a sufficient number of grain boundaries. The orientation of the STD is not as strongly along the <111> as was observed in Ta-A. Crystallographic orientations along the STD in Ta-B generally align from <111> to <100>.

The distance between scan points used to create the EBSD map, i.e. the step size, was 7 μm for specimen Ta-B3 and 10 μm for specimens Ta-B4 and Ta-B5. The step size was reduced for Ta-B3 because the grain size of the unconsumed grains is smaller. Thus, it was desired to increase the number of scan points in each grain to improve the accuracy of grain size and boundary length calculations. A minimum of approximately 8 scan points is required to define the grain size to within 5% [Humphreys 2001]. Grains under 8 scan points in size account for less than 1.5% of the area occupied by polycrystal grains for all maps in this study. The reduced step size is, in part, why the map of Ta-B3 is smaller than of Ta-B4 and Ta-B5. The size of each map was chosen to obtain a reasonable sample of grain boundaries and grain types.

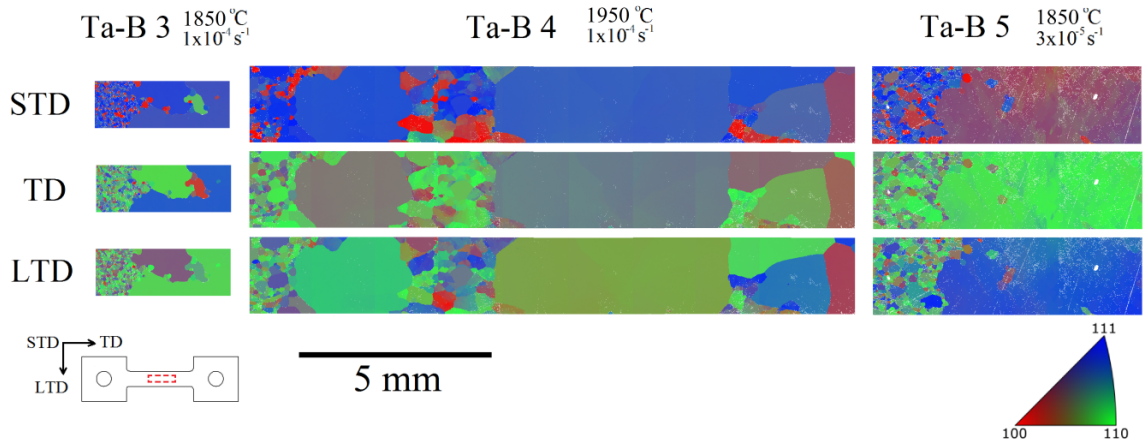

Figure 8.6: EBSD data are shown for three Ta-B specimens. Data are colored by the inverse pole figure coloring scheme to the bottom right and indicate orientations normal to the STD, TD, and LTD specimen directions. Unindexed points are white.

8.3.1 Deformation

Deformation is visualized from EBSD data by first identifying grains and then calculating the ROD and GOS, as described in §3.3.3. ROD and GOS maps created from the EBSD data sets of the specimens from Figure 8.6 are shown in Figures 8.7 and 8.8.

The ROD and GOS maps of tested Ta-B specimens indicate that recrystallization of the polycrystalline microstructure was common. The polycrystal grains in the three materials were 83 ± 25 % recrystallized, where a recrystallized grain is defined as one with a GOS less than 1.5°. Figure 8.7 shows little deformation within any grains in specimen Ta-B3, which was tested to rupture. The deformation substructure expected from straining is not present in the unconsumed polycrystal grains. This is also true for part of Ta-B4, and for Ta-B5. Ta-B4 contains areas of unconsumed polycrystal grains that appear recrystallized and areas that are deformed (i.e., have high ROD and GOS values). In the areas that show deformation, it is not known if the material did not recrystallize or if it recrystallized early in the tensile test and then accumulated strain during tensile deformation. The deformation in the deformed regions of Ta-B4 is consistent with the deformation substructure expected from creep and is similar to that observed in unconsumed polycrystal grains in Ta-A. The grain size of the deformed regions is much larger than is observed in the original annealed material, but it is not known if this is because of grain growth of the original grains or growth following recrystallization. Considerable deformation is observed in the abnormal grain in specimen Ta-B5. The deformation in this grain is consistent with subgrain formation during creep, suggesting that the abnormal grain formed early during the tensile test. All other abnormal grains in the specimens studied for both materials have relatively little deformation. The Ta-B5 specimen, however, likely underwent significantly more deformation following abnormal grain growth than the other specimens. The point at which AGG occurred is not clear from the true stress *versus* true strain tensile data since there was no rapid drop in stress. The abnormal grains in Ta-B3 and Ta-B4 may have formed just prior to, or following, rupture since significant deformation was not observed in these abnormal grains.

The reason for the lack of a distinct stress drop corresponding to AGG is unknown. This may be due to difficulty of growing the grain though the thickness of the specimen or the rate of AGG. Slow AGG would cause a more gradual change from the flow stress of the polycrystalline material to that of the single crystal, which may not be perceptible. If the flow stress of a single crystal is relatively similar to that of a polycrystalline microstructure in Ta-B, the difficulty in detecting DAGG increases because of the small change in stress that must be indentified.

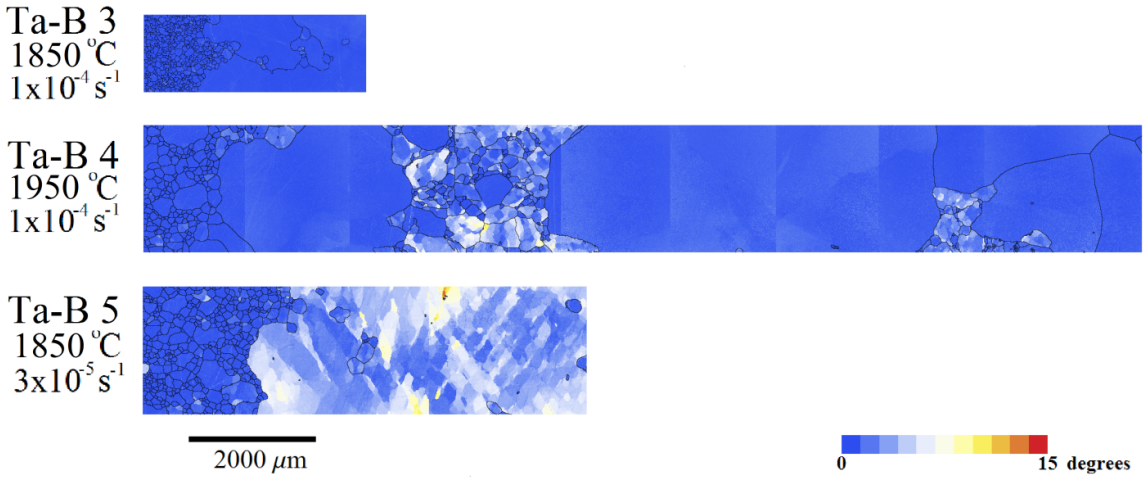

Figure 8.7: Misorientation (ROD) maps are presented for the three Ta-B specimens of Figure 8.5. Each point is colored by its misorientation relative to the average orientation of the grain to which it belongs.

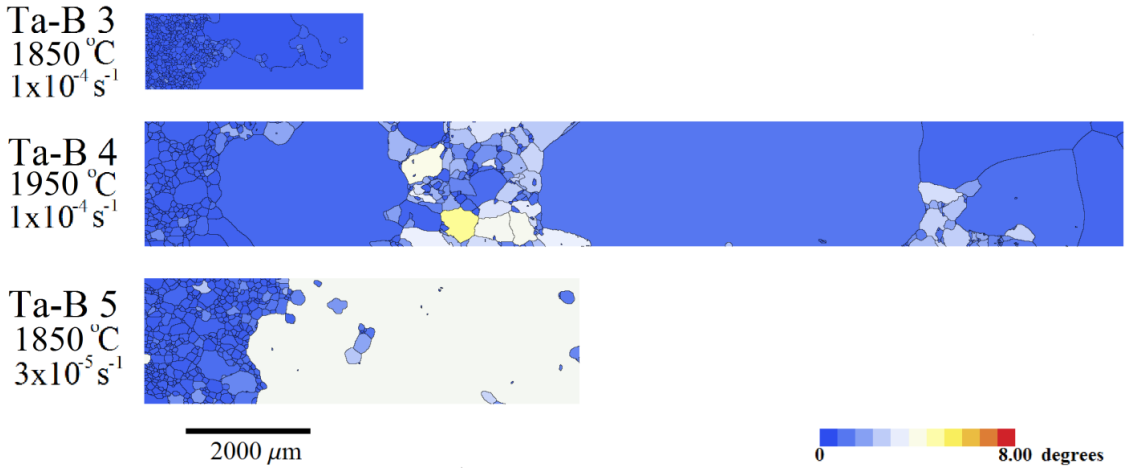

Figure 8.8: Grain orientation spread (GOS) maps are shown for the three Ta-B specimens of Figure 8.5. Each grain is colored to indicate the average misorientation of the points within it from the average orientation of the grain.

Abnormal, polycrystalline, and island grains were defined similarly as in §7.2. This allows for comparison of deformation and grain boundary character based on grain type. Abnormal grains are defined here as those grains that are at least five times the average grain size. Island grains are those that border only abnormal grains, and polycrystal grains are all grains that are not defined as either abnormal or island grains.

The average GOS for each grain type in each specimen is shown in Table 8.2. The GOS values in specimen Ta-B3 were effectively identical for all grain types. In specimen Ta-B4, on average, abnormal grains had a GOS value of approximately half that of the polycrystal grains. However, because some of the polycrystal grains are recrystallized while others are deformed, the average GOS value has a high standard deviation. Polycrystal grains in specimen Ta-B4 oriented similarly to abnormal grains also have a lower GOS value than the average GOS of all of the polycrystal grains. This trend is not consistent with observations of other Ta-A and Ta-B specimens, for which the values were approximately equivalent. However, this may simply indicate that the polycrystal grains often recrystallize to orientations similar to those of the abnormal

grains. In specimen Ta-B5, the GOS values of polycrystal grains and grains oriented similarly to the abnormal grain are similar, but the GOS value of the abnormal grain is much higher. This is likely due to straining following AGG, as discussed previously.

Table 8.2: Average grain orientation spread (GOS) values are given for three grain classifications in the three Ta-B specimens of Figure 8.5.

	GOS, degrees		
	Ta-B3	Ta-B4	Ta-B5
Abnormal grains	0.3 ± 0.2	0.7 ± 0.4	3.6 ± 1.7
Polycrystal grains	0.3 ± 0.2	1.6 ± 0.8	0.6 ± 0.3
Polycrystal grains oriented similarly to abnormal	0.3 ± 0.2	0.5 ± 0.3	0.4 ± 0.3

The Schmid and Taylor factors were calculated for each EBSD map to determine if certain grain types have orientations preferential for slip. The Schmid factor for each map is shown in Figure 8.9, and a summary of the results for each slip system and grain type is given in Table 8.3. No significant difference in Schmid factor is observed between different grain types in each specimen in Figure 8.9, and the data of Table 8.3 confirms this. The Schmid factor for each slip system is effectively the same for each grain type. Maps of the Taylor factor are shown in Figure 8.10, and a summary of this analysis is shown in Table 8.4. As with the Schmid factor, the Taylor factor does not change significantly with grain type. These observations are consistent with the observations of the Schmid factor and the Taylor factor of Ta-A grains in §7.2. There is no indication that the abnormal grains initiate from orientations that have a favorable or unfavorable orientation for slip.

Figure 8.9: Schmid factor maps are shown for the three Ta-B specimens of Figure 8.5. Schmid factor presented at each point is that with the highest value from the three major slip systems: {110}<111>, {112}<111>, and {123}<111>.

Table 8.3: Average Schmid factors for three slip systems, plus combined slip, are shown for various grain types in the three Ta-B specimens of Figure 8.5.

	Schmid factor			
	{110}<111>	{112}<111>	{123}<111>	{110,112,123}<111>
All grains	0.46 ± 0.03	0.46 ± 0.02	0.48 ± 0.02	0.48 ± 0.02
Abnormal grains	0.46 ± 0.03	0.46 ± 0.02	0.47 ± 0.02	0.48 ± 0.02
Polycrystalline	0.46 ± 0.02	0.47 ± 0.02	0.48 ± 0.02	0.48 ± 0.02
Island grains	0.46 ± 0.04	0.46 ± 0.02	0.48 ± 0.02	0.48 ± 0.02

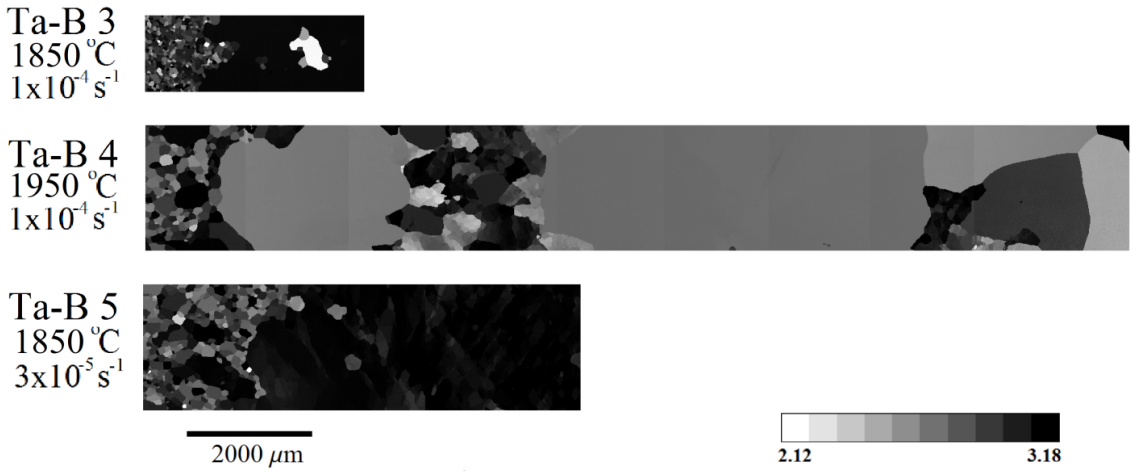

Figure 8.10: Taylor factor (for multiple-slip) maps are shown for the three Ta-B specimens of Figure 8.5.

Table 8.4: Average Taylor factors (multiple-slip) are shown for various grain types in the three Ta-B specimens of Figure 8.5.

	Taylor factor
All grains	2.91 ± 0.23
Abnormal grains	2.89 ± 0.23
Polycrystalline	2.95 ± 0.20
Island grains	2.88 ± 0.19

8.3.2 Grain Boundary Character

The character of the grain boundaries was analyzed similarly as for Ta-A in §7.2 to determine if particular grain boundary types may affect DAGG. A map of each EBSD data set indicating Σ3, Σ5, Σ7, Σ9, Σ11, and low-angle boundaries with a misorientation less than 5° is shown in Figure 8.11. A summary of grain boundary types and and their characters is shown in Table 8.5. Grain boundaries are not separated into RX and non-

RX versions, as was done in §7.2, because the grain boundary characters were similar between both RX and non-RX grains and their neighbors, except in cases where the sample size of boundaries was too small to make an accurate comparison.

In Ta-A, special boundaries, and Σ3 boundaries in particular, are dominant between abnormal grains. This is not the case for Ta-B. Some Σ9 character was observed in specimen Ta-B3 between abnormal grains, but no other special or low-angle boundary character was observed for any of the Ta-B specimens. The grain boundaries between abnormal grains and island grains were similar in character to the boundaries between normal grains, except that abnormal-island grain boundaries are more commonly low-angle. This effect was also observed in Ta-A and has been noted in the literature [Koo 2000]. The boundaries between abnormal and normal grains were similar to those observed between normal grains.

Grain boundary character does not appear to significantly affect AGG in Ta-B. The texture of Ta-B did not favor orienting the <111> crystallographic orientation along the STD as strongly as was observed in Ta-A. The lack of significant special boundary character between abnormal grains in Ta-B supports the notion that the special character in Ta-A was the result of the strong <111> texture. It was previously suggested that the gradual and multiple DAGG drops in Ta-A were the result of the formation of multiple DAGG grains and the impediment of DAGG due to certain grain boundaries. The data of Ta-B suggest that the formation of multiple grains may be more influential than the type of boundary that forms since many abnormal grains often formed in Ta-B without special boundary character, and the tensile behavior exhibited very gradual drops in stress that were often indistinguishable from DRX.

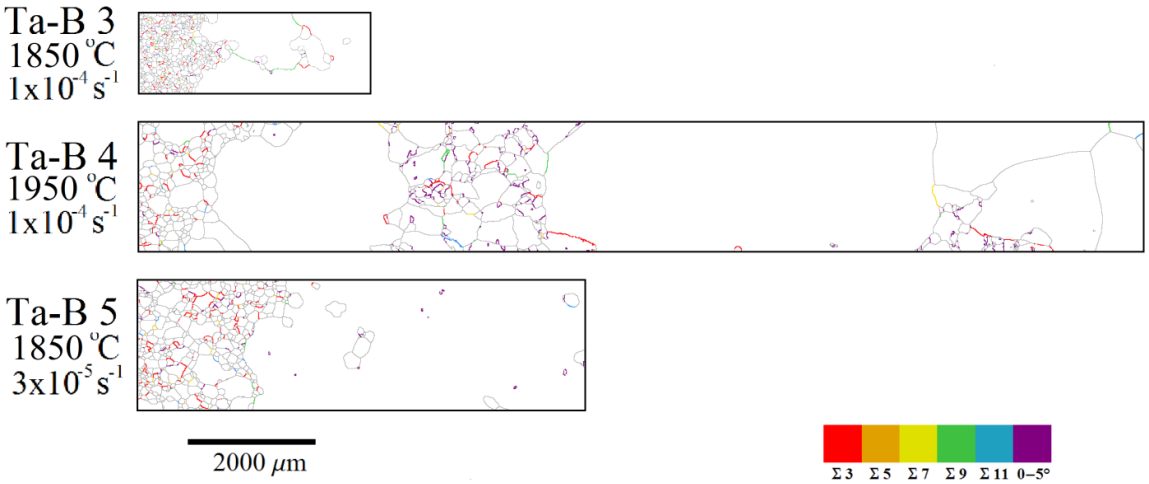

Figure 8.11: Coincident site lattice (CSL) boundaries Σ3, Σ5, Σ7, Σ9, Σ11, and low-angle boundaries, below 5°, are shown for the three Ta-B specimens of Figure 8.5.

Table 8.5: Percentages of grain boundary types between various grain classifications are given for the boundaries in the maps presented in Figure 8.11.

	Σ 3	Σ 5	Σ 7	Σ 9	Σ 11	< 5°	5 to 10°	> 10°
Total	6.1	0.0	1.0	1.2	0.8	9.0	15.7	bal.
Abnormal-Abnormal	0	0	0	12.4	0	0	0	bal.
Abnormal-Island	5.9	0	0	0.9	0	22.8	8.8	bal.
Abnormal-Normal	8.1	0	1.6	2.0	1.1	0.3	3.8	bal.
Normal-Normal	6.0	0	1.0	0.7	0.8	5.8	13.2	bal.

8.4 CONCLUSIONS

1. Constant true-strain rate tests were performed at temperatures of 1650 to 1950 °C and rates of 3×10^{-5} to 1×10^{-4} s^{-1} on a Ta alloyed to restrict normal grain growth, Ta-B.

2. Abnormal grains were observed in several specimens following tensile testing, and DAGG was confirmed in at least one test.
3. Although abnormal grains were observed in 4 specimens, no characteristic sharp drops in stress associated with the initiation of DAGG were observed.
4. Strain softening and recrystallization were observed in the microstructures following testing, indicating that DRX may occur under some conditions.
5. The orientations of the abnormal grains produced were similar to those of DAGG grains in Ta-A, and came primarily from the majority texture of the recrystallized material.
6. Cross-sections of two specimens indicate some preference for growth along the specimen sheet surface, but abnormal grains did not consistently prefer surface growth.
7. The majority of the unconsumed polycrystal grains in the specimens analyzed were recrystallized.
8. Grains of all types have approximately the same slip characteristics, as described by the Schmid and Taylor factors. Thus, there is no preferred orientation of abnormal grains, or other grain types, related to these properties.
9. Special boundary character was not frequently observed between abnormal grains, contrary to observations of Ta-A.
10. Island grains were surrounded by low-angle boundaries more often than for other grain types.

9 Conclusions

9.1 DAGG Under Constant True Stress

DAGG was observed during constant true-stress tensile testing of Mo-PMB at 1650 °C (0.66 T_H). This is the first reported case of DAGG occurring under constant true stress. Under these conditions, DAGG is evidenced by a sharp increase in strain rate. Upon completion of DAGG, the strain rate may briefly remain constant before increasing further as specimen failure begins.

DAGG was observed at true stresses of 28 to 37 MPa. The strain rate continually increases during DAGG; however, the average strain rate during DAGG is faster for higher applied stress. The DAGG boundary migration distance increases with accumulated strain during DAGG, as was observed in constant strain-rate tests of Mo [Worthington 2011]. The velocity of the DAGG boundary is roughly constant with applied stress within the range tested. The constant true-stress data are insufficient to confirm or refute the hypotheses developed in the DAGG grain boundary migration model presented by Worthington [Worthington 2011], which proposed that the velocity of the DAGG boundary is proportional to applied stress to a power of greater than unity, expected to be approximately a power of five (5) for dislocation-climb-controlled creep.

9.2 DAGG in Ta-A

DAGG was observed in a commercial purity Ta (Ta-A) sheet during tensile tests conducted from 1550 to 1850 °C (0.55 to 0.65 T_H) at strain rates from 2×10^{-5} to 5×10^{-4} s^{-1}. This is the first definitive example of DAGG occurring in a material other than Mo. The material had large initial grain sizes of approximately 250 to 550 μm in this temperature

range after annealing for 2 to 3 hours and exhibited a strong initial texture that aligned the <111> crystallographic direction along the STD, a <111>-fiber texture.

DAGG grains were commonly oriented within or near the primary recrystallization texture, but the lack of DAGG grains from outside of this texture may be due to the strength of the initial texture. The critical strain for DAGG initiation did not vary consistently with temperature within the range tested, contrary to previous observations of DAGG in Mo in which the critical strain decreased with increasing temperature [Worthington 2011]. This is thought to be a result of the large recrystallized grain size in the Ta material. The DAGG boundary migration distance in the tensile direction was approximately proportional to the amount of strain accumulated during DAGG. The velocity of the DAGG boundary in Ta-A was similar to that observed previously in Mo [Worthington 2011]. Boundary velocity is likely a function of the applied strain rate but is not related to the amount of strain prior to DAGG initiation or the slip properties of the crystal, including its Schmid and Taylor factors. The DAGG grains are not preferentially oriented favorably, or unfavorably, for slip. The reduction of dislocation density is often a major driving force for grain boundary migration, but the lack of a correlation between the DAGG boundary migration velocity and the critical strain suggests that accumulated strain does not strongly affect DAGG migration rate, which suggests that strain accumulation is most likely related primarily to nucleation of a DAGG grain.

Irregularities observed in the tensile data during DAGG of Ta-A include gradual and intermittent stress drops. The irregular stress drops are likely due to the formation of multiple DAGG grains. The majority of the grain boundaries between DAGG grains in Ta-A have a $\Sigma 3$ character, which may significantly lower grain boundary mobility, providing time for other grains to initiate and grow abnormally. The large initial grain

size may also hinder DAGG by reducing curvature-driven grain boundary migration. DAGG in Ta-A did not show any preference for growth along the surface of the specimen, contrary to observations of DAGG in Mo-PMB by Worthington [Worthington 2011]. It is likely that Mo-PMB has through-thickness variations in texture or grain size that Ta-A does not.

9.3 DAGG IN TA-B

A Ta material alloyed to restrict normal grain growth, Ta-B, was tested from 1650 to 1950 °C (0.58 to 0.68 T_H) and 3×10^{-5} to 1×10^{-4} s^{-1} in an effort to induce DAGG. DAGG grains were observed, but no test data exhibited the sharp drop in true stress expected at DAGG initiation. Microstructural analysis indicated that DRX also likely occurred during testing and may have obscured identification of the characteristic DAGG stress drop. The lack of an identifiable stress drop made DAGG in Ta-B difficult to quantify and compare to other instances of DAGG. Thus, it is not clear if it follows the trends observed in Ta-A and Mo. The original recrystallization texture of Ta-B was similar to that of Ta-A, although more diffuse. The DAGG grains in Ta-B preferred orientations similar to the DAGG grain orientations of Ta-A. Some surface preferred growth was observed, but this preference was not consistent, and the reason for this surface growth preference is unknown. The grain boundaries between abnormal grains in Ta-B rarely had special or low-angle character. Thus, it is likely that the special boundary character in Ta-A was the result of the strong initial texture and not related to any inherent mechanism of DAGG.

9.4 CONCLUSIONS FROM CURRENT INVESTIGATION

The observation of DAGG in Ta suggests that DAGG may occur in additional refractory metals. It is unclear if DAGG is likely to occur in alloys or metals that are not BCC. DAGG occurs under temperatures from approximately 0.6 to 0.7 T_H and strain rates of 10^{-5} to 10^{-4} s^{-1} in both Mo and Ta. Similar conditions are likely to promote DAGG in other materials. The observations of DAGG in Mo and Ta suggest that the growth of one DAGG grain is promoted by: an optimum temperature and strain rate, a small stable grain size, resistance to DRX, and a strong initial texture that does not readily form special boundaries. Avoiding these conditions may reduce the likelihood or extent of DAGG; however, DAGG is still not well understood or easily predicted.

The model proposed by Worthington [Worthington 2011] provides a possible explanation of the mechanisms occurring during DAGG. It relies on the formation and annihilation of dislocations to aid the motion of the grain boundary. The results of this investigation are consistent with the model by Worthington, but do not confirm it. Other models, such as that proposed by Cahn [Cahn 2004] for stress-assisted boundary migration, may possibly be applicable to DAGG.

9.5 SUGGESTIONS FOR FUTURE WORK

The present and previous investigations of DAGG have lead to many questions that remain unanswered. Suggestions for future investigations are provided below.

1. Produce DAGG in other BCC materials, especially α-Fe and W.
2. Test a material with a random initial texture to determine if DAGG has a preferential growth orientation independent of the initial texture.
3. Determine the effect of composition and pinning sites by testing high purity materials and materials with varying particle contents and solid-

solution alloys. Characterize particle contents using SEM and transition electron microscopy (TEM). Determine optimum amounts of particle pinning and/or alloying additions to promote growth of one DAGG grain or suppress DAGG.

4. Conduct additional constant true-stress tests to DAGG completion at varying temperatures and a larger range of applied stresses, and compare trends to those predicted by the model presented by Worthington [Worthington 2011].
5. Determine if DAGG only occurs in tension by testing for DAGG under compression and/or torsion.
6. Determine the ability to control DAGG boundary velocity by changing test parameters, such as strain rate, during testing following DAGG initiation.
7. Investigate alternate grain boundary migration models in relation to DAGG, such as the model presented by Cahn *et al* [Cahn 2004].

Appendix A: *Mathematica*™ Script for Characterizing EBSD Data

The following code (indicated in courier font) can be used to create a *Mathematica*™ notebook (ex: file.nb) to analyze EBSD data. The data must me in a ".txt" file with the first and second columns (or second and third columns) specifying the x and y positions (in μm) of each point in the scan. The last nine (9) columns must be the orientation matrix (i.e. a_{11}, a_{12}, a_{13}, a_{21}, a_{22}, a_{23}, a_{31}, a_{32}, a_{33}). Unindexed points must have the last nine points defined as (1,0,0,0,1,0,0,0,1). Comments are in gray and user defined inputs are in red. The directory location must be specified. Part 8 requires the user to specify the location of the file "taylormixed.txt" which is defined in Appendix C.

```
(*************************************************************************)
(*************************************************************************)
(*********************  EBSD Analysis    *********************)
(*************************************************************************)
(*************************************************************************)

ClearAll["Global`*"];

(*************************************************************************)
(***************Part 1: Defining functions*************)
(*************************************************************************)

Vnorm[x_] := x/Sqrt[Plus @@ Table[x[[i]]^2, {i, Length[x]}]];  (*normalizing a vector*)
(*calculating x,y coordinates for plotting on stereographic triangle*)
stereo1[x_] := {x[[1]]/(Norm[x]*(x[[3]]/Norm[x] + 1)), x[[2]]/(Norm[x]*(x[[3]]/Norm[x] +
       1))};
(*reordering elements for plotting on stereographic triangle*)
move[x_] := RotateLeft[Sort[Abs[x], Greater], 1];
(*finds axis of rotation 1x3 vector. input rotation matrix in 1x9 form
       (a11,a12,a13,a21,a22,a23,a31,a32,a33)*)
rotaxis[x_] := {x[[6]] - x[[8]], x[[7]] - x[[3]], x[[2]] - x[[4]]};
(*same as rotaxis but axis vector is normalized*)
rotaxisnorm[x_] := {x[[6]] - x[[8]], x[[7]] - x[[3]], x[[2]] - x[[4]]}/Sqrt[(x[[7]] -
       x[[3]])^2 + (x[[2]] - x[[4]])^2 +   (x[[6]] - x[[8]])^2];
(*finds angle of rotation in radians. Input rotation matrix in 1x9 form
       (a11,a12,a13,a21,a22,a23,a31,a32,a33)*)
rotang[x_] := Re[ArcCos[0.5*(x[[1]] + x[[5]] + x[[9]] - 1)]];
(*finds misorientation angle between two matrices, in degrees. Input rotation matrices in
       3x3 form*)
miso[u_, v_] := (180*rotang[Flatten[v . Transpose[u]]])/Pi;
(*converts the quaternion description of an rotation to a rotation matrix*)
quattomat[x_] := {{x[[1]]^2 - x[[2]]^2 - x[[3]]^2 + x[[4]]^2, 2*(x[[1]]*x[[2]] -
```

```
       x[[4]]*x[[3]]), 2*(x[[1]]*x[[3]] + x[[2]]*x[[4]])},
      {2*(x[[1]]*x[[2]] + x[[3]]*x[[4]]), -x[[1]]^2 + x[[2]]^2 - x[[3]]^2 + x[[4]]^2,
       2*(x[[2]]*x[[3]] -
x[[4]]*x[[1]])}, {2*(x[[1]]*x[[3]] - x[[4]]*x[[2]]), 2*(x[[2]]*x[[3]] + x[[1]]*x[[4]]),-
       x[[1]]^2 - x[[2]]^2 + x[[3]]^2 + x[[4]]^2}};
(*symmetry operations for a cubic material, given in 3x3 rotation matrix form*)
mtest = {{{1, 0, 0},{0, 1, 0},{0, 0, 1}},{{-1, 0, 0},{0, -1, 0},{0, 0, -1}},{{-1, 0,
       0},{0, 1, 0},{0, 0, 1}},{{1, 0, 0},{0, -1, 0},{0, 0, 1}},{{1, 0, 0},{0, 1, 0},{0,
       0, -1}},{{1, 0, 0},{0, -1, 0},{0, 0, -1}},{{-1, 0, 0},{0, 1, 0},{0, 0, -1}},{{-1,
       0, 0},{0, -1, 0},{0, 0, 1}},{{1, 0, 0},{0, 0, -1},{0, 1, 0}},{{1, 0, 0},{0, 0,
       1},{0, -1, 0}},{{0, 0, 1},{0, 1, 0},{-1, 0, 0}},{{0, 0, -1},{0, 1, 0},{1, 0,
       0}},{{0, -1, 0},{1, 0, 0},{0, 0, 1}},{{0, 1, 0},{-1, 0, 0},{0, 0, 1}},{{-1, 0,
       0},{0, 0, 1},{0, -1, 0}},{{-1, 0, 0},{0, 0, -1},{0, 1, 0}},{{0, 0, -1},{0, -1,
       0},{1, 0, 0}},{{0, 0, 1},{0, -1, 0},{-1, 0, 0}},{{0, 1, 0},{-1, 0, 0},{0, 0, -
       1}},{{0, -1, 0},{1, 0, 0},{0, 0, -1}},{{0, 0, 1},{1, 0, 0},{0, 1, 0}},{{0, 1,
       0},{0, 0, 1},{1, 0, 0}},{{0, 0, -1},{-1, 0, 0},{0, 1, 0}},{{0, -1, 0},{0, 0, 1},{-
       1, 0, 0}},{{0, 0, -1},{1, 0, 0},{0, -1, 0}},{{0, 1, 0},{0, 0, -1},{-1, 0, 0}},{{0,
       0, 1},{-1, 0, 0},{0, -1, 0}},{{0, -1, 0},{0, 0, -1},{1, 0, 0}},{{0, 0, -1},{-1, 0,
       0},{0, -1, 0}},{{0, -1, 0},{0, 0, -1},{-1, 0, 0}},{{0, 0, 1},{1, 0, 0},{0, -1,
       0}},{{0, 1, 0},{0, 0, -1},{1, 0, 0}},{{0, 0, 1},{-1, 0, 0},{0, 1, 0}},{{0, -1,
       0},{0, 0, 1},{1, 0, 0}},{{0, 0, -1},{-1, 0, 0},{0, 1, 0}},{{0, -1, 0},{0, 0, 1},{-1,
       0, 0}},{{-1, 0, 0},{0, 0, 1},{0, 1, 0}},{{0, 0, 1},{0, -1, 0},{1, 0, 0}},{{0, 1,
       0},{1, 0, 0},{0, 0, -1}},{{-1, 0, 0},{0, 0, -1},{0, -1, 0}},{{0, 0, -1},{0, -1,
       0},{-1, 0, 0}},{{0, -1, 0},{-1, 0, 0},{0, 0, -1}},{{1, 0, 0},{0, 0, -1},{0, -1,
       0}},{{0, 0, -1},{0, 1, 0},{-1, 0, 0}},{{0, -1, 0},{-1, 0, 0},{0, 0, 1}},{{1, 0,
       0},{0, 0, 1},{0, 1, 0}},{{0, 0, 1},{0, 1, 0},{1, 0, 0}},{{0, 1, 0},{1, 0, 0},{0,
       0, 1}}};
(*symmetry operation for a cubic material, given in quaternion form*)
qmtest = {{0,0,0,1},{1,0,0,0},{0,1,0,0},{0,0,1,0},{0.5`,0.5`,0.5`,0.5`},{-0.5`,-0.5`,-
       0.5`,0.5`},{0.5`,-0.5`,0.5`,0.5`},{-0.5`,0.5`,-0.5`,0.5`},{-
       0.5`,0.5`,0.5`,0.5`},{0.5`,-0.5`,-0.5`,0.5`},{-0.5`,-0.5`,0.5`,0.5`},{0.5`,0.5`,-
       0.5`,0.5`},{1/Sqrt[2],0,0,1/Sqrt[2]},{0,1/Sqrt[2],0,1/Sqrt[2]},{0,0,1/Sqrt[2],1/Sqrt[2]},{-(1/Sqrt[2]
       ),0,0,1/Sqrt[2]},{0,-(1/Sqrt[2]),0,1/Sqrt[2]},{0,0,-(1/Sqrt[2]),1/Sqrt[2]},{1/Sqrt[2],1/Sqrt[2]
       ,0,0},{-(1/Sqrt[2]),1/Sqrt[2],0,0},{0,1/Sqrt[2],1/Sqrt[2],0},{0,-(1/Sqrt[2]),1/Sqrt[2],0},{1/Sqrt[2]
       ,0,1/Sqrt[2],0},{-(1/Sqrt[2]),0,1/Sqrt[2],0},{0,0,0,-1},{-1,0,0,0},{0,-1,0,0},{0,0,-
       1,0},{-0.5`,-0.5`,-0.5`,-0.5`},{0.5`,0.5`,0.5`,-0.5`},{-0.5`,0.5`,-0.5`,-
       0.5`},{0.5`,-0.5`,0.5`,-0.5`},{0.5`,-0.5`,-0.5`,-0.5`},{-0.5`,0.5`,0.5`,-
       0.5`},{0.5`,0.5`,-0.5`,-0.5`},{-0.5`,-0.5`,0.5`,-0.5`},{-(1/Sqrt[2]),0,0,-(1/Sqrt[2]
       )},{0,-(1/Sqrt[2]),0,-(1/Sqrt[2])},{0,0,-(1/Sqrt[2]),-(1/Sqrt[2])},{1/Sqrt[2],0,0,-(1/Sqrt[2]
       )},{0,1/Sqrt[2],0,-(1/Sqrt[2])},{0,0,1/Sqrt[2],-(1/Sqrt[2])},{-(1/Sqrt[2]),-(1/Sqrt[2]),0,0},{1/
       Sqrt[2],-(1/Sqrt[2]),0,0},{0,-(1/Sqrt[2]),-(1/Sqrt[2]),0},{0,1/Sqrt[2],-(1/Sqrt[2]),0},{-(1/Sqrt[2]
       ),0,-(1/Sqrt[2]),0},{1/Sqrt[2],0,-(1/Sqrt[2]),0}}
(*multiplying quaternions.  q={i,j,k,real}*)
quatmult[p_,q_]:=Module[{x},x={p[[4]]*q[[4]]-(p[[1]]*-q[[1]]+p[[2]]*-q[[2]]+p[[3]]*-
       q[[3]]),p[[4]]*-q[[1]]+q[[4]]*p[[1]]+p[[2]]*-q[[3]]-p[[3]]*-q[[2]],p[[4]]*-
       q[[2]]+q[[4]]*p[[2]]+p[[3]]*-q[[1]]-p[[1]]*-q[[3]],
     p[[4]]*-q[[3]]+q[[4]]*p[[3]]+p[[1]]*-q[[2]]-p[[2]]*-q[[1]]};x=x/Norm[x]];
(*inverting a quaternion. q={i,j,k,real}*)
invquat[q_]:={-q[[1]],-q[[2]],-q[[3]],q[[4]]};
(*calculating misorientation angle, in degrees, between two quaternions. q={i,j,k,real}*)
quatmiso[p_,q_]:=Module[{qt,qm},qt={p[[4]]*q[[4]]-(p[[1]]*-q[[1]]+p[[2]]*-q[[2]]+p[[3]]*-
       q[[3]]),p[[4]]*-q[[1]]+q[[4]]*p[[1]]+p[[2]]*-q[[3]]-p[[3]]*-q[[2]],p[[4]]*-
       q[[2]]+q[[4]]*p[[2]]+p[[3]]*-q[[1]]-p[[1]]*-q[[3]],
     p[[4]]*-q[[3]]+q[[4]]*p[[3]]+p[[1]]*-q[[2]]-p[[2]]*-q[[1]]};
   qt=Sort[qt];
   qt=qt/Norm[qt];
   qm=Max[{qt[[4]],(qt[[3]]+qt[[4]])/Sqrt[2],Total[qt]/2}];
   2*ArcCos[qm]*180/Pi];
```

```
(*converting a rotation matrix to quaternion. q={i,j,k,real}*)
mattoquat[x_]:=Module[{s,q,qw,qx,qy,qz},If[ x[[1]]+x[[5]]+x[[9]]>0,
    s=Sqrt[x[[1]]+x[[5]]+x[[9]]+1.0]*2;(*//S=4*qw*)
    qw=0.25*s;
    qx=(x[[8]]-x[[6]])/s;
    qy=(x[[3]]-x[[7]])/s;
    qz=(x[[4]]-x[[2]])/s,
    If [x[[1]]>x[[5]]&&x[[1]]>x[[9]], s=Sqrt[1.0+x[[1]]-x[[5]]-x[[9]]]*2;(*//S=4*qx*)
     qw=(x[[8]]-x[[6]])/s;
     qx=0.25*s;
     qy=(x[[2]]+x[[4]])/s;
     qz=(x[[3]]+x[[7]])/s,
     If[ x[[5]]>x[[9]],
      s=Sqrt[1.0+x[[5]]-x[[1]]-x[[9]]]*2;(*//s=4*qy *)
      qw=(x[[3]]-x[[7]])/s;
      qx=(x[[2]]+x[[4]])/s;
      qy=0.25*s;
      qz=(x[[6]]+x[[8]])/s,
      (*else*)
      s=Sqrt[1.0+x[[9]]-x[[1]]-x[[5]]]*2;(*//s=4*qz *)
      qw=(x[[4]]-x[[2]])/s;
      qx=(x[[3]]+x[[7]])/s;
      qy=(x[[6]]+x[[8]])/s;
      qz=0.25*s]]];q={qx,qy,qz,qw};If[qw<0,q/Norm[q],-q/Norm[q]]];



(*************************************************************************)
(***************** Part 2: Importing data *************)
(*************************************************************************)
(*user inputs:  scale bar size *)
(*variables needed: select *)
(*outputs: strain0, select, stepx, stepy, Length[strain0], xstep, scalefactor, scaletext,
       indexed*)
(*************************************************************************)

SetDirectory["C:/Users/mydata/"];(*location of the txt data file and where outputs will
       be saved*)
strain0=Import["exampledata.txt","Table"];  (*txt data file.  columns 1 and 2 or 2 and 3
       must contain (x,y) pixel position, and last 9 columns must contain the orientation
       matrix*)


ls01=Length[strain0[[1]]]; (*length of data set*)

(*deleting unused columns from imported data*)
If[Length[Cases[strain0[[All,1]],1]]+Length[Cases[strain0[[All,1]],0]]= Length[strain0],
       strain0=strain0[[1;;All,{2,3,ls01-8,ls01-7,ls01-6,ls01-5,ls01-4,ls01-3,ls01-
       2,ls01-1,ls01}]],strain0=strain0[[1;;All,{1,2,ls01-8,ls01-7,ls01-6,ls01-5,ls01-
       4,ls01-3,ls01-2,ls01-1,ls01}]]];


(*defining the number of pixels in the vertical (y) and horizontal (x) directions in the
       mapped data set*)
stepy=Count[strain0[[All,1]],0];
stepx=Round[Length[strain0]/stepy];
xstep=strain0[[2,2]]-strain0[[1,2]]; (*distance of each step, in microns*)


xyset=Table[i,{i,Length[strain0]}]; (*list of all pixels*)
Table[PrependTo[strain0[[i]],xyset[[i]]],{i,Length[strain0]}];   (*adding data line count
       numbers back in first column*)


(*defining helpful variables based on input data*)
(*determining unindexed points for reference later, 1 indexed, 0 not indexed.  The
       rotation matrix of unindexed points in the data set is the identity matrix*)
```

```
indexed=Table[If[strain0[[i,4;;12]]={1.,0.,0.,0.,1.,0.,0.,0.,1.},0,1],{i,Length[strain0]}
       ];
indexedpct=N[100*(1-Sort[Tally[indexed]][[1,2]]/Sort[Tally[indexed]][[2,2]])];
       (*percentage of data that is indexed*)
Print[Text["Map is "],indexedpct,Text[" % indexed"]];

(*Defining variables used for scale bar depending on size of map*)
If[stepx*xstep<500,scalefactor =100/xstep;scaletext=Text[100 µm]];
If[stepx*xstep>500,scalefactor =200/xstep;scaletext=Text[200 µm]];
If[stepx*xstep>1000,scalefactor =500/xstep;scaletext=Text[500 µm]];
If[stepx*xstep>3000,scalefactor =1000/xstep;scaletext=Text[1000 µm]];
If[stepx*xstep>5000,scalefactor =2000/xstep;scaletext=Text[2000 µm]];

(*determining quaternions at each point for averaging orientations for assigning pixels
       to grains and calculating grain avg to pixel misorientation.*)
<<Quaternions`
quat=Table[{0,0,0,0},{Length[strain0]}];
quat=Table[If[indexed[[i]]=1,mattoquat[strain0[[i,4;;12]]],{0,0,0,0}],{i,Length[strain0]}
       ];



(*Exporting variables for this section*)
Export["indexed.txt",indexed];
Export["stepx.txt",stepx];
Export["stepy.txt",stepy];
Export["xstep.txt",xstep];
Export["scalefactor.txt",scalefactor];
Export["scaletext.txt",scaletext];
Export["indexedpct.txt",indexedpct];




(**********************************************************************)
(**Part 3: Plotting raw data, pixel-pixel
     misorientations, and defining grains*)
(**********************************************************************)
(*user inputs: misdeg,maxdeg *)
(*variables needed: strain0, xstep, indexed, stepx, stepy *)
(*outputs: gcl, grains, strain0, Xmap, Ymap, Zmap, misdeg, misscalebar, PPmismap,
       Grainmap, quat *)
(**********************************************************************)

time0 = AbsoluteTime[];

(*Importing variables if needed: *)
If[ValueQ[strain0],strain0,strain0=ToExpression[Import["strain0.txt","List"]]];
If[ValueQ[xstep],xstep,xstep=ToExpression[Import["xstep.txt"]]];
If[ValueQ[indexed],indexed,indexed=ToExpression[Import["indexed.txt","List"]]];
If[ValueQ[stepx],stepx,stepx=ToExpression[Import["stepx.txt"]]];
If[ValueQ[stepy],stepy,stepy=ToExpression[Import["stepy.txt"]]];
If[ValueQ[scalefactor],scalefactor,scalefactor=ToExpression[Import["scalefactor.txt"]]];
If[ValueQ[scaletext],scaletext,scaletext=ToExpression[Import["scaletext.txt"]]];

(*Mapping data relative to x-direction, points colored by inverse pole figure coloring
       scheme*)
dir=Transpose[Table[strain0[[All,i]], {i, 4,6,1}]];
dir=Table[N[move[{dir[[i,1]],dir[[i,2]],dir[[i,3]]}]], {i,Length[dir]}];
ps=Table[N[stereo1[{dir[[i,1]],dir[[i,2]],dir[[i,3]]}]], {i,Length[dir]}];
psrgb=Table[N[{1-(Sqrt[ps[[i,1]]^2+ps[[i,2]]^2])/0.51764,1-(Sqrt[(Abs[ps[[i,1]]]-
       0.414214)^2+ps[[i,2]]^2])/0.4143,1-(Sqrt[(Abs[ps[[i,1]]]-
```

```
        0.366025)^2+(Abs[ps[[i,2]]]-0.366025)^2])/0.51764}], {i,Length[ps]}];
Table[If[ indexed[[i]]=0,psrgb[[i]]={1,1,1}],{i,Length[psrgb]}];
Xmap = Graphics[{Raster[Partition[psrgb,Round[stepx]]],Thick,Black,Line[{{20,-
        9},{scalefactor+20,-9}}],Thick,Black,Line[{{20,-13},{20,-
        5}}],Thick,Black,Line[{{scalefactor+20,-13},{scalefactor+20,-
        5}}],Black,Text[Style[scaletext,40],{scalefactor/2+20,-20}]}]


(*Mapping data relative to y-direction, points colored by inverse pole figure coloring
        scheme*)
dir=Transpose[Table[strain0[[All,i]], {i, 7,9,1}]];
dir=Table[N[move[{dir[[i,1]],dir[[i,2]],dir[[i,3]]}]], {i,Length[dir]}];
ps=Table[N[stereo1[{dir[[i,1]],dir[[i,2]],dir[[i,3]]}]], {i,Length[dir]}];
psrgb=Table[N[{1-(Sqrt[ps[[i,1]]^2+ps[[i,2]]^2])/0.51764,1-(Sqrt[(Abs[ps[[i,1]]]-
        0.414214)^2+ps[[i,2]]^2])/0.4143,1-(Sqrt[(Abs[ps[[i,1]]]-
        0.366025)^2+(Abs[ps[[i,2]]]-0.366025)^2])/0.51764}], {i,Length[ps]}];
Table[If[indexed[[i]]=0,psrgb[[i]]={1,1,1}],{i,Length[psrgb]}];
(*Graphics[Raster[Partition[psrgb,Round[stepx]]]]*)
Ymap =  Graphics[{Raster[Partition[psrgb,Round[stepx]]],Thick,Black,Line[{{20,-
        9},{scalefactor+20,-9}}],Thick,Black,Line[{{20,-13},{20,-
        5}}],Thick,Black,Line[{{scalefactor+20,-13},{scalefactor+20,-
        5}}],Black,Text[Style[scaletext,40],{scalefactor/2+20,-20}]}]


(*Mapping data relative to z-direction, points colored by inverse pole figure coloring
        scheme*)
dir=Transpose[Table[strain0[[All,i]], {i, 10,12,1}]];
dir=Table[N[move[{dir[[i,1]],dir[[i,2]],dir[[i,3]]}]], {i,Length[dir]}];
ps=Table[N[stereo1[{dir[[i,1]],dir[[i,2]],dir[[i,3]]}]], {i,Length[dir]}];
psrgb=Table[N[{1-(Sqrt[ps[[i,1]]^2+ps[[i,2]]^2])/0.51764,1-(Sqrt[(Abs[ps[[i,1]]]-
        0.414214)^2+ps[[i,2]]^2])/0.4143,1-(Sqrt[(Abs[ps[[i,1]]]-
        0.366025)^2+(Abs[ps[[i,2]]]-0.366025)^2])/0.51764}], {i,Length[ps]}];
Table[If[ indexed[[i]]=0,psrgb[[i]]={1,1,1}],{i,Length[psrgb]}];
Zmap =  Graphics[{Raster[Partition[psrgb,Round[stepx]]],Thick,Black,Line[{{20,-
        9},{scalefactor+20,-9}}],Thick,Black,Line[{{20,-13},{20,-
        5}}],Thick,Black,Line[{{scalefactor+20,-13},{scalefactor+20,-
        5}}],Black,Text[Style[scaletext,40],{scalefactor/2+20,-20}]}]



(*mappimg misorientation*)
(*pixel-pixel misorientation mapping: color point if its neighbor to the right or down is
        misoriented more than a theshold amount from the original point*)
misdeg=2.5;(*defining pixel-pixel misorientation threshold for mapping and for grain ID*)
misgradR=Flatten[Table[If[Mod[i,stepx]=0 &&
        indexed[[i+1]]=0,mis=Min[symmis=Table[miso[Partition[strain0[[i,4;;12]],3].mtest[[
        k]],Partition[strain0[[i+1,4;;12]],3]],{k,Length[mtest]}]]],{i,Length[strain0]-
        1}]];  (*looks to right*)
misgradD=Flatten[Table[If[(i+stepx)<Length[dir] &&
        indexed[[i+stepx]]=0,Min[Table[miso[Partition[strain0[[i,4;;12]],3].mtest[[k]],Par
        tition[strain0[[i+stepx,4;;12]],3]],{k,Length[mtest]}]]],{i,Length[strain0]-1}]];
        (*looks up*)
misgrad=misgradR;
Table[If[(misgradD[[i]]>misgrad[[i]]), misgrad[[i]]=misgradD[[i]]],{i, Length[strain0]-
        1}];
Table[If[(misgrad[[i]]=Null), misgrad[[i]]=0],{i, Length[strain0]-1}];


maxdeg=15;  (*designates maximum on scale for mapping.  truncates values used for
        plotting in map*)
(*scaled to make maxdeg and above at max*)
scaledmisgrad=Flatten[Table[misgrad[[i]]/maxdeg,{i, Length[misgrad]}]];(*misgrad scaled
        to make 15 degrees 1, since plot scales from 0 to 1. Values >15 remain but are
        clipped on plot*)
scaledmisgrad=Table[Clip[scaledmisgrad[[i]],{0,1}],{i,Length[scaledmisgrad]}];
scaledmisgrad=Partition[scaledmisgrad,Round[stepx]];
```

```
PPmismap = Graphics[{Raster[scaledmisgrad,ColorFunction-
       >"TemperatureMap"],Thick,Black,Line[{{20,-9},{scalefactor+20,-
       9}}],Thick,Black,Line[{{20,-13},{20,-5}}],Thick,Black,Line[{{scalefactor+20,-
       13},{scalefactor+20,-5}}],Black,Text[Style[scaletext,40],{scalefactor/2+20,-20}]}]



(**********************Grain identification, method involves gradually building grains
       based on the orientation with its neighbors***********)
quat=Table[mattoquat[strain0[[i,4;;12]]],{i,Length[strain0]}]; (*defining quaternion
       description*)
xyset=Table[i,{i,Length[strain0]}]; (*list of numbers for each data point*)
xyset=Delete[xyset,Position[indexed,0]]; (*removing grains that are not indexed *)
grain={1};  (*initializing first grain*)
grains={}; (*to list corresponding pixel label numbers for each grain. number of grains
       will later define length. ex:{{1,2,3,11,12,13},{4,5,14,15}} will be 2 square
       grains one3x3 and other 2x2 *)
m=Min[xyset]; (*first point to be examined*)
end=1;(*setting end variable starting value*)


(*this loop repeats for each grain built*)
While[end=1,
 If[Length[xyset]=1,end=0;Break[]];
 m=Min[xyset]; (*starting point for next grain*)
 grain={m};(*starting current grain, use min of xyset as starting point*)
 list={0}; (*list of pixels added to grain, but neighbors have not been investigated*)
 endgrain=1;  (*signifies end of while loop for each grain if 0*)


 (*this loop repeats for each point of interest in defining a grain*)
 (*first pick one point, then look at four adjacent points.  if they are indexed and
       exist (not past a boarder) then they are included in the analysis.  if the
       misorientation is below the threshold then it is added to the grain and its
       neighbors are later examined.  the process repeats until all neighbors of the
       points belonging to the grain have been tested and there are no more other
       neighbors with a misorientation below the threshold.  symmetry conditions are
       tested, and the orientation of the point is corrected if a symmetry operation
       reduces the misorientation*)
 While[endgrain=1,
  If[m=0,m=1];(*correction for error in first iteration*)
  p=Table[0,{4},{12}]; (*initialize array of neighboring points*)
  pi=strain0[[m]];  (*center point*)
  p={If[m>stepx &&MemberQ[xyset,m-stepx],p[[1]]=strain0[[m-
       stepx]],p[[1]]={0,0,0,0,0,0,0,0,0,0,0,0}],(*locating neighbors to check. look at
       pixels: down, up, left, right*)
     If[m=(Length[strain0]-stepx) &&
       MemberQ[xyset,m+stepx],p[[2]]=strain0[[m+stepx]],p[[2]]={0,0,0,0,0,0,0,0,0,0,0,0}]
       ,
    If[Mod[m,stepx]=1 &&MemberQ[xyset,m-1],p[[3]]=strain0[[m-
       1]],p[[3]]={0,0,0,0,0,0,0,0,0,0,0,0}],
    If[Mod[m,stepx]=0
       &&MemberQ[xyset,m+1],p[[4]]=strain0[[m+1]],p[[4]]={0,0,0,0,0,0,0,0,0,0,0,0}]};
  (*if neighbor is unindexed pixel, look one more over. this is to help reduce artifact
       island grains because an area is surrounded by unindexed pixels*)
  If[p[[1,1]]=0&&MemberQ[xyset,m-2*stepx],If[ m= (2*stepx+1),p[[1]]=strain0[[m-
       2*stepx]],p[[1]]={m-2*stepx,0,0,0,0,0,0,0,0,0,0,0}]];
  If[p[[2,1]]=0&&MemberQ[xyset,m+2*stepx],If[ m=(Length[strain0]-2*stepx-1) &&
       (m+2*stepx)=Length[strain0],p[[2]]=strain0[[m+2*stepx]],p[[2]]={m+2*stepx,0,0,0,0,
       0,0,0,0,0,0,0}]];
  If[p[[3,1]]=0&&MemberQ[xyset,m-2] ,If[Mod[m,stepx+1]>2 ,p[[3]]=strain0[[m-
       2]],p[[3]]={m-2,0,0,0,0,0,0,0,0,0,0,0}]];
  If[p[[4,1]]=0&&MemberQ[xyset,m+2],If[Mod[m,stepx+1]<stepx-1 &&
       m+2<Length[strain0],p[[4]]=strain0[[m+2]],p[[4]]={m+2,0,0,0,0,0,0,0,0,0,0,0}]];


  Table[If[FreeQ[xyset,p[[k,1]]],p[[k]]={0,0,0,0,0,0,0,0,0,0,0,0}];(*remove already
       grain-labeled pixels from list*)
```

```
      If[p[[k,2]]=0,mist=Flatten[Table[miso[Partition[strain0[[p[[k,1]],4;;12]],3].mtest
      [[j]],Partition[pi[[4;;12]],3]],{j,Length[mtest]}]];mis=Min[mist];
   (*mist contains the misorientation between the two pixels for each symmetry
      operation*)
   (*correcting symmetry within grains: pixels have been assigned to grains using
      symmetry, but not corrected so that they are similar.  Without this, grain
      orientation averaging doesnt work well. Get first pixel in grain and compare with
      second pixel. if a symmetry operation provides a smaller misorientation, then
      reasign that pixel's matrix. *)
   If[ mis<misdeg && FreeQ[grain,p[[k,1]]],
    If[Extract[Flatten[Position[mist,mis]],{1}]=
      1,strain0[[p[[k,1]],4;;12]]=Flatten[Partition[strain0[[p[[k,1]],4;;12]],3].Partiti
      on[Flatten[mtest[[Extract[Flatten[Position[mist,mis]],{1}]]]],3]]]];

  If[mis<misdeg && FreeQ[grain,p[[k,1]]] && p[[k,2]]=0,grain=Flatten[{grain,p[[k,1]]}]];
      (*add point to grain if within misorientation and not already added*)
  If[mis<misdeg && p[[k,2]]=0(*&&
      MemberQ[xyset,p[[k,1]]]*),xyset=Complement[xyset,{p[[k,1]]}]];(*if pixel is
      labeled, delete from global list of pixels to be assigned*)
  If[mis<misdeg && p[[k,2]]=0,list=Flatten[{list,p[[k,1]]}]]; (*if the misorientation is
      less than the threshold, misdeg, and the point is not already part of the list,
      add*)
  ,{k,4}];

 list=DeleteDuplicates[list];
 list=Complement[list,{0}];
 xyset=Complement[xyset,{m}];  (*remove current middle pixel from master list of
      points*)
 list=Complement[list,{m}];   (*remove current middle pixel from list of pixels of
      interest for current grain generated*)
 If[Length[list]=0,endgrain=0;Break[]];
 m=Min[list];
 ];(*end inner While*)

grain=Complement[grain,{0}]; (*delete the 0 point that gets added to each grain*)
If[Length[grain]>2,AppendTo[grains,grain],xyset=Complement[xyset,grain]];(*requries
      grains to be a certain size, if not min size then those pixels are skipped and
      will be corrected in the subsequent section*)

(*making array with each row representing a grain and containing the pixel numbers for
      each grain*)
grain={} (*clear grain variable*)
]; (*end main While loop*)

grains=Table[Flatten[grains[[i]]],{i,Length[grains]}];  (*returning grains to original
      format*)
grains=Delete[grains,Position[grains,{0}]];  (*deleting {0} grain used in computations*)

Complement[grains,Flatten[Position[strain0[[All,4]],1.]]];
grains=Cases[grains, Except[{}]];
grains=Cases[grains, Except[{0}]];



(*redefining quat variable since strain0 updated*)
<<Quaternions`
quat=Table[mattoquat[strain0[[i,4;;12]]],{i,Length[strain0]}];

(*correct orientation of pixels not assigned to a grain in previous procedure and assign.
      this method votes on which grain an unassigned pixel belongs by how many of its
      neighbors belong to each surrounding grain.  the orientation is the average
      orientation of its neighboring pixels that belong to the winning grain*)
```

```
xyset=Table[i,{i,Length[strain0]}];
unlist=Complement[xyset,Flatten[grains]];
unst=Table[0,{Length[unlist]}];
AppendTo[grains,{0}];


For[u=1,u=Length[unlist],u++,
 q=Table[{0},{8}];  (*setting up array to fill with neighbors to vote on based on number
       of neighbors in the same grain*)
 If[unlist[[u]]>stepx,q[[1]]=strain0[[(unlist[[u]]-stepx),1]]];(*down*)

If[unlist[[u]]+stepx<Length[strain0],q[[2]]=strain0[[(unlist[[u]]+stepx),1]]]; (*up*)
 If[Mod[unlist[[u]],stepx]=1,q[[3]]=strain0[[(unlist[[u]]-1),1]]];(*left*)
 If[Mod[unlist[[u]],stepx]=0&&
unlist[[u]]<Length[strain0],q[[4]]=strain0[[(unlist[[u]]+1),1]]];(*right*)
       If[Mod[unlist[[u]],stepx]=0 && unlist[[u]]>stepx,q[[5]]=strain0[[(unlist[[u]]+1-
       stepx),1]]];(*down, right*)
       If[Mod[unlist[[u]],stepx]=1&& unlist[[u]]>stepx,q[[6]]=strain0[[(unlist[[u]]-1-
       stepx),1]]];(*down, left*)
 If[Mod[unlist[[u]],stepx]=0 &&
       unlist[[u]]+stepx<Length[strain0],q[[7]]=strain0[[(unlist[[u]]+1+stepx),1]]];
       (*up, right*)
 If[Mod[unlist[[u]],stepx]=1 &&
       unlist[[u]]+stepx<Length[strain0],q[[8]]=strain0[[(unlist[[u]]-1+stepx),1]]];
       (*up, left*)
 Table[If[FreeQ[grains,q[[i]]],q[[i]]={0}],{i,Length[q]}]; (*getting rid of other un-
       grain-indexed from list to choose from*)
 q=Cases[q,Except[{0}]]; (*deleting {0} point*)
 If[Length[q]<1,unlist=Flatten[{unlist,unlist[[u]]}];Goto[skip]]; (*if q doesnt contain
       any suitable neighbors, skip it and add it to the end of the list of pts to
       check*)
 gt=Table[Take[Flatten[Position[grains,q[[j]]]],1],{j,Length[q]}];
 gt={Flatten[Sort[Tally[gt],#1[[2]]>#2[[2]]&]][[1]]}; (*second part of tally gives
       popularity, so its used to rank*)
 g=Take[Flatten[Tally[Delete[gt,Position[gt,{Length[grains]}]] ]],1]; (*using tally to
       vote on grain pixel belongs to*)
 t=Flatten[Intersection[Flatten[grains[[g]]],Flatten[q]]];
 AppendTo[grains[[g]],unlist[[u]]];
 strain0[[unlist[[u]],4;;12]]=Flatten[quattomat[Mean[quat[[t]]]/Norm[ Mean[quat[[t]]]]]];
 quat[[unlist[[u]]]]=mattoquat[strain0[[unlist[[u]],4;;12]]];
 Label[skip];
 ]; (*end For loop*)

Table[grains[[i]]=Flatten[grains[[i]]],{i,Length[grains]}];
grains=Cases[grains, Except[{}]];
grains=Cases[grains, Except[{0}]];



quat=Table[mattoquat[strain0[[i,4;;12]]],{i,Length[strain0]}];
(*correcting quat where inverse quat is given, first separates quats for each grain,
       finds mean of larger set, compares each point in grain to see if it needs to be
       inversed*)
gcluster=Table[FindClusters[quat[[grains[[i]]]],2],{i,Length[grains]}];
gclmean=Table[If[Length[gcluster[[i,1]]]>Length[gcluster[[i,2]]],Mean[gcluster[[i,1]]],Me
       an[gcluster[[i,2]]]],{i,Length[grains]}];
Table[Table[If[quatmiso[gclmean[[i]],invquat[mattoquat[strain0[[grains[[i,j]],4;;12]]]]]<
       quatmiso[gclmean[[i]],mattoquat[strain0[[grains[[i,j]],4;;12]]]],quat[[grains[[i,j
       ]]]]=invquat[quat[[grains[[i,j]]]]];strain0[[grains[[i,j]],4;;12]]=Flatten[quattom
       at[quat[[grains[[i,j]]]]]],{j,Length[grains[[i]]]}],{i,Length[grains]}];



(*plotting grains*)
gcolor=RandomReal[1,{Length[grains],3}]; (*list of random numbers to use for plotting
       grains*)
```

```
gcl=Array[0,{Length[strain0]}];

gcl=Table[If[Length[Position[grains,c]]>0,gcolor[[Take[Flatten[Position[grains,c]],1]]],{
       {1,0,0}}],{c,Length[strain0]}];
gcl=Partition[Flatten[gcl,1],stepx];
Grainmap=Graphics[{Raster[gcl,ColorFunction-> Hue],Thick,Black,Line[{{20,-
       9},{scalefactor+20,-9}}],Thick,Black,Line[{{20,-13},{20,-
       5}}],Thick,Black,Line[{{scalefactor+20,-13},{scalefactor+20,-
       5}}],Black,Text[Style[scaletext,40],{scalefactor/2+20,-20}]}]

(*misorientation scale*)
m1=Graphics[Raster[{Range[0,1,1/maxdeg]},ColorFunction->"TemperatureMap"]];
m2=Graphics[Text[Style["0",Large,Bold],{0,-0.5}]];
m3=Graphics[Text[Style[maxdeg "+  degrees",Large,Bold],{17,-.5}]];
misscalebar=Show[m1,m2,m3]

time1=AbsoluteTime[];
Print[time1-time0," seconds"]



(*Exporting variables and outputs*)
Export["gcl.txt",gcl];
Export["grains.txt",grains];
Export["strain0.txt",strain0];
Export["misdeg.txt",misdeg];
Export["misscalebar.bmp",misscalebar];
Export["Xmap.bmp",Xmap,ImageSize-> 2* stepx];
Export["Ymap.bmp",Ymap,ImageSize-> 2* stepx];
Export["Zmap.bmp",Zmap,ImageSize-> 2* stepx];
Export["PPmismap.bmp",PPmismap,ImageSize-> 2* stepx];
Export["Grainmap.bmp",Grainmap,ImageSize-> 2* stepx];
Export["quat.bmp",quat];




(*************************************************************************)
(*****Part 4: Averaged grain misorientation mapping
       ******)
(*************************************************************************)
(*user inputs:  maxdeg (for plotting)  *)
(*variables needed: grains, stepx, stepy, strain0, maxdeg, scalefactor, scaletext *)
(*outputs: gmisavgq, gavg, gmc, gmcmap, pgrains, gb, gbmap, quat, Pavgmislegend,
       Pavgmismap *)
(*************************************************************************)

(*Importing variables if needed: *)
If[ValueQ[grains],grains,grains=ToExpression[Import["grains.txt","List"]]];
If[ValueQ[stepx],stepx,stepx=ToExpression[Import["stepx.txt"]]];
If[ValueQ[stepy],stepy,stepy=ToExpression[Import["stepy.txt"]]];
If[ValueQ[strain0],strain0,strain0=ToExpression[Import["strain0.txt","List"]]];
If[ValueQ[scalefactor],scalefactor,scalefactor=ToExpression[Import["scalefactor.txt"]]];
If[ValueQ[scaletext],scaletext,scaletext=ToExpression[Import["scaletext.txt"]]];
If[ValueQ[indexed],indexed,indexed=ToExpression[Import["indexed.txt","List"]]];
time0=AbsoluteTime[];

gmisavgq=Table[0,{Length[grains]}];
gavg=Table[0,{Length[grains]}];

(*determining quaternions again since some grains' orientations have been corrected*)
quat=Table[mattoquat[strain0[[i,4;;12]]],{i,Length[strain0]}];
```

```
(*correcting quat where inverse quat is given, first separates quats for each grain,
       finds mean of larger set, compares each point in grain to see if it needs to be
       inversed*)
gcluster=Table[FindClusters[quat[[grains[[i]]]],2],{i,Length[grains]}];
gclmean=Table[If[Length[gcluster[[i,1]]]>Length[gcluster[[i,2]]],Mean[gcluster[[i,1]]],Me
       an[gcluster[[i,2]]]],{i,Length[grains]}];
Table[Table[If[quatmiso[gclmean[[i]],invquat[mattoquat[strain0[[grains[[i,j]],4;;12]]]]]<
       quatmiso[gclmean[[i]],mattoquat[strain0[[grains[[i,j]],4;;12]]]],quat[[grains[[i,j
       ]]]]=invquat[quat[[grains[[i,j]]]]];strain0[[grains[[i,j]],4;;12]]=Flatten[quattom
       at[quat[[grains[[i,j]]]]]],{j,Length[grains[[i]]]}],{i,Length[grains]}];


Do[gmisavgq[[i]]=Mean[Partition[Flatten[Cases[Table[If[indexed[[grains[[i,j]]]]=1,quat[[s
       train0[[grains[[i,j]],1]]]],0],{j,Length[grains[[i]]]}],Except[0]]],4]],{i,Length[
       grains]}];


Table[gmisavgq[[i]]=gmisavgq[[i]]/Norm[gmisavgq[[i]]],{i,Length[gmisavgq]}];


(*orientation of pixels compared to average grain orientation*)
gmc=Table[quatmiso[quat[[i]],Flatten[gmisavgq[[Take[Flatten[Position[grains,i]],1]]]]],{i
       ,Length[quat]}];


If[Max[gmc]>20,

       Table[Table[If[gmc[[grains[[i,j]]]]>20,gmc[[grains[[i,j]]]]=Mean[Sort[gmc[[grains[
       [1]]]]][[1;;Round[Length[grains[[1]]]*.95]]]];quat[[grains[[i,j]]]]=Mean[FindClust
       ers[quat[[grains[[i]]]],2]][[1]]]],{j,Length[grains[[i]]]}],{i,Length[grains]}]];
       (*if gmc (deviation of a pixel's orientation from the average of the grain's
       orientation) is above a threshold of 20 degrees, this reassigns the gmc value for
       that pixel to be equal to the average gmc for the lower 95% of gmc values for that
       grain. this is to filter out the few gmc values (if any) that are really high and
       may skew the average or smaller grains*)


Do[gmisavgq[[i]]=Mean[Partition[Flatten[Cases[Table[If[indexed[[grains[[i,j]]]]=1,quat[[s
       train0[[grains[[i,j]],1]]]],0],{j,Length[grains[[i]]]}],Except[0]]],4]],{i,Length[
       grains]}];


Table[gmisavgq[[i]]=gmisavgq[[i]]/Norm[gmisavgq[[i]]],{i,Length[gmisavgq]}];
gmc=Table[quatmiso[quat[[i]],Flatten[gmisavgq[[Take[Flatten[Position[grains,i]],1]]]]],{i
       ,Length[quat]}];


pgrains=Flatten[Table[Flatten[Take[Flatten[Position[grains,i]],1]],{i,Length[strain0]}]];
       (*shows grain number in order of pixels*)


pgrains=Partition[pgrains,stepx];


(*defining vertical and horizontal lines for plotting grain boundaries*)
vline=Partition[Table[0,{i,Length[strain0]}],stepx];
hline=vline;
Table[If[pgrains[[j,i]]=pgrains[[j,i+1]],vline[[j,i]]=1,vline[[j,i]]=0],{j,stepy},{i,step
       x-1}];
Table[If[pgrains[[j,i]]=pgrains[[j+1,i]],hline[[j,i]]=1,hline[[j,i]]=0],{j,stepy-
       1},{i,stepx}];
vline=Position[vline,1];
hline=Position[hline,1];
vmap=Table[{{vline[[i,2]],(vline[[i,1]]-
       1)},{vline[[i,2]],vline[[i,1]]}},{i,Length[vline]}];
hmap=Table[{{(hline[[i,2]]-
       1),hline[[i,1]]},{hline[[i,2]],hline[[i,1]]}},{i,Length[hline]}];
gb=Partition[Flatten[{vmap,hmap}],4];
gb=Table[Partition[gb[[i]],{2}],{i,Length[gb]}];
gbmap=Graphics[Line[gb]];
```

```
(*plotting referece orientation deviation map, with average grain orientation as
       reference*)
Table[If[gmc[[i]]="Null",gmc[[i]]=gmc[[i]],gmc[[i]]=0],{i,Length[gmc]}];
Table[If[gmc[[i]]=Null, gmc[[i]]=0],{i,Length[gmc]}];
maxdeg=15; (*scaling parameter for maximum degrees plotted*)
gmcs=gmc/maxdeg;
gmcmap=Graphics[Raster[Partition[Flatten[gmcs],stepx],ColorFunction-> "TemperatureMap"]];
m1=Graphics[Raster[{Range[0,1,.1]},ColorFunction->"TemperatureMap"]];
m2=Graphics[Text[Style["0",Large,Bold],{0,-0.5}]];
m3=Graphics[Text[Style[maxdeg " degrees",Large,Bold],{13,-.5}]];
Pavgmismap=Show[gmcmap,gbmap,Graphics[{Thick,Black,Line[{{20,-9},{scalefactor+20,-
       9}}],Thick,Black,Line[{{20,-13},{20,-5}}],Thick,Black,Line[{{scalefactor+20,-
       13},{scalefactor+20,-5}}],Black,Text[Style[scaletext,40],{scalefactor/2+20,-
       20}]}]]
Pavgmislegend=Show[m1,m2,m3]



time1=AbsoluteTime[];
Print[time1-time0," seconds"];

(*exporting variables and outputs*)
Export["gb.txt",gb];
Export["gmc.txt",gmc];
Export["gavg.txt",gavg];
Export["gmisavgq.txt",gmisavgq];
Export["gmcmap.bmp",gmcmap,ImageSize-> 2* stepx];
Export["gbmap.bmp",gbmap,ImageSize-> 2* stepx];
Export["quat.txt",quat];
Export["pgrains.txt",pgrains];
Export["Pavgmismap.bmp",Pavgmismap,ImageSize-> 2* stepx];
Export["Pavgmislegend.bmp",Pavgmislegend];




(*************************************************************************)
(*****Part 5: Mapping grain boundary types******)
(*************************************************************************)
(*user inputs:    *)
(*variables needed: stepx, gb, strain0, scalefactor, scaletext *)
(*outputs: linec, cslmap, lowangmap, CSLmap, csl, gbsingle, lowang, CSLlegend, glinesmap
       *)
(*************************************************************************)

(*Importing variables if needed: *)
If[ValueQ[stepx],stepx,stepx=ToExpression[Import["stepx.txt"]]];
If[ValueQ[gb],gb,gb=ToExpression[Import["gb.txt","List"]]];
If[ValueQ[strain0],strain0,strain0=ToExpression[Import["strain0.txt","List"]]];
If[ValueQ[scalefactor],scalefactor,scalefactor=ToExpression[Import["scalefactor.txt"]]];
If[ValueQ[scaletext],scaletext,scaletext=ToExpression[Import["scaletext.txt"]]];
time0=AbsoluteTime[];

(*mapping grain boundaries and coloring by degrees misorientation*)

(*converting gb coordinates from x,y to pixel numbers on either side of boundary*)
gbsingle=Flatten[gb,1];
gbsingle=Partition[Table[{gbsingle[[i,1]]+(gbsingle[[i,2]])*stepx},{i,Length[gbsingle]}],
       2];
gbsingle=Table[If[Abs[gbsingle[[i,1]]-gbsingle[[i,2]]]={stepx},
       gbsingle[[i]]={gbsingle[[i,1]],gbsingle[[i,2]]-
       stepx+1},gbsingle[[i]]={gbsingle[[i,1]]-
```

```
        stepx+1,gbsingle[[i,2]]}],{i,Length[gbsingle]}];

(*comparing neighboring pixels to determine misorientation angles*)
vlinec=Partition[Table[0,{i,Length[strain0]}],stepx];
hlinec=vlinec;

(*defining grain boundary misorientations (includes symmetry)*)
linec=Flatten[Cases[Flatten[Table[Min[Table[miso[Partition[Flatten[strain0[[gbsingle[[i,1
        ]],4;;12]]],3].mtest[[j]],Partition[Flatten[strain0[[gbsingle[[i,2]],4;;12]]],3]],
        {j,Length[mtest]}]],{i,Length[gbsingle]}]],Except[0]]];
(*plotting just grain boundaries with line thickness scaled to misorientation angle
        (gbmapg) or uniform line thickness (glinesmap)*)
gbmapg=Graphics[Table[{GrayLevel[.75-
        linec[[i]]/60],Thickness[Clip[linec[[i]]/60000+.0005,{0,0.0015}]],Line[gb[[i]]]},{
        i,Length[linec]}],Background->White]
glinesmap=Graphics[Table[{GrayLevel[0.5],Line[gb[[i]]]},{i,Length[linec]}]];

(*defining all possible rotation matrices that define sigma 3,5,7,9,or 11 boundaries*)

(*sigma 3*)
(*possible 60 degree <111> rotation matrices*)
s3m=Array[0,8];
s3m[[1]]=N[RotationMatrix[60*Pi/180,{1,1,1}]];
s3m[[2]]=N[RotationMatrix[60*Pi/180,{-1,1,1}]];
s3m[[3]]=N[RotationMatrix[60*Pi/180,{1,-1,1}]];
s3m[[4]]=N[RotationMatrix[60*Pi/180,{1,1,-1}]];
s3m[[5]]=N[RotationMatrix[60*Pi/180,{-1,-1,1}]];
s3m[[6]]=N[RotationMatrix[60*Pi/180,{1,-1,-1}]];
s3m[[7]]=N[RotationMatrix[60*Pi/180,{-1,1,-1}]];
s3m[[8]]=N[RotationMatrix[60*Pi/180,{-1,-1,-1}]];

(*sigma 5*)
s5m=Array[0,6];
s5m[[1]]=N[RotationMatrix[36.87*Pi/180,{1,0,0}]];
s5m[[2]]=N[RotationMatrix[36.87*Pi/180,{-1,0,0}]];
s5m[[3]]=N[RotationMatrix[36.87*Pi/180,{0,1,0}]];
s5m[[4]]=N[RotationMatrix[36.87*Pi/180,{0,-1,0}]];
s5m[[5]]=N[RotationMatrix[36.87*Pi/180,{0,0,1}]];
s5m[[6]]=N[RotationMatrix[36.87*Pi/180,{0,0,-1}]];

(*sigma 7*)
s7m=Array[0,8];
s7m[[1]]=N[RotationMatrix[38.21*Pi/180,{1,1,1}]];
s7m[[2]]=N[RotationMatrix[38.21*Pi/180,{-1,1,1}]];
s7m[[3]]=N[RotationMatrix[38.21*Pi/180,{1,-1,1}]];
s7m[[4]]=N[RotationMatrix[38.21*Pi/180,{1,1,-1}]];
s7m[[5]]=N[RotationMatrix[38.21*Pi/180,{-1,-1,1}]];
s7m[[6]]=N[RotationMatrix[38.21*Pi/180,{1,-1,-1}]];
s7m[[7]]=N[RotationMatrix[38.21*Pi/180,{-1,1,-1}]];
s7m[[8]]=N[RotationMatrix[38.21*Pi/180,{-1,-1,-1}]];

(*sigma 9*)
s9m=Array[0,12];
s9m[[1]]=N[RotationMatrix[38.94*Pi/180,{1,1,0}]];
s9m[[2]]=N[RotationMatrix[38.94*Pi/180,{-1,1,0}]];
s9m[[3]]=N[RotationMatrix[38.94*Pi/180,{1,-1,0}]];
s9m[[4]]=N[RotationMatrix[38.94*Pi/180,{-1,-1,0}]];
s9m[[5]]=N[RotationMatrix[38.94*Pi/180,{1,0,1}]];
s9m[[6]]=N[RotationMatrix[38.94*Pi/180,{-1,0,1}]];
s9m[[7]]=N[RotationMatrix[38.94*Pi/180,{1,0,-1}]];
s9m[[8]]=N[RotationMatrix[38.94*Pi/180,{-1,0,-1}]];
s9m[[9]]=N[RotationMatrix[38.94*Pi/180,{0,1,1}]];
s9m[[10]]=N[RotationMatrix[38.94*Pi/180,{0,-1,1}]];
```

```
s9m[[11]]=N[RotationMatrix[38.94*Pi/180,{0,1,-1}]];
s9m[[12]]=N[RotationMatrix[38.94*Pi/180,{0,-1,-1}]];


(*sigma 11*)
s11m=Array[0,12];
s11m[[1]]=N[RotationMatrix[50.48*Pi/180,{1,1,0}]];
s11m[[2]]=N[RotationMatrix[50.48*Pi/180,{-1,1,0}]];
s11m[[3]]=N[RotationMatrix[50.48*Pi/180,{1,-1,0}]];
s11m[[4]]=N[RotationMatrix[50.48*Pi/180,{-1,-1,0}]];
s11m[[5]]=N[RotationMatrix[50.48*Pi/180,{1,0,1}]];
s11m[[6]]=N[RotationMatrix[50.48*Pi/180,{-1,0,1}]];
s11m[[7]]=N[RotationMatrix[50.48*Pi/180,{1,0,-1}]];
s11m[[8]]=N[RotationMatrix[50.48*Pi/180,{-1,0,-1}]];
s11m[[9]]=N[RotationMatrix[50.48*Pi/180,{0,1,1}]];
s11m[[10]]=N[RotationMatrix[50.48*Pi/180,{0,-1,1}]];
s11m[[11]]=N[RotationMatrix[50.48*Pi/180,{0,1,-1}]];
s11m[[12]]=N[RotationMatrix[50.48*Pi/180,{0,-1,-1}]];



(*coloring grain boundaries based on misorientation angle*)


(*for 0-5 only*)
lowang=Table[
   If[linec[[i]]=5,{RGBColor[{.5,0,.5}],Thick,Line[gb[[i]]]}],{i,Length[linec]}];


(*coloring grain boundaries based on sigma character*)
csl=Table[{

        (*S11*)If[Min[{Table[Table[rotang[Flatten[Partition[Flatten[strain0[[gbsingle[[i,1
        ]],4;;12]]],3].s11m[[k]].mtest[[j]].Transpose[Partition[Flatten[strain0[[gbsingle[
        [i,2]],4;;12]]],3]]]]*180/Pi,{k,Length[s11m]}],{j,Length[mtest]}],Table[Table[rota
        ng[Flatten[Partition[Flatten[strain0[[gbsingle[[i,2]],4;;12]]],3].s11m[[k]].mtest[
        [j]].Transpose[Partition[Flatten[strain0[[gbsingle[[i,1]],4;;12]]],3]]]]*180/Pi,{k
        ,Length[s11m]}],{j,Length[mtest]}]}]<4.53,{RGBColor[{.118,.565,1}],Thick,Line[gb[[
        i]]]}],

        (*S9*)If[Min[{Table[Table[rotang[Flatten[Partition[Flatten[strain0[[gbsingle[[i,1]
        ],4;;12]]],3].s9m[[k]].mtest[[j]].Transpose[Partition[Flatten[strain0[[gbsingle[[i
        ,2]],4;;12]]],3]]]]*180/Pi,{k,Length[s9m]}],{j,Length[mtest]}],Table[Table[rotang[
        Flatten[Partition[Flatten[strain0[[gbsingle[[i,2]],4;;12]]],3].s9m[[k]].mtest[[j]]
        .Transpose[Partition[Flatten[strain0[[gbsingle[[i,1]],4;;12]]],3]]]]*180/Pi,{k,Len
        gth[s9m]}],{j,Length[mtest]}]}]<5.01,{RGBColor[{.196,.804,.196}],Thick,Line[gb[[i]
        ]]}],

        (*S7*)If[Min[{Table[Table[rotang[Flatten[Partition[Flatten[strain0[[gbsingle[[i,1]
        ],4;;12]]],3].s7m[[k]].mtest[[j]].Transpose[Partition[Flatten[strain0[[gbsingle[[i
        ,2]],4;;12]]],3]]]]*180/Pi,{k,Length[s7m]}],{j,Length[mtest]}],Table[Table[rotang[
        Flatten[Partition[Flatten[strain0[[gbsingle[[i,2]],4;;12]]],3].s7m[[k]].mtest[[j]]
        .Transpose[Partition[Flatten[strain0[[gbsingle[[i,1]],4;;12]]],3]]]]*180/Pi,{k,Len
        gth[s7m]}],{j,Length[mtest]}]}]<5.67,{RGBColor[{1,.843,0}],Thick,Line[gb[[i]]]}],

        (*S5*)If[Min[{Table[Table[rotang[Flatten[Partition[Flatten[strain0[[gbsingle[[i,1]
        ],4;;12]]],3].s5m[[k]].mtest[[j]].Transpose[Partition[Flatten[strain0[[gbsingle[[i
        ,2]],4;;12]]],3]]]]*180/Pi,{k,Length[s5m]}],{j,Length[mtest]}],Table[Table[rotang[
        Flatten[Partition[Flatten[strain0[[gbsingle[[i,2]],4;;12]]],3].s5m[[k]].mtest[[j]]
        .Transpose[Partition[Flatten[strain0[[gbsingle[[i,1]],4;;12]]],3]]]]*180/Pi,{k,Len
        gth[s5m]}],{j,Length[mtest]}]}]<6.71,{RGBColor[{1,.647,0}],Thick,Line[gb[[i]]]}],

        (*S3*)If[Min[{Table[Table[rotang[Flatten[Partition[Flatten[strain0[[gbsingle[[i,1]
        ],4;;12]]],3].s3m[[k]].mtest[[j]].Transpose[Partition[Flatten[strain0[[gbsingle[[i
        ,2]],4;;12]]],3]]]]*180/Pi,{k,Length[s3m]}],{j,Length[mtest]}],Table[Table[rotang[
        Flatten[Partition[Flatten[strain0[[gbsingle[[i,2]],4;;12]]],3].s3m[[k]].mtest[[j]]
        .Transpose[Partition[Flatten[strain0[[gbsingle[[i,1]],4;;12]]],3]]]]*180/Pi,{k,Len
        gth[s3m]}],{j,Length[mtest]}]}]<8.67,{RGBColor[{1,0,0}],Thick,Line[gb[[i]]]}]
```

```
    (*max deviation=15deg*sigma^-1/2, D.G.Brandon: Acta Met., 14,1966,1479.*)(*this part
      looks at each of 24 equivalent positions (plus 8 variations on 111 direction) and
      determines if there is a case where the misorientation between the two pixels and
      sigma3 is under the threshold 8.66.*)
   },{i,Length[linec]}];

(*plotting grain boundary character*)
cslmap=Graphics[csl];
lowangmap=Graphics[lowang];
CSLmap=Show[glinesmap,lowangmap,cslmap,Graphics[{Thick,Black,Line[{{20,-
      9},{scalefactor+20,-9}}],Thick,Black,Line[{{20,-13},{20,-
      5}}],Thick,Black,Line[{{scalefactor+20,-13},{scalefactor+20,-
      5}}],Black,Text[Style[scaletext,40],{scalefactor/2+20,-20}]}]]

(*label for csl map*)
g1=Graphics[Raster[{{{1,0,0},{1,.647,0},{1,.843,0},{.196,.804,.196},{.118,.565,1},
      {.5,0,.5}}}]];
g2=Graphics[Text[Style["S 3",Large,Bold],{0.5,-0.3}]];
g3=Graphics[Text[Style["S 5",Large,Bold],{1.5,-0.3}]];
g4=Graphics[Text[Style["S 7",Large,Bold],{2.5,-0.3}]];
g5=Graphics[Text[Style["S 9",Large,Bold],{3.5,-0.3}]];
g6=Graphics[Text[Style["S 11",Large,Bold],{4.5,-0.3}]];
g7=Graphics[Text[Style["0-5°",Large,Bold],{5.55,-0.3}]];
CSLlegend=Show[g1,g2,g3,g4,g5,g6,g7]

(*redefining some boundaries that are categorized as both sigma and low angle (due to
      symmetry operations) so that sigma character dominates*)
Table[If[linec[[i]]= 10,If[Count[Flatten[csl[[i]]],Thickness[Large]]=
      1,linec[[i]]=180,linec[[i]]=linec[[i]]],linec[[i]]=linec[[i]]],{i,Length[linec]}];



(*exporting variables and outputs*)
Export["gbsingle.txt",gbsingle];
Export["linec.txt",linec];
Export["csl.txt",csl];
Export["lowang.txt",lowang];
Export["lowangmap.bmp",lowangmap,ImageSize-> 2* stepx];
Export["glinesmap.bmp",glinesmap,ImageSize-> 2* stepx];
Export["CSLmap.bmp",CSLmap,ImageSize-> 2* stepx];
Export["CSLlegend.bmp",CSLlegend];
Export["gbmapg.bmp",gbmapg,ImageSize-> 2* stepx];

time1=AbsoluteTime[];
Print[time1-time0," seconds"];



(**********************************************************************)
(***Part 6: determining length fractions of boundary
      types*****)
(**********************************************************************)
(*user inputs: number of abnormal grains (this is programed in for some cases)*)
(*variables needed: linec, grains, gbsingle, csl*)
(*outputs: abgrains, gbchartable, poly, island *)
(**********************************************************************)
time0=AbsoluteTime[];

(*Importing variables if needed: *)
If[ValueQ[linec],linec,linec=ToExpression[Import["linec.txt","List"]]];
If[ValueQ[grains],grains,grains=ToExpression[Import["grains.txt","List"]]];
If[ValueQ[gbsingle],gbsingle,gbsingle=ToExpression[Import["gbsingle.txt","List"]]];
```

```
If[ValueQ[csl],csl,csl=ToExpression[Import["csl.txt","List"]]];
If[ValueQ[select],select,select=ToExpression[Import["select.txt","List"]]];
If[ValueQ[stepx],stepx,stepx=ToExpression[Import["stepx.txt"]]];
If[ValueQ[xstep],xstep,xstep=ToExpression[Import["xstep.txt"]]];
If[ValueQ[gb],gb,gb=ToExpression[Import["gb.txt","List"]]];
If[ValueQ[strain0],strain0,strain0=ToExpression[Import["strain0.txt","List"]]];
If[ValueQ[scalefactor],scalefactor,scalefactor=ToExpression[Import["scalefactor.txt"]]];
If[ValueQ[scaletext],scaletext,scaletext=ToExpression[Import["scaletext.txt"]]];
If[ValueQ[gmc],gmc,gmc=ToExpression[Import["gmc.txt","List"]]];
gbmap=Graphics[Line[gb]]
graingos=Table[Mean[gmc[[grains[[i]]]]] ,{i,Length[grains]}];
abgrains={};

(*********defining abnormal (DAGG) grains as those over 3x the average grain size and
       under 1.5 degree grain orientation spread (recrystallized)********)
gs=Table[N[Sqrt[(4*xstep*xstep*Length[grains[[i]]])/Pi]],{i,Length[grains]}];(*grain
       sizes*)
abgrains1=Flatten[{Table[Position[grains,Sort[grains,Length[#1]>Length[#2]&][[i]]],{i,1}]
       }]; (*automatically include largest grain as an abnormal grain*)
abgrains=Flatten[Position[Table[If[gs[[i]]>Mean[Sort[gs][[;;Length[gs]]]]*3&&graingos[[i]
       ]= 1.5,1,0],{i,Length[grains]}],1]]; (*add others based on size and GOS*)
abgrains=DeleteDuplicates[Flatten[{abgrains1,abgrains}]] (*combine and simplify list*)

(*determine neighbor grains*)
(*locating grain boundary pixels within each grain*)
neipix=Table[Cases[Table[Position[gbsingle,grains[[j,i]]],{i,Length[grains[[j]]]}],Except
       [{}]],{j,Length[grains]}];
neipix=Table[Flatten[neipix[[j]],1],{j,Length[neipix]}]; (*rearranging {}s*)
neipix=Table[Table[gbsingle[[neipix[[j,i,1]]]],{i,Length[neipix[[j]]]}],{j,Length[neipix]
       }]; (*finding grain boundary pixel pairs for each grain, to be compared between
       grains*)
nei=neipix;
(*lists true/false if neighbor comparing each grain to all others*)
nei=Table[Table[Boole[Length[Intersection[nei[[i]],nei[[j]]]]>0],{i,Length[nei]}],{j,Leng
       th[nei]}];
nei=Table[Flatten[Position[nei[[i]],1]],{i,Length[nei]}]; (*listing grain # s of
       neighboring grains (includes self) for each grain*)
nei=Table[Cases[nei[[i]],Except[i]],{i,Length[nei]}]; (*redefines above deleating self
       reference from neighbors*)

rx=Flatten[Position[Table[Boole[graingos[[i]]= 1.5],{i,Length[nei]}],1]]; (*defining
       recrystallized grains as having a GOS<1.5 degrees*)
og=Flatten[Position[Table[Boole[graingos[[i]]> 1.5],{i,Length[nei]}],1]]; (*defining
       original grains as having a GOS>1.5 degrees*)

island=Flatten[Position[Table[Boole[Length[Intersection[nei[[i]],abgrains]]=
       Length[nei[[i]]]],{i,Length[nei]}],1]]; (*grains touching only abnormal grains*)
islandrx=Intersection[island,rx]
islandog=Intersection[island, og]

poly=Complement[Table[i,{i,Length[grains]}],Flatten[{island,abgrains}]];
polyrx=Intersection[poly,rx]
polyog=Intersection[poly, og]

N[Length[Flatten[grains[[polyrx]]]]/Length[Flatten[grains[[poly]]]]] (*fraction of
       polycrystall grains that are recrystallized*)



(*determine neighbors that are both abnormal: search neighbors of each known abnormal for
       other abnormals, take all permutations of each match in case more than one
       neighbor found, sort to get elements in same order for each pair and delete
       duplicates. left with list of abnormal-abnormal pairs*)
```

```
abab=Partition[Flatten[Table[Table[Cases[Permutations[{abgrains[[i]],Intersection[nei[[ab
       grains[[i]]]],abgrains][[j]]},2],{_,_}],{j,Length[Intersection[nei[[abgrains[[i]]]
       ],abgrains]]}],{i,Length[abgrains]}]],2];
abab=Sort[DeleteDuplicates[Table[Sort[abab[[i]]],{i,Length[abab]}]]];
(*determine neighbors with one abnormal and one island, same methos as abab*)
abisland=Partition[Flatten[Table[Table[Cases[Permutations[{abgrains[[i]],Intersection[nei
       [[abgrains[[i]]]],island][[j]]},2],{_,_}],{j,Length[Intersection[nei[[abgrains[[i]
       ]]],island]]}],{i,Length[abgrains]}]],2];
abisland=Sort[DeleteDuplicates[Table[Sort[abisland[[i]]],{i,Length[abisland]}]]];
abislandrx=Partition[Flatten[Table[Table[Cases[Permutations[{abgrains[[i]],Intersection[n
       ei[[abgrains[[i]]]],islandrx][[j]]},2],{_,_}],{j,Length[Intersection[nei[[abgrains
       [[i]]]],islandrx]]}],{i,Length[abgrains]}]],2];
abislandrx=Sort[DeleteDuplicates[Table[Sort[abislandrx[[i]]],{i,Length[abislandrx]}]]];
abislandog=Partition[Flatten[Table[Table[Cases[Permutations[{abgrains[[i]],Intersection[n
       ei[[abgrains[[i]]]],islandog][[j]]},2],{_,_}],{j,Length[Intersection[nei[[abgrains
       [[i]]]],islandog]]}],{i,Length[abgrains]}]],2];
abislandog=Sort[DeleteDuplicates[Table[Sort[abislandog[[i]]],{i,Length[abislandog]}]]];


(*determine neighbors with one abnormal and one poly, same method as abab*)
abpoly=Partition[Flatten[Table[Table[Cases[Permutations[{abgrains[[i]],Intersection[nei[[
       abgrains[[i]]]],poly][[j]]},2],{_,_}],{j,Length[Intersection[nei[[abgrains[[i]]]],
       poly]]}],{i,Length[abgrains]}]],2];
abpoly=Sort[DeleteDuplicates[Table[Sort[abpoly[[i]]],{i,Length[abpoly]}]]];
abpolyrx=Partition[Flatten[Table[Table[Cases[Permutations[{abgrains[[i]],Intersection[nei
       [[abgrains[[i]]]],polyrx][[j]]},2],{_,_}],{j,Length[Intersection[nei[[abgrains[[i]
       ]]],polyrx]]}],{i,Length[abgrains]}]],2];
abpolyrx=Sort[DeleteDuplicates[Table[Sort[abpolyrx[[i]]],{i,Length[abpolyrx]}]]];
abpolyog=Partition[Flatten[Table[Table[Cases[Permutations[{abgrains[[i]],Intersection[nei
       [[abgrains[[i]]]],polyog][[j]]},2],{_,_}],{j,Length[Intersection[nei[[abgrains[[i]
       ]]],polyog]]}],{i,Length[abgrains]}]],2];
abpolyog=Sort[DeleteDuplicates[Table[Sort[abpolyog[[i]]],{i,Length[abpolyog]}]]];


(*determine poly-poly neighbors, same method as abab*)
polypoly=Partition[Flatten[Table[Table[Cases[Permutations[{poly[[i]],Intersection[nei[[po
       ly[[i]]]],poly][[j]]},2],{_,_}],{j,Length[Intersection[nei[[poly[[i]]]],poly]]}],{
       i,Length[poly]}]],2];
polypoly=Sort[DeleteDuplicates[Table[Sort[polypoly[[i]]],{i,Length[polypoly]}]]];
polypolyrx=Partition[Flatten[Table[Table[Cases[Permutations[{poly[[i]],Intersection[nei[[
       poly[[i]]]],polyrx][[j]]},2],{_,_}],{j,Length[Intersection[nei[[poly[[i]]]],polyrx
       ]]}],{i,Length[poly]}]],2];
polypoly=Sort[DeleteDuplicates[Table[Sort[polypoly[[i]]],{i,Length[polypoly]}]]];
polypolyog=Partition[Flatten[Table[Table[Cases[Permutations[{poly[[i]],Intersection[nei[[
       poly[[i]]]],polyog][[j]]},2],{_,_}],{j,Length[Intersection[nei[[poly[[i]]]],polyog
       ]]}],{i,Length[poly]}]],2];
polypolyog=Sort[DeleteDuplicates[Table[Sort[polypolyog[[i]]],{i,Length[polypolyog]}]]];



(*determining pixel pairs for abab, abpoly,... lists to use with csl characterization*)
ababpix=Partition[Flatten[Table[Intersection[neipix[[abab[[i,1]]]],neipix[[abab[[i,2]]]]
       ,{i,Length[abab]}]],2];
abislandpix=Partition[Flatten[Table[Intersection[neipix[[abisland[[i,1]]]],neipix[[abisla
       nd[[i,2]]]]],{i,Length[abisland]}]],2];
abislandrxpix=Partition[Flatten[Table[Intersection[neipix[[abislandrx[[i,1]]]],neipix[[ab
       islandrx[[i,2]]]]],{i,Length[abislandrx]}]],2];
abislandogpix=Partition[Flatten[Table[Intersection[neipix[[abislandog[[i,1]]]],neipix[[ab
       islandog[[i,2]]]]],{i,Length[abislandog]}]],2];
abpolypix=Partition[Flatten[Table[Intersection[neipix[[abpoly[[i,1]]]],neipix[[abpoly[[i,
       2]]]]],{i,Length[abpoly]}]],2];
abpolyrxpix=Partition[Flatten[Table[Intersection[neipix[[abpolyrx[[i,1]]]],neipix[[abpoly
       rx[[i,2]]]]],{i,Length[abpolyrx]}]],2];
abpolyogpix=Partition[Flatten[Table[Intersection[neipix[[abpolyog[[i,1]]]],neipix[[abpoly
       og[[i,2]]]]],{i,Length[abpolyog]}]],2];
polypolypix=Partition[Flatten[Table[Intersection[neipix[[polypoly[[i,1]]]],neipix[[polypo
       ly[[i,2]]]]],{i,Length[polypoly]}]],2];
```

```
polypolyrxpix=Partition[Flatten[Table[Intersection[neipix[[polypolyrx[[i,1]]]],neipix[[po
       lypolyrx[[i,2]]]]],{i,Length[polypolyrx]}]],2];
polypolyogpix=Partition[Flatten[Table[Intersection[neipix[[polypolyog[[i,1]]]],neipix[[po
       lypolyog[[i,2]]]]],{i,Length[polypolyog]}]],2];


(*categorizing boundary types and properties: csl and general angles*)
ababcsl=csl[[Flatten[Table[Position[Partition[Flatten[gbsingle],2],ababpix[[i]]],{i,Lengt
       h[ababpix]}]]]];
abislandcsl=csl[[Flatten[Table[Position[Partition[Flatten[gbsingle],2],abislandpix[[i]]],
       {i,Length[abislandpix]}]]]];
abislandrxcsl=csl[[Flatten[Table[Position[Partition[Flatten[gbsingle],2],abislandrxpix[[i
       ]]],{i,Length[abislandrxpix]}]]]];
abislandogcsl=csl[[Flatten[Table[Position[Partition[Flatten[gbsingle],2],abislandogpix[[i
       ]]],{i,Length[abislandogpix]}]]]];
abpolycsl=csl[[Flatten[Table[Position[Partition[Flatten[gbsingle],2],abpolypix[[i]]],{i,L
       ength[abpolypix]}]]]];
abpolyrxcsl=csl[[Flatten[Table[Position[Partition[Flatten[gbsingle],2],abpolyrxpix[[i]]],
       {i,Length[abpolyrxpix]}]]]];
abpolyogcsl=csl[[Flatten[Table[Position[Partition[Flatten[gbsingle],2],abpolyogpix[[i]]],
       {i,Length[abpolyogpix]}]]]];
polypolycsl=csl[[Flatten[Table[Position[Partition[Flatten[gbsingle],2],polypolypix[[i]]],
       {i,Length[polypolypix]}]]]];
polypolyrxcsl=csl[[Flatten[Table[Position[Partition[Flatten[gbsingle],2],polypolyrxpix[[i
       ]]],{i,Length[polypolyrxpix]}]]]];
polypolyogcsl=csl[[Flatten[Table[Position[Partition[Flatten[gbsingle],2],polypolyogpix[[i
       ]]],{i,Length[polypolyogpix]}]]]];


ababang=linec[[Flatten[Table[Position[Partition[Flatten[gbsingle],2],ababpix[[i]]],{i,Len
       gth[ababpix]}]]]];
abislandang=linec[[Flatten[Table[Position[Partition[Flatten[gbsingle],2],abislandpix[[i]]
       ],{i,Length[abislandpix]}]]]];
abislandrxang=linec[[Flatten[Table[Position[Partition[Flatten[gbsingle],2],abislandrxpix[
       [i]]],{i,Length[abislandrxpix]}]]]];
abislandogang=linec[[Flatten[Table[Position[Partition[Flatten[gbsingle],2],abislandogpix[
       [i]]],{i,Length[abislandogpix]}]]]];
abpolyang=linec[[Flatten[Table[Position[Partition[Flatten[gbsingle],2],abpolypix[[i]]],{i
       ,Length[abpolypix]}]]]];
abpolyrxang=linec[[Flatten[Table[Position[Partition[Flatten[gbsingle],2],abpolyrxpix[[i]]
       ],{i,Length[abpolyrxpix]}]]]];
abpolyogang=linec[[Flatten[Table[Position[Partition[Flatten[gbsingle],2],abpolyogpix[[i]]
       ],{i,Length[abpolyogpix]}]]]];
polypolyang=linec[[Flatten[Table[Position[Partition[Flatten[gbsingle],2],polypolypix[[i]]
       ],{i,Length[polypolypix]}]]]];
polypolyrxang=linec[[Flatten[Table[Position[Partition[Flatten[gbsingle],2],polypolyrxpix[
       [i]]],{i,Length[polypolyrxpix]}]]]];
polypolyogang=linec[[Flatten[Table[Position[Partition[Flatten[gbsingle],2],polypolyogpix[
       [i]]],{i,Length[polypolyogpix]}]]]];


(*determining length fraction of boundary types of grains*)
total3frac=N[Length[Cases[csl[[;;,5]],Except[Null]]]/Length[csl]]; (*sigma 3 length
       fraction*)
total5frac=N[Length[Cases[csl[[;;,4]],Except[Null]]]/Length[csl]]; (*sigma 5 length
       fraction*)
total7frac=N[Length[Cases[csl[[;;,3]],Except[Null]]]/Length[csl]]; (*sigma 7 length
       fraction*)
total9frac=N[Length[Cases[csl[[;;,2]],Except[Null]]]/Length[csl]]; (*sigma 9 length
       fraction*)
total11frac=N[Length[Cases[csl[[;;,1]],Except[Null]]]/Length[csl]]; (*sigma 11 length
       fraction*)
total0to5frac=N[(LengthWhile[Sort[linec],#= 5&])/Length[linec]]; (*0 to 5 length
       fraction*)
total5to10frac=N[(LengthWhile[Sort[linec],#= 10& ]+LengthWhile[Sort[linec,Greater],#>=
       (5)& ]-Length[linec])/Length[linec]]; (*5 to 10 length fraction*)
```

```
If[Length[ababcsl]>0,
 abab3frac=N[Length[Cases[ababcsl[[;;,5]],Except[Null]]]/Length[ababcsl]]; (*sigma 3
       length fraction*)
 abab5frac=N[Length[Cases[ababcsl[[;;,4]],Except[Null]]]/Length[ababcsl]]; (*sigma 5
       length fraction*)
 abab7frac=N[Length[Cases[ababcsl[[;;,3]],Except[Null]]]/Length[ababcsl]]; (*sigma 7
       length fraction*)
 abab9frac=N[Length[Cases[ababcsl[[;;,2]],Except[Null]]]/Length[ababcsl]]; (*sigma 9
       length fraction*)
 abab11frac=N[Length[Cases[ababcsl[[;;,1]],Except[Null]]]/Length[ababcsl]]; (*sigma 11
       length fraction*)
 abab0to5frac=N[(LengthWhile[Sort[ababang],#<= 5& ])/Length[ababang]]; (*0 to 5 length
       fraction*)
 abab5to10frac=N[(LengthWhile[Sort[ababang],#<= (10)&
       ]+LengthWhile[Sort[ababang,Greater],#>= (5)& ]-
       Length[ababang])/Length[ababang]](*5 to 10 length
       fraction*),abab3frac=abab5frac=abab7frac=abab9frac=abab11frac=abab0to5frac=abab5to
       10frac ="n/a"];


If[Length[abislandcsl]>0,
  abisland3frac=N[Length[Cases[abislandcsl[[;;,5]],Except[Null]]]/Length[abislandcsl]];
       (*sigma 3 length fraction*)
  abisland5frac=N[Length[Cases[abislandcsl[[;;,4]],Except[Null]]]/Length[abislandcsl]];
       (*sigma 5 length fraction*)
  abisland7frac=N[Length[Cases[abislandcsl[[;;,3]],Except[Null]]]/Length[abislandcsl]];
       (*sigma 7 length fraction*)
  abisland9frac=N[Length[Cases[abislandcsl[[;;,2]],Except[Null]]]/Length[abislandcsl]];
       (*sigma 9 length fraction*)
  abisland11frac=N[Length[Cases[abislandcsl[[;;,1]],Except[Null]]]/Length[abislandcsl]];
       (*sigma 11 length fraction*)
  abisland0to5frac=N[(LengthWhile[Sort[abislandang],#<= 5& ])/Length[abislandang]]; (*0
       to 5 length fraction*)
  abisland5to10frac=N[(LengthWhile[Sort[abislandang],#<= (10)&
       ]+LengthWhile[Sort[abislandang,Greater],#>= (5)& ]-
       Length[abislandang])/Length[abislandang]] (*5 to 10 length
       fraction*),abisland3frac=abisland5frac=abisland7frac=abisland9frac=abisland11frac=
       abisland0to5frac=abisland5to10frac="n/a"];


If[Length[abislandrxcsl]>0,

       abislandrx3frac=N[Length[Cases[abislandrxcsl[[;;,5]],Except[Null]]]/Length[abislan
       drxcsl]]; (*sigma 3 length fraction*)

       abislandrx5frac=N[Length[Cases[abislandrxcsl[[;;,4]],Except[Null]]]/Length[abislan
       drxcsl]]; (*sigma 5 length fraction*)

       abislandrx7frac=N[Length[Cases[abislandrxcsl[[;;,3]],Except[Null]]]/Length[abislan
       drxcsl]]; (*sigma 7 length fraction*)

       abislandrx9frac=N[Length[Cases[abislandrxcsl[[;;,2]],Except[Null]]]/Length[abislan
       drxcsl]]; (*sigma 9 length fraction*)

       abislandrx11frac=N[Length[Cases[abislandrxcsl[[;;,1]],Except[Null]]]/Length[abisla
       ndrxcsl]]; (*sigma 11 length fraction*)
  abislandrx0to5frac=N[(LengthWhile[Sort[abislandrxang],#<= 5& ])/Length[abislandrxang]];
       (*0 to 5 length fraction*)
  abislandrx5to10frac=N[(LengthWhile[Sort[abislandrxang],#<= (10)&
       ]+LengthWhile[Sort[abislandrxang,Greater],#>= (5)& ]-
       Length[abislandrxang])/Length[abislandrxang]] (*5 to 10 length
       fraction*),abislandrx3frac=abislandrx5frac=abislandrx7frac=abislandrx9frac=abislan
       drx11frac=abislandrx0to5frac=abislandrx5to10frac="n/a"];


If[Length[abislandogcsl]>0,

       abislandog3frac=N[Length[Cases[abislandogcsl[[;;,5]],Except[Null]]]/Length[abislan
```

```
      dogcsl]]; (*sigma 3 length fraction*)

      abislandog5frac=N[Length[Cases[abislandogcsl[[;;,4]],Except[Null]]]/Length[abislan
      dogcsl]]; (*sigma 5 length fraction*)

      abislandog7frac=N[Length[Cases[abislandogcsl[[;;,3]],Except[Null]]]/Length[abislan
      dogcsl]]; (*sigma 7 length fraction*)

      abislandog9frac=N[Length[Cases[abislandogcsl[[;;,2]],Except[Null]]]/Length[abislan
      dogcsl]]; (*sigma 9 length fraction*)

      abislandog11frac=N[Length[Cases[abislandogcsl[[;;,1]],Except[Null]]]/Length[abisla
      ndogcsl]]; (*sigma 11 length fraction*)
  abislandog0to5frac=N[(LengthWhile[Sort[abislandogang],#<= 5& ])/Length[abislandogang]];
      (*0 to 5 length fraction*)
  abislandog5to10frac=N[(LengthWhile[Sort[abislandogang],#<= (10)&
      ]+LengthWhile[Sort[abislandogang,Greater],#>= (5)& ]-
      Length[abislandogang])/Length[abislandogang]] (*5 to 10 length
      fraction*),abislandog3frac=abislandog5frac=abislandog7frac=abislandog9frac=abislan
      dog11frac=abislandog0to5frac=abislandog5to10frac="n/a"];

If[Length[abpolycsl]>0,
  abpoly3frac=N[Length[Cases[abpolycsl[[;;,5]],Except[Null]]]/Length[abpolycsl]]; (*sigma
      3 length fraction*)
  abpoly5frac=N[Length[Cases[abpolycsl[[;;,4]],Except[Null]]]/Length[abpolycsl]]; (*sigma
      5 length fraction*)
  abpoly7frac=N[Length[Cases[abpolycsl[[;;,3]],Except[Null]]]/Length[abpolycsl]]; (*sigma
      7 length fraction*)
  abpoly9frac=N[Length[Cases[abpolycsl[[;;,2]],Except[Null]]]/Length[abpolycsl]]; (*sigma
      9 length fraction*)
  abpoly11frac=N[Length[Cases[abpolycsl[[;;,1]],Except[Null]]]/Length[abpolycsl]];
      (*sigma 11 length fraction*)
  abpoly0to5frac=N[(LengthWhile[Sort[abpolyang],#<= 5& ])/Length[abpolyang]]; (*0 to 5
      length fraction*)
  abpoly5to10frac=N[(LengthWhile[Sort[abpolyang],#<= (10)&
      ]+LengthWhile[Sort[abpolyang,Greater],#>= (5)& ]-
      Length[abpolyang])/Length[abpolyang]] (*5 to 10 length fraction*)

      ,abpoly3frac=abpoly5frac=abpoly7frac=abpoly9frac=abpoly11frac=abpoly0to5frac=abpol
      y5to10frac="n/a"];

If[Length[abpolyrxcsl]>0,
  abpolyrx3frac=N[Length[Cases[abpolyrxcsl[[;;,5]],Except[Null]]]/Length[abpolyrxcsl]];
      (*sigma 3 length fraction*)
  abpolyrx5frac=N[Length[Cases[abpolyrxcsl[[;;,4]],Except[Null]]]/Length[abpolyrxcsl]];
      (*sigma 5 length fraction*)
  abpolyrx7frac=N[Length[Cases[abpolyrxcsl[[;;,3]],Except[Null]]]/Length[abpolyrxcsl]];
      (*sigma 7 length fraction*)
  abpolyrx9frac=N[Length[Cases[abpolyrxcsl[[;;,2]],Except[Null]]]/Length[abpolyrxcsl]];
      (*sigma 9 length fraction*)
  abpolyrx11frac=N[Length[Cases[abpolyrxcsl[[;;,1]],Except[Null]]]/Length[abpolyrxcsl]];
      (*sigma 11 length fraction*)
  abpolyrx0to5frac=N[(LengthWhile[Sort[abpolyrxang],#<= 5& ])/Length[abpolyrxang]]; (*0
      to 5 length fraction*)
  abpolyrx5to10frac=N[(LengthWhile[Sort[abpolyrxang],#<= (10)&
      ]+LengthWhile[Sort[abpolyrxang,Greater],#>= (5)& ]-
      Length[abpolyrxang])/Length[abpolyrxang]] (*5 to 10 length fraction*)

      ,abpolyrx3frac=abpolyrx5frac=abpolyrx7frac=abpolyrx9frac=abpolyrx11frac=abpolyrx0t
      o5frac=abpolyrx5to10frac="n/a"];

If[Length[abpolyogcsl]>0,
  abpolyog3frac=N[Length[Cases[abpolyogcsl[[;;,5]],Except[Null]]]/Length[abpolyogcsl]];
      (*sigma 3 length fraction*)
  abpolyog5frac=N[Length[Cases[abpolyogcsl[[;;,4]],Except[Null]]]/Length[abpolyogcsl]];
```

```
      (*sigma 5 length fraction*)
  abpolyog7frac=N[Length[Cases[abpolyogcsl[[;;,3]],Except[Null]]]/Length[abpolyogcsl]];
      (*sigma 7 length fraction*)
  abpolyog9frac=N[Length[Cases[abpolyogcsl[[;;,2]],Except[Null]]]/Length[abpolyogcsl]];
      (*sigma 9 length fraction*)
  abpolyog11frac=N[Length[Cases[abpolyogcsl[[;;,1]],Except[Null]]]/Length[abpolyogcsl]];
      (*sigma 11 length fraction*)
  abpolyog0to5frac=N[(LengthWhile[Sort[abpolyogang],#<= 5& ])/Length[abpolyogang]]; (*0
      to 5 length fraction*)
  abpolyog5to10frac=N[(LengthWhile[Sort[abpolyogang],#<= (10)&
      ]+LengthWhile[Sort[abpolyogang,Greater],#>= (5)& ]-
      Length[abpolyogang])/Length[abpolyogang]] (*5 to 10 length fraction*)

      ,abpolyog3frac=abpolyog5frac=abpolyog7frac=abpolyog9frac=abpolyog11frac=abpolyog0t
      o5frac=abpolyog5to10frac="n/a"];

If[Length[polypolycsl]>0,
  polypoly3frac=N[Length[Cases[polypolycsl[[;;,5]],Except[Null]]]/Length[polypolycsl]];
      (*sigma 3 length fraction*)
  polypoly5frac=N[Length[Cases[polypolycsl[[;;,4]],Except[Null]]]/Length[polypolycsl]];
      (*sigma 5 length fraction*)
  polypoly7frac=N[Length[Cases[polypolycsl[[;;,3]],Except[Null]]]/Length[polypolycsl]];
      (*sigma 7 length fraction*)
  polypoly9frac=N[Length[Cases[polypolycsl[[;;,2]],Except[Null]]]/Length[polypolycsl]];
      (*sigma 9 length fraction*)
  polypoly11frac=N[Length[Cases[polypolycsl[[;;,1]],Except[Null]]]/Length[polypolycsl]];
      (*sigma 11 length fraction*)
  polypoly0to5frac=N[(LengthWhile[Sort[polypolyang],#<= 5& ])/Length[polypolyang]]; (*0
      to 5 length fraction*)
  polypoly5to10frac=N[(LengthWhile[Sort[polypolyang],#<= (10)&
      ]+LengthWhile[Sort[polypolyang,Greater],#>= (5)& ]-
      Length[polypolyang])/Length[polypolyang]] (*5 to 10 length fraction*)

      ,polypoly3frac=polypoly5frac=polypoly7frac=polypoly9frac=polypoly11frac=polypoly0t
      o5frac=polypoly5to10frac="n/a"];

If[Length[polypolyrxcsl]>0,

      polypolyrx3frac=N[Length[Cases[polypolyrxcsl[[;;,5]],Except[Null]]]/Length[polypol
      yrxcsl]]; (*sigma 3 length fraction*)

      polypolyrx5frac=N[Length[Cases[polypolyrxcsl[[;;,4]],Except[Null]]]/Length[polypol
      yrxcsl]]; (*sigma 5 length fraction*)

      polypolyrx7frac=N[Length[Cases[polypolyrxcsl[[;;,3]],Except[Null]]]/Length[polypol
      yrxcsl]]; (*sigma 7 length fraction*)

      polypolyrx9frac=N[Length[Cases[polypolyrxcsl[[;;,2]],Except[Null]]]/Length[polypol
      yrxcsl]]; (*sigma 9 length fraction*)

      polypolyrx11frac=N[Length[Cases[polypolyrxcsl[[;;,1]],Except[Null]]]/Length[polypo
      lyrxcsl]]; (*sigma 11 length fraction*)
  polypolyrx0to5frac=N[(LengthWhile[Sort[polypolyrxang],#<= 5& ])/Length[polypolyrxang]];
      (*0 to 5 length fraction*)
  polypolyrx5to10frac=N[(LengthWhile[Sort[polypolyrxang],#<= (10)&
      ]+LengthWhile[Sort[polypolyrxang,Greater],#>= (5)& ]-
      Length[polypolyrxang])/Length[polypolyrxang]] (*5 to 10 length fraction*)

      ,polypolyrx3frac=polypolyrx5frac=polypolyrx7frac=polypolyrx9frac=polypolyrx11frac=
      polypolyrx0to5frac=polypolyrx5to10frac="n/a"];

If[Length[polypolyogcsl]>0,

      polypolyog3frac=N[Length[Cases[polypolyogcsl[[;;,5]],Except[Null]]]/Length[polypol
      yogcsl]]; (*sigma 3 length fraction*)
```

```
      polypolyog5frac=N[Length[Cases[polypolyogcsl[[;;,4]],Except[Null]]]/Length[polypol
      yogcsl]]; (*sigma 5 length fraction*)

      polypolyog7frac=N[Length[Cases[polypolyogcsl[[;;,3]],Except[Null]]]/Length[polypol
      yogcsl]]; (*sigma 7 length fraction*)

      polypolyog9frac=N[Length[Cases[polypolyogcsl[[;;,2]],Except[Null]]]/Length[polypol
      yogcsl]]; (*sigma 9 length fraction*)

      polypolyog11frac=N[Length[Cases[polypolyogcsl[[;;,1]],Except[Null]]]/Length[polypo
      lyogcsl]]; (*sigma 11 length fraction*)
  polypolyog0to5frac=N[(LengthWhile[Sort[polypolyogang],#<= 5& ])/Length[polypolyogang]];
      (*0 to 5 length fraction*)
  polypolyog5to10frac=N[(LengthWhile[Sort[polypolyogang],#<= (10)&
      ]+LengthWhile[Sort[polypolyogang,Greater],#>= (5)& ]-
      Length[polypolyogang])/Length[polypolyogang]] (*5 to 10 length fraction*)

      ,polypolyog3frac=polypolyog5frac=polypolyog7frac=polypolyog9frac=polypolyog11frac=
      polypolyog0to5frac=polypolyog5to10frac="n/a"];



gbchartable=MatrixForm[{{"             ","Total Length","Frac: Sigma 3", "Sigma 5",
      "Sigma 7", "Sigma 9", "Sigma 11", "Low ang 0-5", "Low ang 5-
      10"},{"Total",Length[csl],total3frac,total5frac,total7frac,total9frac,total11frac,
      total0to5frac,total5to10frac},{"Abnormal-
      Abnormal",Length[ababcsl],abab3frac,abab5frac,abab7frac,abab9frac,abab11frac,abab0
      to5frac,abab5to10frac },{"Abnormal-
      Island",Length[abislandcsl],abisland3frac,abisland5frac,abisland7frac,abisland9fra
      c,abisland11frac,abisland0to5frac,abisland5to10frac},
   {"Abnormal-Island
      (rx)",Length[abislandrxcsl],abislandrx3frac,abislandrx5frac,abislandrx7frac,abisla
      ndrx9frac,abislandrx11frac,abislandrx0to5frac,abislandrx5to10frac},
   {"Abnormal-Island (non-
      rx)",Length[abislandogcsl],abislandog3frac,abislandog5frac,abislandog7frac,abislan
      dog9frac,abislandog11frac,abislandog0to5frac,abislandog5to10frac},{"Abnormal-
      Normal",Length[abpolycsl],abpoly3frac,abpoly5frac,abpoly7frac,abpoly9frac,abpoly11
      frac,abpoly0to5frac,abpoly5to10frac},
   {"Abnormal-Normal
      (rx)",Length[abpolyrxcsl],abpolyrx3frac,abpolyrx5frac,abpolyrx7frac,abpolyrx9frac,
      abpolyrx11frac,abpolyrx0to5frac,abpolyrx5to10frac},
   {"Abnormal-Normal (non-
      rx)",Length[abpolyogcsl],abpolyog3frac,abpolyog5frac,abpolyog7frac,abpolyog9frac,a
      bpolyog11frac,abpolyog0to5frac,abpolyog5to10frac},{"Normal-Normal",
      Length[polypolycsl],polypoly3frac,polypoly5frac,polypoly7frac,polypoly9frac,polypo
      ly11frac,polypoly0to5frac,polypoly5to10frac},{"Normal-Normal (rx)",
      Length[polypolyrxcsl],polypolyrx3frac,polypolyrx5frac,polypolyrx7frac,polypolyrx9f
      rac,polypolyrx11frac,polypolyrx0to5frac,polypolyrx5to10frac},{"Normal-Normal (non-
      rx)",
      Length[polypolyogcsl],polypolyog3frac,polypolyog5frac,polypolyog7frac,polypolyog9f
      rac,polypolyog11frac,polypolyog0to5frac,polypolyog5to10frac}}]


(*exporting variables and outputs*)
Export["abgrains.txt",abgrains];
Export["gmchartable.xls",gbchartable];
Export["poly.txt",poly];
Export["polyrx.txt",polyrx];
Export["polyog.txt",polyog];
Export["island.txt",island];
Export["islandrx.txt",islandrx];
Export["islandog.txt",islandog];
Export["nei.txt",nei];
```

```
Print[AbsoluteTime[]-time0," seconds"]
```

```
(*************************************************************************)
(***Part 7: Determining grain size distribution*****)
(*************************************************************************)
(*user inputs: which grains to choose: all, not boarder, not boarder unless abnormal*)
(*variables needed: grains, xstep, abgrains, stepx, stepy *)
(*outputs: gshisto, gsize *)
(*************************************************************************)

(*Importing variables if needed: *)
If[ValueQ[grains],grains,grains=ToExpression[Import["grains.txt","List"]]];
If[ValueQ[xstep],xstep,xstep=ToExpression[Import["xstep.txt"]]];
If[ValueQ[abgrains],abgrains,abgrains=ToExpression[Import["abgrains.txt","List"]]];
If[ValueQ[stepx],stepx,stepx=ToExpression[Import["stepx.txt"]]];
If[ValueQ[stepy],stepy,stepy=ToExpression[Import["stepy.txt"]]];

xybox=Flatten[Array[(stepx)#1+(#2+1)&,{(stepy-2),(stepx-2)}]]; (*lists pixels not on
       edges, for comparison purposes*)

(*****Three options, include: all grains, all except grains touching boarder, all except
       grains touching boarder unless they are abnormal grains*)
(*gsize=Table[Length[grains[[i]]],{i,Length[grains]}];(*all grains*)*)
(*gsize=Table[If[Length[Complement[grains[[i]],xybox]]=0,Length[grains[[i]]],0],{i,Length
       [grains]}]; (*wo boarder grains*)*)
gsize=Table[If[Length[Complement[grains[[i]],xybox]]=0,Length[grains[[i]]],If[MemberQ[abg
       rains,i],Length[grains[[i]]],0]],{i,Length[grains]}];(*wo boarder grains, except
       includes abnormal grains*)



gsize=Cases[gsize,Except[0]];
(*equivalent grain size, assuming circular grains*)
gsize=Table[N[Sqrt[(4*xstep*xstep*gsize[[i]])/Pi]],{i,Length[gsize]}];
ticks=Range[0,Floor[Max[gsize,100]],50];
gshisto=Histogram[gsize,20(*{}bin width, _ # of bins*),Frame->True,FrameTicks-> {ticks,
       Automatic},PlotRange->{{0,Automatic},{0,Automatic}},FrameLabel->{"Grain Size,
       mm","Frequency"}]

(*exporting variables and outputs*)
Export["gshisto.bmp",gshisto];
Export["gsize.txt",gsize];
```

```
(*************************************************************************)
(********* Part 8: Mapping Schmid and Taylor factors
      (bcc only)***********)
(*************************************************************************)
(*user inputs:    *)
(*variables needed: grains, abgrains, poly, island, strain0, scalefactor, scaletext,
       stepx *)
(*outputs: taylortalbe, schmidscalemap, taylorcombmap, schmidcombmap,... *)
(*************************************************************************)

(*Importing variables if needed: *)
If[ValueQ[grains],grains,grains=ToExpression[Import["grains.txt","List"]]];
```

```
If[ValueQ[abgrains],abgrains,abgrains=ToExpression[Import["abgrains.txt","List"]]];
If[ValueQ[poly],poly,poly=ToExpression[Import["poly.txt","List"]]];
If[ValueQ[island],island,island=ToExpression[Import["island.txt","List"]]];
strain0=ToExpression[Import["strain0.txt","List"]];
If[ValueQ[scalefactor],scalefactor,scalefactor=ToExpression[Import["scalefactor.txt"]]];
If[ValueQ[scaletext],scaletext,scaletext=ToExpression[Import["scaletext.txt"]]];
If[ValueQ[stepx],stepx,stepx=ToExpression[Import["stepx.txt"]]];


(*redefine variables since they now include corrected pixels*)
g0x=Transpose[Table[strain0[[All,i]], {i, 4,6,1}]] ;
g0y=Transpose[Table[strain0[[All,i]], {i, 7,9,1}]] ;
g0z=Transpose[Table[strain0[[All,i]], {i, 10,12,1}]] ;


dir=g0x; (*choose direction to look at*)


(*defining slip systems for bcc*)
(*{110}<-111>*)
s110={{{1,1,0},{-1,1,1}},{{1,1,0},{1,-1,1}},{{1,0,1},{-1,1,1}},{{1,0,1},{1,1,-
       1}},{{0,1,1},{1,-1,1}},{{0,1,1},{1,1,-1}},{{-1,1,0},{1,1,1}},{{-1,1,0},{1,1,-
       1}},{{-1,0,1},{1,1,1}},{{-1,0,1},{1,-1,1}},{{0,-1,1},{1,1,1}},{{0,-1,1},{-
       1,1,1}}};
s110=Table[{Normalize[s110[[i,1]]],Normalize[s110[[i,2]]]},{i,Length[s110]}];


(*{112}<11-1>*)
s112={{{1,1,2},{1,1,-1}},{{-1,1,2},{1,-1,1}},{{1,-1,2},{-1,1,1}},{{1,1,-
       2},{1,1,1}},{{1,2,1},{1,-1,1}},{{-1,2,1},{1,1,-1}},{{1,-2,1},{1,1,1}},{{1,2,-1},{-
       1,1,1}},{{2,1,1},{-1,1,1}},{{-2,1,1},{1,1,1}},{{2,-1,1},{1,1,-1}},{{2,1,-1},{1,-
       1,1}}};
s112=Table[{Normalize[s112[[i,1]]],Normalize[s112[[i,2]]]},{i,Length[s112]}];


(*{123}<11-1>*)
s123={{{1,2,3},{1,1,-1}},{{-1,2,3},{1,-1,1}},{{1,-2,3},{-1,1,1}},{{1,2,-
       3},{1,1,1}},{{2,1,3},{1,1,-1}},{{-2,1,3},{1,-1,1}},{{2,-1,3},{-1,1,1}},{{2,1,-
       3},{1,1,1}},{{2,3,1},{1,-1,1}},{{-2,3,1},{1,1,-1}},{{2,-3,1},{1,1,1}},{{2,3,-1},{-
       1,1,1}},{{3,2,1},{-1,1,1}},{{-3,2,1},{1,1,1}},{{3,-2,1},{1,1,-1}},{{3,2,-1},{1,-
       1,1}},{{3,1,2},{-1,1,1}},{{-3,1,2},{1,1,1}},{{3,-1,2},{1,1,-1}},{{3,1,-2},{1,-
       1,1}},{{1,3,2},{1,-1,1}},{{-1,3,2},{1,1,-1}},{{1,-3,2},{1,1,1}},{{1,3,-2},{-
       1,1,1}}};
s123=Table[{Normalize[s123[[i,1]]],Normalize[s123[[i,2]]]},{i,Length[s123]}];


(*schmid factor in direction 'dir' for {110}<111> slip system*)
schmid110=Table[Max[Table[Abs[N[(dir[[i]].s110[[j,1]])/(Norm[dir[[i]]]*Norm[s110[[j,1]]])
       ]]*Abs[N[(dir[[i]].s110[[j,2]])/(Norm[dir[[i]]]*Norm[s110[[j,2]]])]],{j,Length[s11
       0]}]],{i,Length[dir]}];
schmid110map = Graphics[{Raster[Partition[(schmid110-
       .3)/0.2,Round[stepx]]],Thick,Black,Line[{{20,-9},{scalefactor+20,-
       9}}],Thick,Black,Line[{{20,-13},{20,-5}}],Thick,Black,Line[{{scalefactor+20,-
       13},{scalefactor+20,-5}}],Black,Text[Style[scaletext,40],{scalefactor/2+20,-20}]}]


(*schmid factor in direction 'dir' for {112}<111> slip system*)
schmid112=Table[Max[Table[Abs[N[(dir[[i]].s112[[j,1]])/(Norm[dir[[i]]]*Norm[s112[[j,1]]])
       ]]*Abs[N[(dir[[i]].s112[[j,2]])/(Norm[dir[[i]]]*Norm[s112[[j,2]]])]],{j,Length[s11
       2]}]],{i,Length[dir]}];
schmid112map = Graphics[{Raster[Partition[(schmid112-
       .3)/0.2,Round[stepx]]],Thick,Black,Line[{{20,-9},{scalefactor+20,-
       9}}],Thick,Black,Line[{{20,-13},{20,-5}}],Thick,Black,Line[{{scalefactor+20,-
       13},{scalefactor+20,-5}}],Black,Text[Style[scaletext,40],{scalefactor/2+20,-20}]}]


(*schmid factor in direction 'dir' for {123}<111> slip system*)
schmid123=Table[Max[Table[Abs[N[(dir[[i]].s123[[j,1]])/(Norm[dir[[i]]]*Norm[s123[[j,1]]])
       ]]*Abs[N[(dir[[i]].s123[[j,2]])/(Norm[dir[[i]]]*Norm[s123[[j,2]]])]],{j,Length[s12
       3]}]],{i,Length[dir]}];
```

```
schmid123map = Graphics[{Raster[Partition[(schmid123-
       .3)/0.2,Round[stepx]]],Thick,Black,Line[{{20,-9},{scalefactor+20,-
       9}}],Thick,Black,Line[{{20,-13},{20,-5}}],Thick,Black,Line[{{scalefactor+20,-
       13},{scalefactor+20,-5}}],Black,Text[Style[scaletext,40],{scalefactor/2+20,-20}]}]


(*schmid factor presented as minumum from each slip system at each point*)
schmidcomb=Table[Max[{schmid110[[i]],schmid112[[i]],schmid123[[i]]}],{i,Length[schmid123]
       }];
schmidcombmap= Graphics[{Raster[Partition[(schmidcomb-
       .3)/0.2,Round[stepx]]],Thick,Black,Line[{{20,-9},{scalefactor+20,-
       9}}],Thick,Black,Line[{{20,-13},{20,-5}}],Thick,Black,Line[{{scalefactor+20,-
       13},{scalefactor+20,-5}}],Black,Text[Style[scaletext,40],{scalefactor/2+20,-20}]}]


(*schmid factor scale*)
schmidscalemap=Show[Graphics[Rectangle[{-0.02,-
       0.02},{10.02,1.03}]],Graphics[Raster[{Range[0,1,1/9]}]],Graphics[Text[Style["0.3",
       Large,Bold],{0.5,-0.5}]],Graphics[Text[Style["0.5",Large,Bold],{9.5,-.5}]]]


(*determine average schmid factor in various regions: abnormal, island, and
       polycrystalline region grains*)
schmid110ab=Flatten[Table[schmid110[[grains[[abgrains[[i]]]]]],{i,Length[abgrains]}]];
schmid110poly=Flatten[Table[schmid110[[grains[[poly[[i]]]]]],{i,Length[poly]}]];
schmid110island=Flatten[Table[schmid110[[grains[[island[[i]]]]]],{i,Length[island]}]];


schmid112ab=Flatten[Table[schmid112[[grains[[abgrains[[i]]]]]],{i,Length[abgrains]}]];
schmid112poly=Flatten[Table[schmid112[[grains[[poly[[i]]]]]],{i,Length[poly]}]];
schmid112island=Flatten[Table[schmid112[[grains[[island[[i]]]]]],{i,Length[island]}]];

schmid123ab=Flatten[Table[schmid123[[grains[[abgrains[[i]]]]]],{i,Length[abgrains]}]];
schmid123poly=Flatten[Table[schmid123[[grains[[poly[[i]]]]]],{i,Length[poly]}]];
schmid123island=Flatten[Table[schmid123[[grains[[island[[i]]]]]],{i,Length[island]}]];


schmidcombab=Flatten[Table[schmidcomb[[grains[[abgrains[[i]]]]]],{i,Length[abgrains]}]];
schmidcombpoly=Flatten[Table[schmidcomb[[grains[[poly[[i]]]]]],{i,Length[poly]}]];
schmidcombisland=Flatten[Table[schmidcomb[[grains[[island[[i]]]]]],{i,Length[island]}]];


schmidtable=MatrixForm[{{"             ","Fraction of total area","Average Schmid Factor
       110","std 110","Average Schmid Factor 112","std 112","Average Schmid Factor
       123","std 123","Average Combined Schmid Factor (110,112,123)","std all"},{"All
       grains","1",Mean[schmid110],StandardDeviation[schmid110],Mean[schmid112],StandardD
       eviation[schmid112],Mean[schmid123],StandardDeviation[schmid123],Mean[schmidcomb],
       StandardDeviation[schmidcomb]},
   {"Abnormal
       grains",N[Length[schmidcombab]/Length[schmidcomb]],If[Length[schmidcombab]>0,Mean[
       schmid110ab],"n/a"],If[Length[schmidcombab]>2,StandardDeviation[schmid110ab],"n/a"
       ],If[Length[schmidcombab]>0,Mean[schmid112ab],"n/a"],If[Length[schmidcombab]>2,Sta
       ndardDeviation[schmid112ab],"n/a"],If[Length[schmidcombab]>0,Mean[schmid123ab],"n/
       a"],If[Length[schmidcombab]>2,StandardDeviation[schmid123ab],"n/a"],If[Length[schm
       idcombab]>0,Mean[schmidcombab],"n/a"]
       ,If[Length[schmidcombab]>2,StandardDeviation[schmidcombab],"n/a"]},{"Polycrystalli
       ne",N[Length[schmidcombpoly]/Length[schmidcomb]],Mean[schmid110poly],StandardDevia
       tion[schmid110poly],Mean[schmid112poly],StandardDeviation[schmid112poly],Mean[schm
       id123poly],StandardDeviation[schmid123poly],Mean[schmidcombpoly],StandardDeviation
       [schmidcombpoly]},{"Island
       grains",N[Length[schmidcombisland]/Length[schmidcomb]],If[Length[schmidcombisland]
       >0,Mean[schmid110island],"n/a"],

       If[Length[schmidcombisland]>0,StandardDeviation[schmid110island],"n/a"],If[Length[
       schmidcombisland]>0,Mean[schmid112island],"n/a"],

       If[Length[schmidcombisland]>0,StandardDeviation[schmid112island],"n/a"],If[Length[
       schmidcombisland]>0,Mean[schmid123island],"n/a"],
```

```
       If[Length[schmidcombisland]>0,StandardDeviation[schmid123island],"n/a"],If[Length[
       schmidcombisland]>0,Mean[schmidcombisland],"n/a"],
    If[Length[schmidcombisland]>0,StandardDeviation[schmidcombisland],"n/a"]}}]


(*import referece file for determining taylor factor.  Taylor factor was determined at
       0.5 degree increments for a standard stereographic triangle. The values here are
       interpolated from that data set to reduce computation time*)
taylorcombstd=Import["C:/Users/user/Desktop/taylormixed.txt","List"];


(*defining points at 0.5 degree increments on standard triangle*)
tp=Partition[Flatten[Table[Table[{theta,phi},{phi,0,ArcTan[Sin[theta]],.5Degree}],{theta,
       0,45Degree,.5Degree}]],2];


(*interpolating to obtain taylor factor*)
taylorcomb=Flatten[Table[{bp=move[dir[[i]]];If[bp[[1]]=0,bp[[1]]=0.000001];If[bp[[2]]=0,b
       p[[2]]=0.000001];If[bp[[3]]=0,bp[[3]]=0.000001];bp=bp/Norm[bp];theta=N[ArcTan[bp[[
       1]]/bp[[3]]]];phi=N[ArcTan[bp[[2]]/Sqrt[bp[[3]]^2+bp[[2]]^2]]];corners=Sort[Neares
       t[tp,{theta,phi},3]]; (*the nearest 3 points are found, then the fourth point is
       determined. if the nearest 4 points are used, the 4 points often do not make a
       box*)
       corners=Sort[DeleteDuplicates[Partition[Flatten[{corners,{corners[[3,1]],corners[[
       2,2]]},{corners[[3,1]],corners[[1,2]]},{corners[[1,1]],corners[[2,2]]},{corners[[1
       ,1]],corners[[3,2]]}]],2]]];
     If[Length[Intersection[corners,tp]]>3,
      ct=Table[taylorcombstd[[Flatten[Position[tp,corners[[i]]]]]],{i,4}];
      If[Length[DeleteCases[ct,{}]]>3,
       dx=(theta-corners[[1,1]])/(corners[[3,1]]-corners[[1,1]]);
       dy=(phi-corners[[1,2]])/(corners[[2,2]]-corners[[1,2]]);
 (ct[[3]]*Clip[dy]+ct[[4]]*(1-Clip[dy]))*Clip[dx]+(ct[[1]]*Clip[dy]+ct[[2]]*(1-
       Clip[dy]))*(1-
       Clip[dx]),taylorcombstd[[Flatten[Position[tp,Flatten[Nearest[tp,{theta,phi}]]]]]]]
       ,

     taylorcombstd[[Flatten[Position[tp,Flatten[Nearest[tp,{theta,phi}]]]]]]]
     },{i,Length[dir]}]];


(*plotting taylor factor*)
taylorcombmap= Graphics[{Raster[Partition[1-(taylorcomb-2.121)/(3.182-
       2.121),Round[stepx]]],Thick,Black,Line[{{20,-9},{scalefactor+20,-
       9}}],Thick,Black,Line[{{20,-13},{20,-5}}],Thick,Black,Line[{{scalefactor+20,-
       13},{scalefactor+20,-5}}],Black,Text[Style[scaletext,40],{scalefactor/2+20,-20}]}]
       (*lower taylor factor is white, slips easier*)


taylorscale=Show[Graphics[Rectangle[{-0.02,-
       0.02},{10.02,1.03}]],Graphics[Raster[{Range[1,0,-
       1/9]}]],Graphics[Text[Style[SetPrecision[2.121,3],Large,Bold],{0.5,-
       0.5}]],Graphics[Text[Style[SetPrecision[3.182,3],Large,Bold],{9.5,-.5}]]]


(*determine average taylor factor in various regions: abnormal, island, and
       polycrystalline region grains*)
taylorab=Flatten[Table[taylorcomb[[grains[[abgrains[[i]]]]]],{i,Length[abgrains]}]];
taylorpoly=Flatten[Table[taylorcomb[[grains[[poly[[i]]]]]],{i,Length[poly]}]];
taylorisland=Flatten[Table[taylorcomb[[grains[[island[[i]]]]]],{i,Length[island]}]];


taylortable=MatrixForm[{{"             ","Fraction of total area","Average Taylor
       Factor","stdev"},{"All
       grains","1",Mean[taylorcomb],StandardDeviation[taylorcomb]},{"Abnormal
       grains",N[Length[taylorab]/Length[taylorcomb]],If[Length[taylorab]>0,Mean[taylorab
       ],"n/a"] ,If[Length[taylorab]>0,StandardDeviation[taylorab],"n/a"]},

       {"Polycrystalline",N[Length[taylorpoly]/Length[taylorcomb]],Mean[taylorpoly],Stand
       ardDeviation[taylorpoly]},{"Island
```

```
grains",N[Length[taylorisland]/Length[taylorcomb]],If[Length[taylorisland]>0,Mean[
taylorisland],"n/a"],If[Length[taylorisland]>0,StandardDeviation[taylorisland],"n/
a"]}}]


(*exporting variables and outputs*)
Export["schmid110map.bmp",schmid110map,ImageSize-> 2* stepx];
Export["schmid112map.bmp",schmid112map,ImageSize-> 2* stepx];
Export["schmid123map.bmp",schmid123map,ImageSize-> 2* stepx];
Export["schmid110.txt",schmid110];
Export["schmid112.txt",schmid112];
Export["schmid123.txt",schmid123];
Export["schmidcombmap.bmp",schmidcombmap,ImageSize-> 2* stepx];
Export["schmidscalemap.bmp",schmidscalemap];
Export["schmidtable.xls",schmidtable];
Export["taylorcomb.txt",taylorcomb];
Export["taylorcombmap.bmp",taylorcombmap,ImageSize-> 2* stepx];
Export["taylorscale.bmp",taylorscale];
Export["taylortable.xls",taylortable];

Print[AbsoluteTime[]-timetotal0," seconds total"];



(*****************************************************************)
(****** Part 9: mapping inverse pole and pole figures
       ********)
(*********************************************************************)
(*user inputs:   make sure labels for inverse poles x,y, and z are correct for specimen
       orientation, and for pole figures wrt TD, RD, and ND *)
(*variables needed: abgrains, strain0, gmsiavg *)
(*outputs: ipolex, ipoley, ipolez, ipolexwab, ipoleywab, ipolezwab, pole100, pole110,
       pole112, pole111 *)
(*********************************************************************)

(*Importing variables if needed: *)
If[ValueQ[gmisavgq],gmisavgq,gmisavgq=ToExpression[Import["gmisavgq.txt","List"]]];
If[ValueQ[abgrains],abgrains,abgrains=ToExpression[Import["abgrain.s.txt","List"]]];
If[ValueQ[strain0],strain0,strain0=ToExpression[Import["strain0.txt","List"]]];


g0x=Transpose[Table[strain0[[All,i]], {i, 4,6,1}]] ;
g0y=Transpose[Table[strain0[[All,i]], {i, 7,9,1}]] ;
g0z=Transpose[Table[strain0[[All,i]], {i, 10,12,1}]] ;

(*Plotting inverse pole figures*)

(*setting up triangle*)
step=100;
c=Range[0,1,1/step];
c0=ConstantArray[0,step];
c1=ConstantArray[1,step];
L001101={c,c0,c1};
L1=Table[N[stereo1[{L001101[[1,m]],L001101[[2,m]],L001101[[3,m]]}]], {m,step}];
L001111={c,c,c1};
L2=Table[N[stereo1[{L001111[[1,m]],L001111[[2,m]],L001111[[3,m]]}]], {m,step}];
L101111={c1,c,c1};
L3=Table[N[stereo1[{L101111[[1,m]],L101111[[2,m]],L101111[[3,m]]}]], {m,step}];
(*plot formation of stereo pole figure border lines*)
pstereo=Graphics[ListLinePlot[{L1,L2,L3}, PlotStyle->Directive[Black],Axes->False]];
```

```
dir=g0x; (*direction for inverse pole figure reference*)
(*points to be plotted on inv pole figure*)
dir=Table[N[move[{dir[[i,1]],dir[[i,2]],dir[[i,3]]}]], {i,Length[dir]}];
ps=Table[N[stereo1[{dir[[i,1]],dir[[i,2]],dir[[i,3]]}]], {i,Length[dir]}];
px=ListPlot[ps,PlotStyle->Directive[Opacity[0.10],PointSize[0.005],Black]];  (*change
       opacity and pointsize here**************)


dir=g0y; (*direction for inverse pole figure reference*)
(*points to be plotted on inv pole figure*)
dir=Table[N[move[{dir[[i,1]],dir[[i,2]],dir[[i,3]]}]], {i,Length[dir]}];
ps=Table[N[stereo1[{dir[[i,1]],dir[[i,2]],dir[[i,3]]}]], {i,Length[dir]}];
py=ListPlot[ps,PlotStyle->Directive[Opacity[0.10],PointSize[0.005],Black]];  (*change
       opacity and pointsize here**************)


dir=g0z; (*direction for inverse pole figure reference*)
(*points to be plotted on inv pole figure*)
dir=Table[N[move[{dir[[i,1]],dir[[i,2]],dir[[i,3]]}]], {i,Length[dir]}];
ps=Table[N[stereo1[{dir[[i,1]],dir[[i,2]],dir[[i,3]]}]], {i,Length[dir]}];
pz=ListPlot[ps,PlotStyle->Directive[Opacity[0.10],PointSize[0.005],Black]];  (*change
       opacity and pointsize here**************)



(*for plotting single points for single crystals using gmisavg (average misorientation
       for the grain) *)
If[Length[abgrains]= 1,
 g0x2=Flatten[quattomat[gmisavgq[[abgrains[[1]]]]]][[1;;3]] ;
 g0y2=Flatten[quattomat[gmisavgq[[abgrains[[1]]]]]][[4;;6]] ;
 g0z2=Flatten[quattomat[gmisavgq[[abgrains[[1]]]]]][[7;;9]] ;


 dir2=g0x2; (*direction********)
 dir2=N[move[dir2]];(*points to be plotted on inv pole figure*)
 ps2=N[stereo1[dir2]];
 px2=Graphics[{PointSize[0.03],Red,Point[ps2]}];


 dir2=g0y2; (*direction********)
 dir2=N[move[dir2]];
 ps2=N[stereo1[dir2]];
 py2=Graphics[{PointSize[0.03],Red,Point[ps2]}];


 dir2=g0z2; (*direction*******)
 dir2=N[move[dir2]];
 ps2=N[stereo1[dir2]];
 pz2=Graphics[{PointSize[0.03],Red,Point[ps2]}]];


If[Length[abgrains]>1,
  g0x2=Table[Flatten[quattomat[gmisavgq[[abgrains[[i]]]]]],
       {i,Length[abgrains]}][[All,1;;3]];
  g0y2=Table[Flatten[quattomat[gmisavgq[[abgrains[[i]]]]]],
       {i,Length[abgrains]}][[All,4;;6]] ;
  g0z2=Table[Flatten[quattomat[gmisavgq[[abgrains[[i]]]]]],
       {i,Length[abgrains]}][[All,7;;9]] ;


  dir2=g0x2; (*direction***********)
  dir2=Table[N[move[{dir2[[i,1]],dir2[[i,2]],dir2[[i,3]]}]], {i,Length[dir2]}];
  (*points to be plotted on inv pole figure*)
  ps2=Table[N[stereo1[{dir2[[i,1]],dir2[[i,2]],dir2[[i,3]]}]], {i,Length[dir2]}];
  px2=ListPlot[ps2,PlotStyle->Directive[PointSize[0.03],Red]];


  dir2=g0y2; (*direction***********)
  dir2=Table[N[move[{dir2[[i,1]],dir2[[i,2]],dir2[[i,3]]}]], {i,Length[dir2]}];
  ps2=Table[N[stereo1[{dir2[[i,1]],dir2[[i,2]],dir2[[i,3]]}]], {i,Length[dir2]}];
```

```
  py2=ListPlot[ps2,PlotStyle->Directive[PointSize[0.03],Red]];

  dir2=g0z2; (*direction***********)
  dir2=Table[N[move[{dir2[[i,1]],dir2[[i,2]],dir2[[i,3]]}]], {i,Length[dir2]}];
  ps2=Table[N[stereo1[{dir2[[i,1]],dir2[[i,2]],dir2[[i,3]]}]], {i,Length[dir2]}];
  pz2=ListPlot[ps2,PlotStyle->Directive[PointSize[0.03],Red]];


text111=Graphics[Text[Style["111",Large,Bold],{.395,.355}]];
text101=Graphics[Text[Style["101",Large,Bold],{.40,-0.017}]];
text001=Graphics[Text[Style["001",Large,Bold],{0.015,-.017}]];

text=Graphics[Text[Style["TD",Large,Bold],{0.1,0.35}]]; (*****label for X direction inv
       pole figure*****************************)
ipolex=Show[{pstereo,px,text111,text101,text001,text},PlotRange->{{-0.01,0.425},{-
       0.05,.39}},AspectRatio->.92]
text=Graphics[Text[Style["LTD",Large,Bold],{0.1,0.35}]]; (*****label for Y direction inv
       pole figure*****************************)
ipoley=Show[{pstereo,py,text111,text101,text001,text},PlotRange->{{-0.01,0.425},{-
       0.05,.39}},AspectRatio->.92]
text=Graphics[Text[Style["STD",Large,Bold],{0.1,0.35}]]; (*****label for Z direction inv
       pole figure*****************************)
ipolez=Show[{pstereo,pz,text111,text101,text001,text},PlotRange->{{-0.01,0.425},{-
       0.05,.39}},AspectRatio->.92]


(*inv poles with abgrains highlighted*)
If[Length[abgrains]>0,
  text=Graphics[Text[Style["TD",Large,Bold],{0.1,0.35}]]; (*****label for X direction inv
       pole figure*****************************)
  ipolexwab=Show[{pstereo,px,px2,text111,text101,text001,text},PlotRange->{{-
       0.01,0.425},{-0.05,.39}},AspectRatio->.92];
  text=Graphics[Text[Style["LTD",Large,Bold],{0.1,0.35}]]; (*****label for Y direction
       inv pole figure*****************************)
  ipoleywab=Show[{pstereo,py,py2,text111,text101,text001,text},PlotRange->{{-
       0.01,0.425},{-0.05,.39}},AspectRatio->.92];
  text=Graphics[Text[Style["STD",Large,Bold],{0.1,0.35}]]; (*****label for Z direction
       inv pole figure*****************************)
  ipolezwab=Show[{pstereo,pz,pz2,text111,text101,text001,text},PlotRange->{{-
       0.01,0.425},{-0.05,.39}},AspectRatio->.92]];

ipolexwab
ipoleywab
ipolezwab

(*plotting pole figure*)

(* stereographic projection background image*)
bound1=ListLinePlot[{{1,0},{-1,0}},DisplayFunction->Identity,PlotStyle-
       >Directive[Black]];
bound2=ListLinePlot[{{0,1},{0,-1}},DisplayFunction->Identity,PlotStyle-
       >Directive[Black]];
boundc=Circle[{0,0},1];
boundc1={Circle[{-1,0},1.4142,{-
       45*Degree,45*Degree}],Circle[{1,0},1.4142,{135*Degree,225*Degree}],Circle[{0,1},1.
       4142,{225*Degree,315*Degree}],Circle[{0,-1},1.4142,{45*Degree,135*Degree}]};
boundl1=ListLinePlot[{{Cos[45*Degree],Sin[45*Degree]},{-Cos[45*Degree],-
       Sin[45*Degree]}},DisplayFunction->Identity,PlotStyle->Directive[Black]];
boundl2=ListLinePlot[{{-Cos[45*Degree],Sin[45*Degree]},{Cos[45*Degree],-
       Sin[45*Degree]}},DisplayFunction->Identity,PlotStyle->Directive[Black]];

(*parts of g-matrix as shown in inv-pole script. a11,a12,a13; a21,...;...a33*)
g0=Table[Transpose[{{strain0[[i,4]],strain0[[i,5]],
```

```
                        strain0[[i,6]]},{strain0[[i,7]],strain0[[i,8]],
        strain0[[i,9]]},{strain0[[i,10]],strain0[[i,11]],strain0[[i,12]]}}],{i,Length[stra
        in0]}];

(* columns 1 and 2 are x and y coordinates of the EBSD maps *)
spacing=strain0[[2,1]]-strain0[[1,1]];
columns=(Last[strain0][[1]]/spacing) +1;

(* rotating data from ebsd measurement orientation to actual*)
g0=Table[g0[[i]],{i,Length[g0]}];

p100g0=Partition[Flatten[Table[{Vnorm[{1.,0,0}].g0[[i]],Vnorm[{0,1.,0}].g0[[i]],Vnorm[{0,
        0,1.}].g0[[i]]},{i,Length[g0]}]],3];
p110g0=Partition[Flatten[Table[{Vnorm[{-
        1.,0,1}].g0[[i]],Vnorm[{1.,0,1.}].g0[[i]],Vnorm[{0,1.,1.}].g0[[i]],Vnorm[{0,-
        1.,1.}].g0[[i]],Vnorm[{1.,1.,0}].g0[[i]],Vnorm[{-
        1.,1.,0}].g0[[i]]},{i,Length[g0]}]],3];
p111g0=Partition[Flatten[Table[{Vnorm[{-1.,-1.,1.}].g0[[i]],Vnorm[{-
        1.,1.,1.}].g0[[i]],Vnorm[{1.,1.,1.}].g0[[i]],Vnorm[{1.,-
        1.,1.}].g0[[i]]},{i,Length[g0]}]],3];
p112g0=Partition[Flatten[Table[{Vnorm[{1.,1.,2.}].g0[[i]],Vnorm[{1.,2.,1.}].g0[[i]],Vnorm
        [{2.,1.,1.}].g0[[i]],Vnorm[{1.,-1.,2.}].g0[[i]],Vnorm[{-
        1.,1.,2.}].g0[[i]],Vnorm[{1.,1.,-2.}].g0[[i]],Vnorm[{1.,-2.,1.}].g0[[i]],Vnorm[{-
        1.,2.,1.}].g0[[i]],Vnorm[{1.,2.,-1.}].g0[[i]],Vnorm[{-
        2.,1.,1.}].g0[[i]],Vnorm[{2.,-1.,1.}].g0[[i]],Vnorm[{2.,1.,-
        1.}].g0[[i]]},{i,Length[g0]}]],3];


(*100 pole figure*)
xy1=Table[N[{p100g0[[i,2]]/(p100g0[[i,3]]+1),-
        p100g0[[i,1]]/(p100g0[[i,3]]+1)}],{i,Length[p100g0]}];
xy2=Table[N[{-p100g0[[i,2]]/(-p100g0[[i,3]]+1),p100g0[[i,1]]/(-
        p100g0[[i,3]]+1)}],{i,Length[p100g0]}];
xy100g0=Table[Which[xy1[[i,1]]^2+xy1[[i,2]]^2<1,xy1[[i]],xy2[[i,1]]^2+xy2[[i,2]]^2<1,xy2[
        [i]],True,xy1[[i]]],{i,Length[xy1]}];
boundxy100g0=ListPlot[xy100g0,DisplayFunction->Identity,PlotStyle-
        >Directive[Opacity[0.10],PointSize[0.005],Black]];
text=Graphics[Text[Style["100",Large,Bold],{-1,1}]];
toplab=Graphics[Text[Style[" ",Medium,Bold],{0,1.06}]];
botlab=Graphics[Text[Style[" ",Medium,Bold],{1.1,0}]];
pole100=Show[{Graphics[boundc],Graphics[{boundc1}],bound1,bound2,boundl1,boundl2,
        boundxy100g0,text, toplab, botlab},AspectRatio->1,PlotRange->All,DisplayFunction-
        >$DisplayFunction]

(*110 pole figure*)
xy1=Table[N[{p110g0[[i,2]]/(p110g0[[i,3]]+1),-
        p110g0[[i,1]]/(p110g0[[i,3]]+1)}],{i,Length[p110g0]}];
xy2=Table[N[{-p110g0[[i,2]]/(-p110g0[[i,3]]+1),p110g0[[i,1]]/(-
        p110g0[[i,3]]+1)}],{i,Length[p110g0]}];
xy110g0=Table[Which[xy1[[i,1]]^2+xy1[[i,2]]^2<1,xy1[[i]],xy2[[i,1]]^2+xy2[[i,2]]^2<1,xy2[
        [i]],True,xy1[[i]]],{i,Length[xy1]}];
boundxy110g0=ListPlot[xy110g0,DisplayFunction->Identity,PlotStyle-
        >Directive[Opacity[0.10],PointSize[0.005],Black]];
text=Graphics[Text[Style["110",Large,Bold],{-1,1}]];
toplab=Graphics[Text[Style[" ",Medium,Bold],{0,1.06}]];
botlab=Graphics[Text[Style[" ",Medium,Bold],{1.1,0}]];
pole110=Show[{Graphics[boundc],Graphics[{boundc1}],bound1,bound2,boundl1,boundl2,
        boundxy110g0,text, toplab, botlab},AspectRatio->1,PlotRange->All,DisplayFunction-
        >$DisplayFunction]

(*111 pole figure*)
xy1=Table[N[{p111g0[[i,2]]/(p111g0[[i,3]]+1),-
```

```
        p111g0[[i,1]]/(p111g0[[i,3]]+1)}],{i,Length[p111g0]}];
xy2=Table[N[{-p111g0[[i,2]]/(-p111g0[[i,3]]+1),p111g0[[i,1]]/(-
        p111g0[[i,3]]+1)}],{i,Length[p111g0]}];
xy111g0=Table[Which[xy1[[i,1]]^2+xy1[[i,2]]^2<1,xy1[[i]],xy2[[i,1]]^2+xy2[[i,2]]^2<1,xy2[
        [i]],True,xy1[[i]]],{i,Length[xy1]}];
boundxy111g0=ListPlot[xy111g0,DisplayFunction->Identity,PlotStyle-
        >Directive[Opacity[0.10],PointSize[0.005],Black]];
text=Graphics[Text[Style["111",Large,Bold],{-1,1}]];
toplab=Graphics[Text[Style[" ",Medium,Bold],{0,1.06}]];
botlab=Graphics[Text[Style[" ",Medium,Bold],{1.1,0}]];
pole111=Show[{Graphics[boundc],Graphics[{boundc1}],bound1,bound2,boundl1,boundl2,
        boundxy111g0,text, toplab, botlab},AspectRatio->1,PlotRange->All,DisplayFunction-
        >$DisplayFunction]


(*112 pole figure*)
xy1=Table[N[{p112g0[[i,2]]/(p112g0[[i,3]]+1),-
        p112g0[[i,1]]/(p112g0[[i,3]]+1)}],{i,Length[p112g0]}];
xy2=Table[N[{-p112g0[[i,2]]/(-p112g0[[i,3]]+1),p112g0[[i,1]]/(-
        p112g0[[i,3]]+1)}],{i,Length[p112g0]}];
xy112g0=Table[Which[xy1[[i,1]]^2+xy1[[i,2]]^2<1,xy1[[i]],xy2[[i,1]]^2+xy2[[i,2]]^2<1,xy2[
        [i]],True,xy1[[i]]],{i,Length[xy1]}];
boundxy112g0=ListPlot[xy112g0,DisplayFunction->Identity,PlotStyle-
        >Directive[Opacity[0.10],PointSize[0.005],Black]];
text=Graphics[Text[Style["112",Large,Bold],{-1,1}]];
toplab=Graphics[Text[Style[" ",Medium,Bold],{0,1.06}]];
botlab=Graphics[Text[Style[" ",Medium,Bold],{1.1,0}]];
pole112=Show[{Graphics[boundc],Graphics[{boundc1}],bound1,bound2,boundl1,boundl2,
        boundxy112g0,text, toplab, botlab},AspectRatio->1,PlotRange->All,DisplayFunction-
        >$DisplayFunction]



(*exporting variables and outputs*)
Export["ipolex.bmp",ipolex, ImageResolution-> 600];
Export["ipoley.bmp",ipoley];
Export["ipolez.bmp",ipolez];
If[Length[abgrains]>0,Export["ipolexwab.bmp",ipolexwab];
  Export["ipoleywab.bmp",ipoleywab];
  Export["ipolezwab.bmp",ipolezwab]];
Export["pole100.bmp",pole100];
Export["pole110.bmp",pole110];
Export["pole111.bmp",pole111];
Export["pole112.bmp",pole112];


time1=AbsoluteTime[];
Print[time1-time0," seconds"]


(*************************************************************************)
(******** Part 10: mapping grain orientation spread
      (GOS, Kunze et al 1993), and associated
      analysis of different regions **********)
(*************************************************************************)
(*user inputs:    *)
(*variables needed: abgrains, poly, gmsiavgq, scalefactor, scaletext, gbmap *)
(*outputs: graingos *)
(*************************************************************************)


(*Importing variables if needed: *)
If[ValueQ[gmisavgq],gmisavgq,gmisavgq=ToExpression[Import["gmisavgq.txt","List"]]];
If[ValueQ[abgrains],abgrains,abgrains=ToExpression[Import["abgrains.txt","List"]]];
If[ValueQ[strain0],strain0,strain0=ToExpression[Import["strain0.txt","List"]]];
If[ValueQ[scalefactor],scalefactor,scalefactor=ToExpression[Import["scalefactor.txt"]]];
```

```
If[ValueQ[scaletext],scaletext,scaletext=ToExpression[Import["scaletext.txt"]]];
If[ValueQ[grains],grains,grains=ToExpression[Import["grains.txt","List"]]];
If[ValueQ[gb],gb,gb=ToExpression[Import["gb.txt","List"]]];
If[ValueQ[poly],poly,poly=ToExpression[Import["poly.txt","List"]]];
If[ValueQ[gmc],gmc,gmc=ToExpression[Import["gmc.txt","List"]]];
gbmap=Graphics[Line[gb]];


(*for each pixel, compare its orientation to the average orientation of the grain it
      belongs*)(*symmerty has already been corrected, so dont need to compare with
      symetrically equivalent orientations as well*)


(*averaging within each grain*)
graingos=Table[Mean[gmc[[grains[[i]]]]] ,{i,Length[grains]}]; (*list of grains, with
      number corresponding to its average misorientation*)
pixgos=Table[graingos[[Flatten[Position[grains,strain0[[i,1]]]][[1]]]],{i,Length[strain0]
      }];
pixgos=pixgos/8;(*scaling*)
(*plotting*)
maxdeg=8; (*scaling parameter*)
Table[graingos[[i]]=graingos[[i]]/maxdeg,{i,Length[graingos]}];
gosmap=Graphics[Raster[Partition[Flatten[pixgos],stepx],ColorFunction->
      "TemperatureMap"]];
m1=Graphics[Raster[{Range[0,1,.1]},ColorFunction->"TemperatureMap"]];
m2=Graphics[Text[Style["0",Large,Bold],{0,-0.5}]];
m3=Graphics[Text[Style[SetPrecision[maxdeg,3]" degrees",Large,Bold],{13,-.5}]];
Gosmap=Show[gosmap,gbmap,Graphics[{Thick,Black,Line[{{20,-9},{scalefactor+20,-
      9}}],Thick,Black,Line[{{20,-13},{20,-5}}],Thick,Black,Line[{{scalefactor+20,-
      13},{scalefactor+20,-5}}],Black,Text[Style[scaletext,40],{scalefactor/2+20,-
      20}]}]]
Goslegend=Show[m1,m2,m3]


(*weighted average of poly grain gos*)
plengths=Table[Length[grains[[poly[[i]]]]],{i,Length[poly]}];
pwavggos=Total[Table[Mean[gmc[[grains[[poly[[i]]]]]]]*plengths[[i]],{i,Length[poly]}]]/To
      tal[plengths];
pwstdgos=Total[Table[StandardDeviation[gmc[[grains[[poly[[i]]]]]]]*plengths[[i]],{i,Lengt
      h[poly]}]]/Total[plengths];


(*determining GOS of grains oriented similarly (within 5 degrees) to an abnormal grain.
      this part only runs if abnormal grain exists*)
If[Length[abgrains]>0,If[Length[abgrains]=1,
   (*weighted average of abnormal grain gos*)
   abwavggos=Mean[gmc[[Flatten[grains[[abgrains]]]]]];
   abwstdgos=StandardDeviation[gmc[[Flatten[grains[[abgrains]]]]]];
   (*finding grains in poly region that are similar in orientation to the abnormal
      grain(s)*)

      similarabpoly=Table[quatmiso[Flatten[gmisavgq[[abgrains]]],gmisavgq[[poly[[i]]]]],
      {i,Length[poly]}];

      Table[If[similarabpoly[[i]]<5,similarabpoly[[i]]=1,similarabpoly[[i]]=0],{i,Length
      [similarabpoly]}];

      If[Length[Position[similarabpoly,1]]>0,If[Length[Position[similarabpoly,1]]=1,simi
      larabpoly=poly[[Flatten[Position[similarabpoly,1]]]]];
    (*weighted average of poly grain gos, with similar orientation to one or more
      abnormal grains*)

      simwavggos=Mean[gmc[[Flatten[grains[[similarabpoly]]]]]];simwstdgos=StandardDeviat
      ion[gmc[[Flatten[grains[[similarabpoly]]]]]],
    similarabpoly=poly[[Partition[Flatten[Position[similarabpoly,1]],2][[All,2]]]];
    (*weighted average of poly grain gos, with similar orientation to one or more
      abnormal grains*)
```

```
    simabplengths=Table[Length[grains[[similarabpoly[[i]]]]],{i,Length[similarabpoly]}];

      simwavggos=Mean[gmc[[Flatten[grains[[similarabpoly]]]]]];simwstdgos=StandardDeviat
      ion[gmc[[Flatten[grains[[similarabpoly]]]]]],simwavggos="n/a"];
  maxmisindagg=Max[gmc[[Flatten[grains[[abgrains]]]]]],


  (*weighted average of abnormal grain gos*)
  abwavggos=Mean[gmc[[Flatten[grains[[abgrains]]]]]];
  abwstdgos=StandardDeviation[gmc[[Flatten[grains[[abgrains]]]]]];
  (*finding grains in poly region that are similar in orientation to the abnormal
      grain(s)*)

      similarabpoly=Table[Table[quatmiso[gmisavgq[[abgrains[[j]]]],gmisavgq[[poly[[i]]]]
      ],{i,Length[poly]}],{j,Length[abgrains]}];

      Table[Table[If[similarabpoly[[j,i]]<5,similarabpoly[[j,i]]=1,similarabpoly[[j,i]]=
      0],{i,Length[similarabpoly[[j]]]}],{j,Length[similarabpoly]}];

      If[Length[Position[similarabpoly,1]]>0,If[Length[Position[similarabpoly,1]]=1,simi
      larabpoly=poly[[Flatten[Position[similarabpoly,1]]]];
    (*weighted average of poly grain gos, with similar orientation to one or more
      abnormal grains*)

      simwavggos=Mean[gmc[[Flatten[grains[[similarabpoly]]]]]];simwstdgos=StandardDeviat
      ion[gmc[[Flatten[grains[[similarabpoly]]]]]],
    similarabpoly=poly[[Partition[Flatten[Position[similarabpoly,1]],2][[All,2]]]];
    (*weighted average of poly grain gos, with similar orientation to one or more
      abnormal grains*)
    simabplengths=Table[Length[grains[[similarabpoly[[i]]]]],{i,Length[similarabpoly]}];

      simwavggos=Mean[gmc[[Flatten[grains[[similarabpoly]]]]]];simwstdgos=StandardDeviat
      ion[gmc[[Flatten[grains[[similarabpoly]]]]]],simwavggos="n/a"];
  maxmisindagg=Table[Max[gmc[[grains[[abgrains[[i]]]]]]],{i,Length[abgrains]}]],
 abwavggos=simwavggos=maxmisindagg="n/a"];

similarabpoly
abgrains
gostable=MatrixForm[{{"Mean GOS for abnormal grains (weighted by grain size): ",
       abwavggos},{"Stdev GOS for abnormal grains (weighted by grain size): ",
       abwstdgos},{"Mean GOS for grains oriented within 5 degrees of a DAGG grain
       (weighted by grain size): ", simwavggos},{"Stdev GOS for grains oriented within 5
       degrees of a DAGG grain (weighted by grain size): ", simwstdgos},{"Mean GOS for
       polycrystalline grains (weighted by grain size): ",pwavggos},{"Stdev GOS for
       polycrystalline grains (weighted by grain size): ",pwstdgos},{"Fraction
       recrystallized grains (of total):
       ",N[Length[Flatten[grains[[polyrx]]]]/Length[Flatten[grains]]]},{"Fraction
       recrystallized grains (of poly):
       ",N[Length[Flatten[grains[[polyrx]]]]/Length[Flatten[grains[[poly]]]]]},{"Max
       misorientation within DAGG grains: ", maxmisindagg}}]


daggorients=Table[gmisavgq[[abgrains[[i]]]],{i,Length[abgrains]}];


Export["Gosmap.bmp",Gosmap,ImageSize-> 2* stepx];
Export["Goslegend.bmp",Goslegend];
Export["gostable.xls",gostable];
Export["daggorients.txt",daggorients];
Export["similarabpoly.txt",similarabpoly];
```

Appendix B: Rotation Matrices Describing Σ3, Σ5, Σ7, Σ9, and Σ11 Boundaries

The following matrices describe the rotation matrices that define the Σ boundary specified for each variation of its axis and angle.

Σ 3: 60° rotation about <111>

$$\begin{bmatrix} 2/3 & -1/3 & 2/3 \\ 2/3 & 2/3 & -1/3 \\ -1/3 & 2/3 & 2/3 \end{bmatrix} \quad \begin{bmatrix} 2/3 & -1/3 & -2/3 \\ 2/3 & 2/3 & 1/3 \\ 1/3 & -2/3 & 2/3 \end{bmatrix}$$

$$\begin{bmatrix} 2/3 & -2/3 & 1/3 \\ 1/3 & 2/3 & 2/3 \\ -2/3 & -1/3 & 2/3 \end{bmatrix} \quad \begin{bmatrix} 2/3 & 1/3 & -2/3 \\ -2/3 & 2/3 & -1/3 \\ 1/3 & 2/3 & 2/3 \end{bmatrix}$$

$$\begin{bmatrix} 2/3 & -2/3 & -1/3 \\ 1/3 & 2/3 & -2/3 \\ 2/3 & 1/3 & 2/3 \end{bmatrix} \quad \begin{bmatrix} 2/3 & 1/3 & 2/3 \\ -2/3 & 2/3 & 1/3 \\ -1/3 & -2/3 & 2/3 \end{bmatrix}$$

$$\begin{bmatrix} 2/3 & 2/3 & 1/3 \\ -1/3 & 2/3 & -2/3 \\ -2/3 & 1/3 & 2/3 \end{bmatrix} \quad \begin{bmatrix} 2/3 & 2/3 & -1/3 \\ -1/3 & 2/3 & 2/3 \\ 2/3 & -1/3 & 2/3 \end{bmatrix}$$

Σ 5: 36.87° rotation about <100>

$$\begin{bmatrix} 1 & 0 & 0 \\ 0 & 4/5 & -3/5 \\ 0 & 3/5 & 4/5 \end{bmatrix} \quad \begin{bmatrix} 4/5 & 0 & -3/5 \\ 0 & 1 & 0 \\ 3/5 & 0 & 4/5 \end{bmatrix}$$

$$\begin{bmatrix} 1 & 0 & 0 \\ 0 & 4/5 & 3/5 \\ 0 & -3/5 & 4/5 \end{bmatrix} \quad \begin{bmatrix} 4/5 & -3/5 & 0 \\ 3/5 & 4/5 & 0 \\ 0 & 0 & 1 \end{bmatrix}$$

$$\begin{bmatrix} 4/5 & 0 & 3/5 \\ 0 & 1 & 0 \\ -3/5 & 0 & 4/5 \end{bmatrix} \quad \begin{bmatrix} 4/5 & 3/5 & 0 \\ -3/5 & 4/5 & 0 \\ 0 & 0 & 1 \end{bmatrix}$$

Σ 7: 38.21° rotation about <111>

$$\begin{bmatrix} 6/7 & -2/7 & 3/7 \\ 3/7 & 6/7 & -2/7 \\ -2/7 & 3/7 & 6/7 \end{bmatrix} \quad \begin{bmatrix} 6/7 & -2/7 & -3/7 \\ 3/7 & 6/7 & 2/7 \\ 2/7 & -3/7 & 6/7 \end{bmatrix}$$

$$\begin{bmatrix} 6/7 & -3/7 & 2/7 \\ 2/7 & 6/7 & 3/7 \\ -3/7 & -2/7 & 6/7 \end{bmatrix} \quad \begin{bmatrix} 6/7 & 2/7 & -3/7 \\ -3/7 & 6/7 & -2/7 \\ 2/7 & 3/7 & 6/7 \end{bmatrix}$$

$$\begin{bmatrix} 6/7 & -3/7 & -2/7 \\ 2/7 & 6/7 & -3/7 \\ 3/7 & 2/7 & 6/7 \end{bmatrix} \quad \begin{bmatrix} 6/7 & 2/7 & 3/7 \\ -3/7 & 6/7 & 2/7 \\ -2/7 & -3/7 & 6/7 \end{bmatrix}$$

$$\begin{bmatrix} 6/7 & 3/7 & 2/7 \\ -2/7 & 6/7 & -3/7 \\ -3/7 & 2/7 & 6/7 \end{bmatrix} \quad \begin{bmatrix} 6/7 & 3/7 & -2/7 \\ -2/7 & 6/7 & 3/7 \\ 3/7 & -2/7 & 6/7 \end{bmatrix}$$

Σ 9: 38.94° rotation about <110>

$$\begin{bmatrix} 8/9 & 1/9 & 4/9 \\ 1/9 & 8/9 & -4/9 \\ -4/9 & 4/9 & 7/9 \end{bmatrix} \quad \begin{bmatrix} 8/9 & 4/9 & -1/9 \\ -4/9 & 7/9 & -4/9 \\ -1/9 & 4/9 & 8/9 \end{bmatrix}$$

$$\begin{bmatrix} 8/9 & -1/9 & 4/9 \\ -1/9 & 8/9 & 4/9 \\ -4/9 & -4/9 & 7/9 \end{bmatrix} \quad \begin{bmatrix} 8/9 & 4/9 & 1/9 \\ -4/9 & 7/9 & 4/9 \\ 1/9 & -4/9 & 8/9 \end{bmatrix}$$

$$\begin{bmatrix} 8/9 & -1/9 & -4/9 \\ -1/9 & 8/9 & -4/9 \\ 4/9 & 4/9 & 7/9 \end{bmatrix} \quad \begin{bmatrix} 7/9 & -4/9 & 4/9 \\ 4/9 & 8/9 & 1/9 \\ -4/9 & 1/9 & 8/9 \end{bmatrix}$$

$$\begin{bmatrix} 8/9 & 1/9 & -4/9 \\ 1/9 & 8/9 & 4/9 \\ 4/9 & -4/9 & 7/9 \end{bmatrix} \quad \begin{bmatrix} 7/9 & -4/9 & -4/9 \\ 4/9 & 8/9 & -1/9 \\ 4/9 & -1/9 & 8/9 \end{bmatrix}$$

$$\begin{bmatrix} 8/9 & -4/9 & 1/9 \\ 4/9 & 7/9 & -4/9 \\ 1/9 & 4/9 & 8/9 \end{bmatrix} \quad \begin{bmatrix} 7/9 & 4/9 & 4/9 \\ -4/9 & 8/9 & -1/9 \\ -4/9 & -1/9 & 8/9 \end{bmatrix}$$

$$\begin{bmatrix} 8/9 & -4/9 & -1/9 \\ 4/9 & 7/9 & 4/9 \\ -1/9 & -4/9 & 8/9 \end{bmatrix} \quad \begin{bmatrix} 7/9 & 4/9 & -4/9 \\ -4/9 & 8/9 & 1/9 \\ 4/9 & 1/9 & 8/9 \end{bmatrix}$$

Σ 11: 50.48° rotation about <110>

$$\begin{bmatrix} 9/11 & 2/11 & 6/11 \\ 2/11 & 9/11 & -6/11 \\ -6/11 & 6/11 & 7/11 \end{bmatrix} \quad \begin{bmatrix} 9/11 & 6/11 & -2/11 \\ -6/11 & 7/11 & -6/11 \\ -2/11 & 6/11 & 9/11 \end{bmatrix}$$

$$\begin{bmatrix} 9/11 & -2/11 & 6/11 \\ -2/11 & 9/11 & 6/11 \\ -6/11 & -6/11 & 7/11 \end{bmatrix} \quad \begin{bmatrix} 9/11 & 6/11 & 2/11 \\ -6/11 & 7/11 & 6/11 \\ 2/11 & -6/11 & 9/11 \end{bmatrix}$$

$$\begin{bmatrix} 9/11 & -2/11 & -6/11 \\ -2/11 & 9/11 & -6/11 \\ 6/11 & 6/11 & 7/11 \end{bmatrix} \quad \begin{bmatrix} 7/11 & -6/11 & 6/11 \\ 6/11 & 9/11 & 2/11 \\ -6/11 & 2/11 & 9/11 \end{bmatrix}$$

$$\begin{bmatrix} 9/11 & 2/11 & -6/11 \\ 2/11 & 9/11 & 6/11 \\ 6/11 & -6/11 & 7/11 \end{bmatrix} \quad \begin{bmatrix} 7/11 & -6/11 & -6/11 \\ 6/11 & 9/11 & -2/11 \\ 6/11 & -2/11 & 9/11 \end{bmatrix}$$

$$\begin{bmatrix} 9/11 & -6/11 & 2/11 \\ 6/11 & 7/11 & -6/11 \\ 2/11 & 6/11 & 9/11 \end{bmatrix} \quad \begin{bmatrix} 7/11 & 6/11 & 6/11 \\ -6/11 & 9/11 & -2/11 \\ -6/11 & -2/11 & 9/11 \end{bmatrix}$$

$$\begin{bmatrix} 9/11 & -6/11 & -2/11 \\ 6/11 & 7/11 & 6/11 \\ -2/11 & -6/11 & 9/11 \end{bmatrix} \quad \begin{bmatrix} 7/11 & 6/11 & -6/11 \\ -6/11 & 9/11 & 2/11 \\ 6/11 & 2/11 & 9/11 \end{bmatrix}$$

Appendix C: *Mathematica*™ Script for Calculating Taylor factor Over a Standard Triangle

The following code (distinguished by courier font) can be copied and pasted to create a *Mathematica*™ notebook (ex: file.nb). Comments are in gray. A directory location must be specified.

```
(*Calculating and plotting taylor factor over standard triangle.  Use output txt file as
reference in EBSD analysis program in Appendix A*)

(*defining useful functions*)
stereo1[x_] := {x[[1]]/(Norm[x]*(x[[3]]/Norm[x] + 1)), x[[2]]/(Norm[x]*(x[[3]]/Norm[x] +
1))};
move[x_] := RotateLeft[Sort[Abs[x], Greater], 1];

SetDirectory["C:/Users/user/Desktop/"];

(*drawing standard triangle for plotting taylor factor*)
step=100;
c=Range[0,1,1/step];
c0=ConstantArray[0,step];
c1=ConstantArray[1,step];
L001101={c,c0,c1};
L1=Table[N[stereo1[{L001101[[1,m]],L001101[[2,m]],L001101[[3,m]]}]], {m,step}];
L001111={c,c,c1};
L2=Table[N[stereo1[{L001111[[1,m]],L001111[[2,m]],L001111[[3,m]]}]], {m,step}];
L101111={c1,c,c1};
L3=Table[N[stereo1[{L101111[[1,m]],L101111[[2,m]],L101111[[3,m]]}]], {m,step}];
(*plot formation of stereo pole figure border lines*)
pstereo=Graphics[ListLinePlot[{L1,L2,L3}, PlotStyle->Directive[Black,
Thickness[.005]],Axes->False]];

(*matrix of positions covering standard triangle in 0.5 degree incriments*)
dir=Partition[Flatten[Table[Table[{(1+Tan[theta]^2+(1+Tan[theta]^2)*Tan[phi]^2)^(-
1/2),Tan[theta]*(1+Tan[theta]^2+(1+Tan[theta]^2)*Tan[phi]^2)^(-
1/2),Sqrt[1+Tan[theta]^2]*Tan[phi]*(1+Tan[theta]^2+(1+Tan[theta]^2)*Tan[phi]^2)^(-
1/2)},{phi,0.0001,ArcTan[Sin[theta]],.5Degree}],{theta,0.0001,45Degree,.5Degree}]],3];
dir=Table[N[move[{dir[[i,1]],dir[[i,2]],dir[[i,3]]}]], {i,Length[dir]}];
(*points to be plotted on inv pole figure*)
ps=Table[N[stereo1[{dir[[i,1]],dir[[i,2]],dir[[i,3]]}]], {i,Length[dir]}];



(*a110, a112, and a123 define the slip system components (Eq. 3.22) for slip systems
{110}<111>, {112}<111>, and {123}<111>*)

a110={{0,0.707106781373095`,-
0.707106781373095`,0.5773502690459181`,0.5773502690459181`,0.5773502690459181`},{0.707106
781373095`,0,-
0.707106781373095`,0.5773502690459181`,0.5773502690459181`,0.5773502690459181`},{0.707106
781373095`,-
0.707106781373095`,0,0.5773502690459181`,0.5773502690459181`,0.5773502690459181`},{0.7071
06781373095`,0,0.703553409061008`,0.5773502690459181`,0.5773502690459181`,-
0.5773502690459181`},{0,0.707106781373095`,0.707106781373095`,0.5773502690459181`,0.57735
```

```
02690459181`,-0.5773502690459181`},{0.707106781373095`,-
0.707106781373095`,0,0.5773502690459181`,0.5773502690459181`,-
0.5773502690459181`},{0.707106781373095`,0.707106781373095`,0,0.5773502690459181`,-
0.5773502690459181`,0.5773502690459181`},{0.707106781373095`,0,-
0.707106781373095`,0.5773502690459181`,-
0.5773502690459181`,0.5773502690459181`},{0,0.707106781373095`,0.707106781373095`,0.57735
02690459181`,-0.5773502690459181`,0.5773502690459181`},{0,0.707106781373095`,-
0.707106781373095`,-
0.5773502690459181`,0.5773502690459181`,0.5773502690459181`},{0.707106781373095`,0,0.7071
06781373095`,-
0.5773502690459181`,0.5773502690459181`,0.5773502690459181`},{0.707106781373095`,0.707106
781373095`,0,-0.5773502690459181`,0.5773502690459181`,0.5773502690459181`}};
a112={{0.40824829`,0.40824829`,-
0.816496581`,0.577350269`,0.577350269`},{0.40824829`,-
0.816496581`,0.40824829`,0.577350269`,0.577350269`,0.577350269`},{-
0.816496581`,0.40824829`,0.40824829`,0.577350269`,0.577350269`,0.577350269`},{0.40824829`
,0.40824829`,0.816496581`,0.577350269`,0.577350269`,-0.577350269`},{-
0.40824829`,0.816496581`,0.40824829`,0.577350269`,0.577350269`,-
0.577350269`},{0.816496581`,-0.40824829`,0.40824829`,0.577350269`,0.577350269`,-
0.577350269`},{-0.40824829`,0.40824829`,0.816496581`,0.577350269`,-
0.577350269`,0.577350269`},{0.816496581`,0.40824829`,-0.40824829`,0.577350269`,-
0.577350269`,0.577350269`},{0.40824829`,0.816496581`,0.40824829`,0.577350269`,-
0.577350269`,0.577350269`},{0.816496581`,0.40824829`,0.40824829`,-
0.577350269`,0.577350269`,0.577350269`},{0.40824829`,0.816496581`,-0.40824829`,-
0.577350269`,0.577350269`,0.577350269`},{-0.40824829`,0.40824829`,-0.816496581`,-
0.577350269`,0.577350269`,0.577350269`}};


a123 = {{0.534522484`,-
0.801783726`,0.267261242`,0.577350269`,0.577350269`,0.577350269`},{0.534522484`,0.2672612
42`,-0.801783726`,0.577350269`,0.577350269`,0.577350269`},{-0.267261242`,-
0.534522484`,0.801783726`,0.577350269`,0.577350269`,0.577350269`},{-0.534522484`,-
0.267261242`,0.801783726`,0.577350269`,0.577350269`,0.577350269`},{-
0.801783726`,0.267261242`,0.534522484`,0.577350269`,0.577350269`,0.577350269`},{-
0.801783726`,0.534522484`,0.267261242`,0.577350269`,0.577350269`,0.577350269`},{0.8017837
26`,-0.534522484`,0.267261242`,0.577350269`,0.577350269`,-0.577350269`},{0.801783726`,-
0.267261242`,0.534522484`,0.577350269`,0.577350269`,-
0.577350269`},{0.534522484`,0.267261242`,0.801783726`,0.577350269`,0.577350269`,-
0.577350269`},{0.267261242`,0.534522484`,0.801783726`,0.577350269`,0.577350269`,-
0.577350269`},{-0.267261242`,0.801783726`,0.534522484`,0.577350269`,0.577350269`,-
0.577350269`},{-0.534522484`,0.801783726`,0.267261242`,0.577350269`,0.577350269`,-
0.577350269`},{0.801783726`,0.534522484`,0.267261242`,-
0.577350269`,0.577350269`,0.577350269`},{0.801783726`,0.267261242`,0.534522484`,-
0.577350269`,0.577350269`,0.577350269`},{0.534522484`,-0.267261242`,0.801783726`,-
0.577350269`,0.577350269`,0.577350269`},{0.267261242`,-0.534522484`,0.801783726`,-
0.577350269`,0.577350269`,0.577350269`},{-0.267261242`,-0.801783726`,0.534522484`,-
0.577350269`,0.577350269`,0.577350269`},{-0.534522484`,-0.801783726`,0.267261242`,-
0.577350269`,0.577350269`,0.577350269`},{-0.801783726`,-
0.534522484`,0.267261242`,0.577350269`,-0.577350269`,0.577350269`},{-0.801783726`,-
0.267261242`,0.534522484`,0.577350269`,-0.577350269`,0.577350269`},{-
0.534522484`,0.267261242`,0.801783726`,0.577350269`,-0.577350269`,0.577350269`},{-
0.267261242`,0.534522484`,0.801783726`,0.577350269`,-
0.577350269`,0.577350269`},{0.267261242`,0.801783726`,0.534522484`,0.577350269`,-
0.577350269`,0.577350269`},{0.534522484`,0.801783726`,0.267261242`,0.577350269`,-
0.577350269`,0.577350269`}};


am={a110,a112,a123};
am=Partition[Flatten[am],6];


(*calculating taylor factor at each 0.5 degree increment*)
mt=Table[{am[[k,2]]*am[[k,5]],am[[k,3]]*am[[k,6]],
.5*(am[[k,2]]*am[[k,6]]+am[[k,3]]*am[[k,5]]),.5*(am[[k,1]]*am[[k,6]]+am[[k,3]]*am[[k,4]])
,.5*(am[[k,1]]*am[[k,5]]+am[[k,2]]*am[[k,4]])},{k,Length[am]}];


taylorfactor=Flatten[Table[{bp=dir[[i]];bp=bp/Norm[bp];theta=N[ArcTan[bp[[1]]/bp[[3]]]];p
```

```
hi=N[ArcTan[bp[[2]]/Sqrt[bp[[3]]^2+bp[[2]]^2]]];de=.5*Partition[Flatten[{{3*Cos[phi]^2*Co
s[theta]^2-
1},{3*Cos[phi]^2*Sin[theta]*Cos[theta]},{3*Sin[phi]*Cos[phi]*Cos[theta]},{3*Cos[phi]^2*Si
n[theta]*Cos[theta]},{3*Cos[phi]^2*Sin[theta]^2-
1},{3*Sin[phi]*Cos[phi]*Sin[theta]},{3*Sin[phi]*Cos[phi]*Cos[theta]},{3*Sin[phi]*Cos[phi]
*Sin[theta]},{3*Sin[phi]^2-
1}}],3];per=Subsets[Range[Length[am]],{5}];pernd=Table[mt[[per[[i]]]],{i,Length[per]}];pe
rnd=pernd[[Flatten[Position[Table[MatrixRank[Transpose[pernd[[i]]]],{i,Length[pernd]}],5]
]]];detp=Chop[Table[Det[pernd[[i]]],{i,Length[pernd]}]];pernd=Delete[pernd,Position[detp,
0]];taylor=Min[Table[Total[Abs[Inverse[Transpose[pernd[[i]]]].Flatten[de][[{5,9,6,3,2}]]]
],{i,Length[pernd]}]]},{i,Length[dir]}]];

plotfn=taylorfactor;

(*finding taylor factor for <100>, <110>, and <111> directions for corners of inverse
pole figure*)
bp={0,0,1};
bp=move[bp];
If[bp[[1]]==0,bp[[1]]=0.000001];
If[bp[[2]]==0,bp[[2]]=0.000001];
If[bp[[3]]==0,bp[[3]]=0.000001];
bp=bp/Norm[bp];
theta=N[ArcTan[bp[[1]]/bp[[3]]]];
phi=N[ArcTan[bp[[2]]/Sqrt[bp[[3]]^2+bp[[2]]^2]]];
de=.5*Partition[Flatten[{{3*Cos[phi]^2*Cos[theta]^2-
1},{3*Cos[phi]^2*Sin[theta]*Cos[theta]},{3*Sin[phi]*Cos[phi]*Cos[theta]},{3*Cos[phi]^2*Si
n[theta]*Cos[theta]},{3*Cos[phi]^2*Sin[theta]^2-
1},{3*Sin[phi]*Cos[phi]*Sin[theta]},{3*Sin[phi]*Cos[phi]*Cos[theta]},{3*Sin[phi]*Cos[phi]
*Sin[theta]},{3*Sin[phi]^2-
1}}],3];per=Subsets[Range[Length[am]],{5}];pernd=Table[mt[[per[[i]]]],{i,Length[per]}];pe
rnd=pernd[[Flatten[Position[Table[MatrixRank[Transpose[pernd[[i]]]],{i,Length[pernd]}],5]
]]];detp=Chop[Table[Det[pernd[[i]]],{i,Length[pernd]}]];pernd=Delete[pernd,Position[detp,
0]];t001=Min[Table[Total[Abs[Inverse[Transpose[pernd[[i]]]].Flatten[de][[{5,9,6,3,2}]]]],
{i,Length[pernd]}]];

bp={0,1,1};
bp=move[bp];
If[bp[[1]]==0,bp[[1]]=0.000001];
If[bp[[2]]==0,bp[[2]]=0.000001];
If[bp[[3]]==0,bp[[3]]=0.000001];
bp=bp/Norm[bp];
theta=N[ArcTan[bp[[1]]/bp[[3]]]];
phi=N[ArcTan[bp[[2]]/Sqrt[bp[[3]]^2+bp[[2]]^2]]];
de=.5*Partition[Flatten[{{3*Cos[phi]^2*Cos[theta]^2-
1},{3*Cos[phi]^2*Sin[theta]*Cos[theta]},{3*Sin[phi]*Cos[phi]*Cos[theta]},{3*Cos[phi]^2*Si
n[theta]*Cos[theta]},{3*Cos[phi]^2*Sin[theta]^2-
1},{3*Sin[phi]*Cos[phi]*Sin[theta]},{3*Sin[phi]*Cos[phi]*Cos[theta]},{3*Sin[phi]*Cos[phi]
*Sin[theta]},{3*Sin[phi]^2-
1}}],3];per=Subsets[Range[Length[am]],{5}];pernd=Table[mt[[per[[i]]]],{i,Length[per]}];pe
rnd=pernd[[Flatten[Position[Table[MatrixRank[Transpose[pernd[[i]]]],{i,Length[pernd]}],5]
]]];detp=Chop[Table[Det[pernd[[i]]],{i,Length[pernd]}]];pernd=Delete[pernd,Position[detp,
0]];t110=Min[Table[Total[Abs[Inverse[Transpose[pernd[[i]]]].Flatten[de][[{5,9,6,3,2}]]]],
{i,Length[pernd]}]];

bp={1,1,1};
bp=move[bp];
If[bp[[1]]==0,bp[[1]]=0.000001];
If[bp[[2]]==0,bp[[2]]=0.000001];
If[bp[[3]]==0,bp[[3]]=0.000001];
bp=bp/Norm[bp];
theta=N[ArcTan[bp[[1]]/bp[[3]]]];
phi=N[ArcTan[bp[[2]]/Sqrt[bp[[3]]^2+bp[[2]]^2]]];
de=.5*Partition[Flatten[{{3*Cos[phi]^2*Cos[theta]^2-
1},{3*Cos[phi]^2*Sin[theta]*Cos[theta]},{3*Sin[phi]*Cos[phi]*Cos[theta]},{3*Cos[phi]^2*Si
```

```
n[theta]*Cos[theta]},{3*Cos[phi]^2*Sin[theta]^2-
1},{3*Sin[phi]*Cos[phi]*Sin[theta]},{3*Sin[phi]*Cos[phi]*Cos[theta]},{3*Sin[phi]*Cos[phi]
*Sin[theta]},{3*Sin[phi]^2-
1}}],3];per=Subsets[Range[Length[am]],{5}];pernd=Table[mt[[per[[i]]]],{i,Length[per]}];pe
rnd=pernd[[Flatten[Position[Table[MatrixRank[Transpose[pernd[[i]]]],{i,Length[pernd]}],5]
]]];detp=Chop[Table[Det[pernd[[i]]],{i,Length[pernd]}]];pernd=Delete[pernd,Position[detp,
0]];t111=Min[Table[Total[Abs[Inverse[Transpose[pernd[[i]]]].Flatten[de][[{5,9,6,3,2}]]]],
{i,Length[pernd]}]];

(*taylor plotting*)
contourdiv=0.1;
text111=Graphics[Text[Style["[111]",18(*,Bold*)],{.41,.355}]];
lab111=Graphics[Text[SetPrecision[t111,4],N[stereo1[{1,1,1}]],Background->White]];
text101=Graphics[Text[Style["[101]",18(*,Bold*)],{.40,-0.019}]];
lab101=Graphics[Text[SetPrecision[t110,4],N[stereo1[{1,0,1}]],Background->White]];
text001=Graphics[Text[Style["[001]",18(*,Bold*)],{0.015,-.019}]];
lab001=Graphics[Text[SetPrecision[t001,4],N[stereo1[{0,0,1}]],Background->White]];
pxc=ListContourPlot[Table[{ps[[i,1]],ps[[i,2]],plotfn[[i]]},{i,Length[ps]}],ContourShadin
g->None,ContourStyle->{Black},Contours-
>Table[j,{j,Floor[Min[plotfn],contourdiv],Ceiling[Max[plotfn],contourdiv],contourdiv}],Co
ntourLabels->(Text[#3,{#1,#2},Background->White]&)];

ipole=Show[{pstereo,pxc,lab111,lab101,lab001,text111,text101,text001(*,text*)},PlotRange-
>{{-0.01,0.44},{-0.05,.39}},AspectRatio->.92]

Export["taylorcontcomb.bmp",ipole,ImageResolution-> 600];
Export["dir.txt",dir];
Export["ps.txt",ps];
Export["taylorcomb.txt",taylorcomb];
```

Output inverse pole figure:

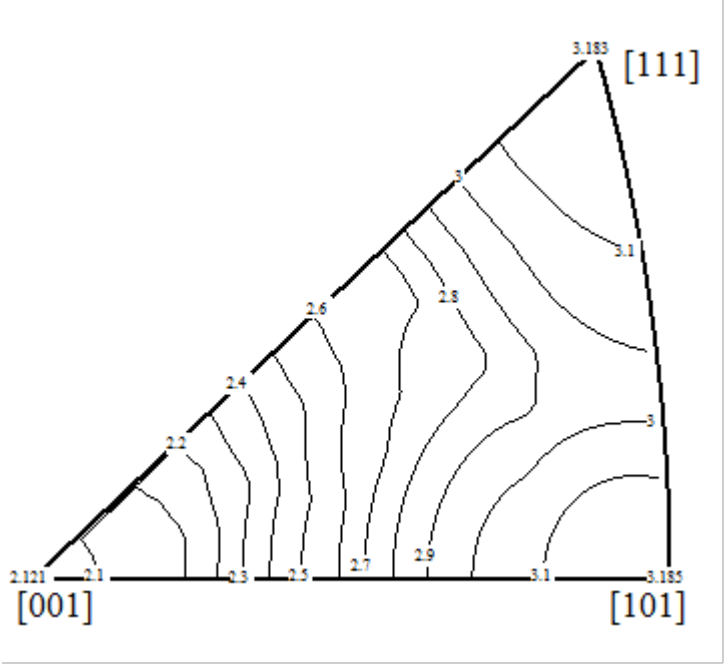

Appendix D: Constant True-Stress Specimen Data Sheets

Mo cs 1 and **Mo cs 2** tests invalid due to improper load control settings.

Mo cs 3

Stress: 30 MPa
Temp: 1650C

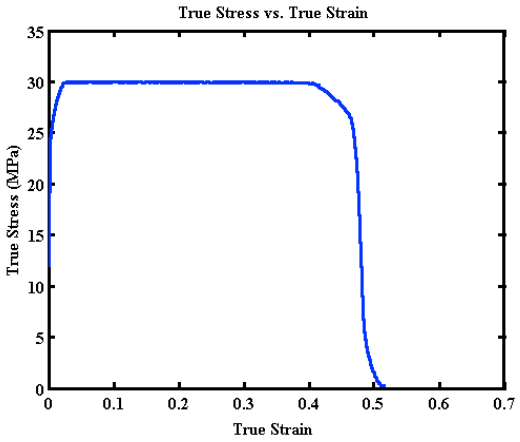

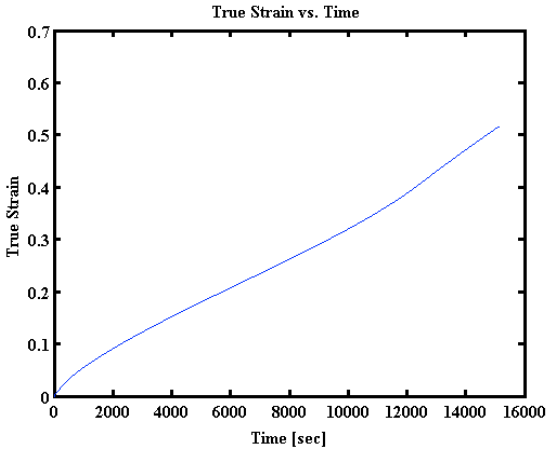

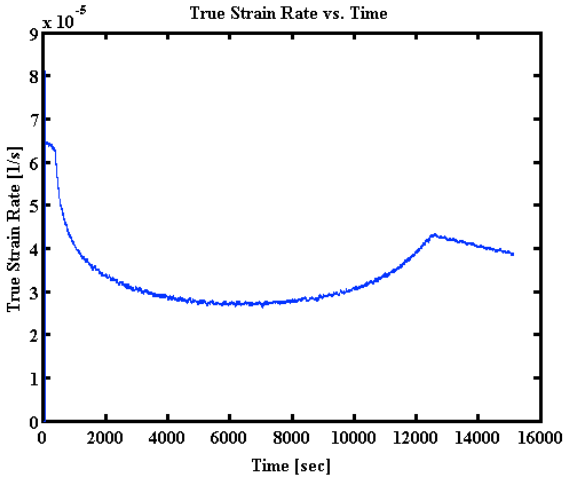

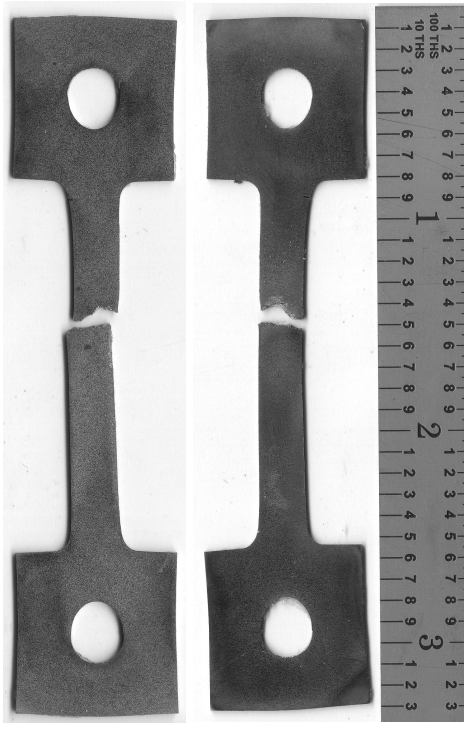

Mo cs 4
Stress: 35 MPa
Temp: 1650C

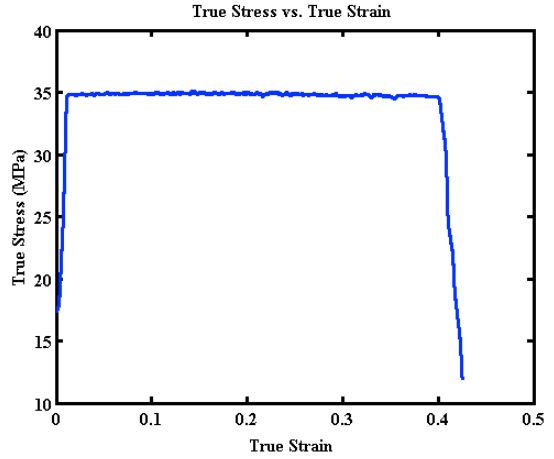

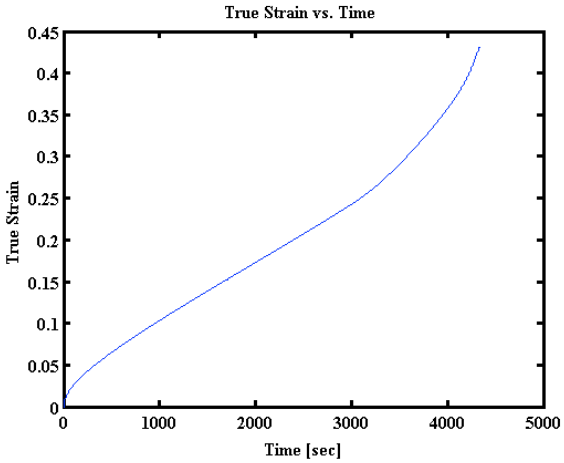

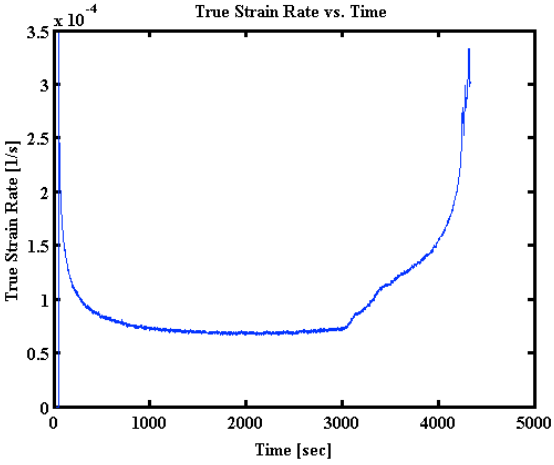

Mo cs 5
Stress: 35 MPa
Temp: 1650C

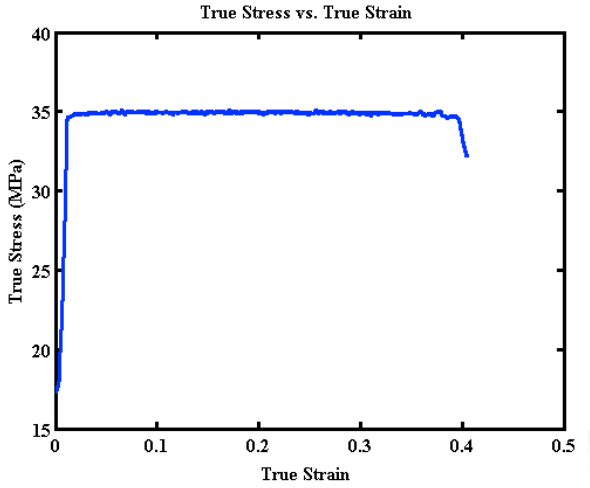

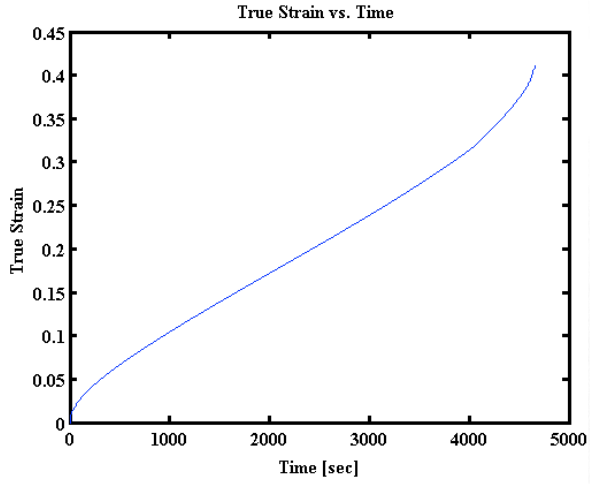

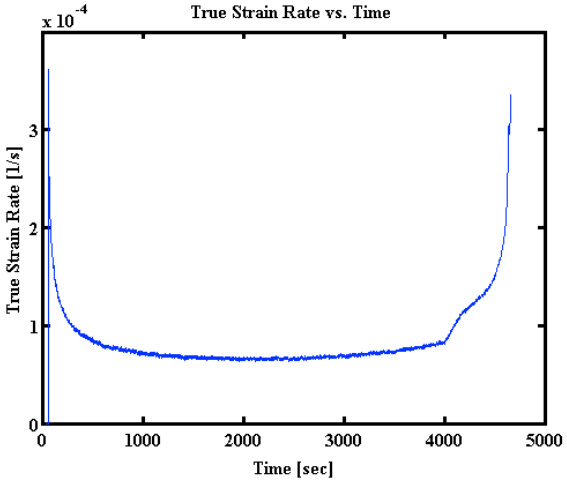

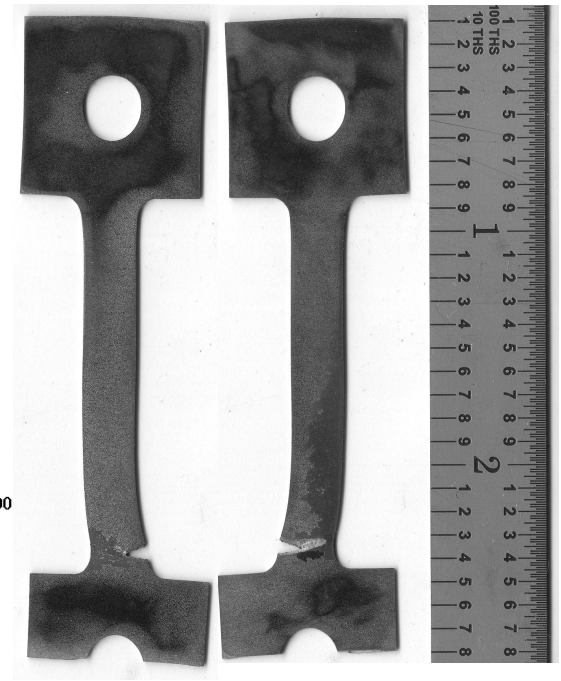

Mo cs 6
Stress: 35 MPa
Temp: 1650C

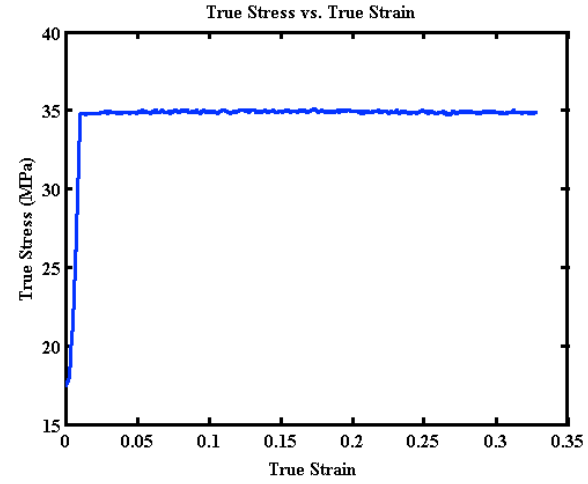

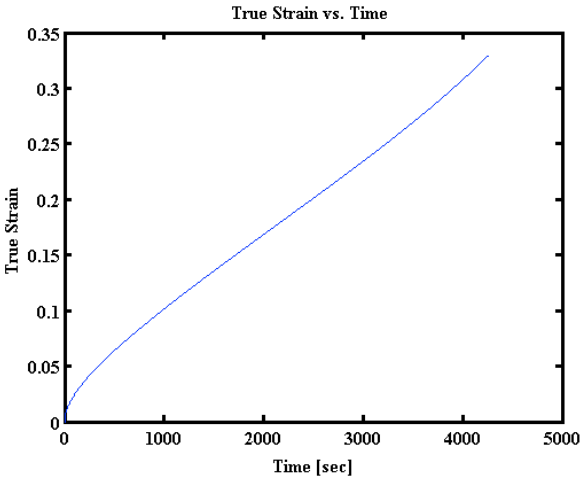

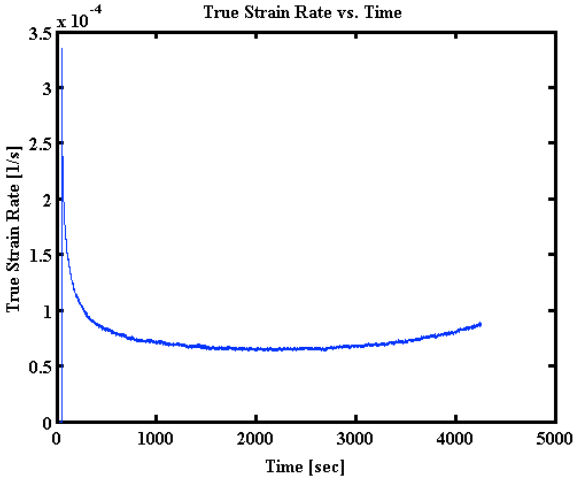

Mo cs 7
Stress: 35 MPa
Temp: 1650C

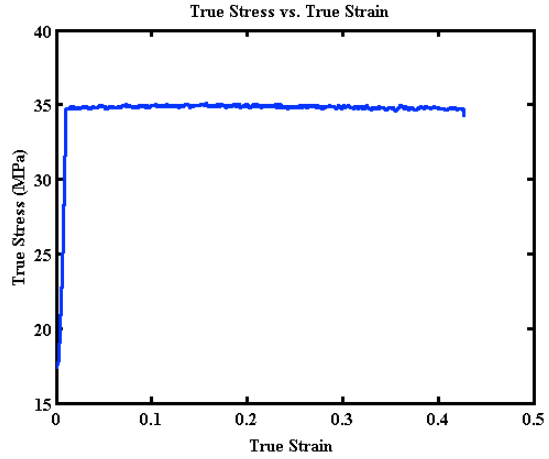

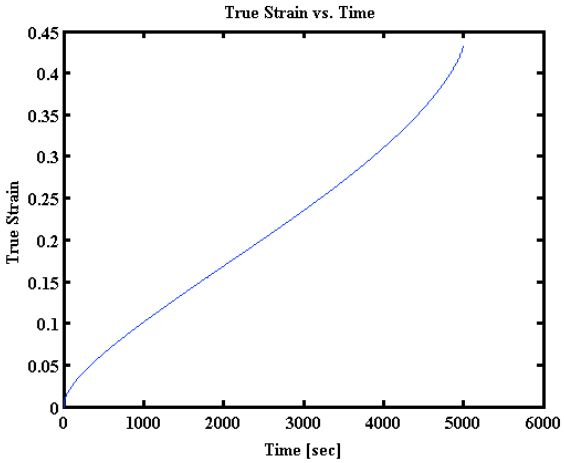

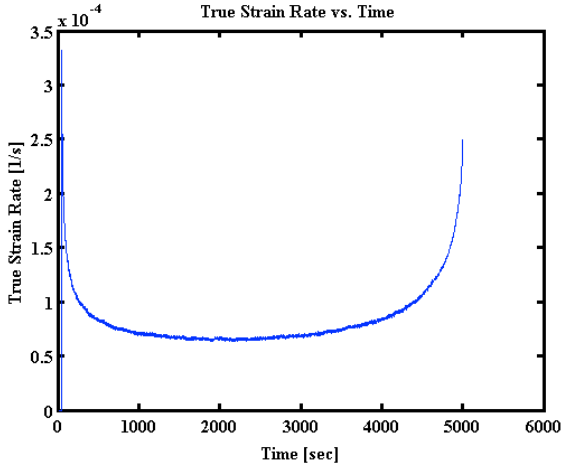

Mo cs 8

Stress: 30 MPa
Temp: 1650C

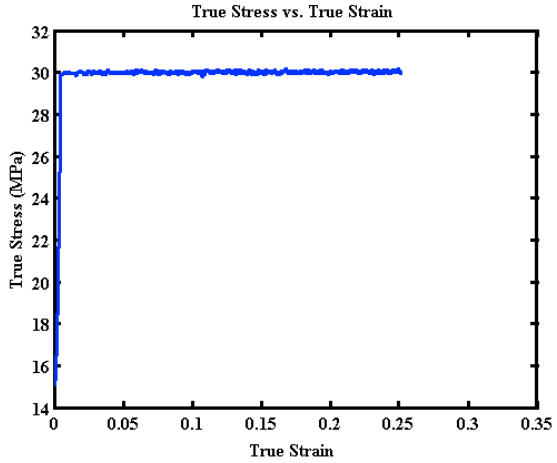

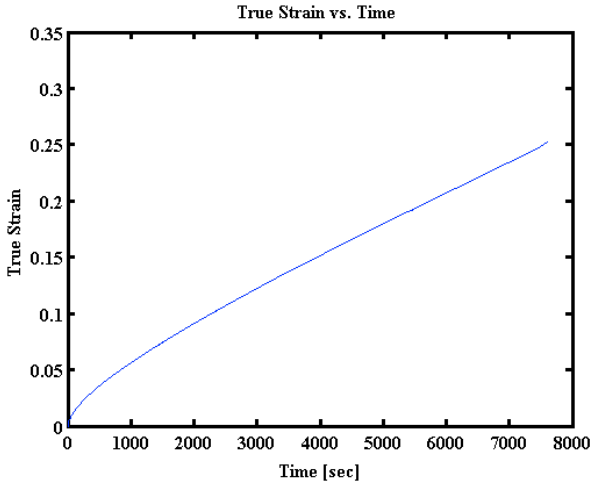

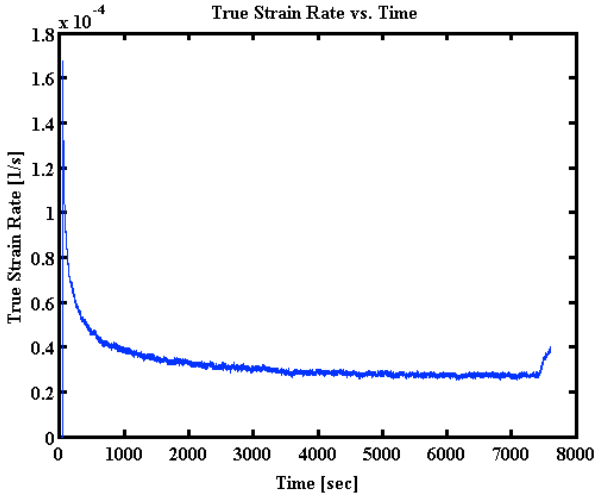

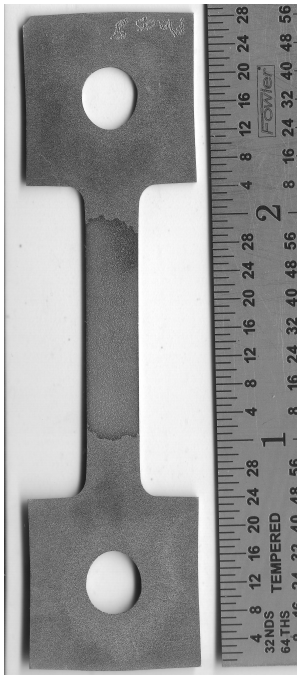

Mo cs 9
Stress: 37 MPa
Temp: 1650C

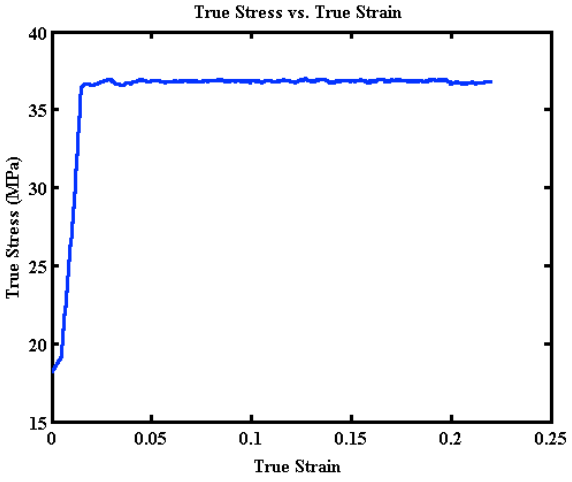

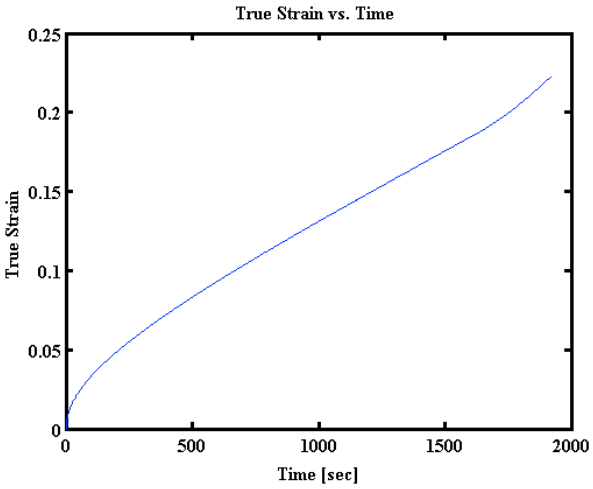

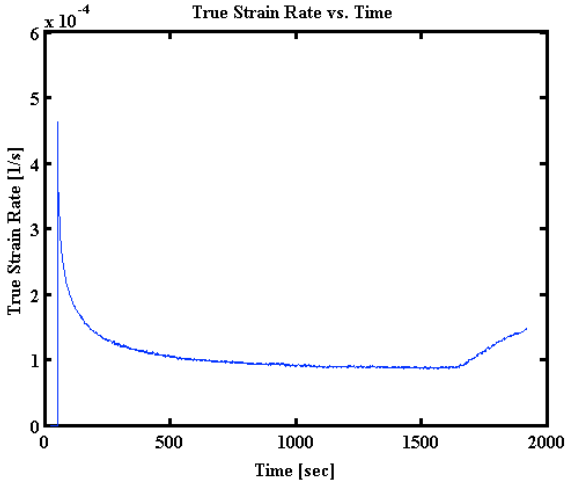

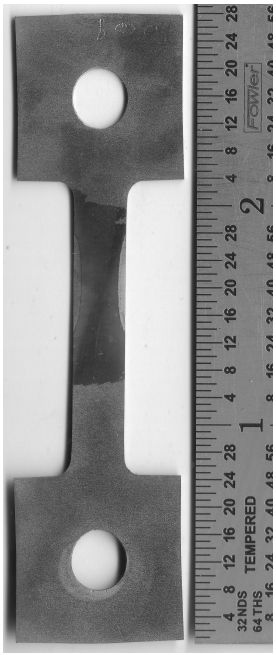

Mocs 10

Stress: 40 MPa
Temp: 1650C

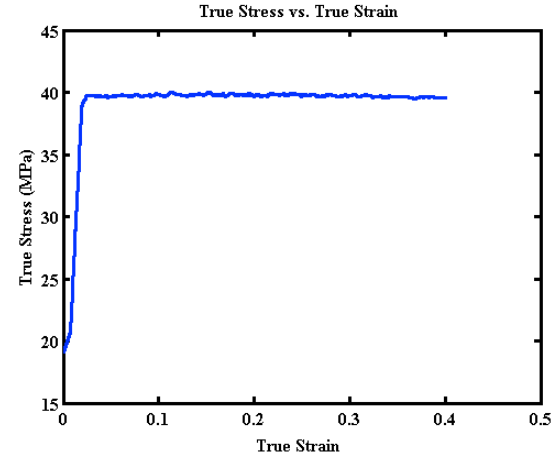

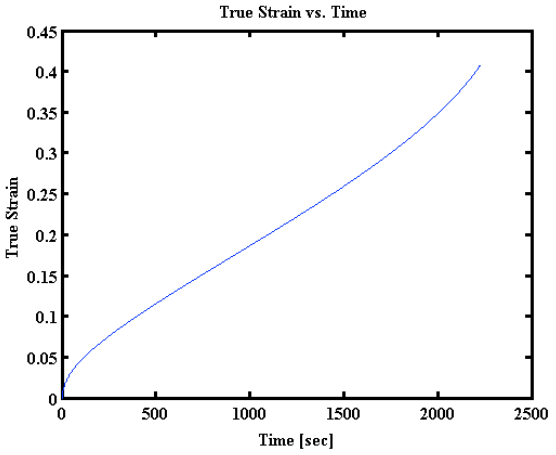

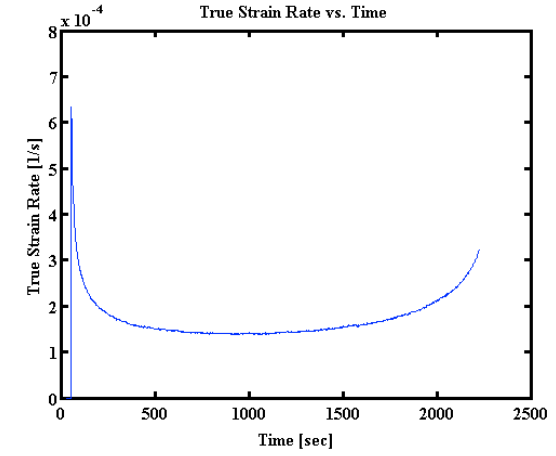

Mo cs 11
Stress: 40 MPa
Temp: 1650C

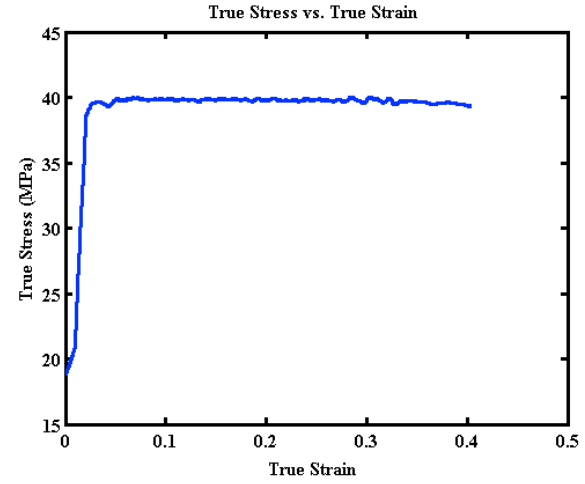

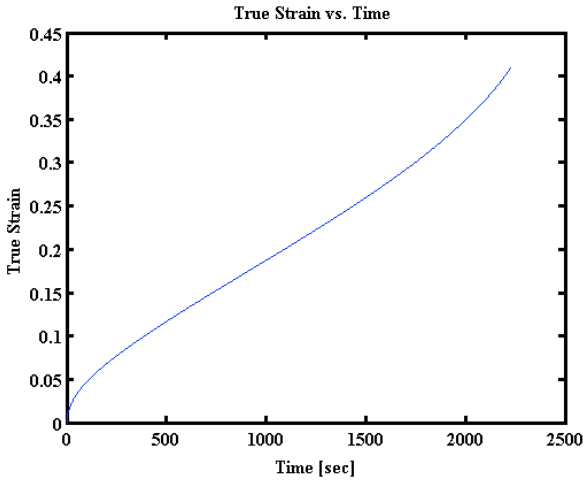

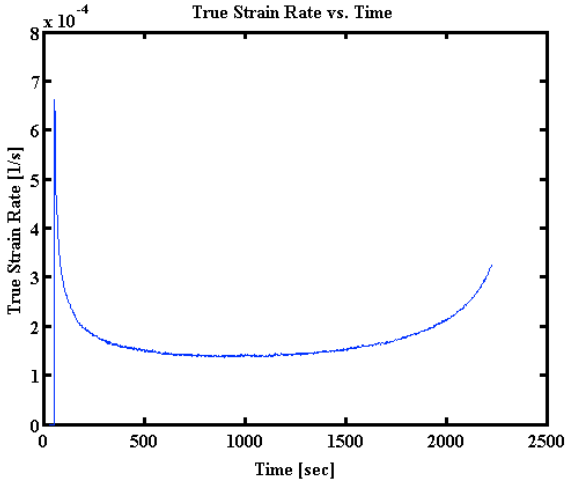

Mo cs 12
Stress: 38.5 MPa
Temp: 1650C

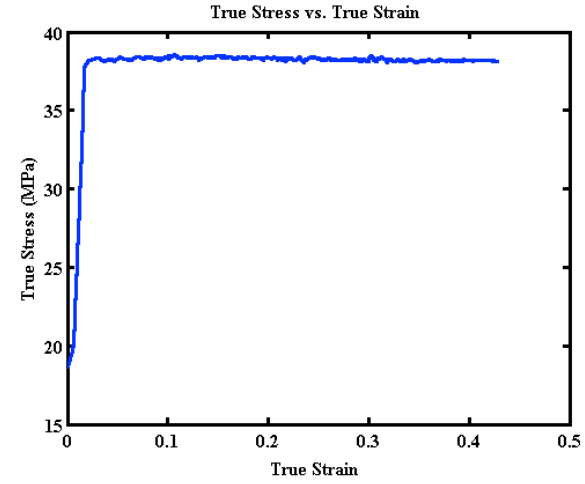

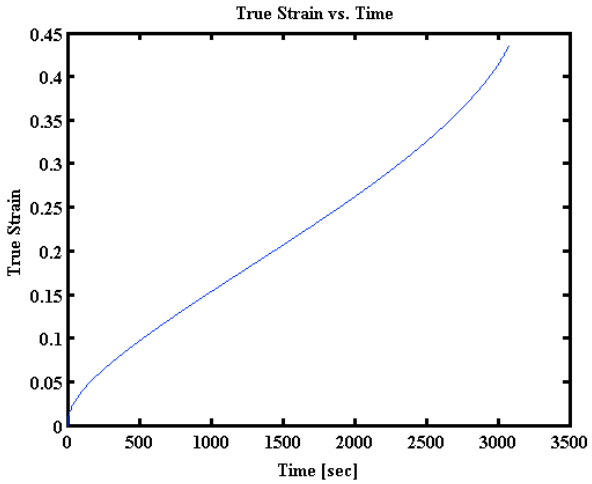

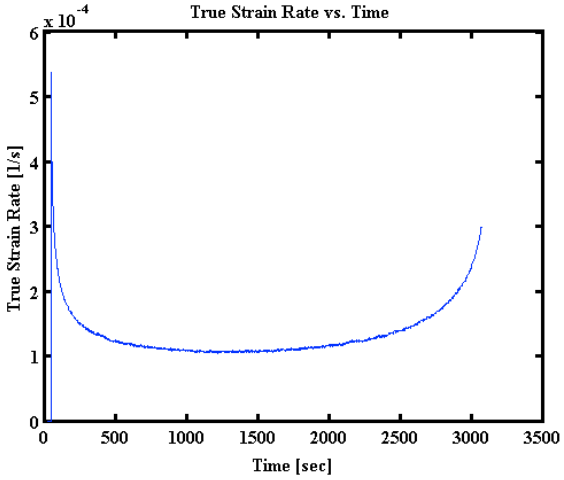

Mo cs 13
Stress: 37 MPa
Temp: 1650C

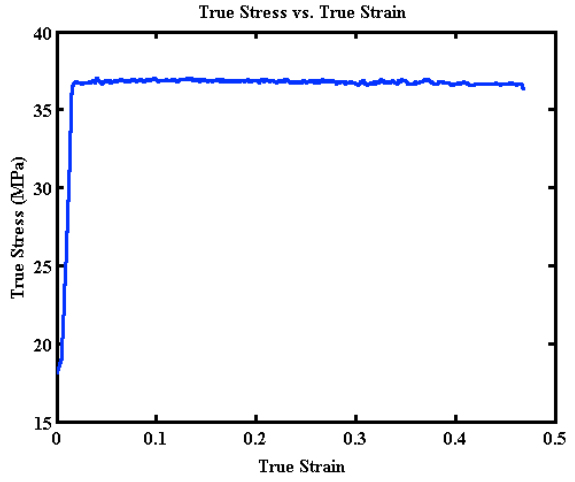

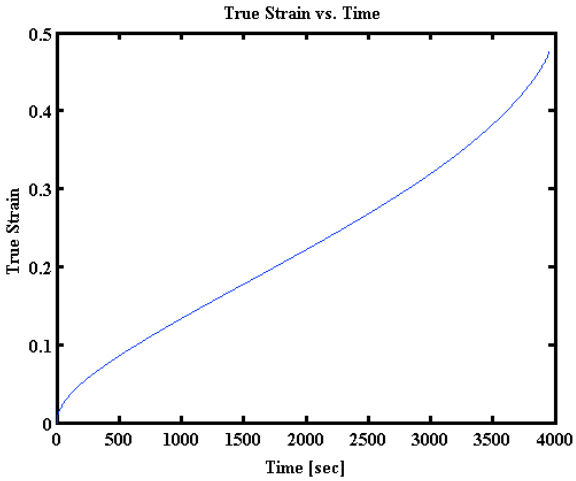

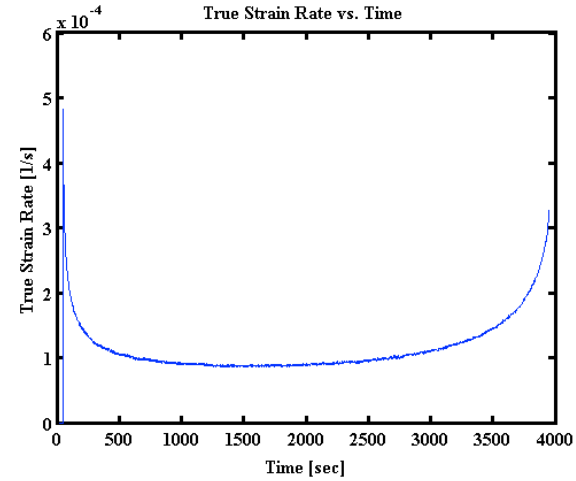

Mo cs 14
Stress: 32 MPa
Temp: 1650C

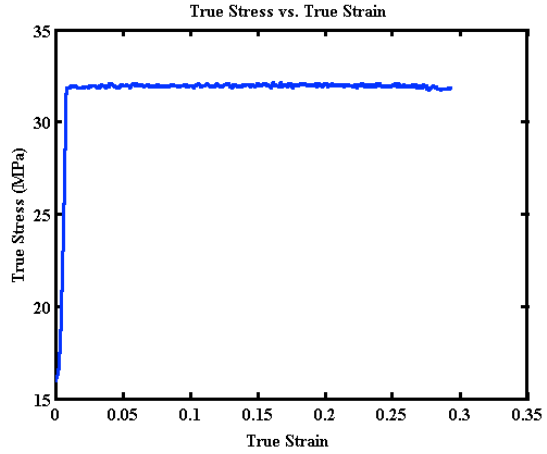

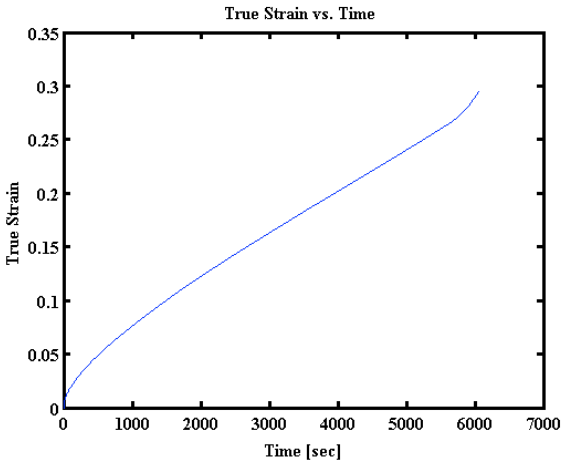

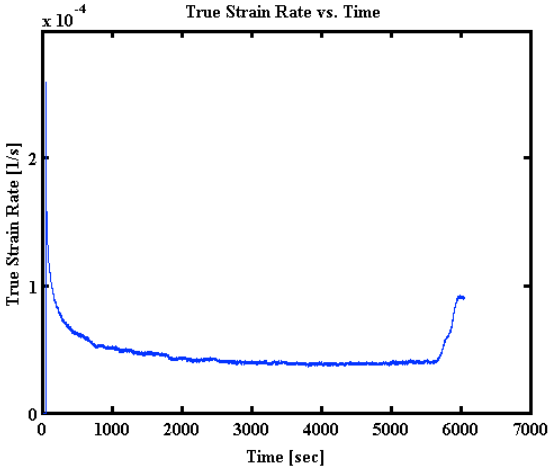

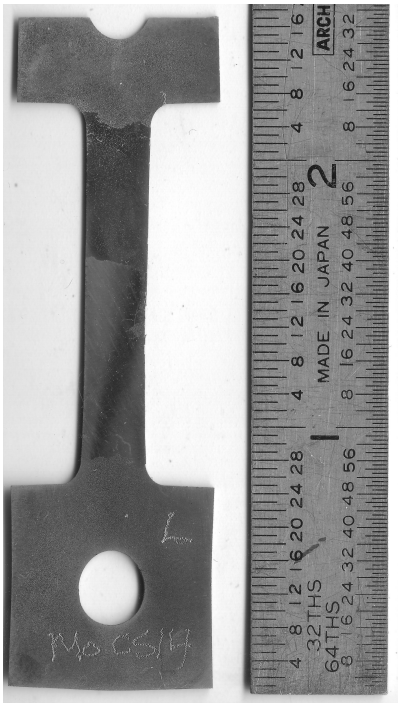

Mo cs 15
Stress: 28 MPa
Temp: 1650C

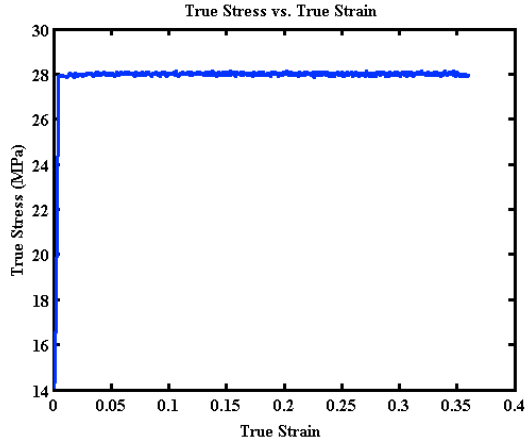

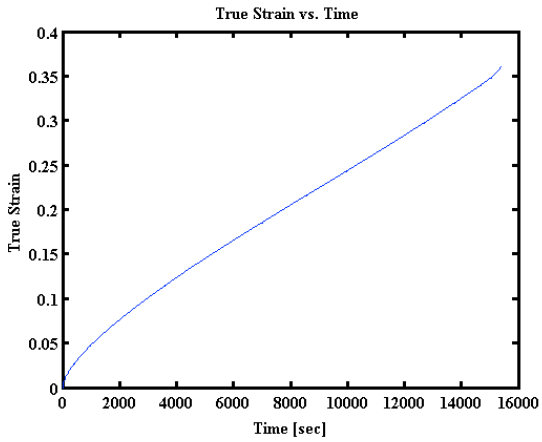

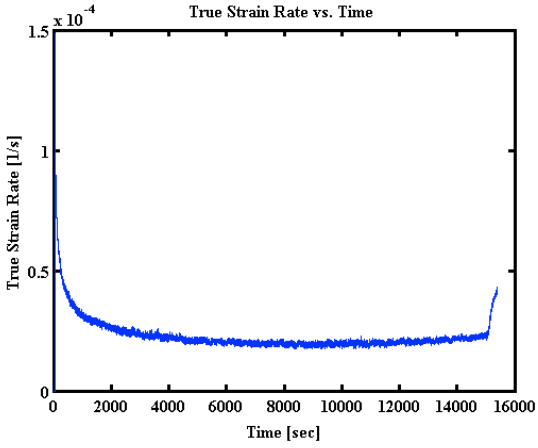

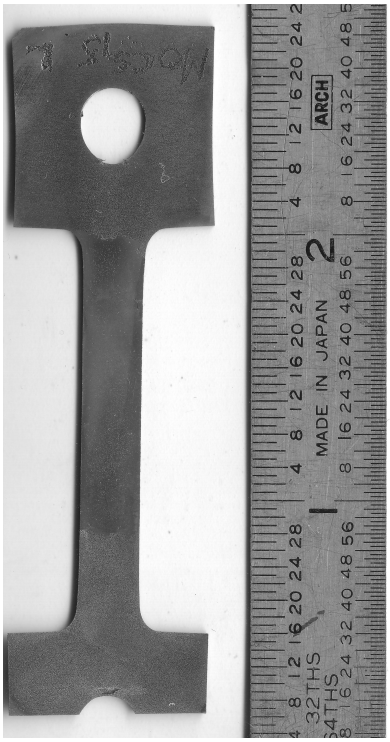

Mo cs 16
Stress: 32 MPa
Temp: 1650C

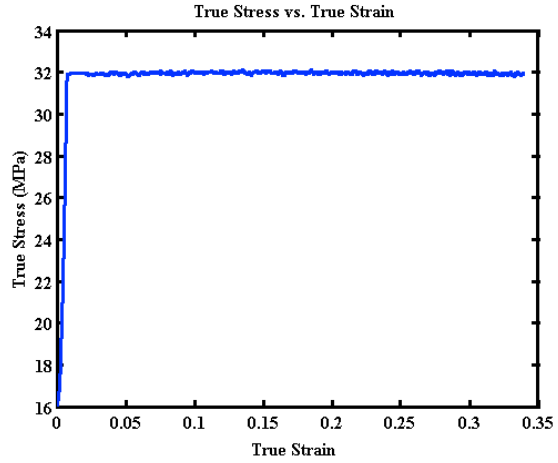

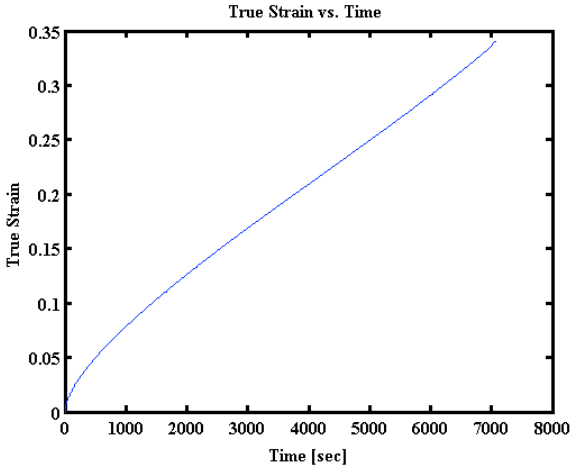

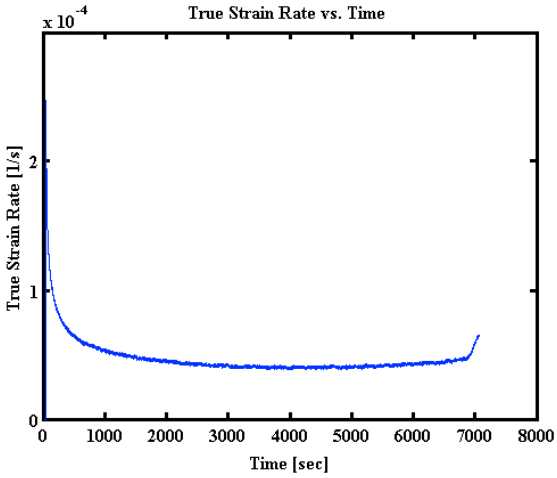

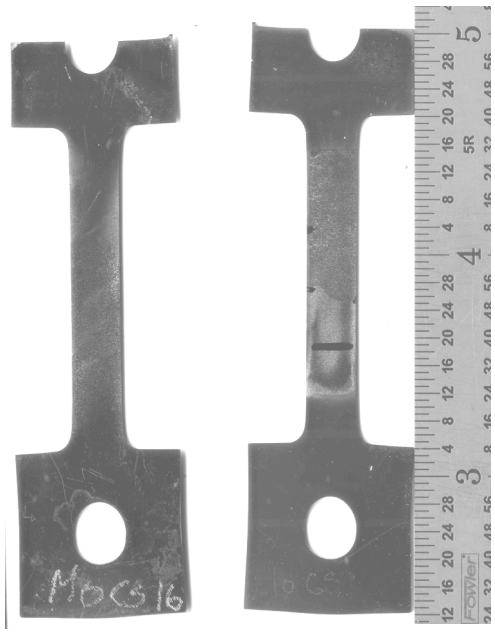

Mo cs 17
Stress: 30 MPa
Temp: 1650C

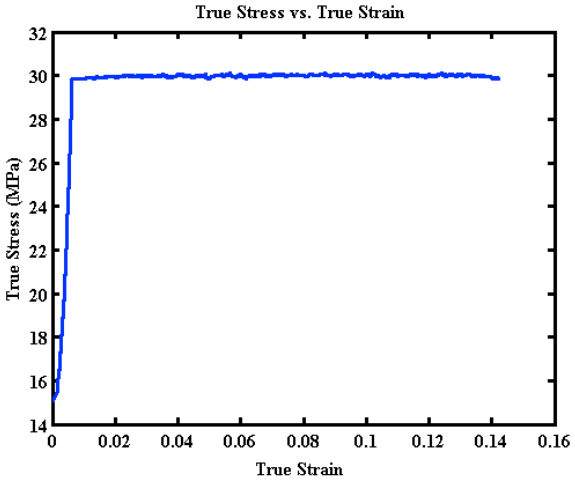

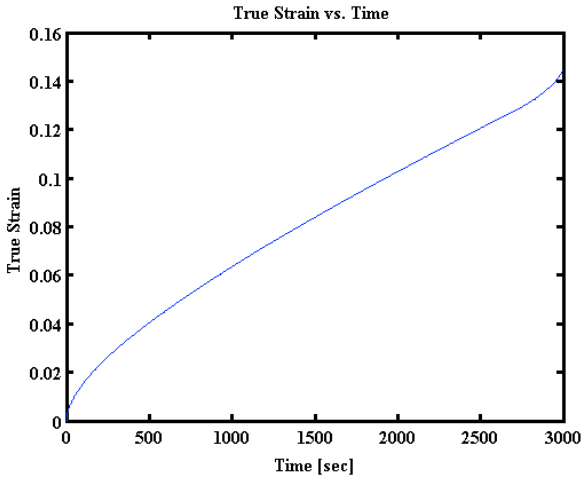

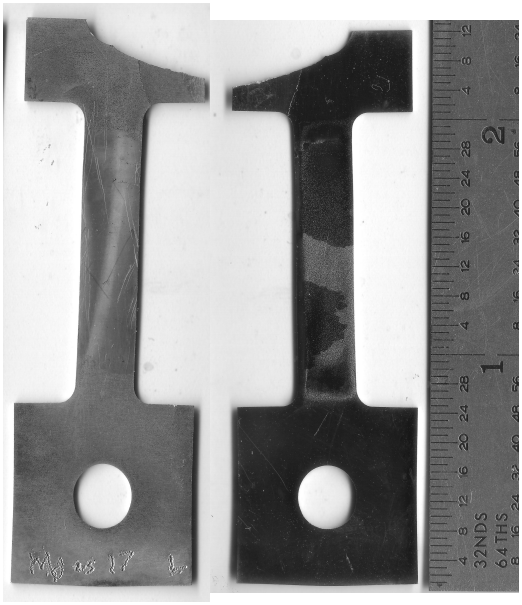

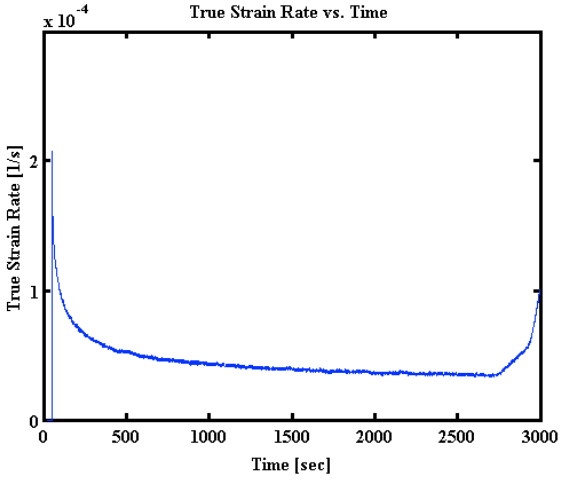

Appendix E: Constant True-Strain Rate Specimen Data Sheets for Ta-A

Ta 1

Temperature: 1850 °C

Strain rate: 1×10^{-4}

Preload: 4.0 lb

DAGG observed: Yes

Notes: Some temperature fluctuation occurred in steady-state just prior to DAGG drop.

1 large DAGG grain, ~39mm

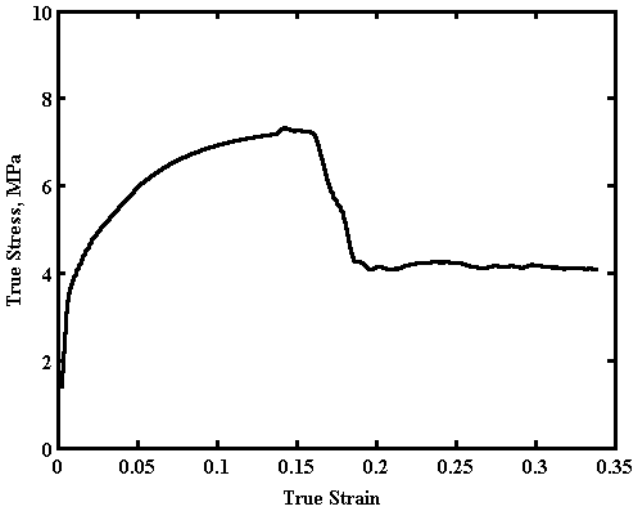

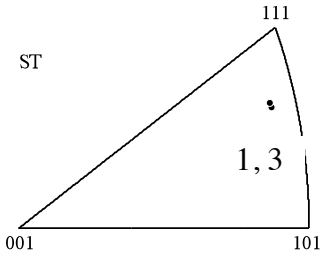

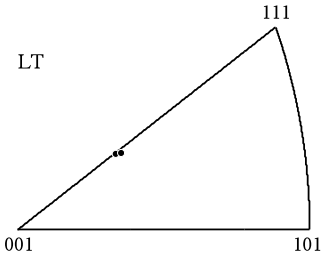

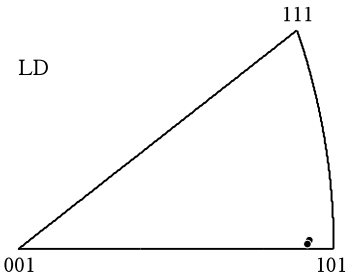

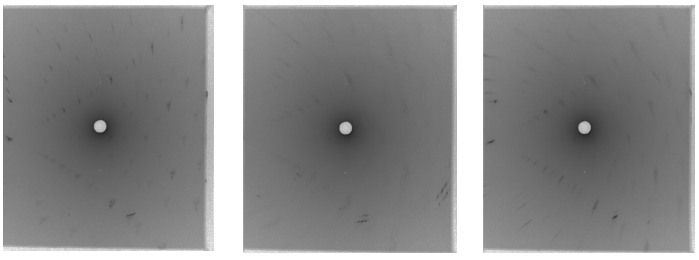

1 2 3

Ta 2

Temperature: 1850 °C

Strain rate: 1×10^{-4}

Preload: 0 lbs

DAGG observed: Yes

Notes: Significant temperature variation upon initial straining. Excessive slack cause by zero preload.

Smoothed true stress vs. true strain

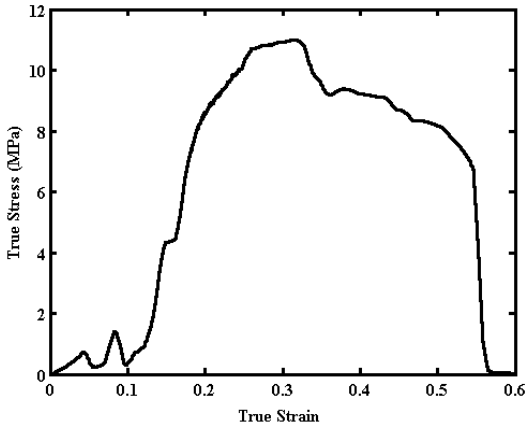

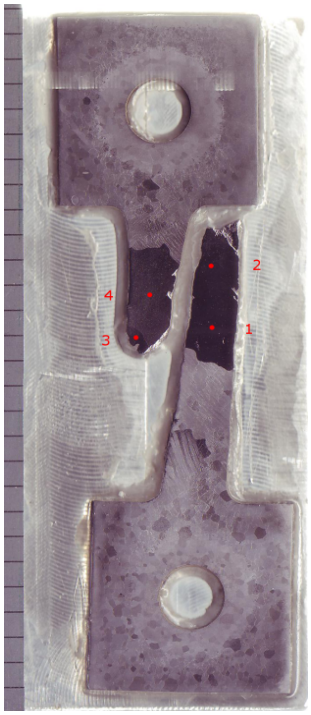

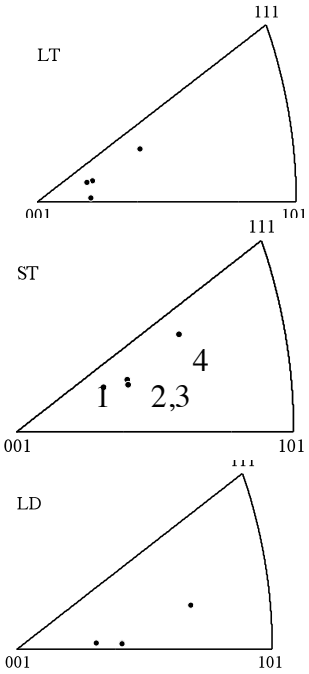

True stress vs. true strain (original)

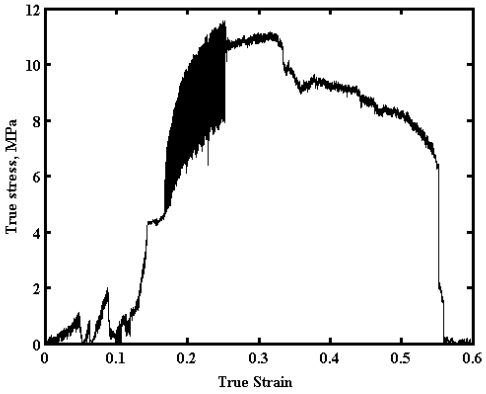

due to temperature control fluctuation.

Ta 3

Temperature: 1850 °C

Strain rate: 1×10^{-4}

Preload: 1 lbs

DAGG observed: Yes

Notes: 2 grains of ~5mm. DAGG start and stop is not clear from true stress vs. true strain data.

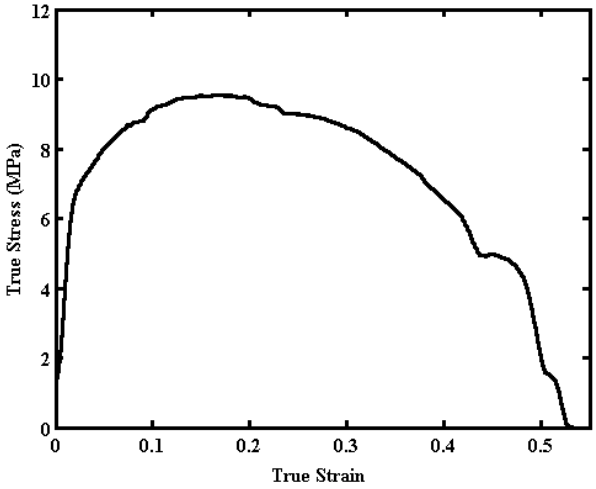

Ta 4

Temperature: 1850 °C

Strain rate: 1×10^{-4}

Preload: 1 lbs

DAGG observed: Yes

Notes: Test data lost. 2 large DAGG grains formed with similar orientations.

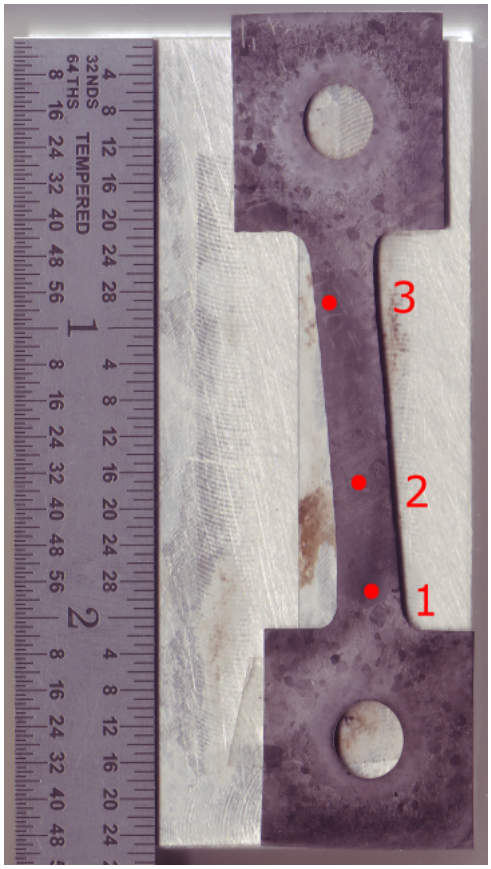

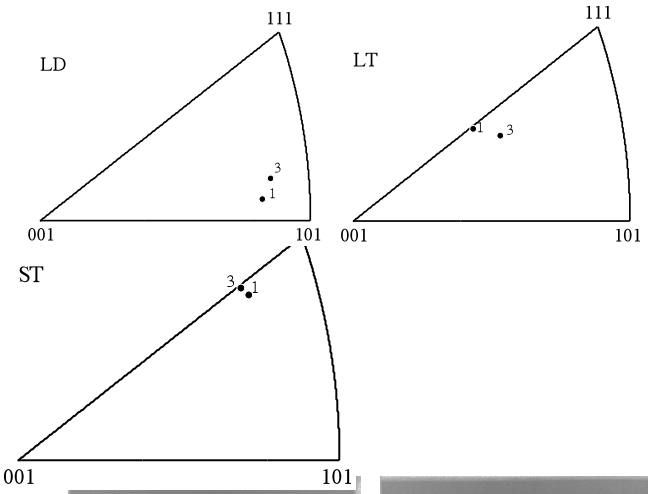

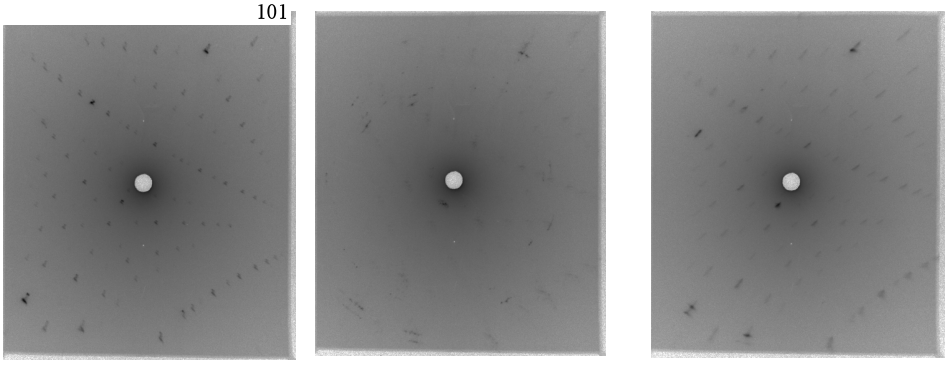

1 2 3

Ta 5

Temperature: 1850 °C

Strain rate: 1.1×10^{-4}

Preload: 2 lbs

DAGG observed: Yes

Notes: Test data incomplete. One large DAGG grain found.

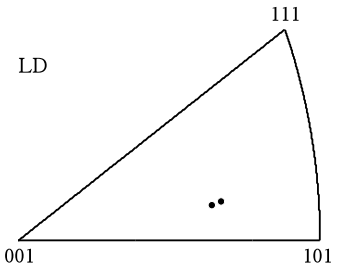

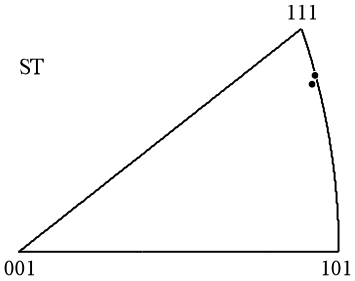

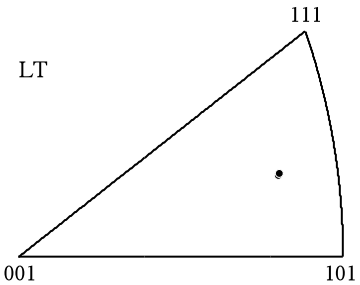

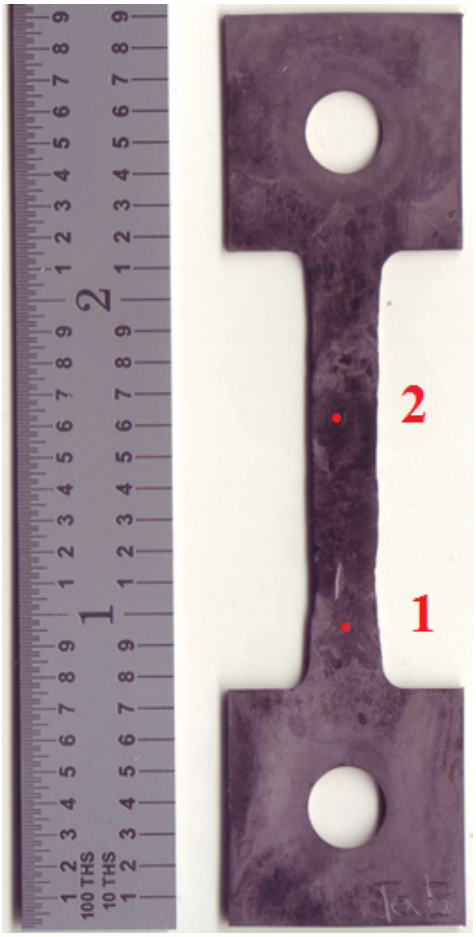

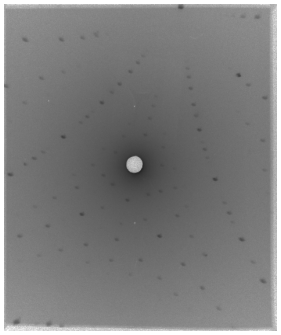

1

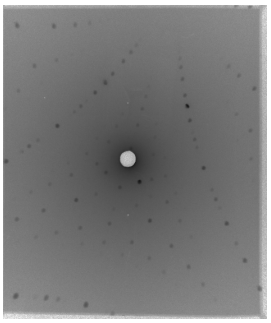

2

Ta 6

Temperature: 1850 °C

Strain rate: 1×10^{-4}

Preload: 2 lbs

DAGG observed: Yes

Notes: 2 DAGG grains ~14, 10mm, with significant shear banding.

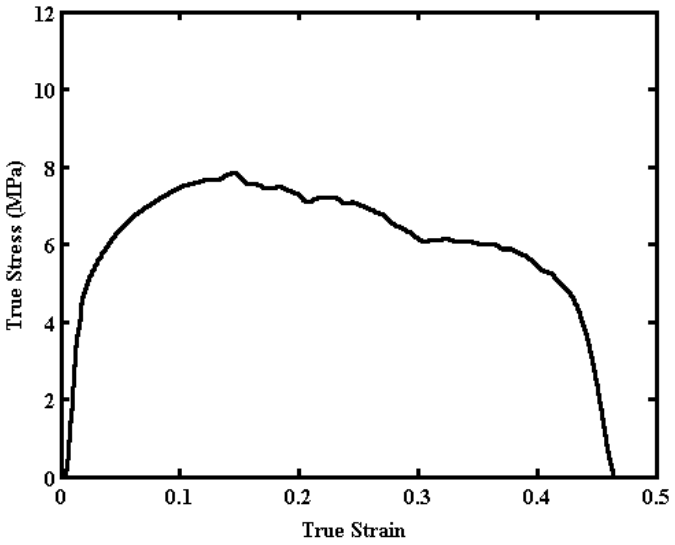

Ta 7

Temperature: 1750 °C

Strain rate: 1×10^{-4}

Preload: 4 lbs

DAGG observed: Yes

Notes: 2-3 DAGG grains observed

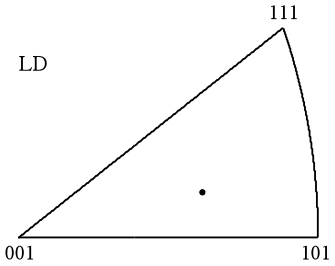

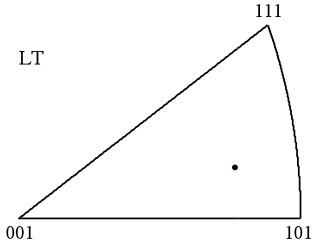

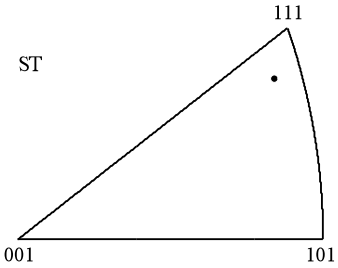

1

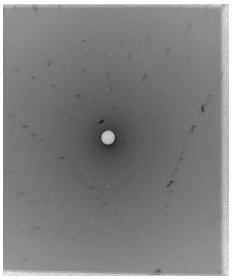

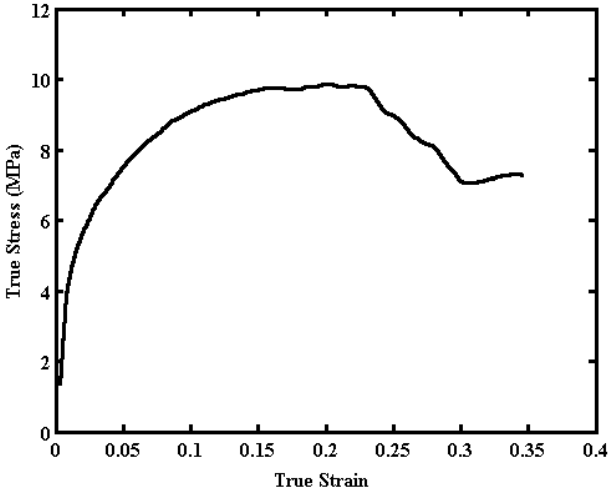

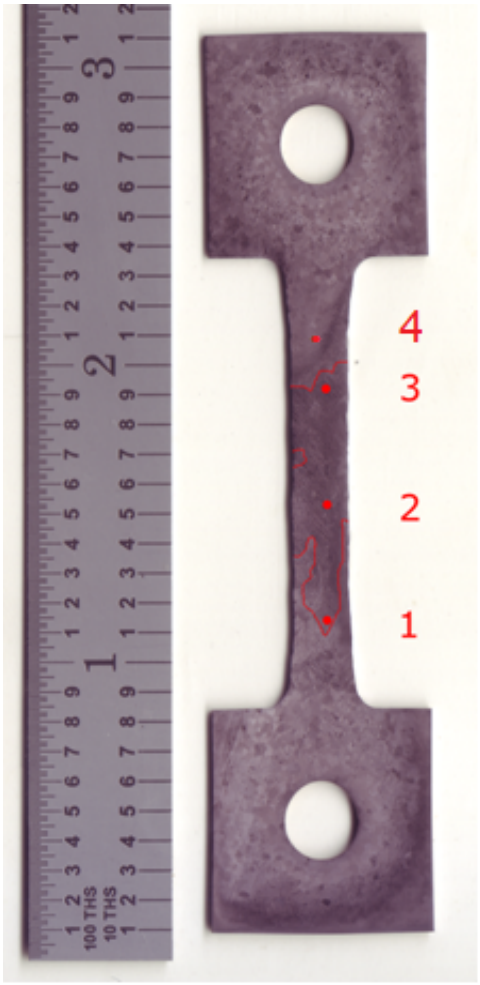

Ta 8

Temperature: 1800 °C

Strain rate: 1.0×10^{-4}

Preload: 4 lbs

DAGG observed: Yes, 2 DAGG grains

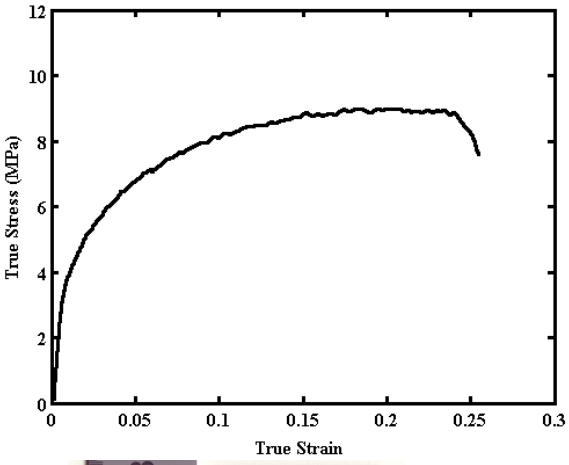

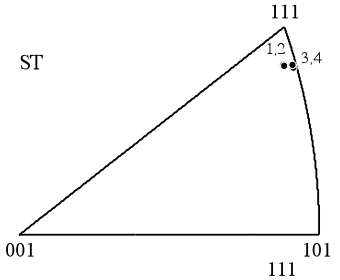

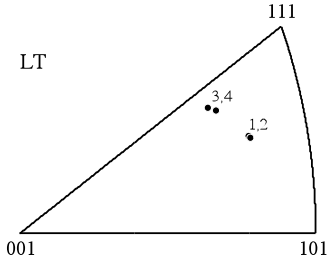

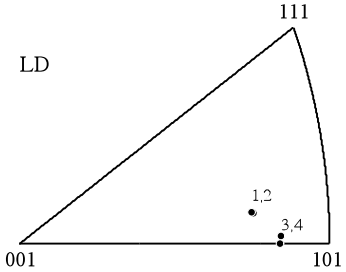

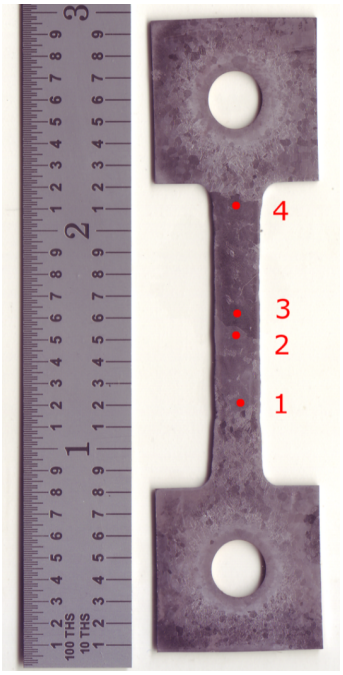

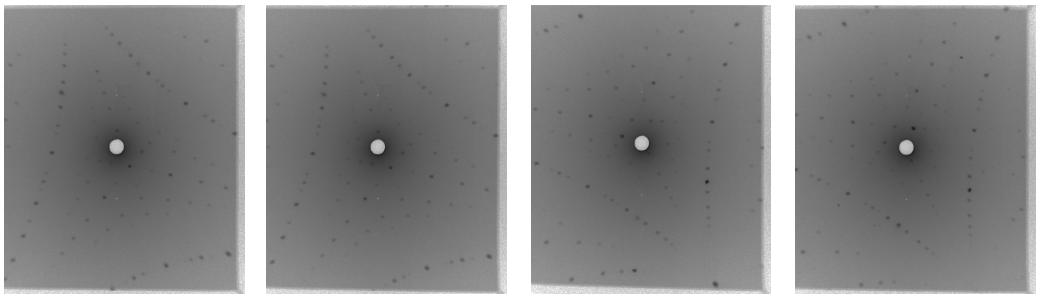

1 2 3 4

Ta 9

Temperature: 1850 °C

Strain rate: 1 $\times 10^{-4}$

Preload: 4 lbs

DAGG observed: Not shown in test data, observed in microsctucture

Notes: 6 DAGG grains ~4mm avg, none at least 10 mm

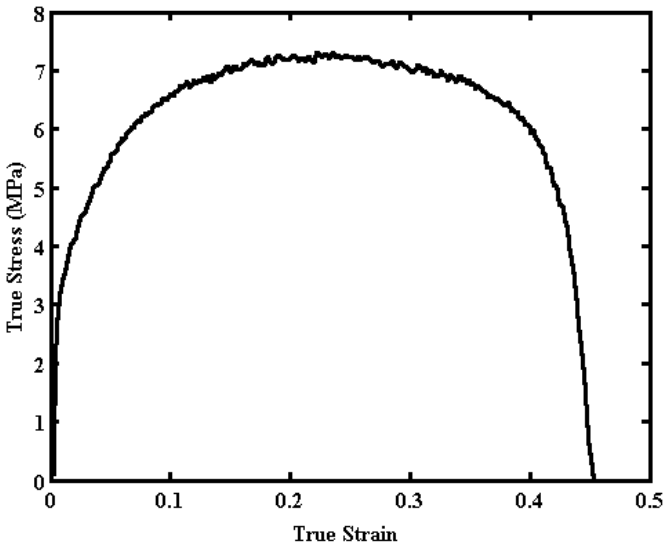

Ta 10

Temperature: 1750 °C

Strain rate: 0.8×10^{-4}

Preload: 4 lbs

DAGG observed: Yes

Notes: At least 1 DAGG grain. Test stopped just after load drop from DAGG, so grain did not continue growing.

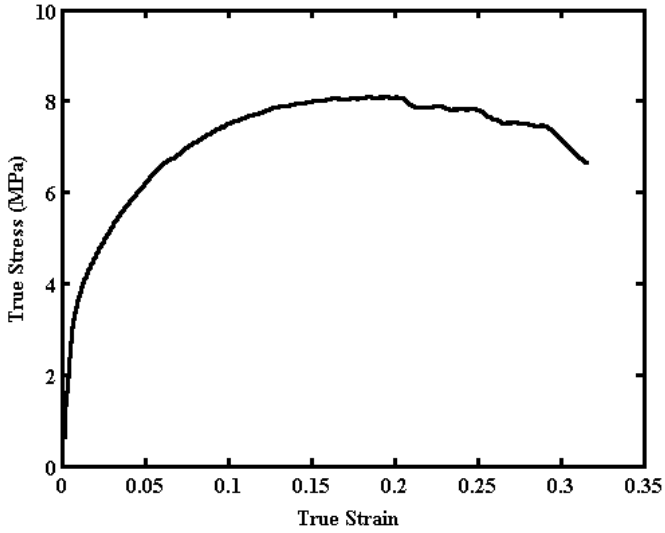

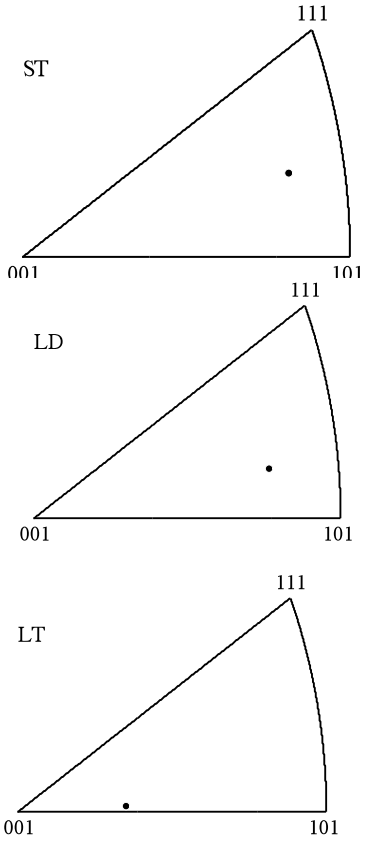

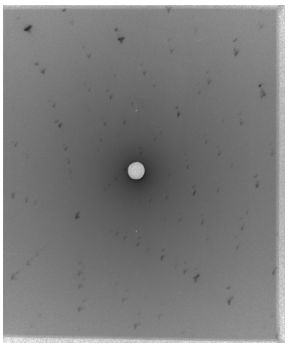

Ta 11

Temperature:	1650 °C
Strain rate:	1 $\times 10^{-4}$
Preload:	4 lbs
DAGG observed:	Yes

Notes: Computer error at end of heatup. Initial load lost.
2 DAGG grains of ~3 mm. Test stopped just after DAGG drop. No grains over 10 mm observed.

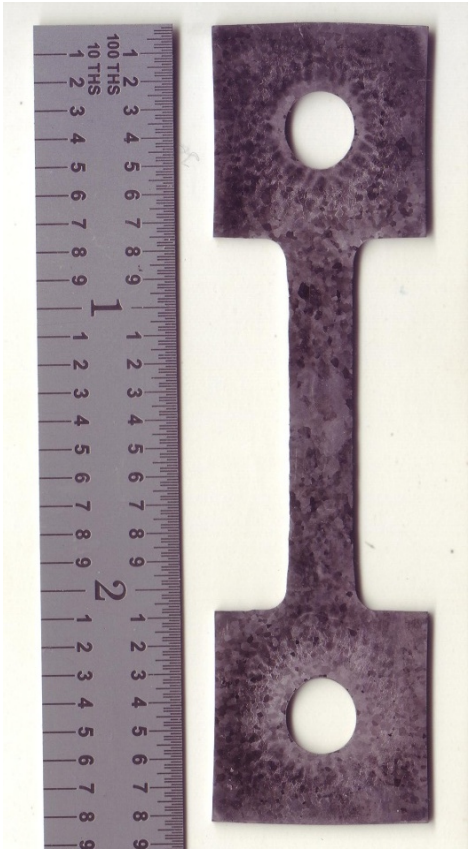

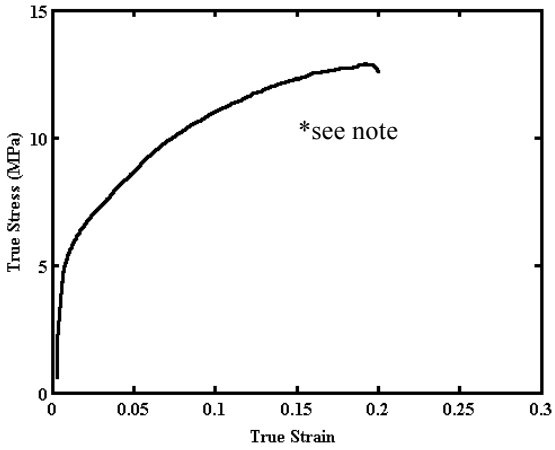

*Stress values unreliable due to computer crash and loss of load value at start of test. Data is plotting with assumption that load on specimen was same as heatup load. Initial position known from separate record, thus true strain is correct.

Ta 12

Temperature: 1550 °C

Strain rate: 1×10^{-4}

Preload: 4 lbs

DAGG observed: Yes

Notes: 7 DAGG grains ~3 mm avg. No grains over 10 mm observed.

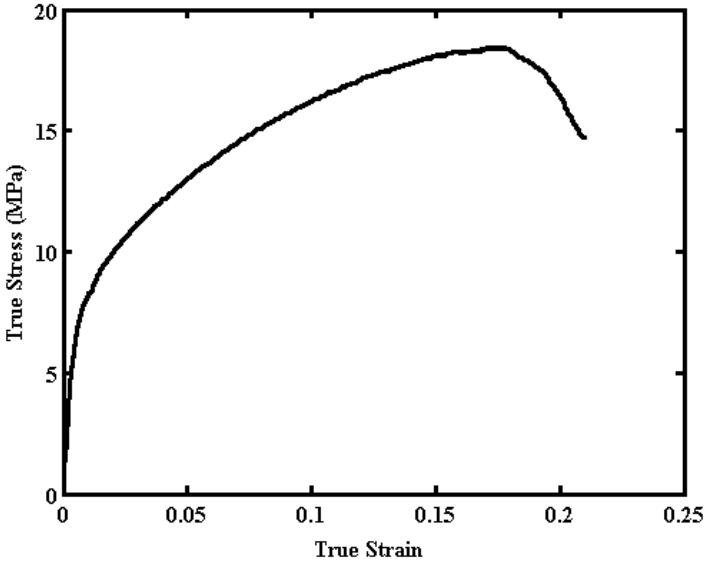

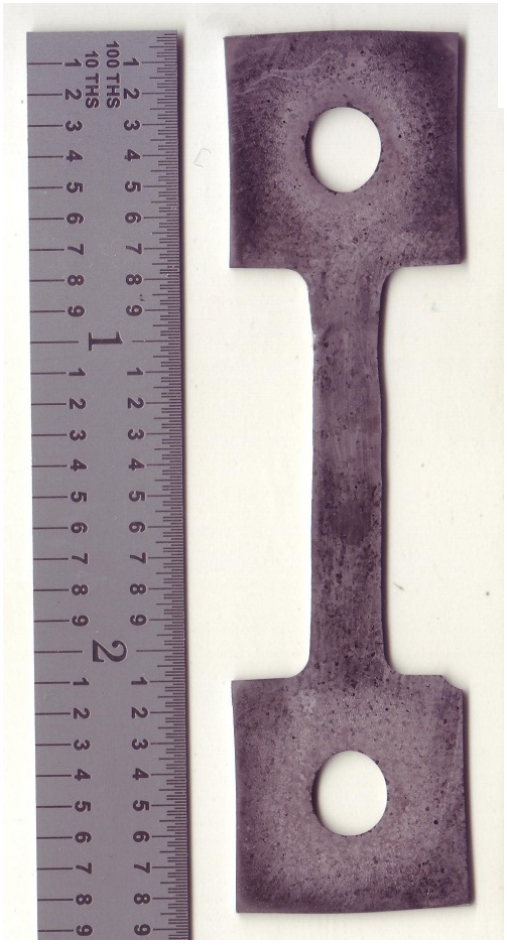

Ta 14

Temperature: 1850 °C

Strain rate: 5 $\times 10^{-4}$

Preload: 4 lbs

DAGG observed: Yes

Notes: Fast heatup (700s). Many DAGG grains, ~6 over 2mm, largest ~11 mm.

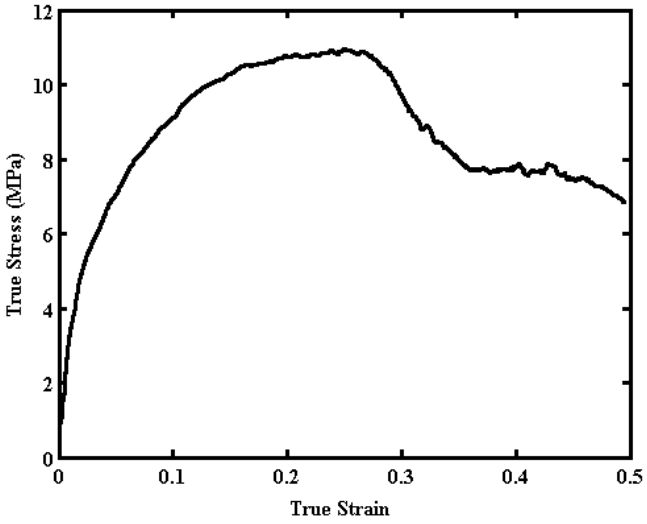

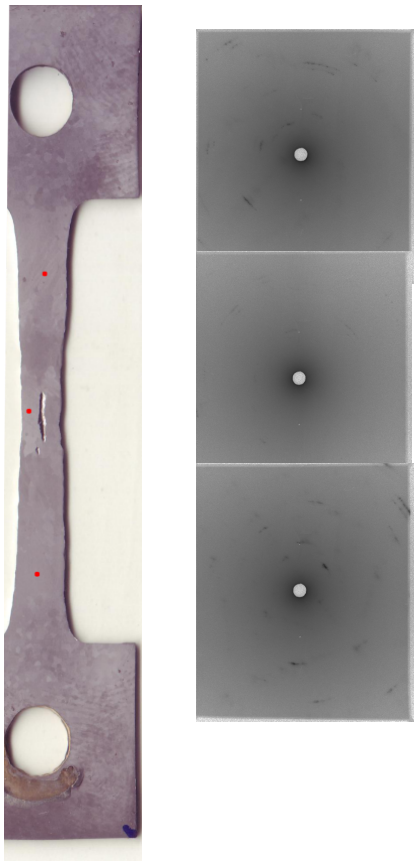

Ta 15

Temperature: 1850 °C

Strain rate: 3 $\times 10^{-4}$

Preload: 4 lbs

DAGG observed: Yes

Notes: Fast heat-up (700s), ~4 DAGG grains over 2 mm, largest ~8 mm.

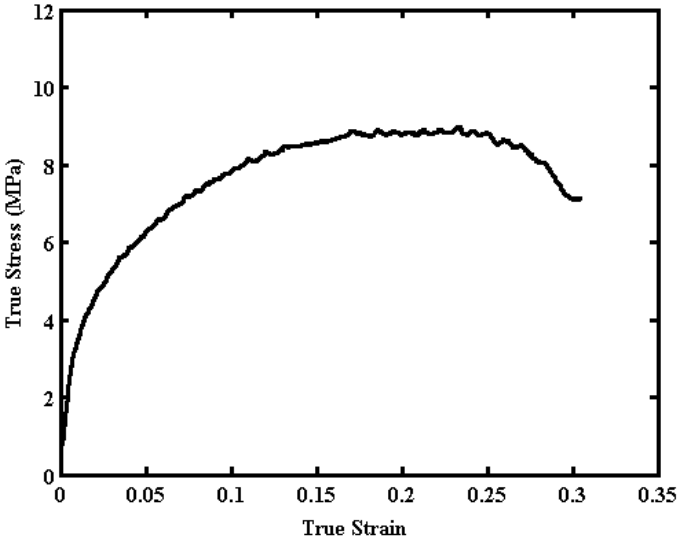

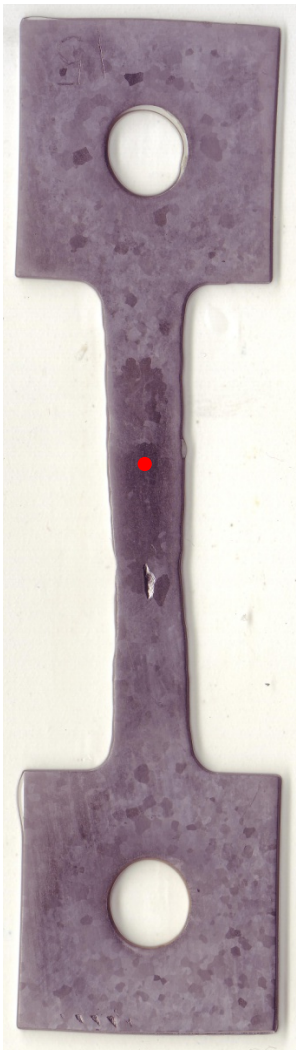

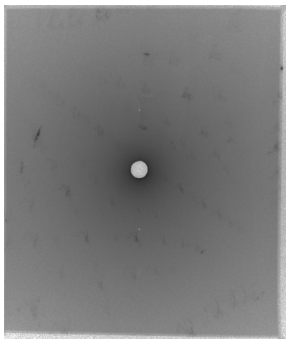

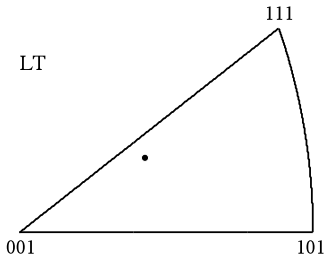

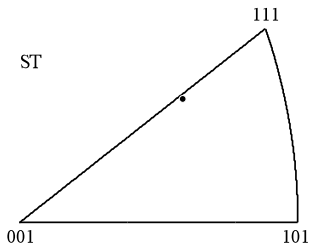

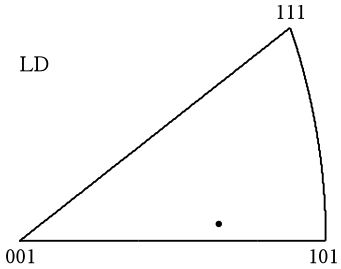

Ta 16

Temperature: 1850 °C

Strain rate: 2×10^{-4}

Preload: 5 lbs

DAGG observed: Yes

Notes: Fast heatup (700s), 3 DAGG grains, largest ~ 9 mm.

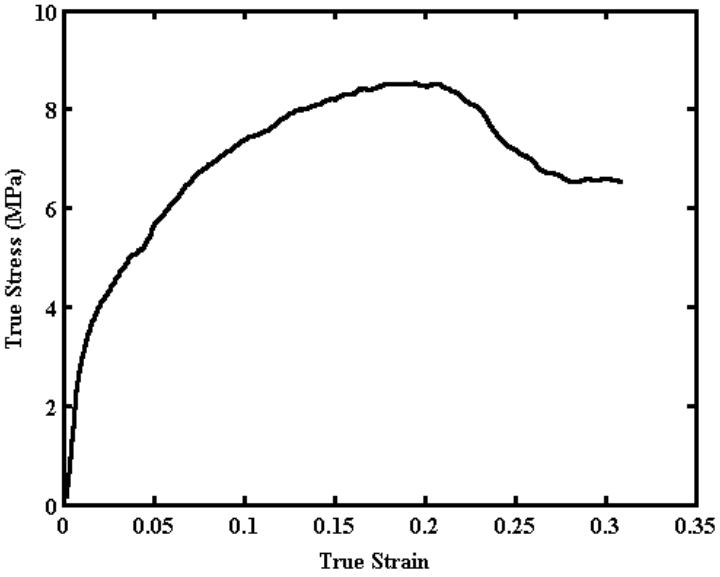

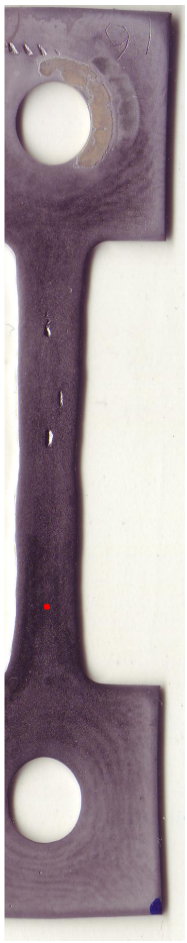

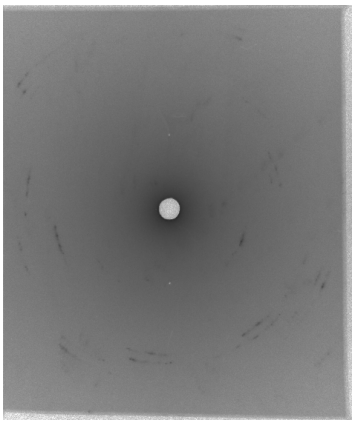

Ta 17

Temperature: 1850 °C

Strain rate: 2 $\times 10^{-4}$

Preload: 4 lbs

DAGG observed: Yes

Notes: 30 min heatup. 3 DAGG grains, largest ~10 mm.

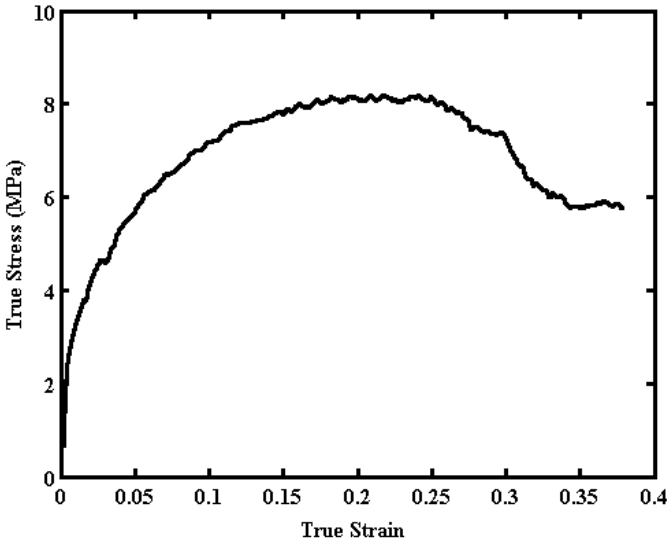

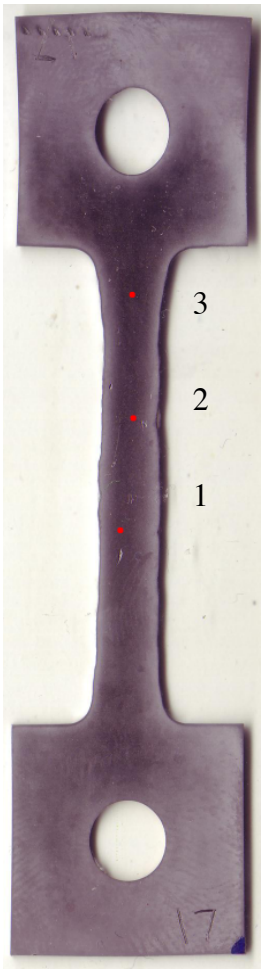

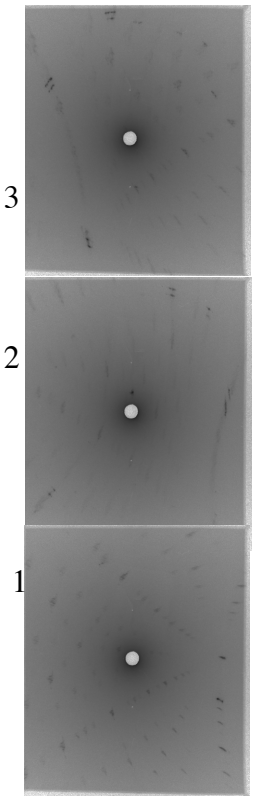

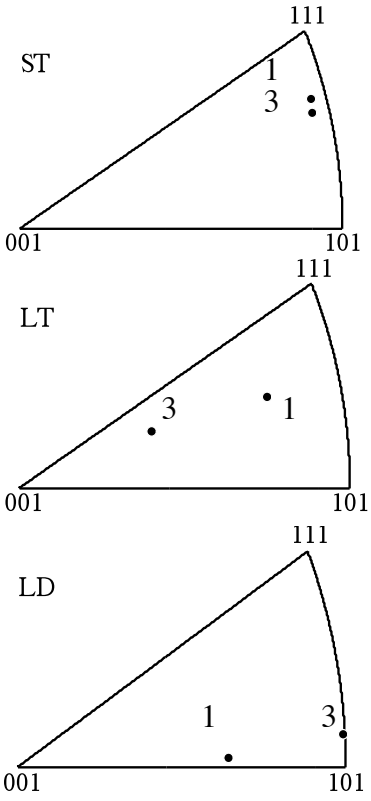

Ta 18

Temperature:	1650 °C
Strain rate:	5 $\times 10^{-5}$
Preload:	5 lbs
DAGG observed:	Yes

Notes: 1200s heatup, 3 DAGG grains, largest ~12 mm.

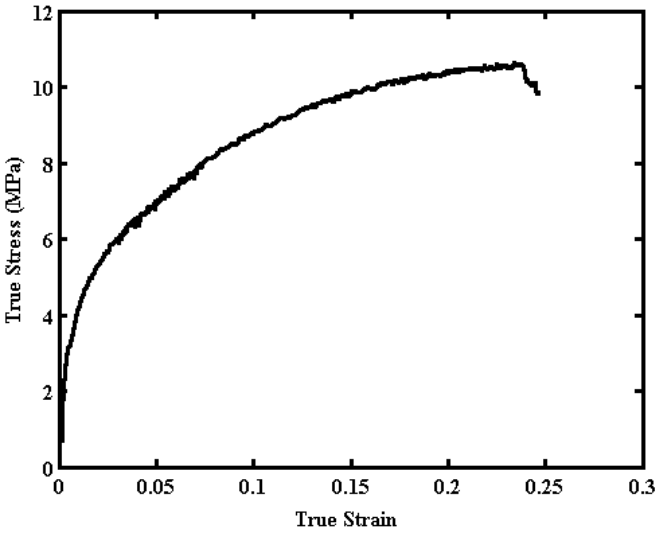

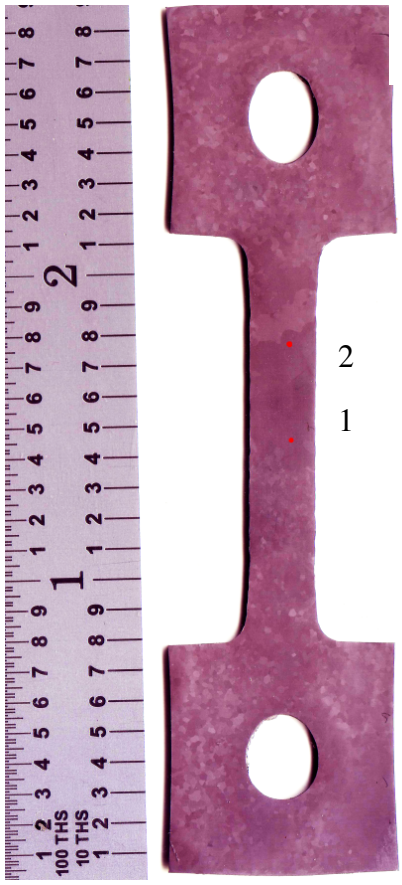

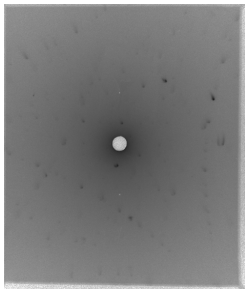

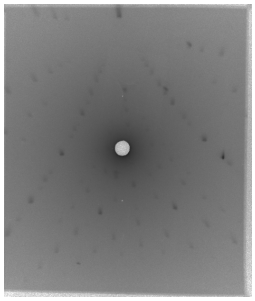

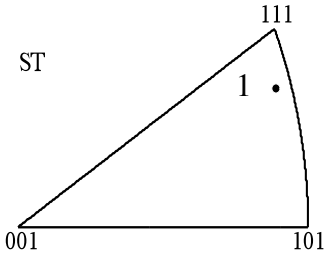

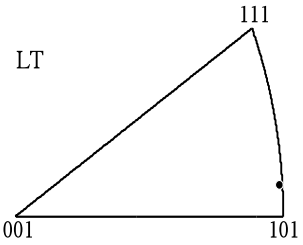

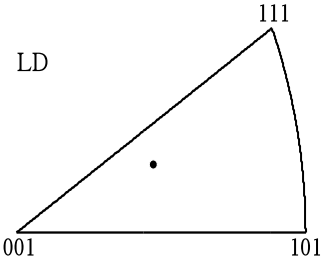

Ta 19

Temperature:	1650 °C
Strain rate:	3 $\times 10^{-5}$
Preload:	5 lbs
DAGG observed:	Yes

Notes: 2500s heatup, 1 DAGG grain ~24 mm.
Thermocouple problems likely increased temperature of test, thus decreasing flow stress on specimen.

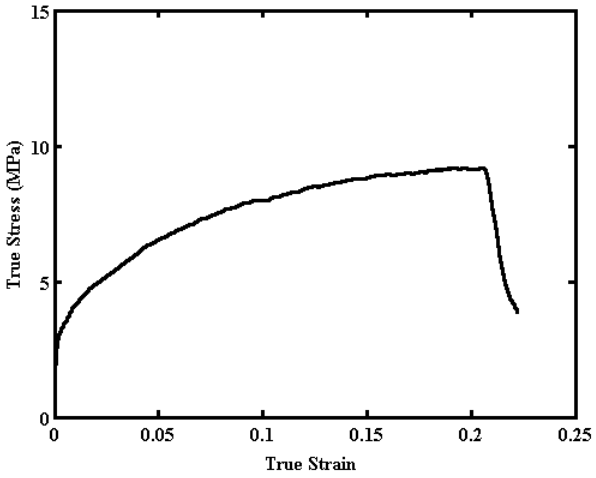

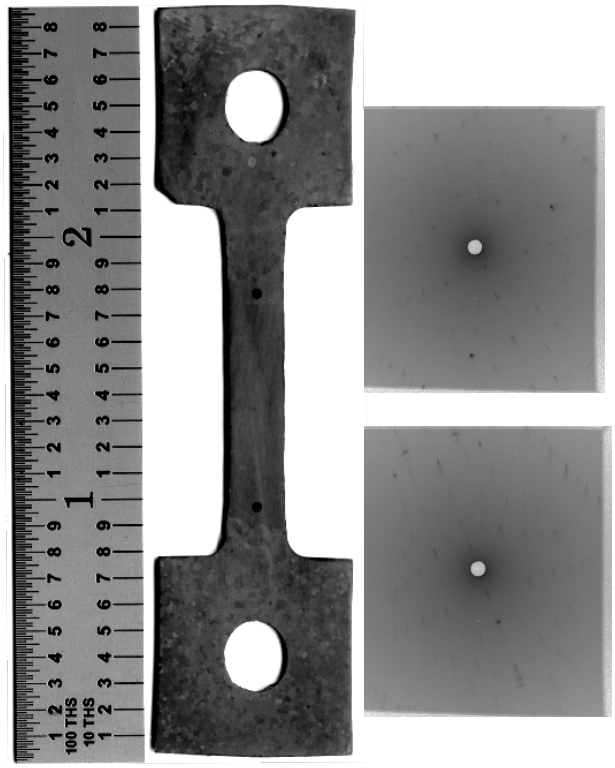

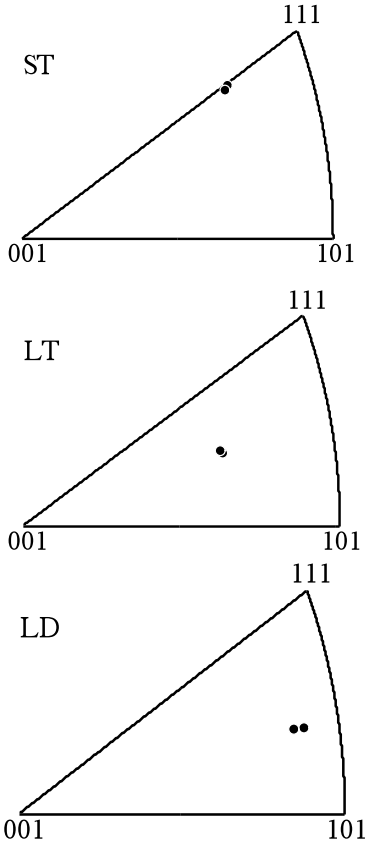

Ta 20

Temperature: 1450 °C

Strain rate: 3×10^{-5}

Preload: 5 lbs

DAGG observed: Yes

Notes:

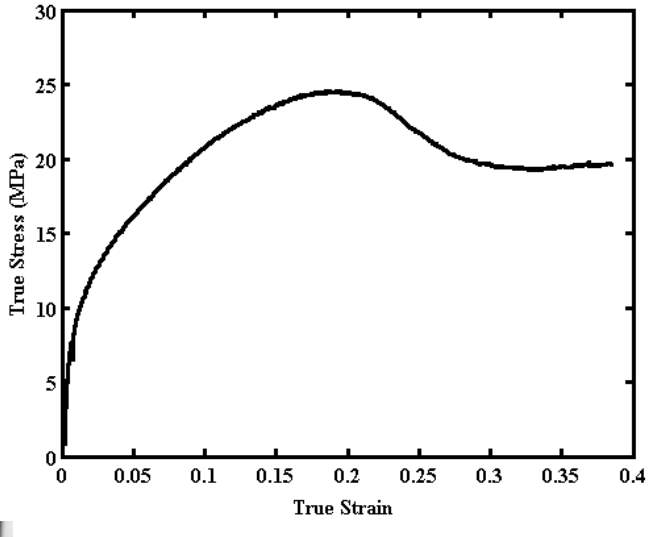

Ta 21

Temperature: 1650 °C

Strain rate: 3×10^{-5}

Preload: 5 lbs

DAGG observed: Yes

Notes: Data lost after heatup (before start of test), so stress is only approximate and is based on assumption that load was still equal to preload (5lbs) at start of test, but will likely be slightly lower due to recovery.

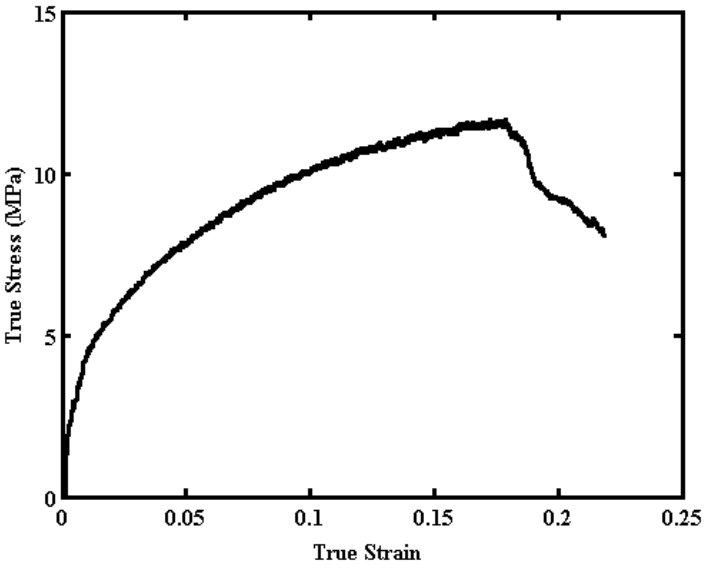

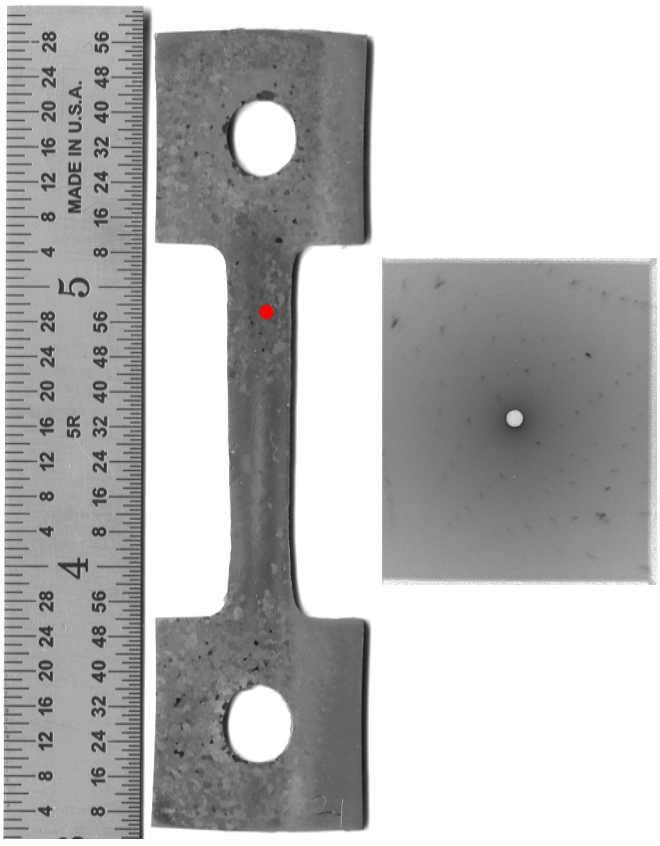

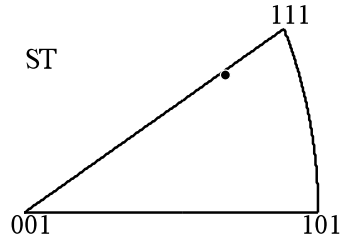

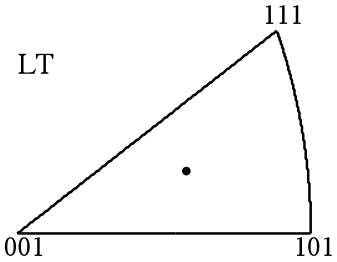

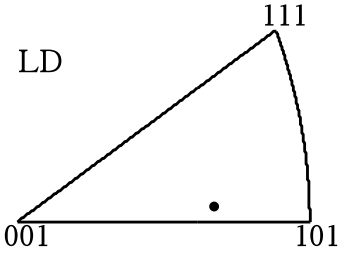

Ta 22

Temperature: 1550 °C

Strain rate: 3×10^{-5}

Preload: 5 lbs

DAGG observed: Yes

Notes:

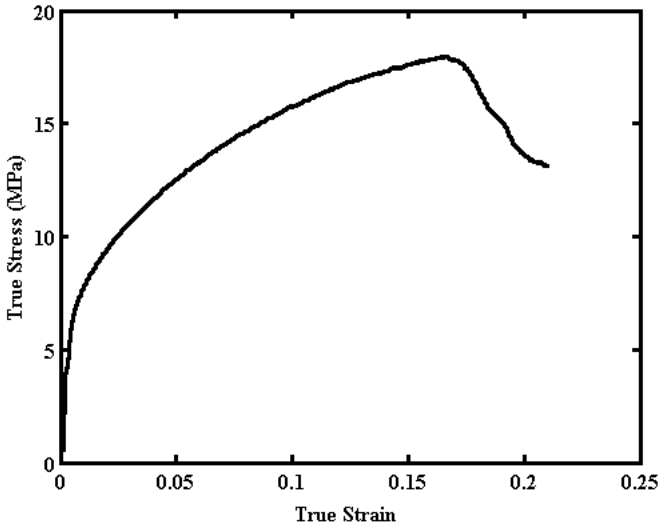

Ta 23

Temperature: 1750 °C

Strain rate: 3 $\times 10^{-5}$

Preload: 5 lbs

DAGG observed: Yes

Notes: specimen bent during furnace cooldown and was cut in two places to make flat for metallography.

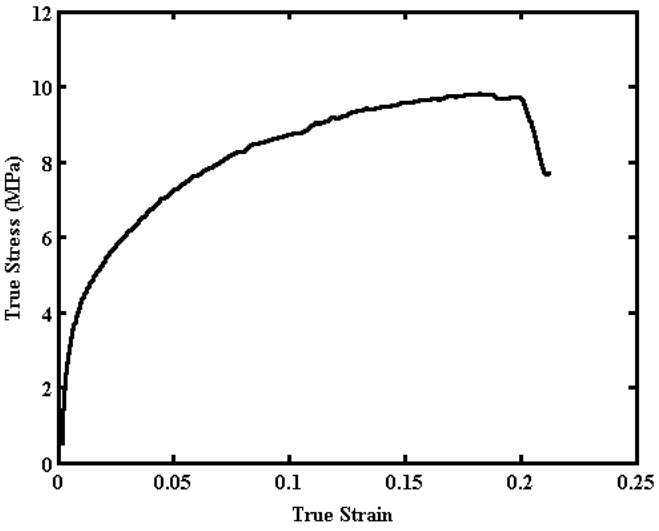

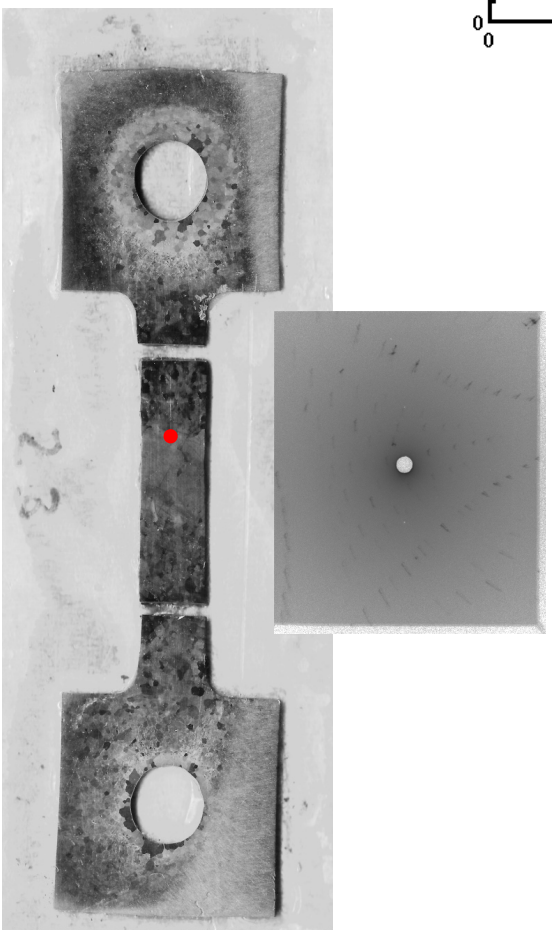

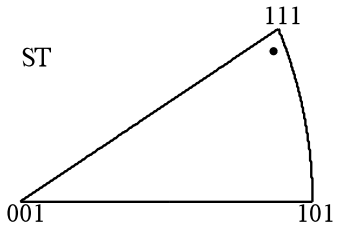

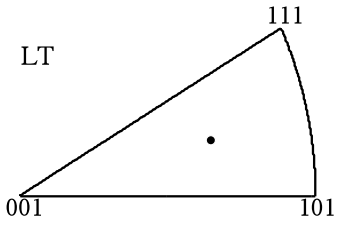

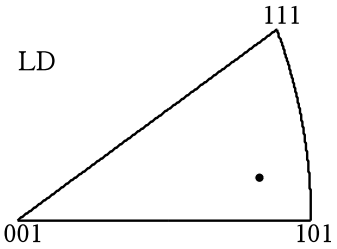

Ta 24

Temperature: 1850 °C

Strain rate: 3 $\times 10^{-5}$

Preload: 5 lbs

DAGG observed: Yes

Notes:

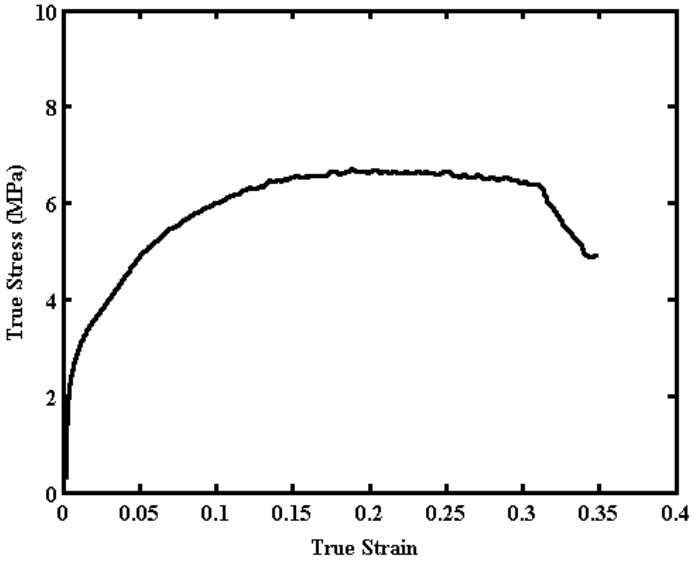

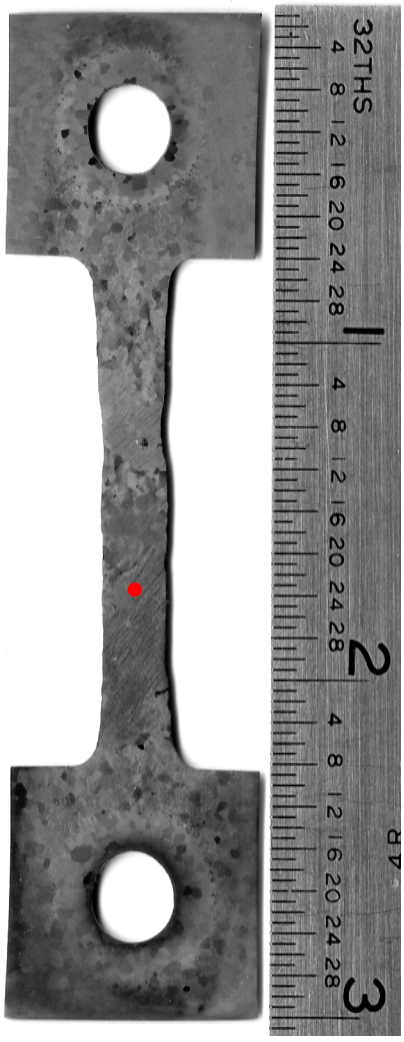

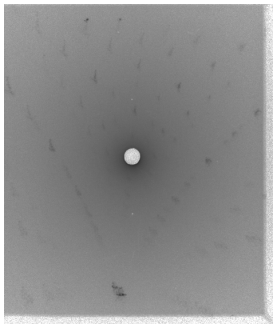

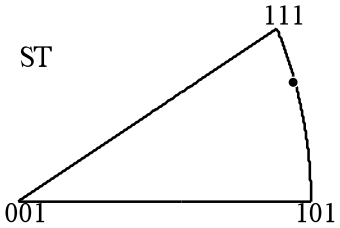

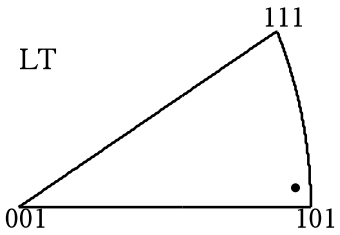

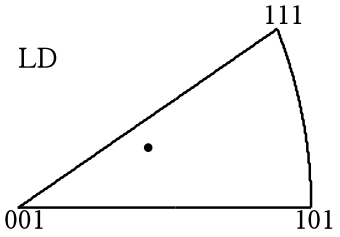

Ta 25

Temperature: 1650°C

Strain rate: 3×10^{-5}

Preload: 5 lbs

DAGG observed: Yes

Notes: Data lost

Ta 26

Temperature:	1650 °C
Strain rate:	3 $\times 10^{-5}$
Preload:	5 lbs
DAGG observed:	Yes

Notes: Specimen may have shifted in grips during testing

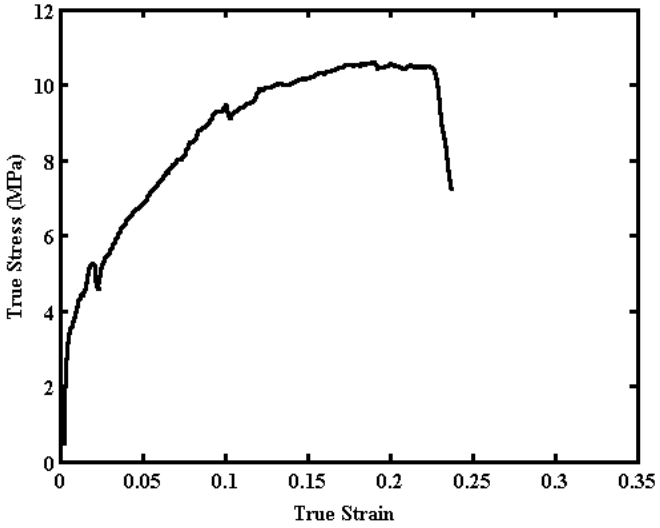

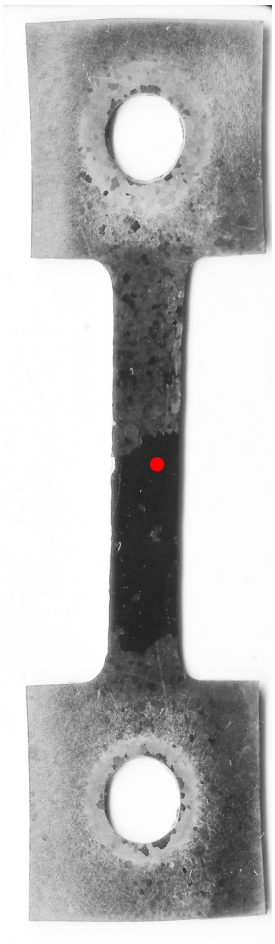

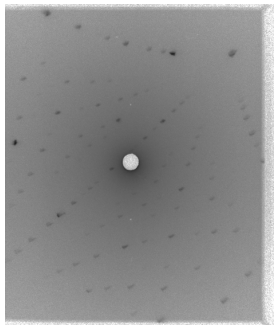

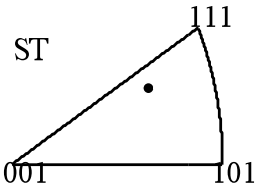

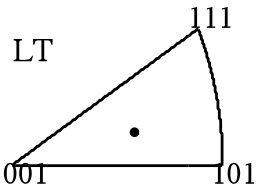

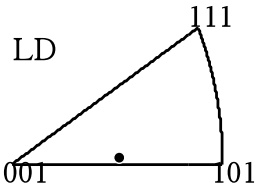

Ta 27

Temperature: 1750 °C

Strain rate: 3×10^{-5}

Preload: 5 lbs

DAGG observed: Yes

Notes:

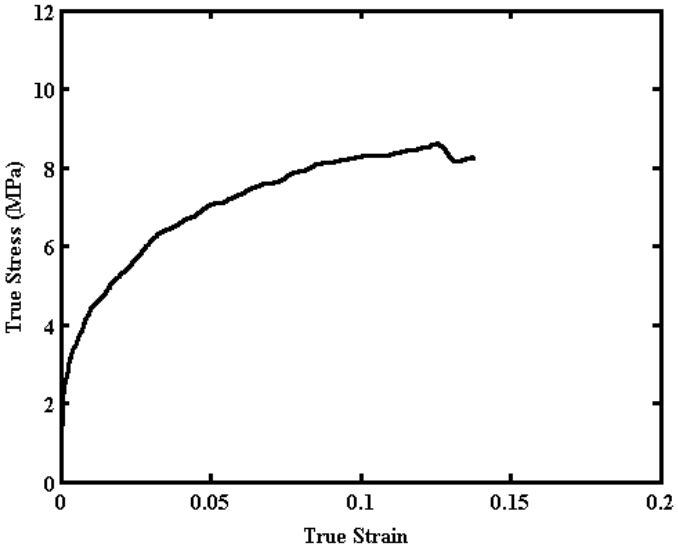

Ta 28

Temperature:	1550 °C
Strain rate:	3 $\times 10^{-5}$
Preload:	5 lbs
DAGG observed:	Yes

Notes:

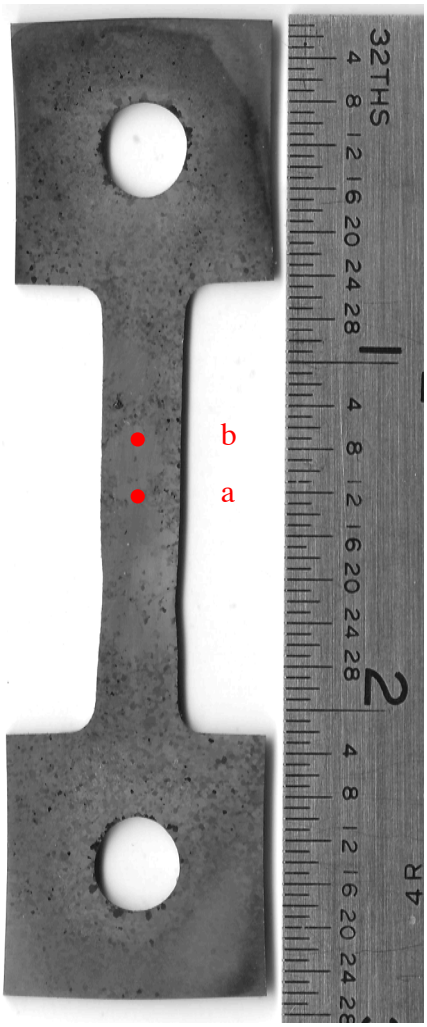

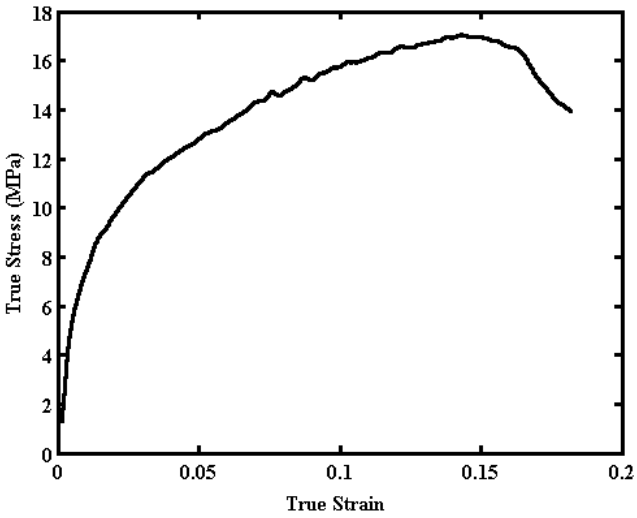

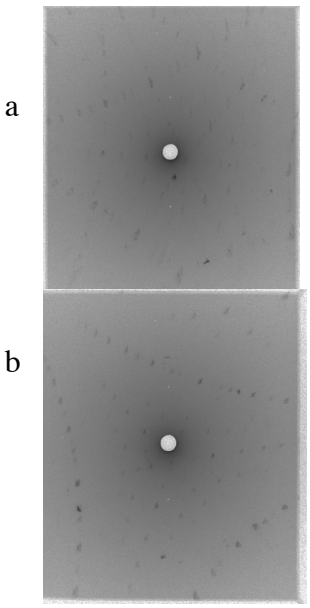

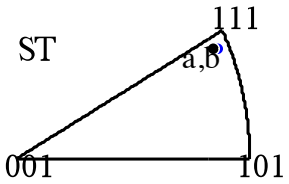

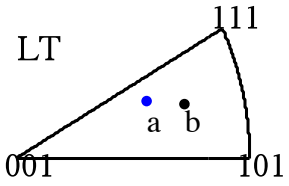

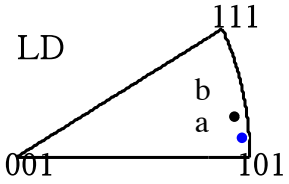

Ta 29

Temperature: 1750 °C

Strain rate: 3 $\times 10^{-5}$

Preload: 5 lbs

DAGG observed: Yes, but not apparent from microstructural observations

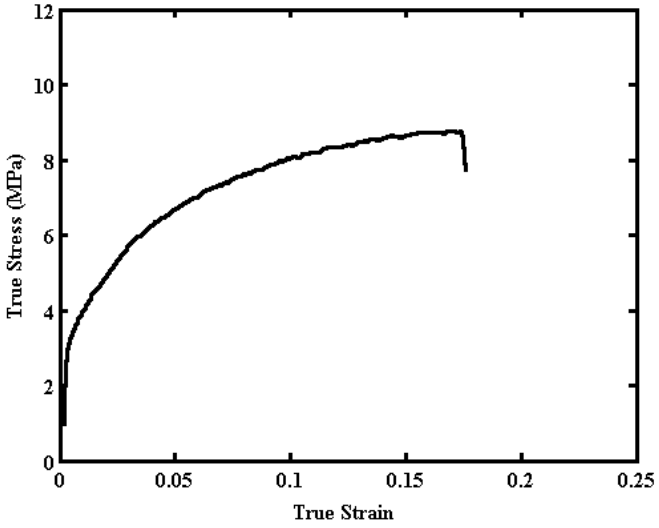

Ta 30

Temperature: 1650 °C

Strain rate: 3×10^{-5}

Preload: 5 lbs

DAGG observed: Yes

Notes: Two small DAGG grains formed

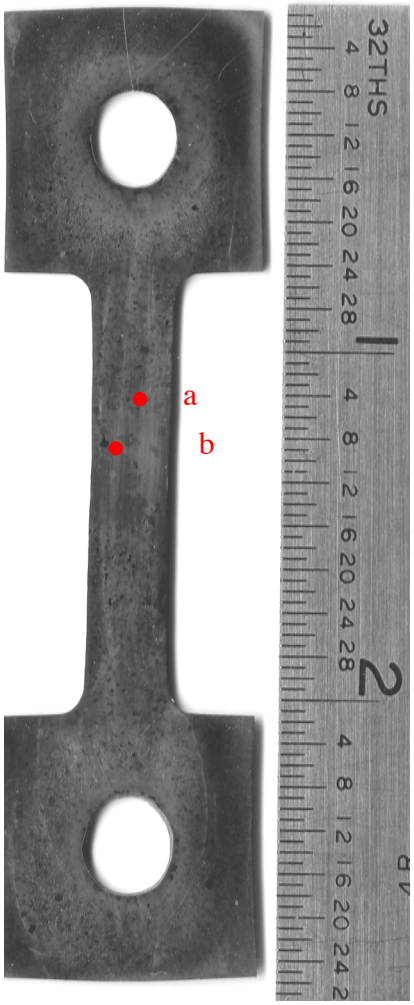

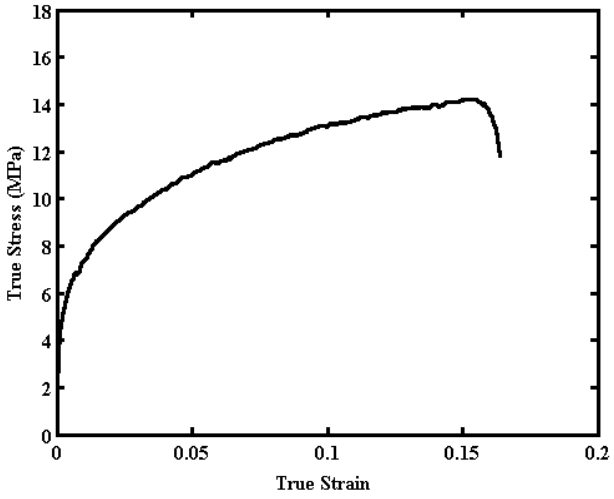

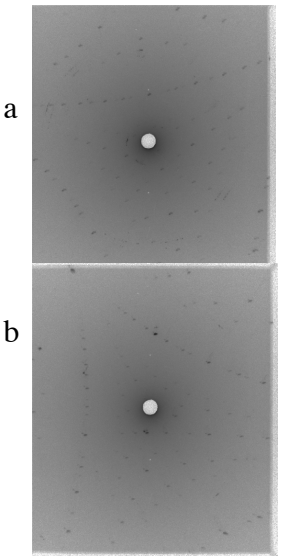

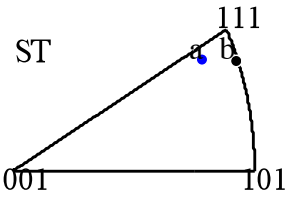

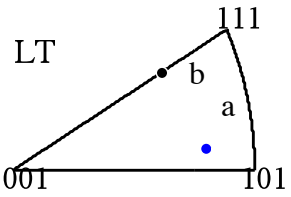

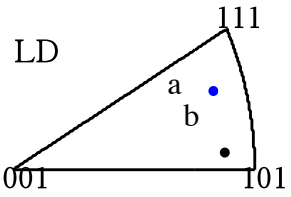

Ta 31

Temperature: 1650 °C

Strain rate: 3×10^{-5}

Preload: 5 lbs

DAGG observed: Yes

Notes:

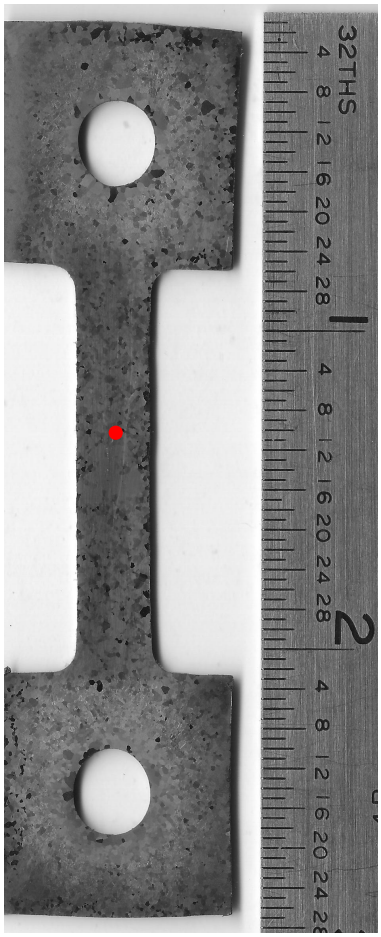

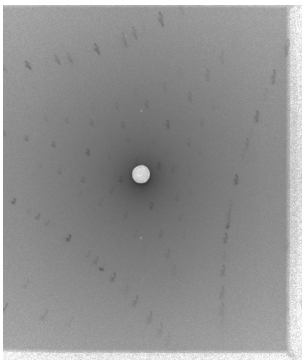

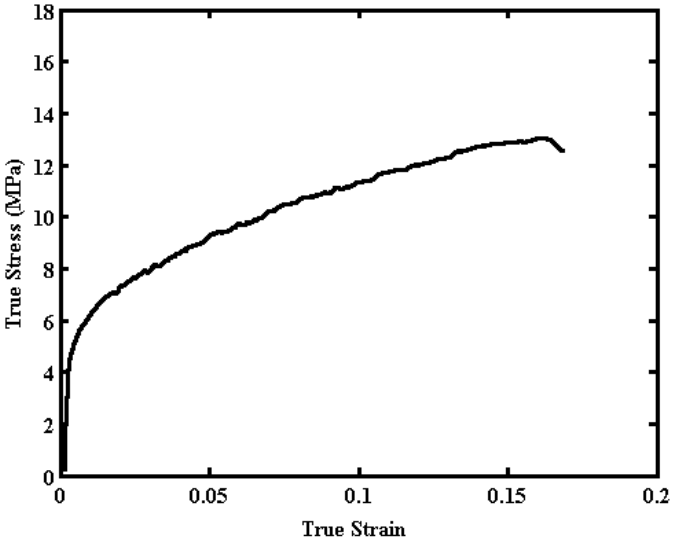

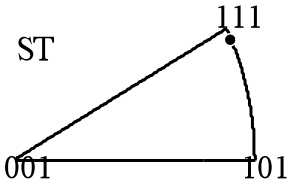

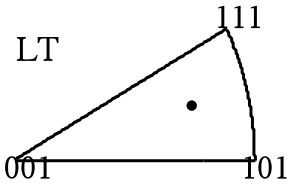

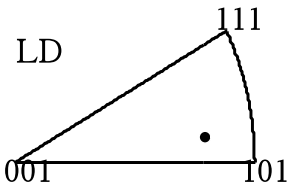

Ta 32

Temperature: 1650 °C

Strain rate: 3×10^{-5}

Preload: 5 lbs

DAGG observed: Yes

Notes:

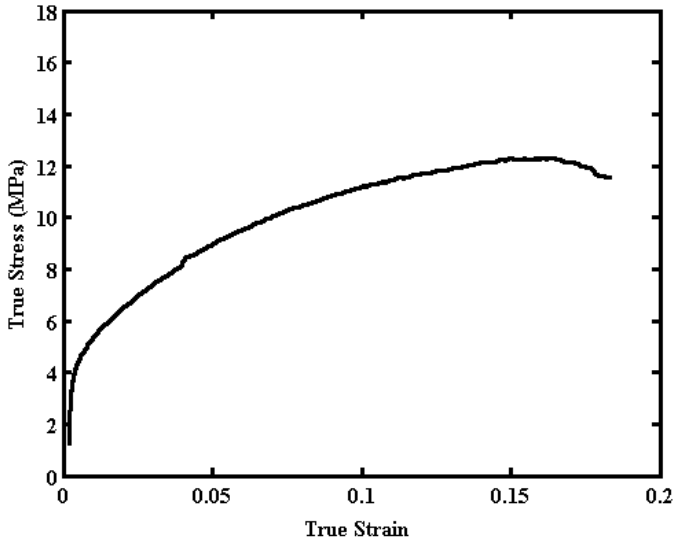

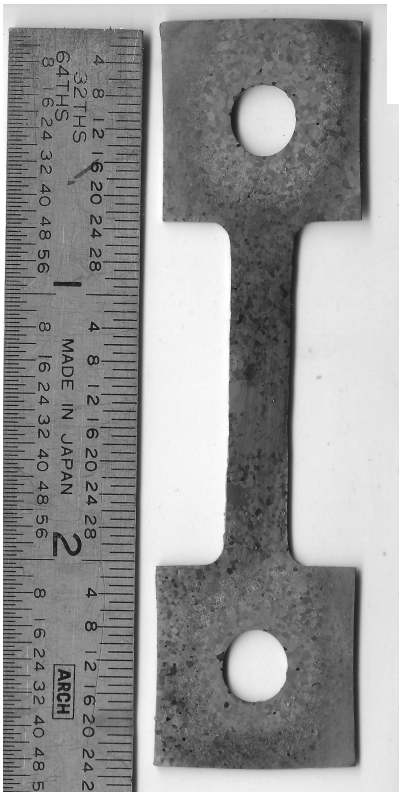

Ta 33

Temperature: 1650 °C

Strain rate: 3×10^{-5}

Preload: 5 lbs

DAGG observed: Yes

Notes:

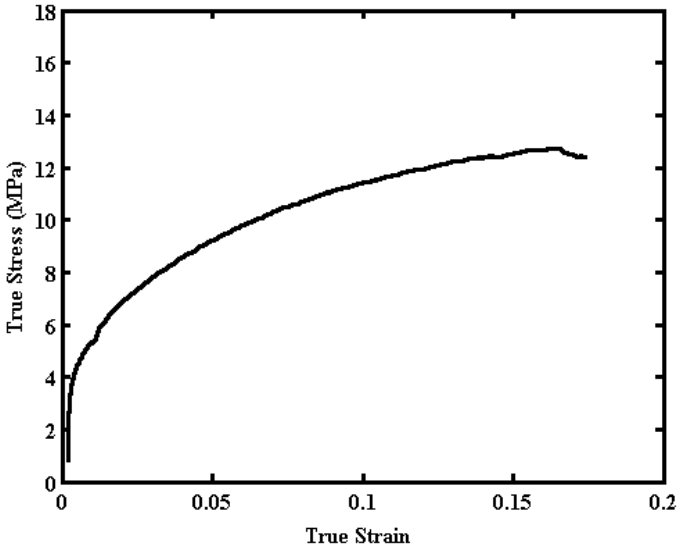

Ta 34

Temperature: 1650 °C

Strain rate: 3×10^{-5}

Preload: 5 lbs

DAGG observed: Yes

Notes:

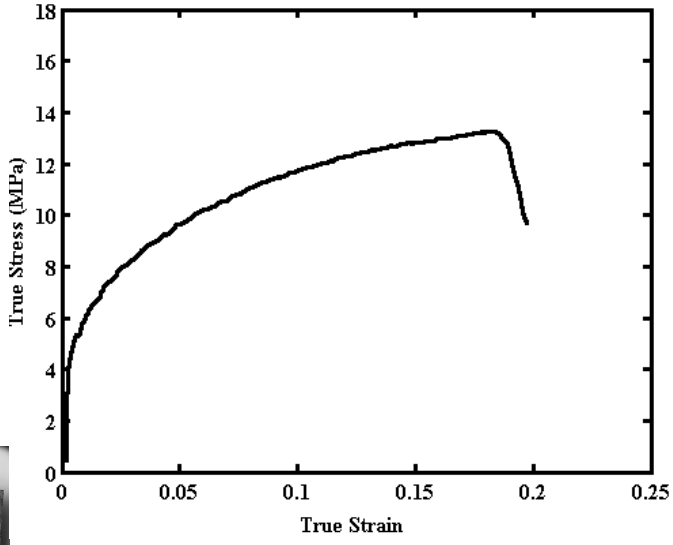

Ta 35

Temperature: 1650 °C

Strain rate: 3×10^{-5}

Preload: 5 lbs

DAGG observed: Yes

Notes:

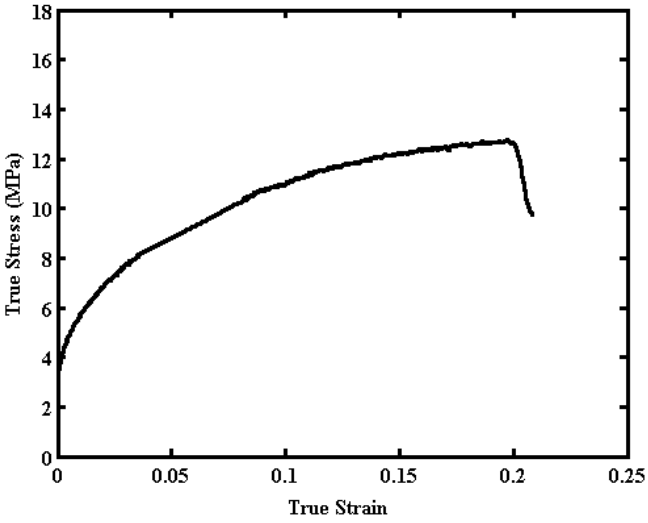

Ta 36

Temperature: 1650 °C

Strain rate: 3×10^{-5}

Preload: 5 lbs

DAGG observed: Yes

Notes:

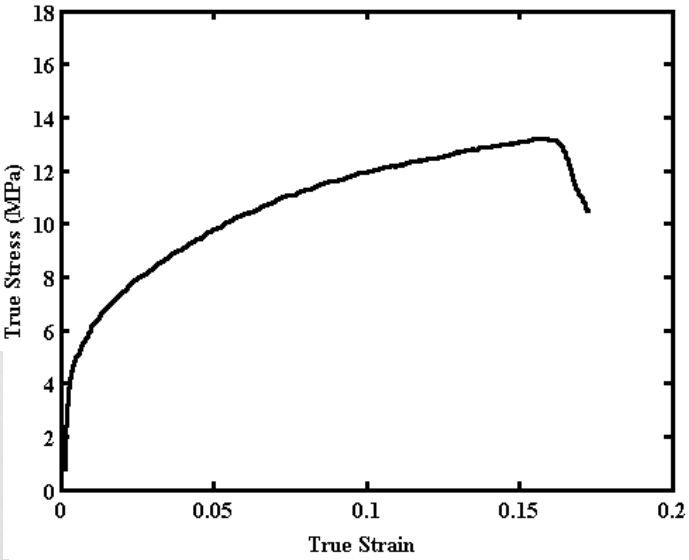

Ta 37

Temperature: 1650 °C

Strain rate: 3×10^{-5}

Preload: 5 lbs

DAGG observed: Yes

Notes:

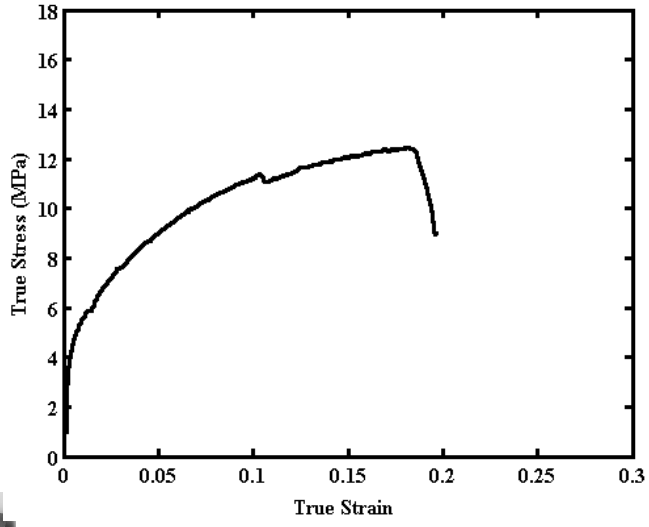

Ta 38

Temperature: 1750 °C

Strain rate: 3×10^{-5}

Preload: 5 lbs

DAGG observed: Yes

Notes:

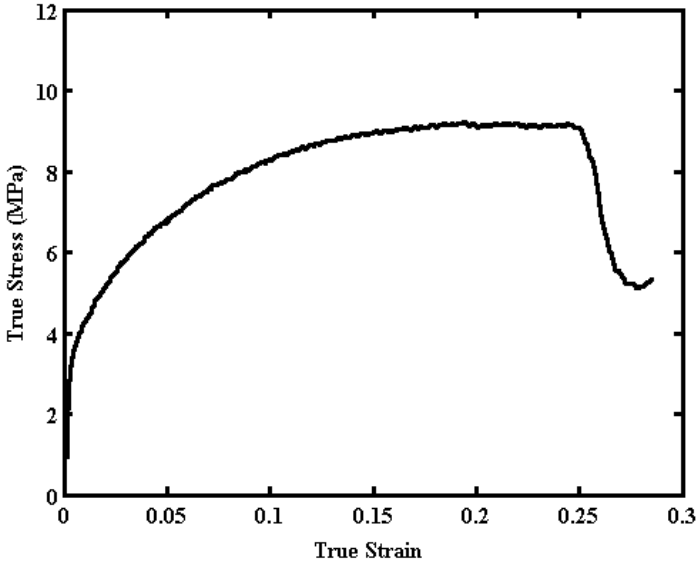

Ta 39

Temperature: 1650 °C

Strain rate: 3×10^{-5}

Preload: 5 lbs

DAGG observed: Yes

Notes:

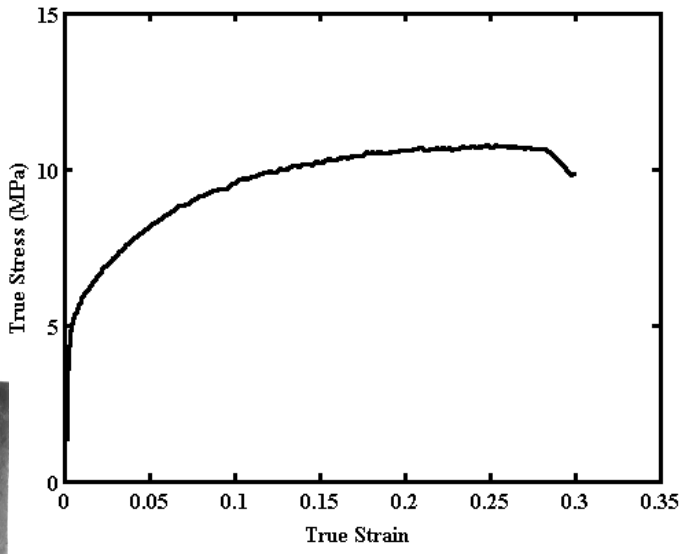

Ta 40: Computer error. Test aborted.

Ta 41

Temperature: 1650 °C

Strain rate: 1×10^{-4}

Preload: 5 lbs

DAGG observed: Yes

Notes:

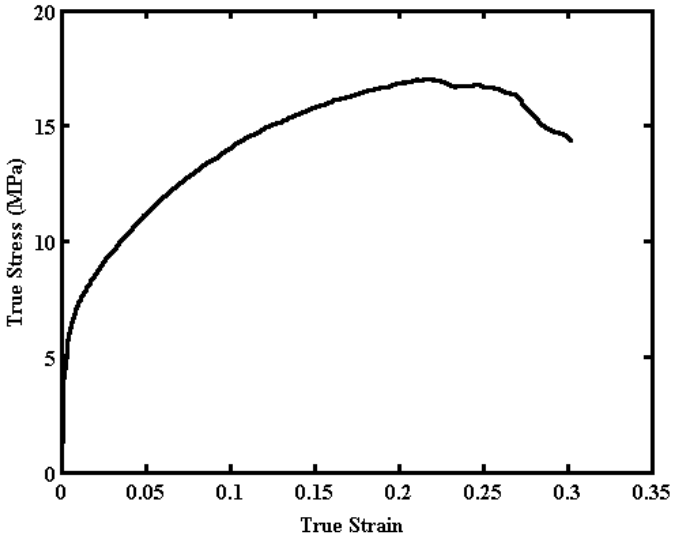

Ta 42

Temperature: 1650 °C

Strain rate: 1×10^{-4}

Preload: 5 lbs

DAGG observed: Yes

Notes:

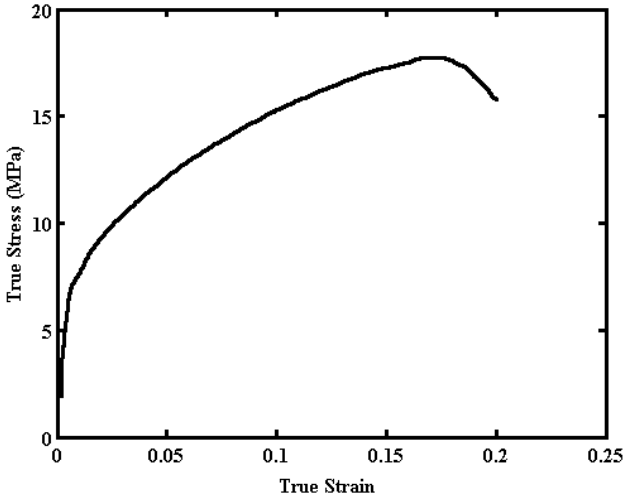

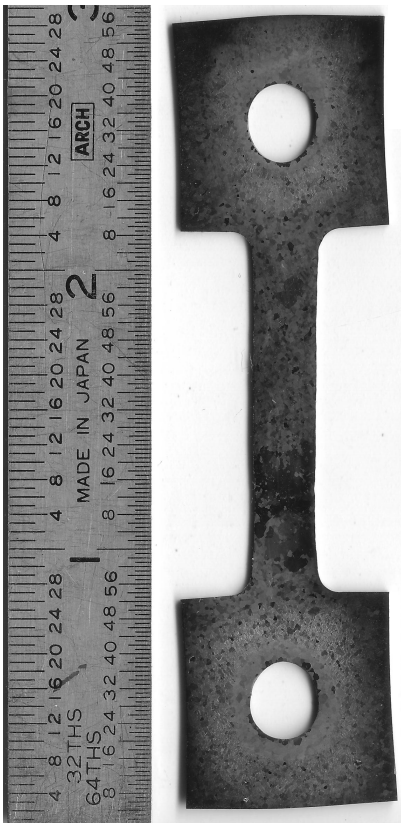

Ta 43

Temperature: 1650 °C

Strain rate: 2×10^{-4}

Preload: 5 lbs

DAGG observed: Yes

Notes:

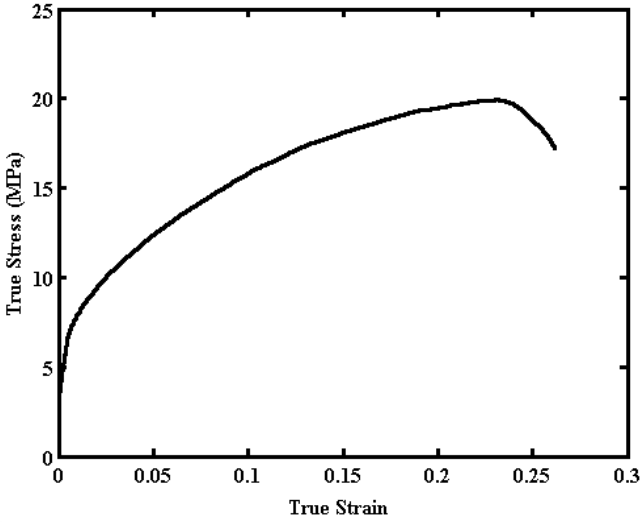

Ta 44

Temperature: 1650 °C

Strain rate: 2×10^{-5}

Preload: 5 lbs

DAGG observed: Yes

Notes:

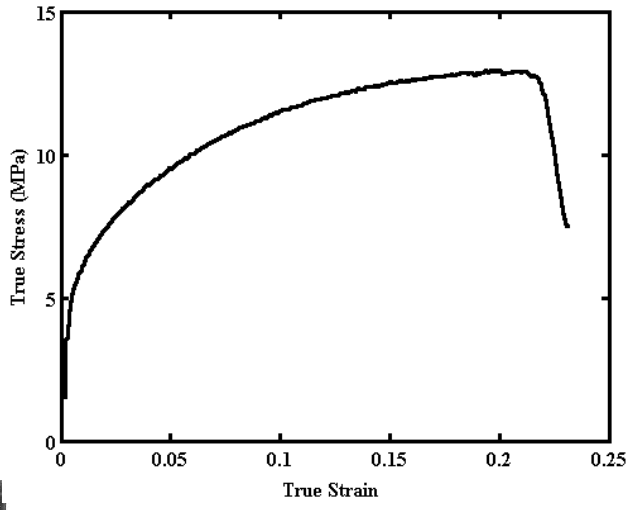

Ta 45

Temperature: 1650 °C

Strain rate: 2×10^{-4}

Preload: 5 lbs

DAGG observed: Yes

Notes:

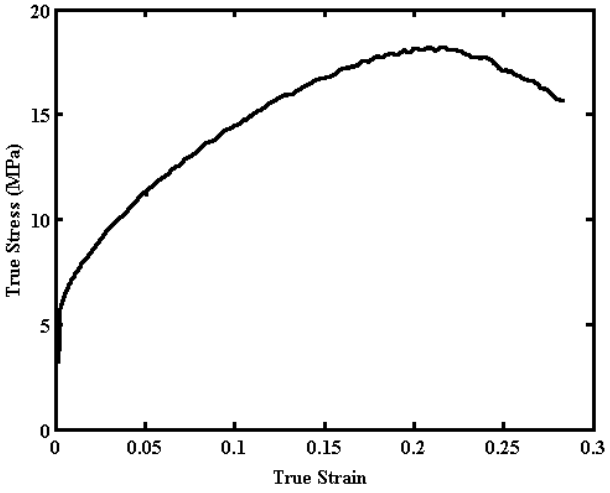

Ta 46

Temperature:	1650 °C
Strain rate:	5×10^{-5}
Preload:	5 lbs
DAGG observed:	Yes
Notes:	

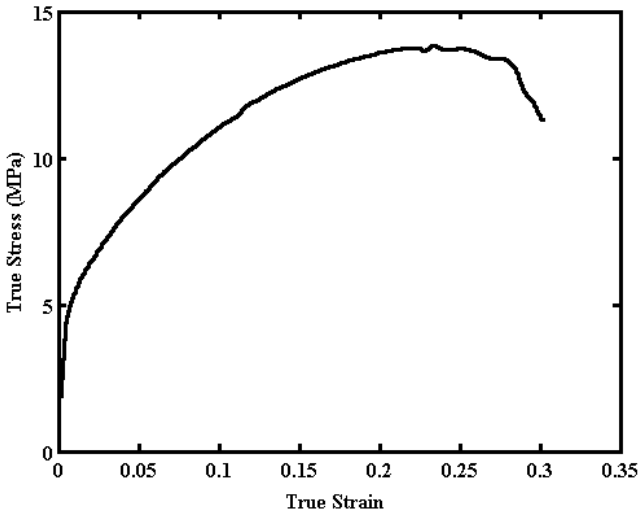

Ta 47

Temperature: 1650 °C

Strain rate: 2×10^{-5}

Preload: 5 lbs

DAGG observed: Yes

Notes:

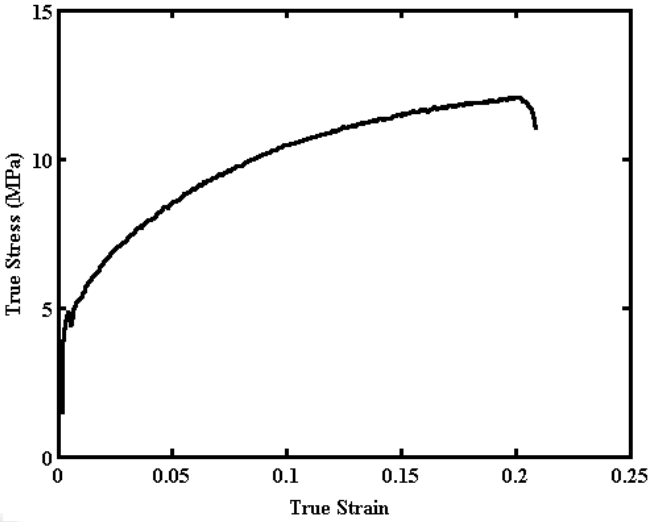

Ta 48

Temperature:	1550 °C
Strain rate:	1×10^{-4}
Preload:	5 lbs
DAGG observed:	Yes
Notes:	

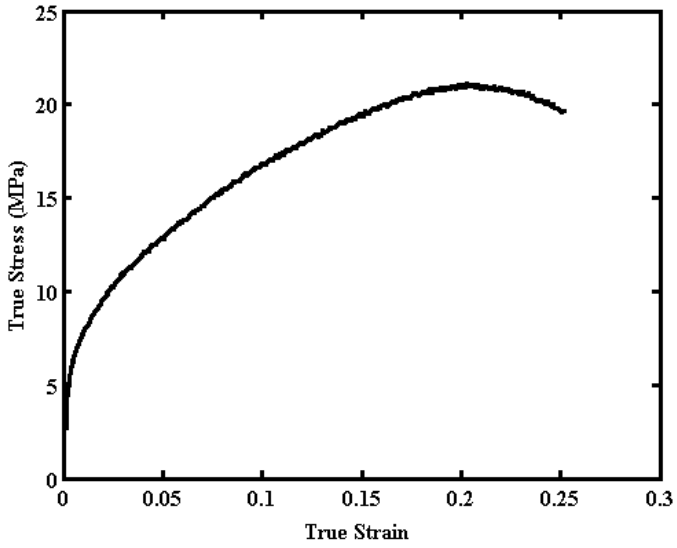

Ta 49

Temperature: 1800 °C

Strain rate: 1×10^{-4}

Preload: 5 lbs

DAGG observed: Yes

Notes:

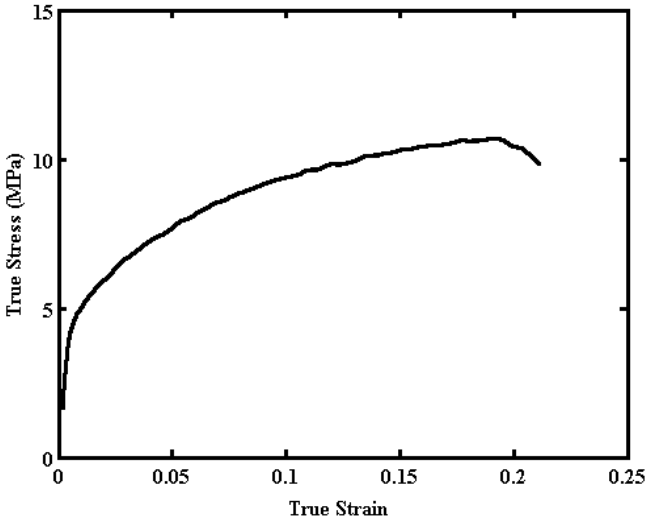

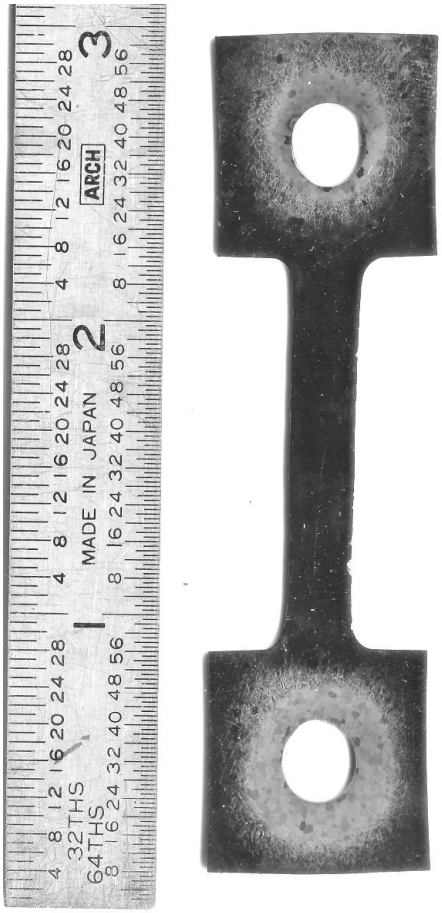

Ta 50

Temperature: 1850 °C

Strain rate: 3×10^{-5}

Preload: 5 lbs

DAGG observed: Yes

Notes:

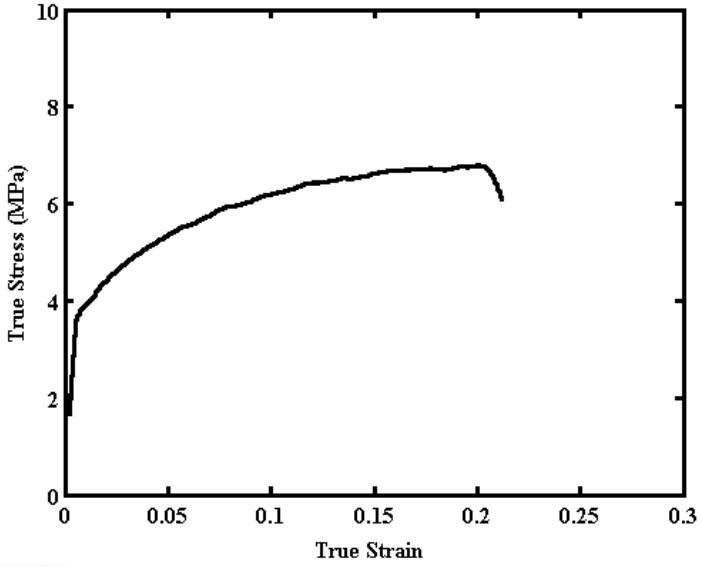

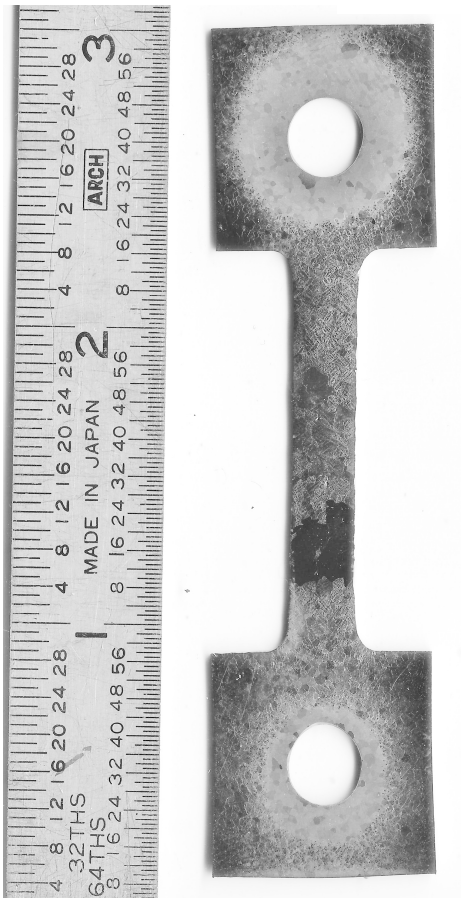

Appendix F: Constant True-Strain Rate Specimen Data Sheets for Ta-B

Ta B 1

Temperature: 1650 °C
Strain rate: 3×10^{-5}
Preload: 5 lbs
DAGG observed: No
Notes:

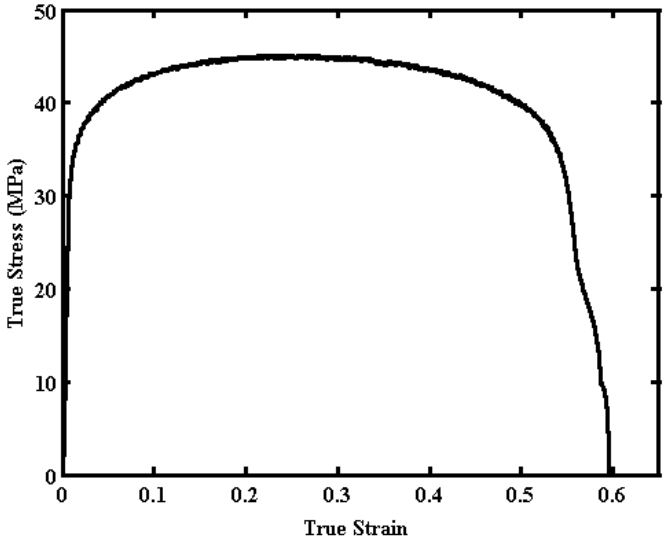

Ta B 2

Temperature: 1750 °C
Strain rate: 1×10^{-4}
Preload: 5 lbs
DAGG observed: No
Notes:

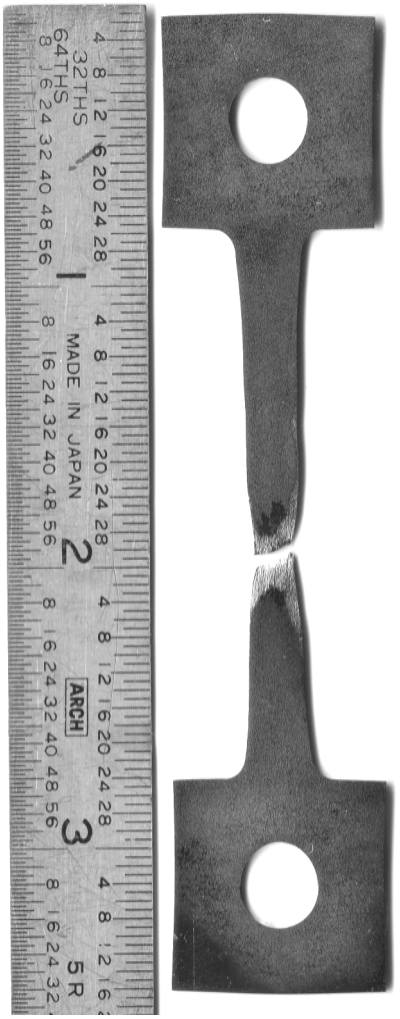

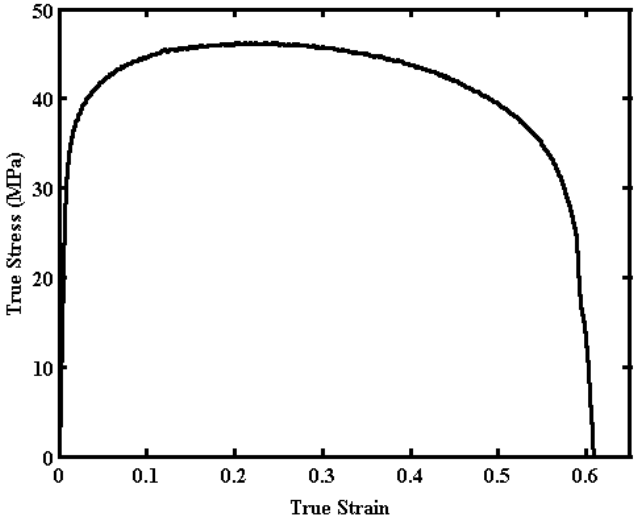

Ta B 3

Temperature: 1850 °C
Strain rate: 1×10^{-4}
Preload: 5 lbs
DAGG observed: No
Notes:

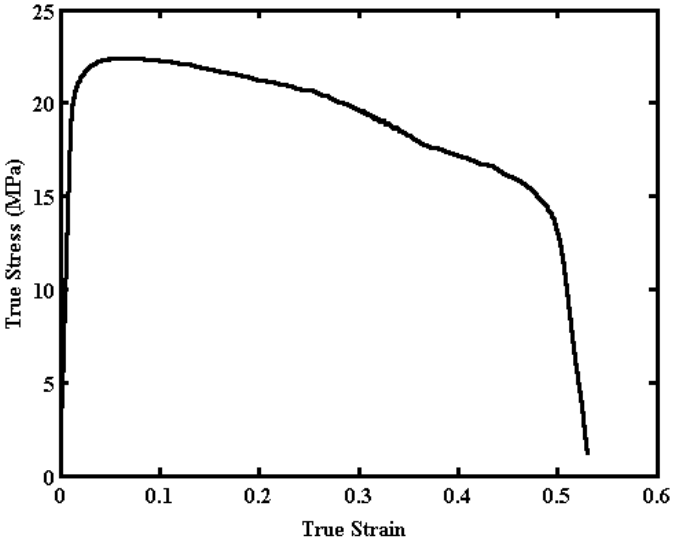

Ta B 4

Temperature: 1950 °C
Strain rate: 1×10^{-4}
Preload: 5 lbs
DAGG observed: No
Notes:

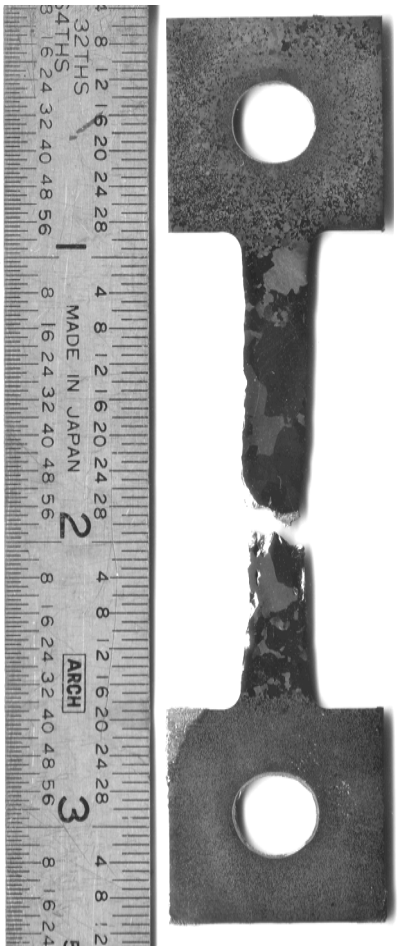

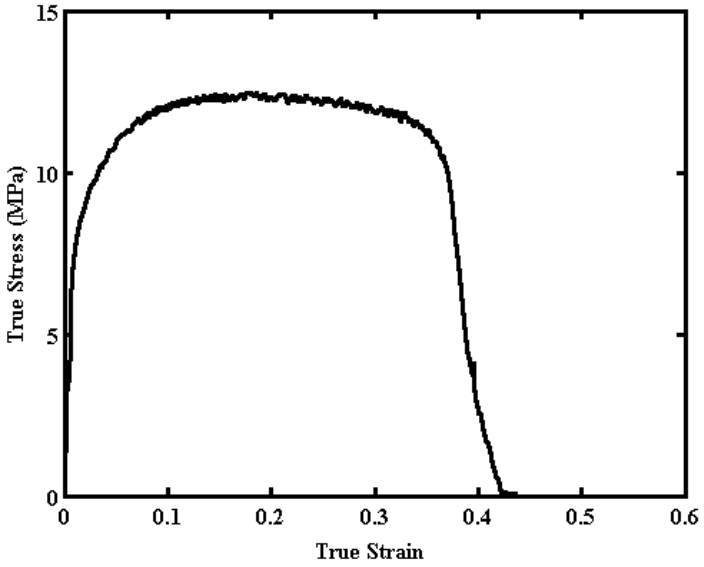

Ta B 5

Temperature: 1850 °C
Strain rate: 3×10^{-5}
Preload: 5 lbs
Notes:

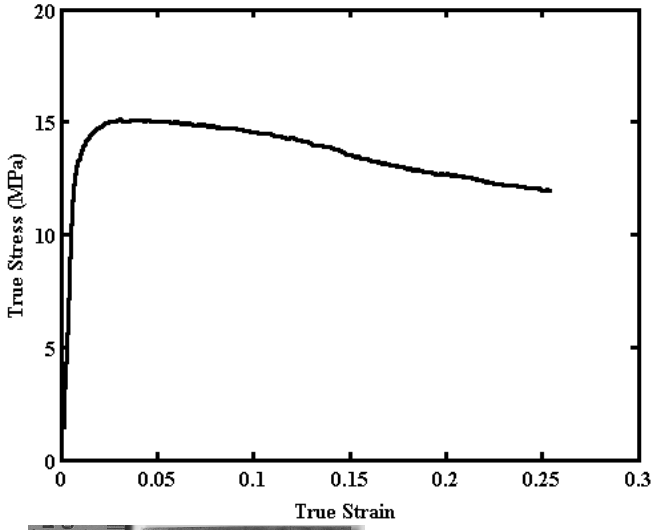

Ta B 6

Temperature: 1750 °C
Strain rate: 3×10^{-5}
Preload: 5 lbs
Notes:

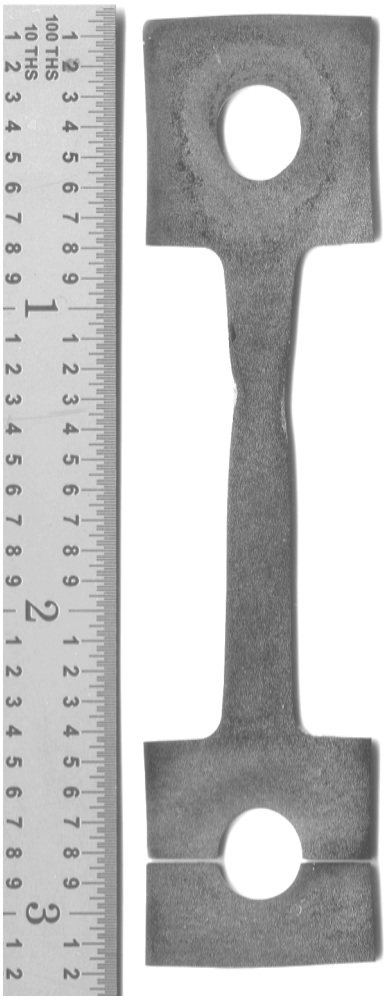

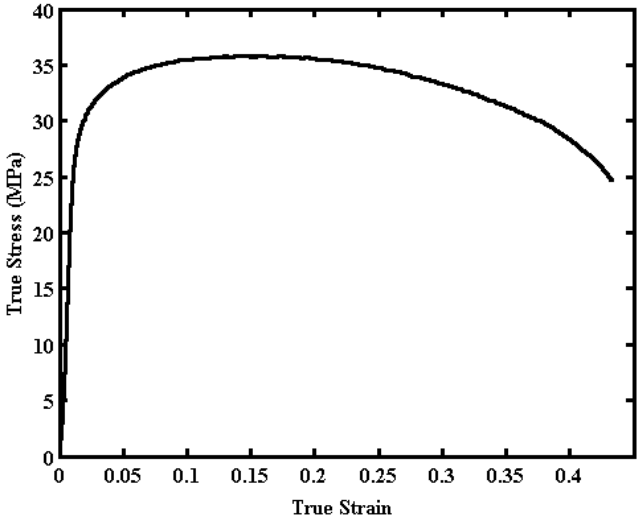

References

[Andersen 1995a] I. Andersen, Ø. Grong, "Analytical Modelling Of Grain Growth In Metals And Alloys In The Presence Of Growing And Dissolving Precipitates--I. Normal Grain Growth," *Acta metall, mater*. Vol.43, No. 7, pp. 2673-2688, 1995.

[Andersen 1995b] I. Andersen, Ø. Grong, N. Ryum, "Analytical Modelling Of Grain Growth In Metals And Alloys In The Presence Of Growing And Dissolving Precipitates--II. Abnormal Grain Growth," *Acta metall, mater*. Vol.43, No. 7, pp. 2689-2700, 1995

[Ardakani 1992] M.G. Ardakani, F.J. Humphreys, in *Recrystallization '92*, eds. Fuentes and Gil Sevillano. Trans Tech Publications, 213.

[ASTM 1996] ASTM International: *Standard Test Methods for Determining Average Grain Size*, Standard Designation E 112-96, ASTM International, West Conshohocken, PA, 1996.

[ASTM 2005] ASTM International: *Standard Specification for Tantalum and Tantalum Alloy Plate, Sheet, and Strip*, Designation B 708 - 05, ASTM International, West Conshohocken, PA, 1996.

[Bachmann 2010] F. Bachmann, R. Hielscher, H. Schaeben, "Texture Analysis with MTEX - Free and Open Source Software Toolbox," *Solid State Phenomena*, Vol. 160, pp. 63-68, 2010.

[Beck 1949] P.A. Beck, M. L. Holzworth, and P. R. Sperry, " Effect of a Dispersed Phase on Grain Growth in Al-Mn Alloys," *Trans. Am. Inst. Min. Metall. Eng*, Vol. 180, pp. 163-192, 1949.

[Bennett 2007] T.A. Bennett, P.N. Kalu, A.D. Rollett, "On the character of host-island grain interfaces in Fe-1%Si alloy," *Scripta Materialia*, Vol. 57, pp. 41-44, 2007.

[Bishop 1951] Bishop J.F.W. and Hill, R., (i) A theory of the plastic distortion of a polycrystalline aggregate under combined stresses, *Philosophical Magazine*, 42, 414-427, 1951, (ii) A theoretical derivation of the plastic properties of a polycrystalline face-centered metal, *Philosophical Magazine*, Vol. 42, pp. 1298-1307, 1951.

[Brandon 1966] D.G. Brandon, "The Structure of High-Angle Grain Boundaries," *Acta Metallurgica*, Vol. 14, pp. 1479-1484, 1966.

[Brewer 2002] Brewer, L.N., Othon, M.A., Young, L.M. & Angeliu, T.M., "Misorientation mapping for visualization of plastic strain via electron back-scattered diffraction," *Microscopy and Micro-analysis 2002*, Voelkel, E., Piston, D., Gauvin, R., Lockley, A.J., Bailey, G.W. & McKernan, S. (Eds.), pp. 684CD–685CD. Quebec City, Quebec, Canada: Cambridge University Press. 2002.

[Briant 2000] C.L. Briant, E. MacDonald, R.W. Balliett, T. Luong, "Recrystallization textures in tantalum sheet and wire," *International Journal of Refractory Metals and Hard Materials*, Vol. 18, pp. 1-8, 2000.

[Bridgman 1931] P.W. Bridgman: U.S. Patent No. 1,793,672, 1931.

[Buchheit 2005] T. E. Buchheit, G.W. Wellman, C.C. Battaile, "Investigating the limits of polycrystal plasticity modeling," *International Journal of Plasticity*, Vol. 21, pp. 221–249, 2005.

[Burke 1952] J. E. Burke, D. Turnbull. "Recrystallization and grain growth," *Progress in Metal Physics*, Vol. 3, pp. 220–244, 1952.

[Cahn 2004] J.W. Cahn, J.E. Taylor, "A unified approach to motion of grain boundaries, relative tangential translation along grain boundaries, and grain rotation," *Acta Materialia*, Vol. 52, pp. 4887-4898, 2004.

[Cahn 2006a] J.W. Cahn, Y. Mishinb, A. Suzuki, "Coupling grain boundary motion to shear deformation," *Acta Materiallia*, Vol. 54, Is. 19, pp. 4953-4975, 2006.

[Cahn 2006b] J.W. Cahn, Y. Mishin, A Suzuki, "Duality of dislocation content of grain boundaries," *Philosophical Magazine*, Vol. 86, No. 25-26, pp. 3965-3980, 2006.

[Chin 1967] G.Y. Chin, W. L. Mammel, and M. T. Dolan. "Computerized plastic deformation by slip." *Trans. Met. Soc. AIME*, Vol. 239, pp. 1111-1112, 1967.

[Chin 1970] G. Y. Chin, B. C. Wonsiewicz, "Stress States for {123} (111} Multiple Slip," *Metallurgical Transactions*, Vol. 1, pp. 551-556, 1970.

[Cho 2005] J.H. Cho, A.D. Rollett, K.H. Oh, "Determination of a Mean Orientation in Electron Backscatter Diffraction Measurements," *Metallurgical and Materials Transactions A*, Vol. 36A, pp. 3427-3438, 2005.

[Christian 1983] J.W. Christian, "Some Surprising Features of the Plastic Deformation of Body-Centered Cubic Metals and Alloys," *Metallurgical Transactions A*, Vol.14 A, pp.1237-1256, 1983.

[Ciulik 2005] J.R. Ciulik, "Creep and Dynamic Abnormal Grain Growth of Commercial-Purity Molybdenum," PhD thesis, The University of Texas at Austin, August 2005.

[Ciulik 2007] J. Ciulik, E.M. Taleff, "Power-law creep of powder-metallurgy grade molybdenum sheet," *Materials Science and Engineering A*, Vol. 463, pp. 197–202, 2007.

[Ciulik 2009] J.R. Ciulik, E.M. Taleff, "Dynamic abnormal grain growth: A new method to produce single crystals," *Scripta Materialia*, vol. 61, pp. 895-898, 2009.

[Clark 1991] J.B. Clark, R.K. Garrett, Jr., T.L. Jungling, R.A. Vandermeer, C.L. Vold, "Effect of Processing Variables on Texture and Texture Gradients in Tantalum," *Metallurgical Transactions A*, Vol. 22A, pp. 2039-2048, 1991.

[Czochralski 1918] J. Czochralski, "Ein neues Verfahren zur Messung des Kristallisationsgeschwindigkeit der Metalle [A new method for the measurement of crystallization rate of metals]," *Z. phys. Chem.* Vol. 92, pp. 219-221, 1918.

[Duesbery 1973] M. S. Duesbery, V. Vitek, D. K. Bowen, "The effect of shear stress on the screw dislocation core structure in body-centred cubic lattices." *Proceedings of the Royal Society of London. A. Mathematical and Physical Sciences*, Vol. 332, No. 1588, pp. 85-111, 1973.

[Duesbery 1984] M.S. Duesbery, "On Non-Glide Stresses and Their Influence on the Screw Dislocation Core in Body-Centred Cubic Metals. I. The Peierls Stress." *Proceedings of the Royal Society of London. A. Mathematical and Physical Sciences*, Vol. 392, No. 1802, pp. 145-173, 1984.

[Duesbery 1989] M.S. Duesbery, "The dislocation core and plasticity." *Elsevier Science Publishers, Dislocations in Solids,* Vol. 8, pp. 67-173, 1989.

[Duesbery 1998] M. S. Duesbery, V. Vitek, "Plastic Anisotropy In B.C.C. Transition Metals," *Acta mater*., Vol. 46, No. 5, pp. 1481-1492, 1998.

[Dunn 1966] C.G. Dunn and J.L. *Walter, Recrystallization, Grain Growth and Textures*, ASM, Ohio, 1966.

[Escaig 1974] B. Escaig, "Dissociation and Mechanical Properties. Dislocation Splitting and the Plastic Glide Process in Crystals." *Le Journal de Physique Colloques*. Vol. 35, pp. 151-166, 1974.

[Farraro 1979] R.J. Farraro, R.B. McLellan, "High Temperature Elastic Properties of Polycrystalline Niobium, Tantalum, and Vanadium," *Metallurgical Transactions A*, Vol. 10A, pp. 1699-1702, 1979.

[Frost 1988] H.J. Frost, C. V. Thompson. "Computer simulation of microstructural evolution in thin films." *Journal of Electronic Materials*, Vol. 17, no. 5, pp. 447-458, 1988.

[Frost 1990] H.J. Frost, C. V. Thompson, and D. T. Walton. "Simulation of thin film grain structures—I. Grain growth stagnation." *Acta Metallurgica et Materialia*, Vol. 38, no. 8, pp. 1455-1462, 1990.

[Frost 1992] H.J. Frost, C.V. Thompson, D.T. Walton, "Simulation of Thin Film Grain Structures- II. Abnormal Grain Growth," *Acta metal. mater*., Vol. 40, No. 4, pp. 779-793, 1992.

[Gao 2005] N. Gao, S.C. Wang, H.S. Ubhi, M.J. Starink, "A comparison of grain size determination by light microscopy and EBSD analysis," *Journal of Materials Science*, Vol. 40, Is. 18, pp. 4971-4974, 2005.

[Gianola 2006] D.S. Gianola, S. Van Petegem, M. Legros, S. Brandstetter, H. Van Swygenhoven, K.J. Hemker, "Stress-assisted discontinuous grain growth and its effect on the deformation behavior of nanocrystalline aluminum thin films," *Acta Materialia*, Vol. 54, pp. 2253-2263, 2006.

[Gifkins 1952] R.C. Gifkins, "Grain Movements During Creep." *Nature*, Vol. 169, pp. 238-239, 1952.

[Gifkins 1953a] R.C. Gifkins, "The Influence Of Thallium On The Creep Of Lead." *Journal of the Institute of Metals*, Vol. 81, no. 8, pp. 417-425, 1953.

[Gifkins 1953b] R.C. Gifkins, "Structural Studies Of The Creep Of Lead." *Journal of the Institute of Metals*, Vol. 82, no. 1, pp. 39-47, 1953.

[Gifkins 1957] R.C. Gifkins, "The Effect Of Stress On The Recrystallization Of Lead During Creep." *Journal of the Institute of Metals*, Vol. 86, no. 1, pp. 15-16, 1957.

[Gifkins 1959] R.C. Gifkins, "Boundary Migration Of High-Purity Lead During Creep And Grain Growth." *Transactions Of The American Institute Of Mining And Metallurgical Engineers*, Vol. 215, no. 6, pp. 1015-1022, 1959.

[Gladman 1966] T. Gladman, "On the Theory of the Effect of Precipitate Particles on Grain Growth in Metals," *Proc. R. Soc. Lond. A,* Vol. 294, pp. 298-309, 1966.

[Gorkaya 2010] T. Gorkaya, T. Burlet, D.A. Moldov, G. Gottstein, "Experimental method for true in situ measurements of shear-coupled grain boundary migration," *Scripta Materialia*, Vol. 63, pp. 633-838, 2010.

[Gottstein 1979] G. Gottstein, D. Zabardjadi, and H. Mecking, "Dynamic recrystallization in tension-deformed copper single crystals," *Metal Science*, March-April 1979, pp. 223-227, 1979.

[Gottstein 1983a] G. Gottstein, U.F. Kocks, "Dynamic Recrystallization and Dynamic Recovery in <111> Single Crystals of Nickel and Copper," *Acta metall*., Vol. 31, pp. 175-188, 1983.

[Gottstein 1983b] G. Gottstein, "Dynamic recrystallization of Cu single crystals during tensile deformation in creep." *Metal science*, Vol. 17, no. 10, pp. 497-502, 1983.

[Gottstein 2009] G. Gottstein and L. S. Shvindlerman, *Grain Boundary Migration in Metals: Thermodynamics, Kinetics, Applications,* 2nd ed. Boca Raton, FL: CRC Press, 2009.

[Green 1965] W.V. Green, “High-Temperature Creep of Tantalum,” *Transactions of the Metallurgical Society of AIME*, Vol. 233, pp. 1818-1825, 1965.

[Gröger 2005] R. Gröger, V. Vitek, "Breakdown of the Schmid law in bcc molybdenum related to the effect of shear stress perpendicular to the slip direction," *Materials Science Forum*, Vol. 482, pp. 123-126, 2005.

[Gumbsch 2003] P. Gumbsch, "Brittle fracture and the brittle-to-ductile transition of tungsten." *Journal of nuclear materials*, Vol. 323, no. 2, pp. 304-312, 2003.

[Hillert 1965] M. Hillert, "On the theory of normal and abnormal grain growth." *Acta Metallurgica*, Vol. 13, no. 3, pp. 227-238, 1965.

[HKL] Oxford Instruments plc, Oxon, United Kingdom.

[Holm 2003] E. A. Holm, M. A. Miodownik, A. D. Rollett, “On abnormal subgrain growth and the origin of recrystallization nuclei,” *Acta Materialia*, Vol. 51, No. 9, pp. 2701–2716, 2003.

[Horacsek 1980] O. Horacsek, “Properties and failure modes of incandescent tungsten filaments,” *EEPROC*, Vol. 127, Pt. A, No. 3, 1980.

[Hosford 1969] W.F. Hosford, G.Y. Chin, “Stress States for {111}<112> Multiple Slip and Twinning,” *Trans. metal. soc. AIME*, Vol. 245, pp. 877-880, 1969.

[Hosford 1993] W.F. Hosford, *Mechanics of Crystals and Textured Polycrystals*, Oxford University Press, 1993.

[Huang 2000] Y. Huang, F.J. Humphreys, “Subgrain Growth and Low Angle Boundary Mobility in Aluminum Crystals of Orientation {110}<001>,” *Acta mater.*, Vol. 48, pp. 2017-2030, 2000.

[Hull 2001] D. Hull and D.J. Bacon. *Introduction to dislocations*. Butterworth-Heinemann, Oxford, 4th edition, 2001.

[Humbert 1996] M. Humbert, N. Gey, J. Muller, C. Esling, “Determination of a Mean Orientation from a Cloud of Orientations. Application to Electron Back-Scattering Pattern Measurements,” *J. Appl. Cryst.*, Vol. 29, pp. 662-666, 1996.

[Humphreys 1997] F. J. Humphreys, "A Unified Theory Of Recovery, Recrystallization And Grain Growth, Based On The Stability And Growth Of Cellular Microstructures-I. The Basic Model," *Acta mater*. Vol. 45, No. 10, pp. 4231-4240, 1997.

[Humphreys 2001] F.J. Humphreys, "Review: Grain and subgrain characterisation by electron backscatter diffraction," *Journal of Materials Science*, Vol. 36, pp. 3833-3854, 2001.

[Humphreys 2004] F.J. Humphreys, M. Hatherly, A. Rollett, *Recrystallization and Related Annealing Phenomena.* Burlington: Elsevier Science, 2004.

[Ito 2001] K. Ito, V. Vitek, "Atomistic study of non-Schmid effects in the plastic yielding of bcc metals," *Philosophical Magazine A*, Vol. 81, No. 5, pp. 1387-1407, 2001.

[Janssens 2006] K.G.F. Janssens, D. Olmsted, E.A. Holm, S.M. Foiles, S.J. Plimpton, P.M. Derlet, "Computing the mobility of grain boundaries," *Nature Materials*, Vol. 5, no. 2, pp. 124-127, 2006.

[Kassner 2009] M.E. Kassner, *Fundamentals of Creep in Metals and Alloys*, Elsevier: Amsterdam; London, 2nd ed. 2009.

[Kim 2008] S.G. Kim, Y.B. Park. "Grain boundary segregation, solute drag and abnormal grain growth." *Acta Materialia*, Vol. 56, no. 15, pp. 3739-3753, 2008.

[Kocks 1976] U.F. Kocks, "Laws for work-hardening and low-temperature creep," *ASME, Transactions, Series H-Journal of Engineering Materials and Technology* 98, pp. 76-85, 1976.

[Koo 2000] J.B. Koo, D.Y. Yoon, M.F. Henry, "Island grains of low misorientation angles formed during abnormal grain growth in Cu," *Metallurgical and Materials Transactions A*, Vol. 31, no. 5, pp. 1489-1491, 2000.

[Kunze 1993] K. Kunze, S.I. Wright, B.L. Adams, D.J. Dingley, "Advances in Automatic EBSP Single Orientation Measurements," *Textures and Microstructures*, Vol. 20, pp. 41-54, 1993.

[Liang 1999] R. Liang, A.S. Khan, "A critical review of experimental results and constitutive models for BCC and FCC metals over a wide range of strain rates and temperatures," *International Journal of Plasticity*, Vol. 15, pp. 963-980, 1999.

[Maag 1969] W.L. Maag, and W.F. Mattson. *Statistical Analysis Of High-Temperature Creep-Rate Data For Alloys Of Tantalum, Molybdenum, And Columbium*. No. N--69-36653; NASA-TN-D--5424. National Aeronautics and Space Administration, Cleveland, Ohio. Lewis Research Center, 1969.

[Mathematica 2010] Mathematica 8.0, Wolfram Research, Champaign, Illinois, 2010.

[Matthies 1988] S. Matthies, H-R. Wenk, G. W. Vinel, "Some basic concepts of texture analysis and comparison of three methods to calculate orientation distributions from pole figures." *Journal of applied crystallography*, Vol. 21, no. 4, pp. 285-304, 1988.

[Mecking 1978] H. Mecking, G. Gottstein, in *Recrystallization of metallic materials*, ed. F. Haessner, Dr. Riederer-Verlag, GmbH, Stuttgart, 195.

[Mehl 1948] R.F. Mehl, *Recrystallization***,** American Society for Metals (Ed.), Metals Handbook, American Society for Metals, Cleveland, Ohio, pp. 259–263, 1948.

[Mingard 2009] K.P. Mingard, B. Roebuck, E.G. Bennett, M.G. Gee, H. Hordenstrom, G. Sweetman, P. Chan, "Comparison of EBSD and conventional methods of grain size measurement of hard metals," *Int. Journal of Refractory Metals and Hard Materials*, Vol. 27, pp. 213-223, 2009.

[Morawiec 1989] A. Morawiec, J. Pospiech, "Some Information of Quaternions Useful in Texture Calculations," *Textures and Microstructures*, Vol. 10, pp. 211-216, 1989.

[Mullins 1956] W.W. Mullins, "Two-Dimensional Motion of Idealized Grain Boundaries," *Journal of Applied Physics*, Vol. 27, No. 8, pp. 900-904, 1956.

[Mullins 1958] W.W. Mullins, "The effect of thermal grooving on grain boundary motion." *Acta metallurgica*, Vol. 6, no. 6, pp. 414-427, 1958.

[Nakashima 1994] S. Nakashima, K. Takashima, J. Harase, "Effect of Thickness on Secondary Recrystallization of Fe-3%Si," *Acta metal. mater.* Vol. 42, No. 2, pp. 539-547, 1994.

[Olmsted 2009a] David L. Olmsted, Stephen M. Foiles, Elizabeth A. Holm, "Survey of computed grain boundary properties in face-centered cubic metals: I. Grain boundary energy," *Acta Materialia*, Vol. 57, pp. 3694–3703, 2009.

[Olmsted 2009b] David L. Olmsted, Elizabeth A. Holm, Stephen M. Foiles, "Survey of computed grain boundary properties in face-centered cubic metals—II: Grain boundary mobility," Acta Materialia, Vol. 57, pp. 3704–3713, 2009.

[Laugier] J. Laugier and B. Bochu. *OrientExpress* from the LMGP (Laboratoire des Materiaux et du Génie Physique de l'Ecole Supérieure de Physique de Grenoble http://www.inpg.fr/LMGP/) Suite. http://www.ccp14.ac.uk/tutorial/lmgp/index.html.

[Palmer 1987] J.E. Palmer, C.V. Thompson, and H.I. Smith. "Grain growth and grain size distributions in thin germanium films." *Journal of applied physics*, Vol. 62, no. 6, pp. 2492-2497, 1987.

[Park 1998] Y.B. Park, D.N. Lee, G. Gottstein, "The Evolution of Recrystallization Textures in Body Centered Cubic Metals," *Acta mater.*, Vol. 46, pp. 3371-3379, 1998.

[Pearson 1896] K. Pearson, "Mathematical Contributions to the Theory of Evolution.--On a Form of Spurious Correlation Which May Arise When Indices Are Used in the Measurement of Organs," *Proceedings of the Royal Society of London* 60, No. 359-367, pp. 489-498, 1896.

[Raabe 1994] D. Raabe, G. Schlenkert, H. Weisshaupt, K. Lücke, "Texture and microstructure of rolled and annealed tantalum," *Materials Science and Technology*, Vol. 10, pp. 299-305, 1994.

[Randle 2009] V. Randle, "Electron backscatter diffraction: Strategies for reliable data acquisition and processing," *Materials Characterization*, vol. 60, p. 913-922, 2009.

[Reid 1973] Reid, C.N., *Deformation Geometry for Materials Scientists,* Pergamon Press Ltd., 1973.

[Rios 1987] P.R. Rios, "A Theory for Grain Boundary Pinning by Particles," *Acta metall.*, Vol. 35, No. 12, pp. 2805-2814, 1987.

[Rios 1992] P.R. Rios, "Abnormal Growth in the Presence of Coarsening Particles," *Acta metall.*, Vol. 40, No. 4, pp. 649-651, 1992.

[Rios 1994] P.R. Rios, "Abnormal Grain Growth in Materials Containing Particles," *Acta metall. mater.*, Vol. 42, No. 3, pp. 839-843, 1994.

[Roberts 1979] W. Roberts, H. Bóden, B. Ahlblom, "Dynamic recrystallization kinetics," *Metal Science*, Vol. 13, No. 3-4, pp. 195-205, 1979.

[Rohrer 2011] G.S. Rohrer, "Grain boundary energy anisotropy: a review," *J. Mater. Sci.*, Vol. 46, pp. 5881-5895, 2011.

[Rollett 1989] A.D. Rollett, D.J. Srolovitz, and M. P. Anderson. "Simulation and theory of abnormal grain growth—anisotropic grain boundary energies and mobilities." *Acta metallurgica*, Vol. 37, no. 4, pp. 1227-1240, 1989.

[Rollett 1997a] A.D. Rollett, W. W. Mullins. "On the growth of abnormal grains." *Scripta materialia*, Vol. 36, No. 9, pp. 975-980, 1997.

[Rollett 1997b] A.D. Rollett, E. A. Holm. "Abnormal grain growth--The origin of recrystallization nuclei?," No. SAND--97-1712C; CONF-9610242--6. Sandia National Labs., Albuquerque, NM (United States), 1997.

[Rollett 1998] A.D. Rollett, S.I. Wright, in *Texture and anisotropy : preferred orientations in polycrystals and their effect on materials properties*, eds. U.F. Kocks, C.N. Tomé, H.-R. Wenk, Cambridge University Press, New York, pp. 178-239, 1998.

[Rosenberg 1971] J.M. Rosenberg, H.R. Piehler, "Calculation of the Taylor Factor and Lattice Rotations for Bcc Metals Deforming by Pencil Glide," *Met. Trans.* Vol. 2, p.257-259, 1971.

[Sachs 1928] G. Sachs, "On the Derivation of a Condition of Flow." *Z. Verein. Deutsch. Ing*, Vol. 72, pp. 734-736, 1928.

[Schmid 1935] Schmid, E. and Boas, W, *Kristallplastizität*, Springer, Berlin, 1935.

[Schwartzberg 1959] F.R. Schwartzberg, H. R. Ogden, and R. I. Jaffee. *Ductile-brittle transition in the refractory metals*. No. AD-216526; DMIC-114; PB-151070. Battelle Memorial Inst., Defense Metals Information Center, Columbus, Ohio, 1959.

[Sherby 1967] O. D. Sherby and P. M. Burke, "Mechanical behavior of crystalline solids at elevated temperature," *Progress in Materials Science*, vol. 13, pp. 325-390, 1967.

[Srolovitz 1985] Srolovitz, D. J., G. S. Grest, and M. P. Anderson. "Computer simulation of grain growth—V. Abnormal grain growth." *Acta Metallurgica*, Vol. 33, no. 12, pp. 2233-2247, 1985.

[Stuitje 1980] P.J.T. Stuitje, and G. Gottstein. "Dynamische Recrystallisation in Zugverformten Silbereinkristallen." *Z. Metallic*, Vol. 279, pp. 279-285, 1980.

[Taylor 1926] G.I. Taylor, C.F. Elam, "The Distortion of Iron Crystals," *Proceedings of the Royal Society of London. Series A, Containing Papers of a Mathematical and Physical Character*, Vol. 112, No. 761, pp. 337-361, 1926.

[Taylor 1928] G.I. Taylor, "The deformation of crystals of β-brass." *Proc. R. Soc. Lond. A*, Vol. 118, pp. 1–24, 1928.

[Taylor 1938] G. I. Taylor, "Plastic strain in metals." *J Inst Met*, vol. 62, pp. 307-324, 1938.

[Thanh 2009] P. Thanh. "Strain-assisted abnormal grain growth." TMS Annual Meeting & Exhibition, February 15-19 2009.

[Thompson 1987] C.V. Thompson, H.J. Frost, F. Spaepen, "The Relative rates of Secondary and Normal Grain Growth," *Acta metall.*, Vol. 35, No. 4, pp. 887-890, 1987.

[Tran 2008] T.B. Tran, B.V. Fell, C.A. Guebels, J.-P. Delplanque, J.R. Groza., "Towards single crystals using strain induced grain growth. part i: Experimental results," TMS Annual Meeting & Exhibition, Louisiana, New Orleans., March 9-13 2008.

[Tsurekawa 1994] S. Tsurekawa, T. Tanaka, and H. Yoshinaga. "Grain boundary structure, energy and strength in molybdenum." *Materials Science and Engineering: A*, Vol. 176, no. 1, pp. 341-348, 1994.

[Tsurekawa 1999] S. Tsurekawa, and Tadao Watanabe. "Grain Boundary Microstructure Dependent–Intergranular Fracture in Polycrystalline Molybdenum." *MRS Proceedings*, Vol. 586, No. 1, Cambridge University Press, 1999.

[Vitek 1970] V. Vitek, R. C. Perrin, and D. K. Bowen. "The core structure of ½ (111) screw dislocations in bcc crystals." *Philosophical Magazine*, Vol.21, no. 173, pp. 1049-1073, 1970.

[Voce 1948] E. Voce, "The relationship between stress and strain for homogeneous deformation." *J. Inst. Met.*, Vol. 74, pp. 537-562, 1948.

[Voce 1955] E. Voce, "A practical strain-hardening function." *Metallurgia*, Vol. 51, no. 307, pp. 219-226, 1955.

[von Misses 1928] R. von Mises, "Mechanik der plastischen Formänderung von Kristallen," *ZAMM-Journal of Applied Mathematics and Mechanics/Zeitschrift für Angewandte Mathematik und Mechanik*, Vol. 8, no. 3, pp. 161-185, 1928.

[Walter 1960] J.L. Walter, and C. G. Dunn. "An effect of impurity atoms on the energy relationship of (100) and (110) surfaces in high purity silicon iron." *Acta metallurgica*, Vol. 8, no. 8, pp. 497-503, 1960.

[Weertman 1968] J. Weertman, "Dislocation climb theory of steady-state creep." *ASM Trans. Quart.*, Vol. 61, no. 4, pp. 681-694, 1968.

[Winning 2001a] M.Winning, G. Gottstein, L.S. Schvindlerman, "Stress Induced Grain Boundary Motion," *Acta mater.*, Vol. 49, pp. 211-219, 2001.

[Winning 2001b] M.Winning, G. Gottstein, L.S. Schvindlerman, "Migration of grain boundaries under the influence of an external shear stress," *Materials Science and Engineering A*, Vol. 317, pp. 17-20, 2001.

[Winning 2002] M.Winning, G. Gottstein, L.S. Schvindlerman, "On the mechanisms of grain boundary migration," *Acta Materialia*, Vol. 50, pp. 353-363, 2002.

[Winning 2010] M. Winning, A. D. Rollett, G. Gottstein, D. J. Srolovitz, A. Lim, and L. S. Shvindlerman. "Mobility of low-angle grain boundaries in pure metals." *Philosophical Magazine*, Vol. 90, no. 22, pp. 3107-3128, 2010.

[Wörner 1987] C.H. Wörner, A. Cabo, "On the Grain Growth Inhibition by Second Phase Particles," *Acta metall*., Vol. 35, No. 11, pp. 2801-2804, 1987.

[Worthington 2007] D.L. Worthington, J.C. Cooley, D.J. Thoma, "Strain assisted abnormal grain growth of uranium 238," Poster Presented at TMS 2007 Annual Meeting Exhibition, Orlando, Florida, February 2007.

[Worthington 2011] D.L. Worthington, "Characteristics of Dynamic Abnormal Grain Growth in Commercial-Purity Molybdenum," PhD thesis, The University of Texas at Austin, December 2011.

[Worthington 2013] D.L. Worthington, N.A. Pedrazas, E.M. Taleff, "Dynamic Abnormal Grain Growth in Molybdenum," *Metallurgical and Materials Transactions A*, 2013, submitted.

[Wright 1993] S.I. Wright, S.I, "A review of automated orientation imaging microscopy (OIM),". *J Comput Assist Microsc* **5**, 207–221, 1993.

[Wright 1994a] S.I. Wright, G. T. Gray, and A. D. Rollett. "Textural and microstructural gradient effects on the mechanical behavior of a tantalum plate." *Metallurgical and Materials Transactions A*, Vol. 25, no. 5, pp. 1025-1031, 1994.

[Wright 1994b] S.I. Wright, S.R. Bingert, and M.D. Johnson. *Effect of annealing temperature on the texture of rolled tantalum and tantalum-10 wt% tungsten*. No. LA-UR--94-3431; CONF-9410213--3. Los Alamos National Lab., NM (United States), 1994.

[Wright 2011] S.I. Wright, M.M. Nowell, D.P. Field, "A Review of Strain Analysis Using Electron Backscatter Diffraction," *Microsc. Microanal*. 17, 316–329, 2011.

[Yang 2001] C.C. Yang, A.D. Rollett, W.W. Mullins, "Measuring Relative grain Boundary Energies and Mobilities in an Aluminum Foil from Triple Junction Geometry," *Scripta materialia*, Vol. 44, No. 12, pp. 2735-2740, 2001.

[Zener 1944] C. Zener, and J. H. Holloman, "Effect of Strain Rate Upon Plastic Flow of Steel," *J. Appl. Physics*, Vol. 15, pp. 22-32, 1944.

[Zener 1948] C. Zener, Private communication to C.S. Smith. Cited in *Trans. Am. Inst. Min. Engrs*, Vol. 175, p. 15, 1948.

Vita

Nicholas Alan Pedrazas graduated as salutatorian from Carnegie Vanguard High School in Houston, TX. He then pursued his undergraduate degree in mechanical engineering at The University of Texas at Austin (UT). In the spring of 2006 he studied abroad at the Technical University of Denmark (DTU). Shortly after returning, he began to do research under Dr. Eric Taleff at UT as an undergraduate research assistant. He obtained his Bachelor of Science degree in Mechanical Engineering from UT in December 2007 and continued in Dr. Taleff's group for graduate school. He completed his Master of Science in Engineering degree in August 2009 with his thesis titled: "Solid-State Production of Single-Crystal Aluminum and Aluminum-Magnesium Alloys."

npedrazas@gmail.com

This dissertation was typed by the author.